1990

Electrochemical Studies Of Vanadium Oxides For Use In Lithium Batteries

Eddie Edmund Andrukaitis

NOTICE

The quality of this microform is heavily dependent upon the quality of the original thesis submitted for microfilming. Every effort has been made to ensure the highest quality of reproduction possible.

If pages are missing, contact the university which granted the degree.

Some pages may have indistinct print especially if the original pages were typed with a poor typewriter ribbon or if the university sent us an inferior photocopy.

Reproduction in full or in part of this microform is governed by the Canadian Copyright Act, R.S.C. 1970, c. C-30, and subsequent amendments.

AVIS

La qualité de cette microforme dépend grandement de la qualité de la thèse soumise au microfilmage. Nous avons tout fait pour assurer une qualité supérieure de reproduction.

S'il manque des pages, veuillez communiquer avec l'université qui a conféré le grade.

La qualité d'impression de certaines pages peut laisser à désirer, surtout si les pages originales ont été dactylographiées à l'aide d'un ruban usé ou si l'université nous a fait parvenir une photocopie de qualité inférieure.

La reproduction, même partielle, de cette microforme est soumise à la Loi canadienne sur le droit d'auteur, SRC 1970, c. C-30, et ses amendements subséquents

ELECTROCHEMICAL STUDIES OF VANADIUM OXIDES FOR USE IN LITHIUM BATTERIES

by

EDDIE EDMUND ANDRUKAITIS

Department of Chemistry

Submitted in partial fulfillment

of the requirements for the degree of

Doctor of Philosophy

Faculty of Graduate Studies

The University of Western Ontario

London, Ontario

January 1990

ISBN 0-315-55276-X

ABSTRACT

Vanadium oxides of varying stoichiometries have been studied for their potential use in rechargeable solid state lithium batteries. Deposits of hydrated diammonium hexavanadates have been prepared electrochemically on various conducting anode substrates. Coherent electrodeposits of highly oriented, crystalline $M_4V_6O_{16+\delta}$, where M = NH_4, K, Rb and Cs and $0.00 < \delta < 0.10$, have also been made for the first time electrochemically on various conducting cathode substrates. Also, mixed crystalline phases of formula $M_{4-x}N_xV_6O_{16+\delta}$, where M, N = NH_4, K, Rb and Cs, $M \neq N$ and $0.00 < \delta < 0.13$, have been made. The mechanism of formation of a deposit at the anode involves formation of a hydrated V_2O_5 sol in a pH gradient at the anode, and subsequent electrophoretic deposition of the sol as an oriented crystalline deposit. The sol spreads to the cathode by convection, migration and diffusion, where the particles adhere with evidence of nucleation and growth on the cathode. These electrodeposits have been studied using both electrochemical (RDE, impedance, galvanostatic and potentiostatic methods) and non-electrochemical techniques (X-ray diffraction, chemical analysis, SEM, ESCA, and DTA with simultaneous TGA) to determine their structure, stoichiometry and use as reversible insertion electrodes.

The deposits containing NH_4^+ can be decomposed to crystalline V_2O_5 by heating in air, or to non-stoichiometric V_6O_{13} by heating in argon or in vaccuum (low O_2 partial pressure) at 300°C for several hours, with retention of their orientation on the substrate. The first (endothermic) step of the thermal decomposition involves loss of $2NH_3 + H_2O$. In the second (exothermic) step, on heating in air, recrystallization and oxidation of V(IV) to V(V) is observed with the

addition of 1/2 O to form V_2O_5. This oxidation is not seen on heating under reduced O_2 partial pressure (Ar or vacuum) and reduction continues until $V_6O_{13+\delta}$ is formed, where δ is a function of how much residual O_2 is left exposed to the deposit. Lithium could be reversibly inserted into and removed from the V_2O_5 form of the deposit up to a mole ratio $Li/V_2O_5 = 1.2$. For non-stoichiometric V_6O_{13} the ratio of $Li/V_6O_{13} = 4.4$. However, electrodes that were not decomposed cycled poorly and inserted only a small amount of lithium, < 1% of total V.

Single-cell batteries consisting of a Li anode, a polymer electrolyte such as MEEP, PEO or tetraglyme (supported in a porous material such as Celgard) and a vanadium pentoxide cathode have been studied. The batteries show favorable cycle lifetimes (>300) and high cathode capacity.

ACKNOWLEDGEMENTS

I would like to thank Dr. P.W.M. Jacobs and Dr. J.W. Lorimer for their invaluable guidance and encouragement. They both provided me with excellent supervision and support on this thesis, making it the most thought-provoking and enjoyable part of my education.

Acknowledgement is also given to the Natural Sciences and Engineering Research Council of Canada and the Ontario Ministry of University Affairs for financial support.

Lastly, I would like to thank my parents, who taught me that you can accomplish your goals in life if your desire is strong enough.

TABLE OF CONTENTS

LIST OF PHOTOGRAPHIC PLATES

thermogravometric (DTG) and thermogravometric analysis (TGA) were carried out on samples under an air or inert (argon) atmosphere using a Mettler Recording Vacuum Thermoanalyzer 127. Samples were 50 to 150 mg in weight for best results. Differential Scanning Calorimetry (DSC; Perkin-Elmer DSC-1B) required smaller samples (10-20 mg) than DTA but the upper temperature range was limited to 700 K.

3.4.7 Electrochemical Impedance Spectroscopy

This electrochemical technique involved the use of a Solartron 1250 Frequency Response Analyzer with a Solartron 1286 Electrochemical Interface. The same cell holder was that described in fig. 3.1. Single cell batteries could readily be analyzed at various cycle numbers and temperatures in the range from 10 to 85°C in the two-electrode configuration shown. The cell was heated by wrapping the glass cylinder with heating tape and its temperature was monitored using a Pt/Pt-Rh thermocouple and strip chart recorder.

The frequency range used for all impedance studies was from 65 KHz to 100 mHz with a signal amplitude of 10 mV peak-to-peak. For specific information on cathode electrodes separate measurements were made with blocking electrodes (see section 4.3.4).

3.4.8 Other Techniques

Mass spectrometry used a Finnigan MAT 8230 apparatus with a D-probe for solid samples, which provides direct exposure to the electron flux. Atomic Absorption Spectroscopy (AA) used a Varian Model 1275 Spectrophotometer with a lithium lamp. Samples were prepared by dissolving deposits in 0.2 mol/L H_2SO_4 and measuring the absorption at 670.8 nm. Standard solutions contained Li_2CO_3 in 0.2 mol/L H_2SO_4. Fourier Transform Infra-Red Spectroscopy (FTIR) was performed on a

LIST OF FIGURES

LIST OF SYMBOLS

Symbol	Description
a	activity of species
c^{σ}	concentration at the electrode surface
C	capacitance
C_{dl}	double layer capacitance
d	distance between crystal layers in x-ray diffraction
D	diffusion coefficient
E	potential against a reference electrode
E_{cf}	configurational contribution to potential
E_e	equilibrium potential
E_e^0	standard potential
E_i	initial potential for sweep experiment
E_p	peak potential (A or C denotes anodic or cathodic respectively)
$E_{p/2}$	half-peak potential
ΔE_p	change in peak potential
F	Faraday constant = 96484.6 C mol^{-1}
F_u	number of formula units
i	current
i_o	exchange current
i_p	peak current (A or C denotes anodic or cathodic respectively)
I	current density
I_o	exchange current density
I_p	peak current density
I_L	diffusion-limited current density
k	rate constant for a chemical reaction
k^0	standard rate constant for an electron transfer couple
n	number of electrons involved in overall electrode reaction
n_α	number of electrons before and including rate-determining step
N	number of ions
N_A	Avogadro constant = 6.022045×10^{23} mol^{-1}
R	gas constant = 8.31441 J K^{-1} mol^{-1} *or* resistance
R_u	resistance between reference and working electrode
R_{ct}	charge transfer resistance
S_{cf}	configurational entropy
t	time
T	temperature
V	cell voltage *or* applied voltage *or* volume
Z	impedance
Z_w	Warburg impedance
Z'	real component of impedance
Z''	imaginary component of impedance
α	transfer coefficient (subscript A or C denotes anodic or cathodic respectively) *or* number of lithium sites per vanadium atom
θ	diffraction angle in x-ray patterns
λ	wavelength of x-ray radiation
λ_f	ionic conductivity of species f
μ_{cf}	chemical potential
σ	Warburg coefficient
ν	potential scan rate *or* kinematic viscosity
ω	angular rotation rate *or* angular frequency of ac excitation

LIST OF APPENDICES

CHAPTER 1

INTRODUCTION

1.1 Objectives

The overall objective of the work described in this thesis was the fabrication and chemical and electrochemical analysis of new reversible cathode materials for lithium batteries. It was considered important to offer an explanation for the complicated electrochemical behaviour occurring at the cathode and how it influences the overall battery performance, stability and other important characteristics. This could be done using several classical and modern electrochemical techniques. Techniques from surface science were also employed as either confirmatory tests or to check the morphology of electrode materials. An extension of the simple lattice-gas model approach used in the past for other simpler systems such as Li_xTiS_2 [1], Li_xTaS_2 and $Li_xMo_6Se_8$ [2] was attempted. Setting up instrumental techniques which were new to our laboratory, in order to study these electrodes as reversible electrode materials, was also an important aspect of this project. This aspect included the interfacing and extensive programming of a PC to interact with a PAR electrochemistry system and HP plotter.

This thesis will cover both the electrodeposition and mechanism of formation of various vanadium oxides, their conversion to useful pure vanadium oxide electrodes, and a detailed experimental and theoretical study of vanadium oxide deposits as reversible electrode materials.

1.2 Review of Past Research

1.2.1 Development of Advanced Batteries

Research into new high-energy density batteries was begun in the early sixties, as the improvements in battery performance were deemed essential as its use for various energy storage needs grew. High-energy secondary (rechargeable) batteries have been used in a broad range of applications from electric traction to energy storage devices coupled to wind and solar power generators. These being intermittent power sources, a reserve power supply is necessary when they are not in operation.

The main requirements of the anode in a battery are a high theoretical energy density and compatibility with the (organic) electrolyte used. The electrolyte itself is required to be compatible with both the anode and cathode and should have a high ionic conductivity and selective solvation properties. The requirements of a cathode typically are: a low molar mass, high potential versus the alkali metal anode, stability and low solubility in the electrolyte, electrochemical activity, and good electrical conductivity.

Several commercially-available primary lithium batteries of the seventies typically employed a cathode of SO_2 or C_xF with an organic electrolyte. Work in the late seventies began to focus more on insertion electrode materials since earlier batteries (including the Pb battery) involved the formation of new phases whose growth restricts the power density and eventually causes complete loss of the active electrode material. However, insertion electrodes may avoid the formation of new phases. The use of such electrodes was first discussed

both by Armand [3] and Steele [4]. One of the most widely studied electrode materials during this time was the Li_xTiS_2 ($0 < x < 1$) insertion electrode, which has a theoretical specific energy (energy/unit mass) of about 500 W h/kg and an open circuit voltage of 2.4-1.9 V. In the literature, the term, energy density (energy per unit volume), is sometimes improperly used when the term, specific energy (energy per unit mass) is implied. TiS_2 is used in probably one of the most technologically advanced intercalation batteries, where the intercalation of Li to form Li_xTiS_2 results in a homogeneous single phase which is perfectly non-stoichiometric for the range $0 \leq x \leq 1$. In practical systems the TiS_2 is mixed with about 10% PTFE (teflon-(poly(tetrafluoroethylene)), pressed at 300°C into a metal mesh, surrounded by a polypropylene separator, and immersed in an organic electrolyte such as propylene carbonate or dioxolane with lithium perchlorate. Such a system has a specific energy of about 100 W h/kg [5].

Recently a secondary lithium battery using a MoS_2 cathode with a liquid organic electrolyte has been developed [6]. By cycling a C-cell between 2.3 and 1.3 V a capacity of 2 A h and life expectancy of 500 cycles is attained. Cell output doubles that of commercial nickel-cadmium (Nicad batteries) and more than triples that of lead-acid cells with a value of about 76 W h/kg.

Layered chalcogenides such as TiS_2 and MoS_2 [5,6] as cathode materials have the ability to insert reversibly and remove an ion such as Li^+ or Na^+ with very little change in their structure. Cavities in the structure allow for the passage of small ions.

1.2.2 The Vanadium Oxides

The commonest compounds containing vanadium (V) are vanadium pentoxide (V_2O_5) and ammonium metavanadate (NH_4VO_3). The pentoxide has limited solubility in water (0.0043 mol/L) [7] and is more acidic than oxides of vanadium in lower oxidation states, but does dissolve in acidic solutions. At pH values between about 2 and 6.5, vanadium in aqueous solutions exists as a complex mixture of monomeric and polymeric anions, where the proportions depend on pH and concentration of V(V).

Interest has been shifted over the past few years to framework oxides like V_2O_5 [8-11] as cathode materials. These framework compounds consist of shear structures derived from a ReO_3-type lattice, as shown in fig 1.1 [10]. The ReO_3 structure contains an extended network of channels intesecting in three perpendicular directions. These channels arise from the sharing of the square faces of individual, vacant cavities. The vanadium oxides V_2O_5, V_6O_{13} and VO_2 are derived from this structure by a shear of the ideal MO_3 lattice, which contains perovskite-like cavities where some of the square faces are capped by an additional oxide ion. A schematic diagram of the V_2O_5 structure is shown in fig 1.2 where its layer-like structure can be seen more clearly

.

The advantages of using a cathode containing V_2O_5 include a higher theoretical capacity (about 1 W h/cm^3), a lower sensitivity to moisture and air, a greater resistance to solvent intercalation [8,11] and a higher potential versus lithium. The Li/V_2O_5 battery system is theoretically the most favourable because of its high potential, high specific energy and good rate-capability. The good rate behaviour has been associated with the structure of V_2O_5 which contains cavities that

allow for easy lithium intercalation [8]. The pentoxide is an *n*-type semiconductor with an energy gap of 2.5eV [12].

There are some disadvantages to a $Li_xV_2O_5$ structure including low electronic conductivity which decreases with the amount of lithium inserted [11], irreversible reduction for Li/V mole ratios > 0.5, and, because of high potentials (3.8 V vs. Li/Li^+), solution decomposition can occur on charging. The latter can possibly be resolved, however, by developing new eletrolyte systems [13,14]. One solution to these problems in the past has been the use of suboxides of vanadium such as V_6O_{13} [15,16], which have been found to be two orders of magnitude more conductive even when fully lithiated. The V_6O_{13} does not have a close-packed structure and consists of alternating double and zig-zag chains of distorted VO_6 octahedra interconnected by corner-shared oxygens and providing infinite channels parallel to the [*010*] plane for lithium ion diffusion. The theoretical specific energy of the Li/V_6O_{13} cell system is about 800 W h/kg, with an average voltage of 2.5 V and 1 lithium per vanadium.

1.2.3 Electrochemical Deposition of Cathode Materials

Electrochemical deposition of solid-state electrodes into which hydrogen or lithium can be inserted has been demonstrated in only a few cases [17,18]. In 1987, Yoshino *et al.* [17] deposited onto an ITO (indium-doped tin oxide) glass substrate a thin film of hydrated non-stoichiometric V_2O_5 from a solution of polyvanadic acid sol. An electrochromic display device (ECD) was made using the film as two electrodes (working and counter) separated by an electrolyte of lithium perchlorate in propylene carbonate. A colour change of yellow to green

was observed with a switching potential of ±1.5 V and a response time of 2-20 s. Another electrodeposit of non-stoichiometric mixed-valent tungsten oxide has been made by cyclic voltammetry in a colloidal suspension of $Na_2WO_4 \cdot 2H_2O$ in 2 mol/L H_2SO_4 by Kulesza and Faulkner in 1988 [18]. They observed reversible electrochromic behaviour of this electrode by the reversible insertion and removal of H^+ from this electrodeposited tungsten bronze H_xWO_3.

As early as 1960, Goncharenko and Suvorova [19] found that a mixed-valence vanadium oxide hydrate of variable composition could be deposited electrochemically on a cathode from an strong alkaline solution ccntaining metavanadate. The stoichiometry was found to be $VO_2 \cdot nV_2O_5 \cdot mH_2O$ where m was approximately 3n and potassium was also detected. Subsequently Goncharenko [20] found that potassium hexavanadate monohydrate could be deposited electrochemically at an anode from alkaline vanadate solutions. Goncharenko and Suvorova [21] found that the mixed-valence vanadium oxide hydrate of variable composition and approximate formula $3K_2O \cdot 2VO_2 \cdot 5V_2O_5 \cdot 15H_2O$ could be deposited on a platinum cathode. They also observed that the addition of potassium or sodium sulfates and chlorides improved the rate of electrodeposition, but did not discuss adequately the mechanism of formation or the exact nature of the deposit. In all their papers the primary concern was the determination of the of deposition of vanadium compounds at the electrode in order to find the optimum conditions for isolation of vanadium compounds by electrolysis from vanadium ores. Typically, they operated in alkaline solutions at high current densities of 5 to 100 mA/cm^2.

Ptitsyn *et al.* [22] reported the formation of V_2O_5 films by

alternate cathodic and anodic polarization of a steel substrate in NH_4VO_3 solution at current densities of 540 and 360 mA/cm^2 respectively. A certain amount of lithium was found to insert into these films from *N,N*-dimethylformamide solutions to form lithium vanadium bronzes; however, a reliable analysis to determine the amount of insertion was not done. They had found previously that solutions containing K^+ did not reduce V_2O_5 contained in composite electrodes [23], but that a reaction at these electrochemically-deposited film-electrodes did occur in $KClO_4$ solutions. These phenomena were attributed to structural imperfections of the electrochemically deposited vanadium oxide, but no further investigation was made of the actual structure and morphology of these films or their mechanism of formation. Thus there remained many unknown aspects of the preparation and properties of these deposits.

Previous to the electrochemical preparation mentioned above, ammonium or alkali metal hexavanadates were made by collection of precipitates from a boiling vanadate solution in presence of a zinc catalyst [24] or by precipitation of alkali metal vanadates by strong acid [25]. The products were then analyzed by chemical analysis and X-ray powder diffraction to determine their stoichiometry. The electrochemical properties of these materials have not been investigated.

1.2.4 Application to Battery Technology

The most common method of forming a vanadium oxide for use as an electrode material has been by the thermal decomposition of ammonium metavanadate (NH_4VO_3) under a controlled temperature and oxygen partial pressure. Many high-temperature vanadium bronzes have been made, by melting correct amounts of a metal and a vanadium oxide at high temperature, and their structures and properties have been studied [26-30]. Among these bronzes, the regions of existence at high temperature have been established for the system $K_2O \cdot VO_2 \cdot V_2O_5$ [27]. In 1970, Bernard *et al.* [24] formed the isomorphic vanadium oxide containing ammonia and water by precipitation from a boiled aqueous ammonium vanadate solution in the presence of a zinc catalyst. The precipitate was collected and found to have a composition range $(NH_4)_{3.56}V_6O_{15.18} \cdot H_2O$ to $(NH_4)_{3.16}V_6O_{15.58} \cdot zH_2O$, with $0.23 \leqslant z \leqslant 1.07$, analogous to the high temperature alkali metal vanadates.

In the past, other researchers have produced cathodes consisting of mixtures of various materials which are pressed at high pressures to form a pellet which can be used as an insertion electrode. Little is known about the properties of these types of composite electrodes and the relative contribution made by the solid electrolyte and electrode phases to the mass transport. Such systems need to be carefully analyzed so that the relevant material specifications can be defined. Vanadium oxide electrodes prepared electrochemically have several potential advantages over the conventional method of preparation from mixtures of thermally-produced vanadium pentoxide bronzes mixed with an electronic conductor (such as carbon black or nickel powder) and a polymer binder (such as PTFE or polyethylene powder): (a) the electrodes

can be prepared directly on a conducting support; (b) electrochemical investigations are not complicated by the presence of extraneous materials; (c) as prepared, cells containing pure vanadium pentoxide electrodes are initially in the fully-charged state; (d) the deposits show marked electrochromic behaviour, which can possibly be exploited in practical devices; (e) the deposits act as ion-selective electrodes, again with the possibility of exploitation in practical devices.

If these vanadium oxide bronzes can be prepared at or near room temperature, several potential advantages accrue over other methods of preparation. Therefore, such an electrode could allow for a wide range of electrochemical studies to be done to examine the kinetics and diffusion processes of lithium into and out of the pure V_2O_5. In earlier batteries made by other researchers, phase changes in the cathode electrode have had an important effect on the charge/discharge character. This is primarily due to the phase changes of the cathode material that occurs during cycling of a battery. While the electrolyte/lithium interface typically causes the largest problems, the choice of the proper electrolyte may overcome the problem of the highly reactive lithum anode. Recently, stable LiAl alloys, and other materials that alloy with lithium, have also been examined as prospective anodes with better stability than the highly reactive pure lithium metal, but with easy transfer of lithium ion to the electrolyte. The electrolyte/cathode interface is also an important problem since good contact must be made with no reaction between the two materials.

With these considerations in mind, the thesis will primarily focus on the formation of vanadium pentoxide cathode materials and their application to secondary lithium batteries.

Fig. 1.1 Perovskite-related cavities present in ReO_3 a), V_2O_5 b), V_6O_{13} c) and VO_2 d). The arrows indicate possible directions of lithium diffusion.

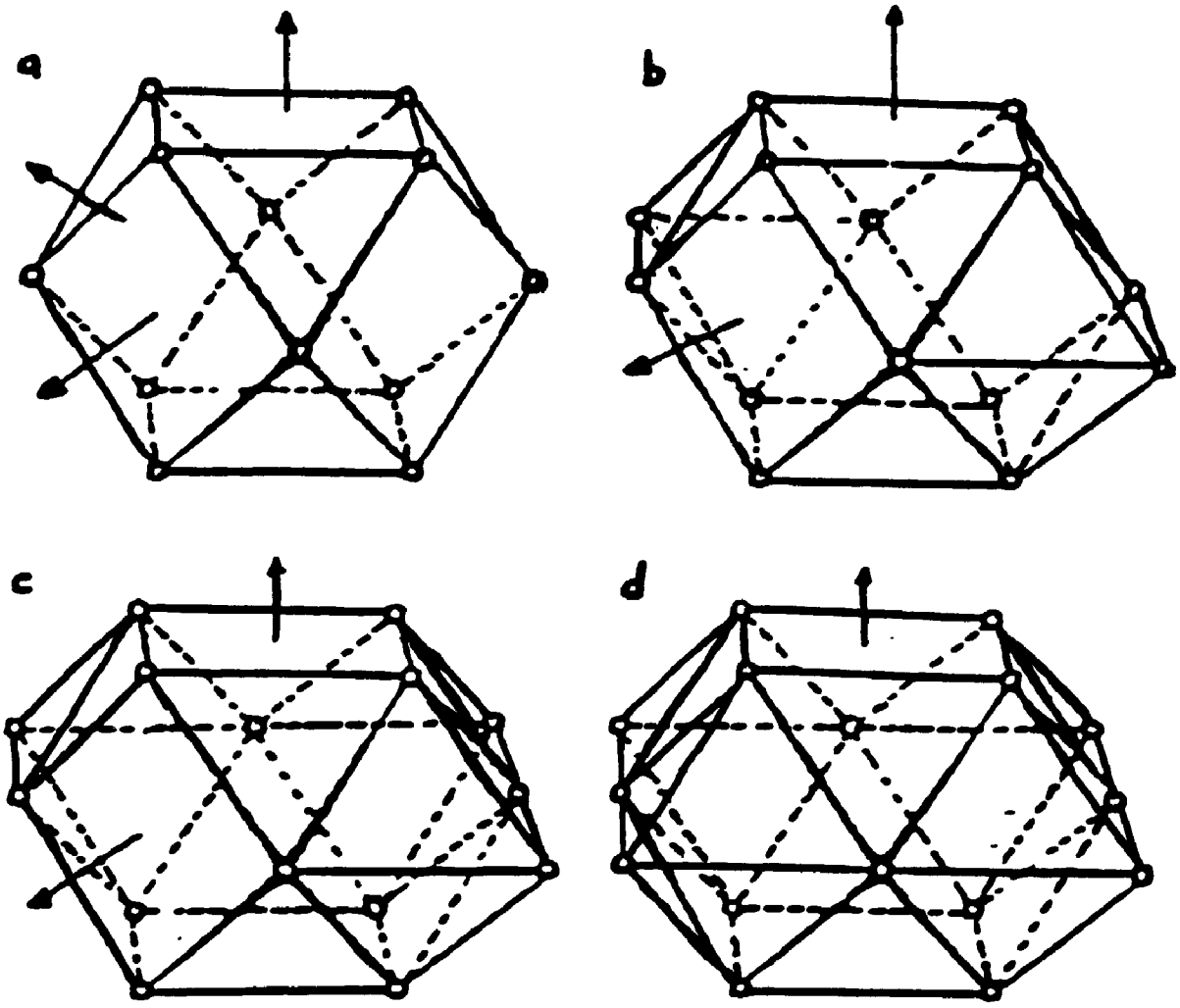
a
b
c
d

Fig. 1.2 Structure of orthorhombic vanadium pentoxide (V_2O_5).

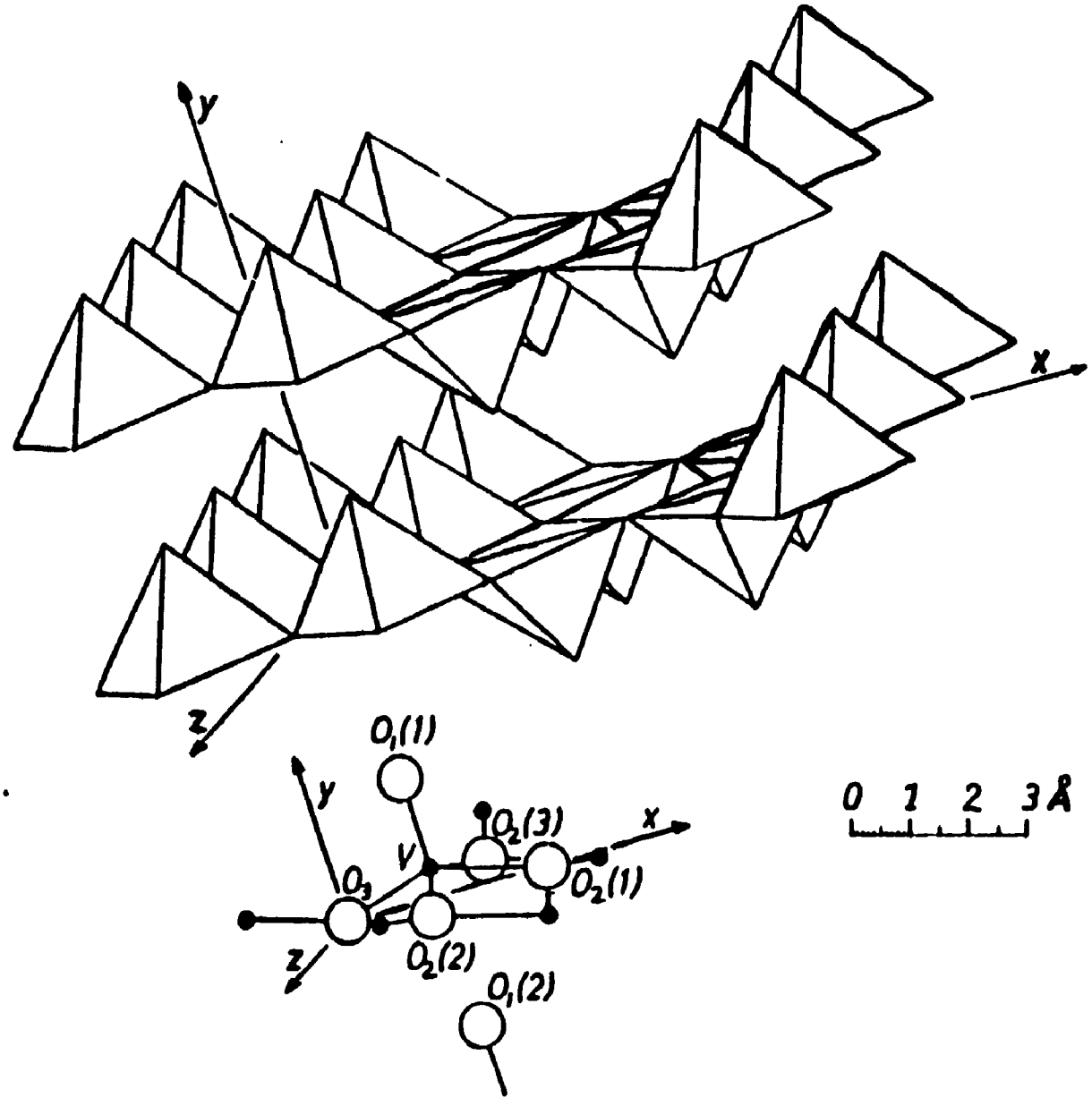
y
x
z
O1(1)
y
O2(3)
x
V
O3
O2(1)
z
O2(2)
O1(2)
0 1 2 3 Å

CHAPTER 2

DISCUSSION OF THE EXPERIMENTAL AND THEORETICAL APPROACH

2.1 Introduction

Since this thesis reports an electrochemical preparation of vanadium oxides, or more precisely, a salt of vanadium oxide on a conducting substrate, it was important to determine the exact nature of the deposit, the mechanism of formation and potential use as a cathode material in order to compare with work done by other battery researchers using similar materials. Thus, a thorough and sometimes exhaustive chemical analysis routine was adopted, along with other semi-quantitative surface analysis techniques, including photoelectron spectroscopy (PES), energy dispersive X-ray analysis (EDAX) and atomic absorption (AA). These helped confirm the presence or absence of certain elements or oxidation states of vanadium. With chemical analysis often being more precise than 1% even for small samples, relative amounts of vanadium in different oxidation states could be obtained. These led to the determination of several new phases.

It was also important to try to describe the structure of several of these new crystalline materials by indexing the X-ray diffraction patterns [31]. Experimental values of X-ray *d*-spacings are determined from Bragg's equation:

$$n\lambda = 2\,d\,\sin\theta \qquad (2.1)$$

where λ is the wavelength of the radiation used (here, CuK_α - λ = 0.15405 nm). The observed *d*-spacings are arranged in order of

decreasing *d*.

The procedure to index X-ray patterns and to determine unit cell dimensions, either for newly-formed crystalline deposits or to check reported data, can be summarized in the following steps:

1) From the low θ-values and assumed type of unit cell, estimate the unit cell dimensions.
2) Use these dimensions to index, approximately, all lines.
3) Using a least squares procedure, find the best fit of the observed d-spacings, and find refined unit cell dimensions.
4) Use the refined unit cell dimensions to recalculate the indices.
5) Repeat from step 3, until all the observed and calculated d-spacings are within the assigned error limit, typically < 0.005 nm.

Once the unit cell dimensions have been determined it is possible to determine a theoretical density of the crystal from the dimensions and number of formula units in the unit cell.

2.2 Electrochemical Methods

Several electrochemical techniques were employed in the formation of cathodes, the analysis of their nature, and their ability to behave as useful reversible cathodes for use in a lithium battery. A brief account of how these were used together with a description of the techniques will be outlined below. Relevant equations to the system under investigation will be given later in the results section of the thesis [32-38].

Cyclic voltammetry is a potential sweep technique in which a linear potential ramp is applied up to a certain value and then is returned to

the original potential (see fig. 2.1(a)). Its use has grown to cover a wide variety of systems, allowing kinetic parameters to be determined for many mechanisms. This technique is usually the first choice when studying a system for the first time. Care must be taken to insure that the *iR* drop is negligible when taking measurements as this will decrease the peak heights and increase the peak separations. This usually becomes a problem with experiments involving large currents. Another concern can be the effect of the contributions of double-layer charging to the total current. However this contribution will usually be small if scan rates are below 100 mV/s or microelectrodes are used. For reversible reactions the peak current density is proportional to the concentration of the electroactive species and to the square roots of the sweep rate and the diffusion coefficient. Irreversible reactions arise when the rate of electron transfer is slow or involves many steps. Surface equilibrium is not maintained, and the shape of the CV curve changes from that seen in fig 2.1(b). A totally irreversible system can usually be identified from a total absence of a reverse peak.

Cyclic voltammetry has been used extensively to study many electrochemical processes such as coupled chemical reactions and surface processes like adsorption and, to a smaller extent, corrosion and deposition mechanisms. Some diagnostic test_ .or CV of reversible processes include the following [37]:

1) $\Delta E_p = E_p^A - E_p^C = 59/n$ mV at 25 °C
2) $|E_p - E_{p/2}| = 59/n$ mV at 25 °C
3) $|I_p^A / I_p^C| = 1$
4) $I_p \propto \nu^{1/2}$

5) E_p independent of ν

6) at potentials beyond E_p, $I^{-2} \propto t$

Symbols shown here and throughout the thesis have been summarized on page *xviii*. Here E_p represents the peak potential and I_p the peak current, with the A or C representing the anodic and cathodics peaks respectively and ν the sweep rate.

Diagnostic tests used for testing for total irreversibility include [37]:

1) No reverse peak

2) $I_p^C \propto \nu^{1/2}$

3) E_p^C shifts $-30/(\alpha_c\, n_\alpha)$ mV for each decade increase in ν (at 25 °C)

4) $|E_p - E_{p/2}| = 48/(\alpha_c\, n_\alpha)$ mV at 25 °C.

It is also possible, depending on sweep rate, for a system that is reversible at one sweep rate to become irreversible at a higher sweep rate, with a quasi-reversible intermediate region also being present. Some diagnostic tests for this situation would include [37]:

1) $|I_p|$ increases with $\nu^{1/2}$ but is not proportional to it

2) $|I_p^A I_p^C| = 1$ provided $\alpha_C = \alpha_A = 0.5$

3) ΔE_p is greater than $59/n$ mV and increses with increasing ν at 25 °C

4) E_p^C shifts negatively with increasing ν

This technique will be used to study both the initial electrochemical deposition of useful cathode materials for battery applications, as well as to help understand the mechanism occurring at the cathode electrode during the deposition process. Cyclic voltammograms are often difficult to interpret, and as a result other electrochemical techniques will also be used to derive further information about the mechanism of formation. Other techniques were also used to study the insertion and removal behaviour of the electrodes and their performance in a lithium battery.

Chronoamperometry is a potential-step technique where the potential of the working electrode is changed almost instantaneously and the current-time response is recorded (see figs 2.2(a) and (b)). Notice from the figures that the current falls as $t^{-1/2}$ and a plot of I vs $t^{-1/2}$ should be linear and pass through the origin (test for diffusion control). The diffusion coefficient can be found from the slope (or from the value of $It^{1/2}$, which should be independent of t).

The current density at time $t = 0$ is kinetically controlled and the rate constant for the electrode reaction can be found in principle. But $I_{t=0}$ cannot be measured for the following reasons:

1) the rise-time of the potentiostat is not zero;

2) the current-measuring system also has a finite rise time;

3) a double layer charging current is present.

As a result, its value must be found by extrapolation to $t = 0$.

This technique will be used specifically to examine the insertion and removal behaviour of the electrochemically-formed electrodes. Several experiments will also be described using the electrodeposited electrodes, with the rotating disc electrode technique.

The technique of electrochemical impedance spectroscopy has several advantages over other classical electrochemical techniques, as there is the possibility of a complete analysis of sometimes complicated processes involving surface and solution reactions [35]. It allows for continuous recording of reaction parameters under more dynamic conditions than for cyclic voltammetry and polarography. There are, however, some important things to consider when using this technique which include linearity, spurious effects and the frequencies used. The usual theories are all linear, but electrochemical processes are by nature non-linear. A general rule to achieve linearity is not to exceed a peak-to-peak amplitude of 10 mV. Falsification of results by spurious effects in the circuitry is a problem; this is usually due to stray capacitance between connecting leads and self-inductance of the leads at high frequencies. Proper cell design can remove most of this problem by proper placement of the working and counter electrodes, with the reference electrode close to the working electrode, without disturbing a uniform current distribution. Finally, the range of frequencies should be as large as possible (at least 10^{-2} to 10^{5} Hz) for proper theoretical analysis of the results.

It is important in any impedance analysis to be able to fit the experimental data to a physical model (an equivalent circuit) to obtain information about cell parameters. Only a brief explanation of what would theoretically be seen in an experiment will be given. For the circuits shown in the impedance diagrams in fig. 2.3 with an impedance of $Z = R + 1/j\omega C$, the real part of Z is simply R and the imaginary part is $-1/\omega C$. The graph of fig. 2.3(a) shows the case for a parallel combination giving a semicircle, and a series resistance (R_u) which

translates the semicircle along the Z' axis. R_u could represent an uncompensated solution resistance between reference and working electrode. The capacitance C_{dl} is an interfacial capacitance and at low frequencies the impedance is purely resistive (C_{dl} has very large reactance).

To illustrate the behaviour of electrochemical impedance spectroscopy for battery systems the cell:

Li / LiX in a polymer solvent / Li (2.2)

will be used. Three semicircles would be expected from such a cell, as shown in figure 2.3(b) [38]. The high-frequency semicircle corresponds to the parallel combination, R_bC_b, in the equivalent circuit and is associated with the bulk electrolyte. The intermediate-frequency semicircle corresponds to the parallel combination, R_eC_e, in the equivalent circuit and is attributed to electrode/electrolyte charging (C_e) and reaction of ions (Li^+) at the electrode. The low-frequency semicircle is skewed, with a linear region at higher frequency which is 45° to the real axis. This semicircle is associated with the diffusion of the electroactive ions (Li^+) and is represented by the Warburg impedance, W, given by [38]:

$$Z_w = A\omega^{-1/2} - jA\omega^{-1/2} \qquad (2.3)$$

where A is a constant given by:

$$A = RT/(n^2F^2(2D)^{1/2}c_{Li^+}) \qquad (2.4).$$

Theory predicts that at even lower frequencies the impedance reaches a maximum and curves over to reach the real axis in the zero frequency limit (fig. 2.3(b). However, as shown later in the thesis, for an intercalation electrode the impedance diverges at low frequency.

The Warburg impedance can also occur by the diffusion of the

electroactive species within an electrode such as the intercalation electrode, Li_xTiS_2 ($0 \leq x \leq 1$). The ratio of the height and width of the Warburg impedance is a constant and the frequency at which the maximum occurs can be estimated from the equation:

$$X = (\omega L/D)^{1/2} \qquad (2.5)$$

where X is a constant.

All three semicircles in fig. 2.3(b) are usually not observed in most cases because of the complexities of real electrolytes [38]. In real cells the semicircles are significantly broadened and electrode spikes non-vertical because of several factors; (a) ion-ion interactions, (b) surface layers on electrodes, (c) inhomogeneity of the polymer electrolyte and (d) roughness of the electrodes.

Electrochemical impedance spectroscopy (EIS) is one of the newest electrochemical methods. Ideally, as with cyclic voltammetry, a lot of information can theoretically be obtained, but, in practice the results are often difficult to interpret. In our case, EIS provides information about the resistances in our cathode materials, in comparison to the electrolyte, as a function of battery cycle time and with the actual amount of lithium present in the layered vanadium oxide cathodes during the charge and discharge of a single cell battery.

The rotating disc electrode (RDE) technique is an example of a convective diffusion system and was developed by V. G. Levich and co-workers in the 1950's [36]. Its use is quite widespread and the theory and experimental design are well understood. The transport of a species in solution can occur by the mechanisms of migration, diffusion and convection which are a result, respectively, of an electrical potential gradient, a concentration gradient from a region of high

concentration to low concentration of the species, or of stirring the solution. Migration effects are negligible when an inert electrolyte at higher concentrations (> 100X) than that of the electroactive species is added to the solution.

There are essentially two regions next to an electrode surface, a diffusion layer (thickness δ) in contact with the electrode surface and a bulk solution region beyond this layer. Convection is responsible for bringing the electroactive species to the diffusion layer and diffusion brings it across the layer to the electrode surface. A steady state condition exists since the faradaic current in the electrode is independent of time for a constant stirring rate.

The limiting current at a rotating disk is given by the Levich equation

$$I_{l,d} = 0.62\ nFAD^{2/3}\ \upsilon^{-1/6}\ \omega^{1/2}\ C^b \qquad (2.6)$$

where
- $I_{l,d}$ = limiting disk current
- C^b = bulk concentration of species
- A = area of disk electrode
- D = diffusion coefficient
- υ = kinematic viscosity of solution
- ω = angular velocity of electrode rotation

This equation is not valid for $\omega \rightarrow \infty$ and the onset of turbulence is expected at $\omega \simeq 6 \times 10^4\ s^{-1}$ in aqueous solutions.

By determining the mass transport-limited currents at the RDE it is possible to calculate the diffusion coefficient in solution. Once a recording of the current during a potential sweep is made at various rotation speeds, a plot of the limiting current at a fixed potential in the sweep vs. $\omega^{1/2}$ is made. This plot should be linear and the

intercept is equal to the charging current which passes in the electrode. The charging current is independent of rotation speed and the slope of the plot of I_L vs. $\omega^{1/2}$ should be independent of the scan rate. The diffusion coefficient of the electroactive species can be calcuated from the slope of the plot (equation (2.6)). The RDE technique may also be employed in conjunction with many of the other techniques developed for static electrodes, such as cyclic voltammetry, potentiostatic steps and chronoamperometric experiments.

2.3 Lattice Gas Model

Recently this model has been found to be a useful basis for describing the thermodynamics of insertion of ions into certain intercalation electrodes [2]. The theory has been worked out in great detail [1] and a few chalcogenide systems such as Li_xTiS_2, Li_xTaS_2 and $Li_xMo_6Se_8$, have been studied [1,2,38,39].

2.3.1 Introduction

The potential of an intercalation electrode is proportional to the chemical potential of a guest (such as lithium) in a host (such as TiS_2 or Mo_6Se_8) where the cell for the electrode reaction consists of the following:

$$\text{Li} \quad / \quad \begin{matrix}\text{electrolyte containing} \\ \text{Li salt}\end{matrix} \quad / \quad \begin{matrix}\text{intercalation} \\ \text{electrolyte}\end{matrix} \qquad (2.7)$$

The potential of lithium in a host as a function of lithium concentration, x , where:

$$x\,\text{Li(s)} + \text{X(s)} = \text{Li}_x\text{X(s)} + x\,e^-$$

is usually measured at open circuit ($i = 0$) and lithium is inserted using constant current. The value of x is found by chemical analysis from the relation, $x = it$. The work done on the cell is the charge times the potential difference (E) which equals the change in molar Gibbs energy of the cell process and is given by;

$$\Delta G = -xFE \qquad (2.8)$$

2.3.2 Extension of the Lattice-Gas Model

In an attempt to account for the shape of the potential-x curves, a theoretical calculation of the potential was made on the basis of a Bragg-Williams type of model, the details of which are given below. This model was originally designed to study insertion of lithium into hydrated vanadium pentoxide gels [42]. However, an attempt at understanding the potential-x curves for the insertion of lithium into crystalline electrodeposits of vandadium oxides will also be discussed in chapter 7. In order to use eqn. (2.23) below, the number of lithium sites per vanadium atom, α, must be known. Murphy *et al.* [8-10] concluded that V_2O_5 should be viewed as a framework structure, containing cavities in which inserted lithium ions have four nearest-neighbour V atoms. Examination of the structure of orthorhombic V_2O_5 indicates that each of these V atoms is shared with a neighbouring cavity, so that $\alpha = 2$. The equation for the potential is then

$$E = -(RT/F)\ln[x^2/(1-x)(2-x)] + a + bx$$

$$= E_{cf} + a + bx \qquad (2.9)$$

where R is the gas constant, T the thermodynamic temperature, F the

Faraday constant, and *a* and *b* constants related to the energy change accompanying the insertion process. The first term is the configurational contribution from mixing lithium ions and V(IV) ions on the V_2O_5 lattice. This equation is analogous to those developed by Crandall *et al.* [42] and by Armand (see [12]), who used a slightly different derivation which was limited to $\alpha = 1$ and no distribution of lattice ions.

According to eqn. (2.9), a plot of $Q = E - E_{cf}$ should be linear in x. For small values of x, the configurational contribution is very sensitive to errors in x, so an initial sharp rise or drop in a plot of the Q function against x is of questionable significance, as will be seen later in Chapter 7.

The electrochemical insertion of lithium into hydrated vanadium pentoxide gels occurs according to the following reaction:

$$V_2O_5 \cdot yH_2O + xLi^+ + xe^- = Li_xV_2O_5 \cdot yH_2O \qquad (2.10)$$

which can be investigated using the cell:

$$Li(s)/LiX/Li_xV_2O_5 \cdot yH_2O(s) \qquad (2.11)$$

The products of the reaction can be considered to be Li^+ and V(IV) in the vanadium pentoxide lattice, so that the cell reaction can be written as:

$$xLi^+(s) + xe^- + V_2O_5 \cdot yH_2O(s) \longrightarrow Li_x[V(IV)_xV(V)_{2-x}]O_5 \cdot yH_2O(s) \qquad (2.12)$$

The corresponding change in Gibbs energy is

$$\Delta G = x\mu(Li^+ \text{ in } V_2O_5) + x\mu[V(IV) \text{ in } V_2O_5] - x(\mu(V(V) \text{ in } V_2O_5) - x\mu(Li)$$
$$= -xFE \qquad (2.13)$$

where E is potential of the cell.

Thus,

$$-FE = \mu(Li^+ \text{ in } V_2O_5) - \mu(Li) + \mu[V(IV) \text{ in } V_2O_5] - \mu(V(V) \text{ in } V_2O_5 \qquad (2.14)$$

The first two terms in this equation together make up the change in Gibbs energy on transferring one mole of lithium ions from the metal to the vanadium pentoxide lattice. If a Bragg-Williams type of model is assumed, there are four contributions to these terms: (a) the standard chemical potentials of Li(s) and Li^+ in V_2O_5; (b) the contribution of the configurational entropy which arises when the lithium ions are distributed randomly on the vanadium pentoxide lattice to form $Li_xV_2O_5 \cdot yH_2O$; (c) terms in x which arise from the interaction between pairs of Li^+ ions and Li^+ ions and V^{4+} ions; (d) constant terms which arise from the interaction between pairs of Li^+ ions, between V^{5+} ions and Li^+ ions, and between both ions (Li^+, V^{4+} , V^{5+}) and water molecules in the lattice.

The final two terms in eqn. (2.14) describe the change in Gibbs energy on converting one mole of V_2O_5 to $V_2O_5^-$. The contributions to these terms are: (a) the standard chemical potentials of V^{4+} in V_2O_5; (b) the contribution of the configurational entropy which arises when V^{5+} is reduced randomly to V^{4+} on the vanadium pentoxide lattice; (c) terms in x which arise from the interaction between pairs of V^{4+} ions and Li^+ ions and V^{4+} ions; (d) constant terms which arise from the interaction between V^{4+} and V^{5+}, and between these ions and water

molecules.

The contributions to the cell potential from the terms involving interaction energies may be written (again in the Bragg-Williams approximation)

$$a + bx$$

In general, for each lithium ion in the V_2O_5 lattice there are αN sites for insertion. During electrochemical insertion of lithium, electrons and lithium ions enter the lattice from opposite sides, so there is initially a strong electric field that drives diffusion in the lattice and may result in a random distribution of Li^+ and V^{4+} at equilibrium. In this case, there are two configurational terms, one for positioning the lithium ions on the lattice, and one for positioning the V^{4+} ions on the lattice. If N is the number of V atoms, N_{Li} the number of lithium ions, k Boltzmann's constant and N_A Avogadro's constant, the number of Li^+ sites is N/α and the number of Li atoms is (for $Li_xV_2O_5$)

$$N_{Li} = xN/2 \tag{2.15}$$

The configurational entropy is then:

$$S_{cf}(Li^+) = k\ln\{(N/\alpha)!/(xN/2)!(N/\alpha - xN/2)!\} \tag{2.16}$$

Use of Stirling's approximation gives:

$$S_{cf}(Li^+) = -(N/\alpha)\ln\{(2 - \alpha x)/2\} - (xN/2)\ln\{\alpha x/(2 - \alpha x)\} \tag{2.17}$$

Since

$$\mu_{cf} = -N_A T\,[\partial S_{cf}/\partial N(Li^+)]_{NT,V} \tag{2.18}$$

then

$$\mu_{cf}(Li+) = \quad = -(2N_A T/N)(\partial S_{cf}/\partial x)_N$$

$$= RT\ln\{\alpha x/(2 - \alpha x)\} \qquad (2.19)$$

Similarly, if the V(IV) ions are distributed randomly on the N available sites,

$$S_{cf}[V(IV)] = k\ln\{N!/(xN/2)!(N - xN/2)!\} \qquad (2.20)$$

and

$$\mu_{cf(V^{4+})} = RT\ln\{x/(2 - x)\} \qquad (2.21)$$

If the positions of the lithium ions and the V(IV) ions are not closely correlated, then the total configurational contribution to the chemical potential is

$$\mu_{cf} = RT\ln[\alpha x^2/(2 - x)(2 - \alpha x)] \qquad (2.22)$$

Addition of eqn. (2.14) and (2.21) gives for the cell potential

$$E = -(RT/F)\ln[\alpha x^2/(2 - x)(2 - \alpha x)] + a + bx$$

$$= E_{cf} + a + bx \qquad (2.23)$$

In practice, a pseudo-reference electrode is used instead of a reversible lithium electrode; the only change introduced is in the significance of the constant a.

Fig. 2.1(a) Potential-time profiles for linear sweep voltammetry.

Fig. 2.1(b) Cyclic voltammogram for a reversible process for the reaction $O + e^- = R$ where only O is present in solution.

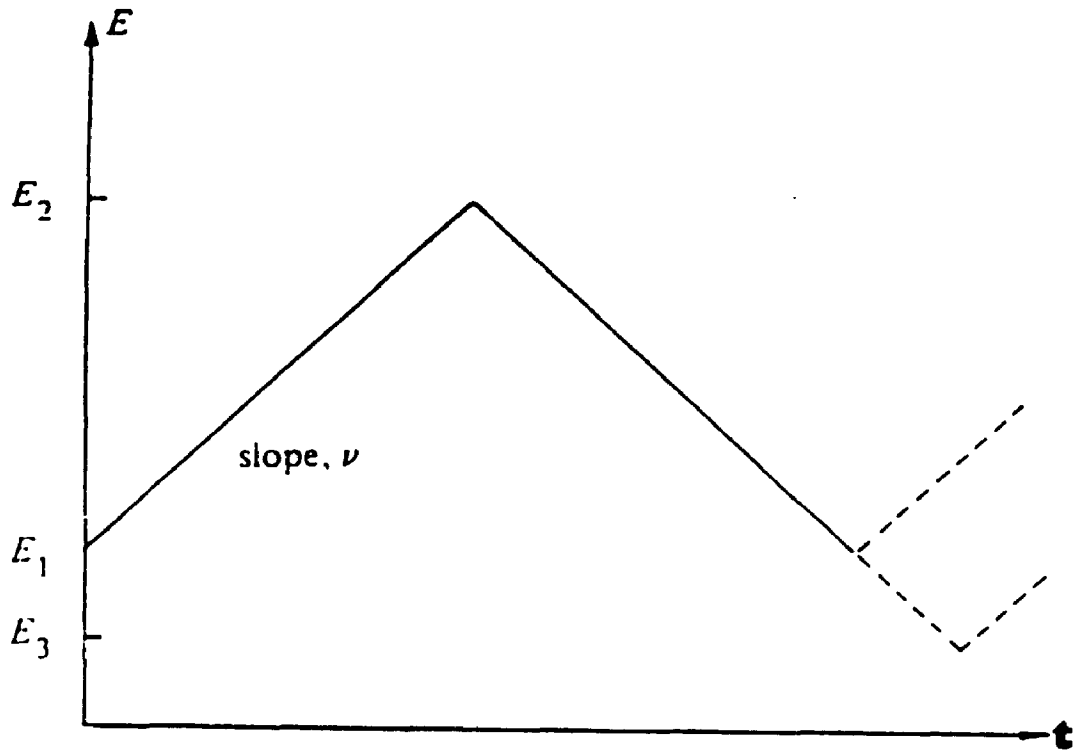
E
E2
E1
E3
slope, ν
t

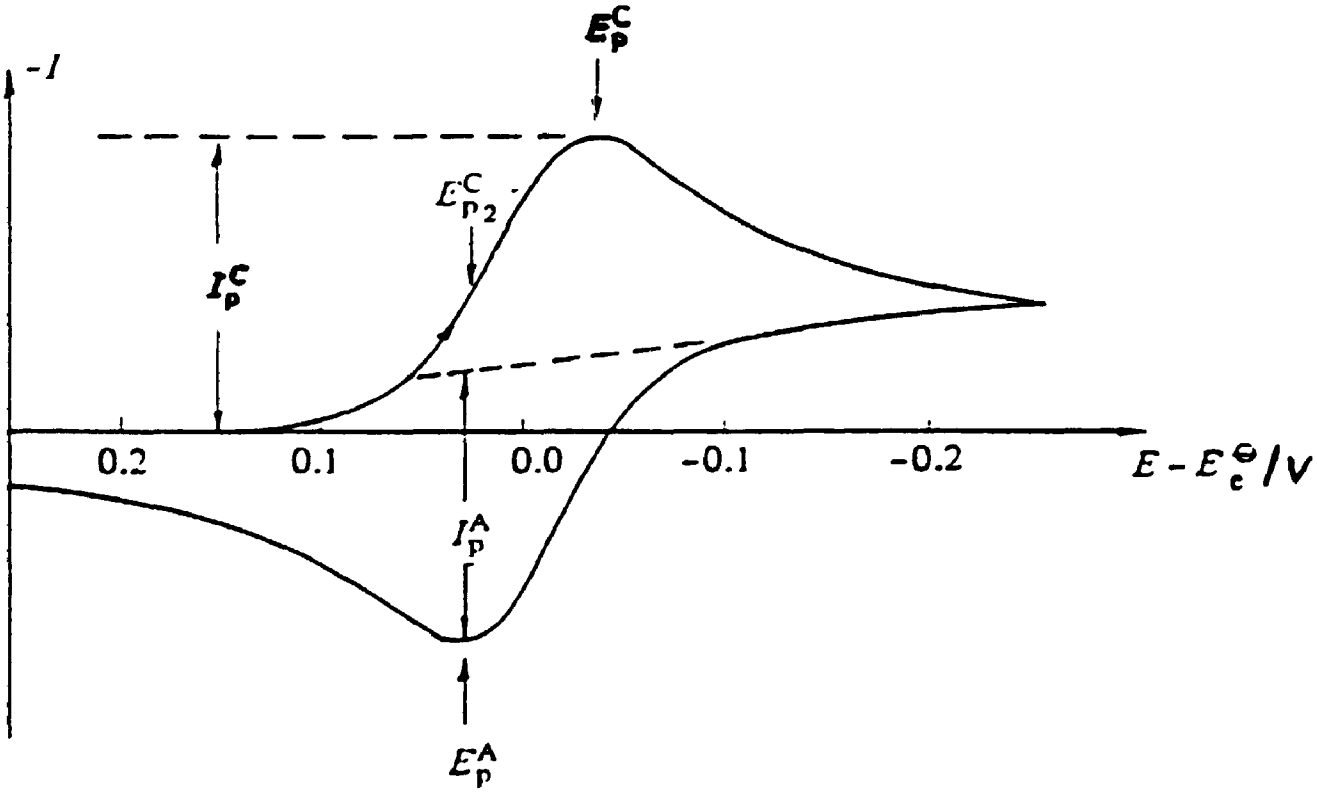
-I
E_p^C
$E_{p/2}^C$
I_p^C
0.2
0.1
0.0
-0.1
-0.2
$E - E_c^\ominus$ /V
I_p^A
E_p^A

Fig. 2.2(a) The potential-time profile for a single potential step chronoamperometric experiment.

Fig. 2.2(b) Current-time response for a potential step experiment, where E_2 is chosen so that (a) the reaction is diffusion controlled. (b) the reaction is kinetically controlled. and (c) there is mixed control.

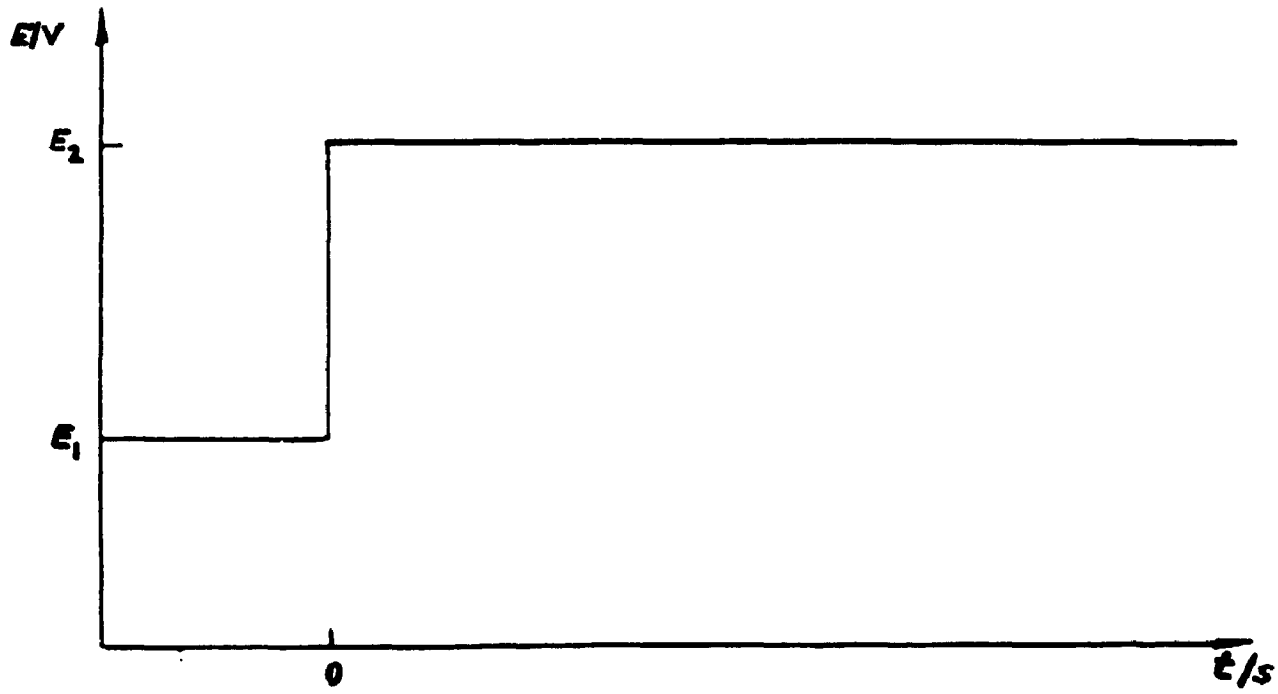
E/V
E2
E1
0
t/s

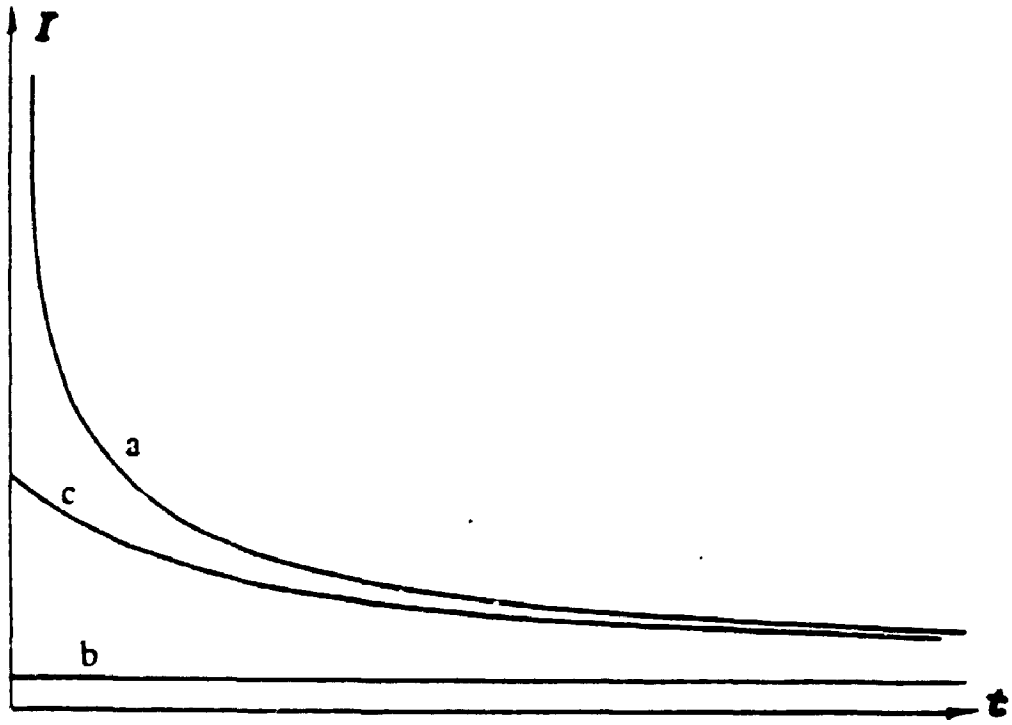
I
a
c
b
t

Fig. 2.3(a) Complex plane impedance for a parallel *RC* circuit, plus an uncompensated solution resistance, R_u, where C_{dl} is the interfacial capacitance.

Fig. 2.3(b) Complex plane impedance spectrum and equivalent circuit for a polymer electrolyte cell with diffusion-controlled migration of an electroactive ion.

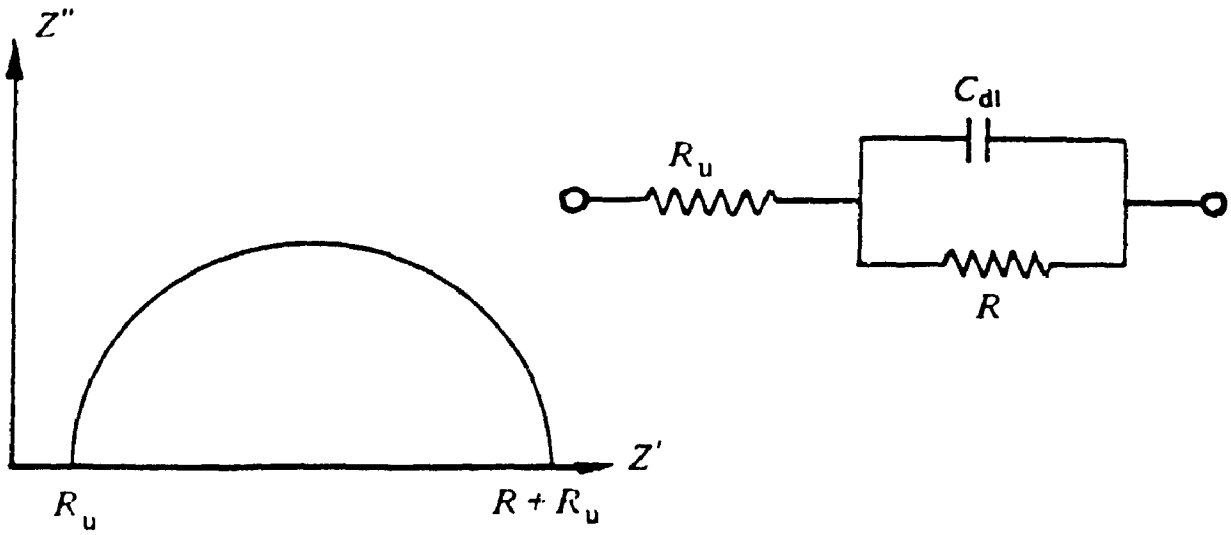
Z''
Z'
R_u
$R + R_u$
C_{dl}
R_u
R

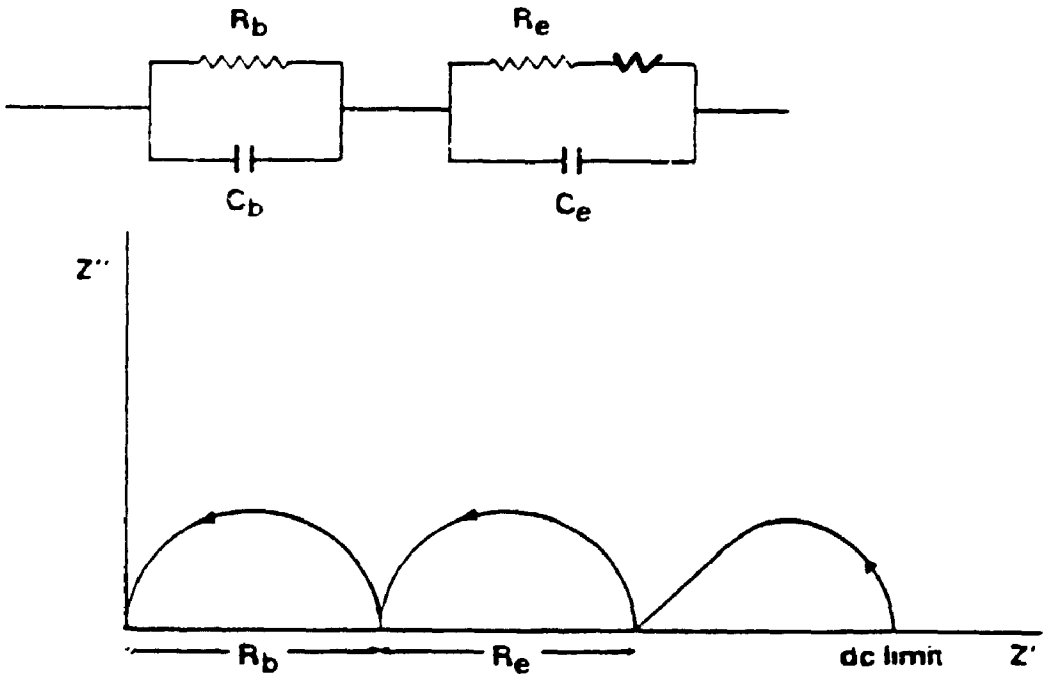
R_b
R_e
C_b
C_e
Z''
R_b
R_e
dc limit
Z'

CHAPTER 3

EXPERIMENTAL EQUIPMENT AND ANALYSIS

3.1 General Materials

All the water used for rinsing and standard aqueous solutions was doubly-distilled using a Corning AG-2 laboratory still. The conductivity of the water was of the order of 1×10^{-6} S cm^{-1}. Non-aqueous solutions of propylene carbonate (GLC grade and Reagent grade) and *N,N*-dimethylformamide (DMF)(BDH Analytical grade) were handled under argon in a glove bag. Lithium perchlorate (Fisher Certified A.C.S. grade) was dried under vacuum above 100°C and stored under argon in a glove box. NH_4VO_3 as well as other materials, were used as received from various suppliers without further purification. Any moisture- or oxygen-reactive materials, such as lithium metal or non-aqueous electrolytes, were also kept in sealed containers in the glove box.

3.2 Solution Preparations

All solutions prepared for electrodeposition have in common two factors, the vanadate ion (VO_3^-) at or near saturation for a specific temperature and an overall pH in the range of 6.5 to 7.0. Several non-aqueous solutions containing salts were also used in the later electrochemical studies.

3.2.1 Aqueous Ammonium Vanadate

This is the most common solution prepared for electrodeposition experiments. First, an excess of 20 g of NH_4VO_3 was added to about 0.5 L of water and heated at > 70°C with stirring for several hours. The

solution was allowed to cool to the desired temperature, usually 40°C, and the clear yellow-orange solution was decanted into the cell used for electrodeposition making sure that as little as possible of the undissolved NH_4VO_3 was added. This ensured saturation in NH_4VO_3 at the temperature of interest.

3.2.2 Aqueous Ammonium Vanadate With Additional Salt

When a supporting electrolyte was used, saturated aqueous NH_4VO_3 was first made at 60°C, and additional salts such as K, Na, and Li sulphates and perchlorates were added and then cooled to the desired temperature as described above. Solutions containing both an alkali metal ion (K^+, Na^+ or Li^+) and NH_4^+ were made by saturating a solution with NH_4VO_3 at 40°C and adding the salt to various concentrations of 0.0, 0.05, 0.10 and 0.5 mol/L.

3.2.3 Alkali Vanadate Solutions and Mixtures

Alkali metal vanadates of K, Na, and Li were prepared by addition of a slight excess of 1 mol/L KOH, NaOH or LiOH, respectively, to saturated NH_4VO_3 (40°C) and then were heated at a higher temperature (> 80°C) for several hours until all the ammonia was released. The pH of the final solutions was adjusted to 6-7 if outside this range. Similarly, Rb and Cs vanadate solutions were made by adding NH_4VO_3 to a Rb or Cs hydroxide solution. Hydroxide solutions of 1 mol/L were prepared either by passing a Rb or Cs halide through an ion exchange column (hydroxide form) or from RbOH and CsOH (Aldrich - 99% pure - 50% by wt.). Mixtures of various combinations of Cs^+ with NH_4^+, Rb^+ or K^+ and Rb^+ with K^+ can be made from combining these vanadate solutions in the desired proportions.

3.2.4 Non-Aqueous Solutions

The drying procedures for these materials are very important since trace amounts of water can attack Li electrodes and also DMF which is very hygroscopic. For this reason molecular sieves (Type 5A) were placed in solutions of DMF to ensure dryness. Propylene carbonate solutions were prepared by passing it through a column of molecular sieves to remove any trace amounts of water. The cell on assembly was placed in a glove box under argon atmosphere where these two materials were stored.

After adding about 75 mL of the non-aqueous electrolyte, such as propylene carbonate to the cell, lithium perchlorate was weighed on a digital Mettler Balance in the glove box and added to the solution in amounts to give a range of concentration from 0.1 to 1.0 mol/L $LiClO_4$. The solutions were stored in sealed containers in a glove bag under argon atmosphere.

3.3 Electrodes and Cells

The fabrication and design of electrodes is crucial in battery studies. Thus, it was important to study electrodes of a predictable nature (i.e., reproducible in structure, morphology, thickness and adhesion to support).

3.3.1 Cathode Materials

Electrodes were supported on a variety of conducting substrates, including SnO_2-coated glass (Corning 0211, 0.05μm thick, 100 Ω/square), platinum foil (0.1 mm), nickel foils (0.025 to 0.125 mm) and stainless steel (1mm). These substrates were cut to the desired size and cleaned ultrasonically (Bransonic 220 bath) in 2 mol/L H_2SO_4 for 3 min, then

twice more in doubly distilled water. If the deposit was needed only on a specific site on the support (i.e., only on one of the two sides of support) the most effective method was to cover the opposite side of this surface with masking tape (3M). Removing the tape at the end of the deposition leaves the metal surface clean and free from deposits which was important for good electrical contact in the electrochemical measurements described below.

3.3.2 Reference Electrodes

Potentials involving aqueous solutions were measured relative to the saturated calomel electrode (SCE - Fisher # 13-639-56) for aqueous electrolytes. The SCE has a potential of +0.2415 V compared to the standard hydrogen electrode at 25°C. For non-aqueous electrolytes a silver-silver chloride electrode was used since the SCE (containing sat. aq. KCl) would expose the solution to water (add 3.550 V to obtain potentials versus Li^+/Li for a 0.25 mol/L $LiClO_4$ in propylene carbonate at 25°C). The Ag-AgCl reference electrode which has a potential of 0.2223 V was made by oxidizing a spiral of silver wire (1.5 mm in diameter) in a 0.1 mol/L HCl solution at a current density of about 0.1 mA/cm^2. for about 5 to 10 min.

3.3.3 Electrolytes

All aqueous electrolyte solutions for electrodeposition have been discussed above. Solution of $HClO_4$ were made at various concentrations from 0.1 to 1.0 mol/L in both aqueous and non-aqueous solutions of DMF and PC.

For battery studies several electrolytes were used, all with $LiClO_4$ as a solute and one of the following as solvent: tetraglyme, (tetraethylene glycol dimethyl ether, $CH_3-[OC_2H_4]_4-OCH_3$, mp -30°C),

poly(bis(methoxyethoxyethoxide)phosphazene) (MEEP), or poly(ethylene oxide) (PEO). The mole ratio of O/Li was 12:1. Because of the low viscosity of tetraglyme at room temperature a porous support was needed to prevent the electrolyte from seeping out from between the electrodes. Celgard 2500 - porosity 45% (Celanese Separations Products) was treated with boiling diethyl ether for 30 minutes and then drying for 60 minutes under vacuum at 50°C. Celgard provided rigid support while still being very porous to the electrolyte. The tetraglyme was used as delivered. It was checked periodically using FTIR for water contamination. The electrolytes were stored until needed in the argon-filled glove box. The electrodes and cell itself were then sealed and the cell was removed and placed in the bag. After 10 minutes of flushing the glove bag with argon the glove bag was closed and the leads were connected.

3.3.4 Single Cell Batteries

Single cell batteries were all designed to fit this same sealed glass cylinder (fig. 3.1). These single cells have the arrangement:

$$\underset{\text{(anode)}}{Li} \;/\; \underset{\text{(in Celgard 25 } \mu\text{m)}}{\text{tetraglyme} + LiClO_4\ (O/Li = 12:1)} \;/\; \underset{\text{(cathode)}}{V_2O_5}$$

This design allowed for evacuation and flushing the cell with argon. Electrical contact was made through spring-loaded stainless steel rods emerging from either end of the cylinder which was made air tight by the use of rubber O-rings. As seen in the figure, the cell had an anode of lithium (Aldrich 0.1 mm thick); a lithium-aluminum alloy was also used (see 3.3.5). The cathode was vanadium oxide on a conducting support, usually Ni or Pt.

3.3.5 Specific Cells

For experiments on pH changes at the electrodes, a cell was used with an anode compartment (20 mL) separated from the cathode compartment (100 mL) by a porous glass frit of area 1 cm^2.

The setup for impedance measurements for the symmetric case where V_2O_5 are blocking electrodes is given by:

$$V_2O_5 \ / \ \text{tetraglyme} + LiClO_4 \ (O/Li = 12:1) \ / \ V_2O_5$$
$$(\text{in Celgard } 25\ \mu m)$$

This cell was designed to fit the glass cylinder shown in fig. 3.1.

Alloys of LiAl were made electrochemically in solutions of propylene carbonate with 0.1 to 1.0 mol/L $LiClO_4$. The cell consisted of a Li anode and a aluminum cathode in the solution, using an Ag-AgCl reference electrode. A constant current, density between 0.1 to 1 mA/cm^2, was passed for a measured time. The current was periodically turned off, which allowed the cell to equilibrate under stirring for 1 min., then current was again passed, and the procedure was repeated. To ensure dryness, a lithium metal scavenger was placed in the cell.

Formation of LiAl alloy electrodes were also done using the cell arrangement

$$\underset{(\text{anode})}{Li} \ / \ \underset{(\text{in Celgard } 25\mu m)}{\text{tetraglyme} + LiClO_4 \ (O/Li = 12:1)} \ / \ \underset{(\text{cathode})}{Al}$$

where aluminum foil (0.1 mm Aldrich 99.9% pure) replaces the V_2O_5 in the single cell arrangement of section 4.3.4. More commonly the alloys were made galvanostatically in the propylene carbonate solutions with $LiClO_4$.

3.4 Apparatus and Equipment

Many different experimental techniques were used in an attempt to characterize prospective cathode electrodes by electrochemical and non-electrochemical means. Summaries of these techniques are given below.

3.4.1 Surface Science Techniques

Laser Raman spectra were recorded directly from deposits on platinum substrates using a Dilor OMARS spectrometer equipped with a Olympus BH2 microscope and green excitation of power 3 mW. Several electrodeposits and battery components were analyzed by scanning electron microscopy (SEM) with the ability to do X-ray energy dispersive analysis (EDAX). Other techniques used were X-ray photoelectron spectroscopy (XPS) and Auger Electron Spectroscopy (AES).

3.4.2 Electrochemical Analysis

Controlled potentials and currents were applied using a PAR Model 170 Electrochemistry System for routine electrochemical procedures such as electrodepositions. Experiments requiring a record of the measurements used a PAR Model 273 potentiostat interfaced to a microcomputer and graphics plotter. Extensive programming in CWBASIC was done to allow for interaction between these three units. Our own software made this electrochemical system very flexible to use with a number of techniques and it has been also used periodically by others. Several programs were written; however, there are two which were used routinely with minor modifications to suit the experiment needed and these are given in appendices 1 and 2.

The first program (appendix 1(a)) allows a choice of either chronamperometry, chronpotentiometry or cyclic voltammetry. A command file (appendix 1(b)) is read from the floppy disk, the experiment is

performed and the data first stored in the PAR 273 memory (up to 6000 data points). The data can then be saved on a floppy disk and printed on the screen. If desired, a hardcopy was made on a HP 7550A plotter. The second program (appendix 2(a)) is used for longer experiments (>5 min) such as those involving insertion and removal studies. It allows for an on-screen point-by-point plot of the data (there must be more than 5 s between points) as it is being stored directly to a floppy disk, to monitor the experiment visually. Thus, by minor changes in the command files (appendix 2(b)) or a few lines in the main program, all parameters are set up for the experiment. For example, open circuit potential measurements were completely automated with stirring, rest, and constant-current insertion steps controlled by the computer interfaced to the potentiostat using the auxiliary interface of the PAR 273.

3.4.3 Chemical Analyses

A modification of the reductimetric titration method for the determination of vanadium in steel was used [43] to provide an efficient, easy to perform, two-step titration that could be used to determine accurately the amount of V(IV) and V(V) present. A known mass of deposit was dissolved in 1 mol/L H_2SO_4 and was titrated with standard $KMnO_4$ solution to determine the amount of V(IV) present. An extra 1 mL of $KMnO_4$ was added after the end point, then 0.5% $NaNO_2$ solution was added dropwise until the pink color disappeared, and then a few drops in excess were added. About 5 mL of a 10% sulfamic acid solution was added to destroy excess nitrite. Titration with standard ammonium iron(II) sulfate gave the total vanadium content in the deposit. The endpoint was detected using either a redox electrode or an indicator (barium

diphenylamine sulfonate), the former being the preferred method. This analysis has proved to be rapid, and had a precision of better than 1 % on a limiting sample size of about 10 mg.

The amount of NH_4^+ present in the deposit was determined by the Kjeldahl method using a microdistillation setup and collecting the NH_3 in a 4% boric acid solution. The solution was then titrated with standard 0.125 mol/L HCl and methyl red indicator. This titration could also be carefully carried out potentiometrically since the endpoint was not very sharp with the indicator. Checks with NH_4Cl (dried > 100 °C) gave results accurate to within 0.5%.

Once it was determined that only V, O, H_2O and NH_3 or an alkali metal (see 3.4.4 for analysis) were present in a sample the water content was determined by differences in the actual mass of the sample from the masses of ammonium or alkali metal and vanadium determined by chemical analysis and the amount of oxygen in combination with these elements. The amount of water in a sample was also determined by TGA (thermal gravimetric analysis) (see 3.4.6).

3.4.4 Gravimetric Analysis and Density Determinations

The quantitative method of determining the amount of alkali metal (K, Rb or Cs) present in an electrodeposit was by gravimetric analysis using sodium tetraphenylboron [44]. A deposit was dissolved in 1 mol/L H_2SO_4, then a solution containing excess sodium tertraphenylboron was added. The sodium salt is soluble, but the K, Rb or Cs (even NH_4^+) salts form precipitates which can be collected, washed with water and dried in an oven at > 100 °C to constant weight.

However, some care must be taken in the collection of the precipitate because of its tendency to creep up the glass walls, forming

very fine particles which could easily pass through filter paper. To circumvent these problems a medium porosity Pyrex^{R} glass filter was used with a double layer of glass filter paper (Reeve Angel-Grade 934AH). By heating the filter and glass crucible to constant weight before and after collecting and washing the precipitate, the mass and hence the amount of alkali metal for known mass of deposit can be determined.

Experimental density values for various deposits were determined using a Berman Density Balance with toluene as the displacement liquid. One drop of Triton X-100 wetting agent (Fisher) was added to the toluene solution. Because of the possibility of finer particles falling through the powder basket and improper "wetting" of the powder sample the "in liquid" weight was measured first to constant weight, then in air when all the toluene has dried off. The density of the toluene had been determined by the formula given by Berman:

$$d_t = d_s + 10^{-3}\,\alpha(T/K-273.15) + 10^{-6}\,\beta(T/K-273.15)^2$$

where d_s = 0.8845 g cm^{-3}, α = 0.9159 and β = 0.368 [45].

3.4.5 X-ray Diffraction

X-ray diffraction spectra were recorded on a Rigaku Geigerflex apparatus with emergent slit 1°, receiving slit 0.3°, a crystal monochromator, and a scan rate of 2°/min. The X-ray source was Cu Kα radiation where λ = 0.15405 nm. Small corrections could be made to the observed diffraction angles by internal calibration using the platinum (001) line obtained from the substrate on which the deposits were made. No special sample preparation was needed other than mounting the sample on a glass slide.

3.4.6 Simultaneous DTA, DTG, and TGA Analysis and DSC

Simultaneous differential thermal analysis (DTA), differential

thermogravometric (DTG) and thermogravometric analysis (TGA) were carried out on samples under an air or inert (argon) atmosphere using a Mettler Recording Vacuum Thermoanalyzer 127. Samples were 50 to 150 mg in weight for best results. Differential Scanning Calorimetry (DSC; Perkin-Elmer DSC-1B) required smaller samples (10-20 mg) than DTA but the upper temperature range was limited to 700 K.

3.4.7 Electrochemical Impedance Spectroscopy

This electrochemical technique involved the use of a Solartron 1250 Frequency Response Analyzer with a Solartron 1286 Electrochemical Interface. The same cell holder was that described in fig. 3.1. Single cell batteries could readily be analyzed at various cycle numbers and temperatures in the range from 10 to 85°C in the two-electrode configuration shown. The cell was heated by wrapping the glass cylinder with heating tape and its temperature was monitored using a Pt/Pt-Rh thermocouple and strip chart recorder.

The frequency range used for all impedance studies was from 65 KHz to 100 mHz with a signal amplitude of 10 mV peak-to-peak. For specific information on cathode electrodes separate measurements were made with blocking electrodes (see section 4.3.4).

3.4.8 Other Techniques

Mass spectrometry used a Finnigan MAT 8230 apparatus with a D-probe for solid samples, which provides direct exposure to the electron flux. Atomic Absorption Spectroscopy (AA) used a Varian Model 1275 Spectrophotometer with a lithium lamp. Samples were prepared by dissolving deposits in 0.2 mol/L H_2SO_4 and measuring the absorption at 670.8 nm. Standard solutions contained Li_2CO_3 in 0.2 mol/L H_2SO_4. Fourier Transform Infra-Red Spectroscopy (FTIR) was performed on a

Bruker IFS 32 with an IBM system 9000 computer.

A rotating disc method (RDE) was also used to study lithium insertion into electrodeposits and the mechanism of cathodic electrodeposition. An electrode of either Pt or glassy carbon was used with the rotation speed accurately controlled using a Pine Instrument Co. analytical rotator (Model ASR2). Rotation speeds of 400, 900, 1600, 2500, 3600, 4900, and 6400 rpm were used.

Cyclic voltammetry experiments were run at various temperatures for the aqueous vanadate solution. The pH was also carefully adjusted over a broad range of 2 to 10 at room temperature and at higher temperatures by titration with known amounts of concentrated standards of either 10 mol/l H_2SO_4 or NaOH.

3.5 Methodology

It was very important to find the best conditions to form useful electrodeposits. Once this was done, the same conditions were maintained so that accurate comparisons could be drawn from one sample to the next without repeating the lengthy analysis necessary to determine accurately the composition of a deposit and its structural morphology.

3.5.1 Electrodeposition

For anodic deposition, the following cell was used:

$$Pt \;/\; NH_4VO_3(sat.\ aq.) \;/\; SnO_2 \text{ glass}$$

(cathode) (anode)

The cell was kept at temperatures from 25 to 70°C during deposition by keeping the cell in a thermostatted water bath. Other conducting substrates such as, carbon cloth (Stackpole PWB-6 or PWB-3/C/C),

stainless steel and nickel were used as anodes.

In general all cathodic electrochemical depositions used the cell:

Pt / sat. MVO_3 (M = K, NH_4, Rb and/or Cs) / Pt

(anode) (25 to 70°C) (cathode)

The methods used were either chronoamperometry (-2 to -3 V), chronopotentiometry (0.1 to 1.0 mA/cm² current density) or cyclic voltammetry at a scan rate of 50 mV/s between potentials of 0.0 and -0.7 V (SCE). Potentials and currents were applied using a PAR Model 273 potentiostat for recording data or a PAR 170 for routine electrode fabrications.

3.5.2 Analysis

To accurately determine the composition of a deposit the following analyses were performed routinely. Once a deposit was made and allowed to dry either by air drying, heating or vacuum methods the sample was collected and stored in a desiccator. Typically, a sample of about 100 mg was used for NH_3 analysis and one of 50 mg for chemical analysis of V(IV) and V(V). EDAX was used to confirm the presence or absence of other alkali metals and SEM to determine the size, orientation and effects of heating the deposits. X-ray diffraction was used on samples usually before chemical analysis and the pattern analyzed with an attempt to match a pattern in the ASTM powder diffraction file. Details of the various analyses are given in later chapters. All other techniques mentioned were used to either confirm other results or as a comparison to theoretical values.

3.5.3 Ion insertion

All ion insertions were performed at constant current densities of 0.1 to 1 mA/cm². Open circuit measurements of the potential were made

for the galvanostatic insertion of an alkali cation into various electrodeposited electrodes in both aqueous and non-aqueous solutions. From these measurements insertion curves of potential against the amount of ion inserted per formula unit were plotted. For ion insertions the following cell was used:

$$\text{Pt} \;/\; 0.1\ \text{mol/L}\ LiClO_4 \;/\; V_2O_5\ \text{on}\ SnO_2\ \text{glass}$$

in propylene carbonate

(anode) (cathode)

with an Ag-AgCl reference electrode. The cell had a volume of 75 mL and a distance of 4 cm between anode and cathode and 3 mm between the reference electrode and cathode. A constant current, density between 0.1 to 1 mA/cm^2, was passed for a measured time. The current was then turned off, the cell was allowed to equilibrate under stirring for 3 min, then the open circuit potential was measured after stirring was stopped. Current was again passed, and the procedure was repeated until the maximum insertion of lithium had occurred.

Open circuit measurements of the potential were made for the insertion of lithium into the deposits and for a cycle of reduction-oxidation-reduction to study insertion of lithium after an oxidation step; here a solution of 0.1 mol/L $LiClO_4$ in propylene carbonate was used, with a Ag-AgCl reference electrode. A constant current (density between 0.1 to 1 mA/cm^2) was passed for a measured time (1 to 3 minutes). The current was then turned off, the cell was allowed to equilibrate under stirring for 1 min, then the open circuit potential was measured after stirring was stopped.

3.5.4 Batteries

Single cell batteries could readily be analyzed at various cycle

numbers and temperatures in the range from 10 to 85°C in a two electrode configuration shown in fig. 3.1. For long term charge-discharge cycling a home-made galvanostat allowed application of a manually adjusted charge and discharge current and for choice of upper and lower potentials between charge and discharge. The potential versus time curves were recorded on a strip chart recorder. Typical charge-discharge current densities ranged from 1.0 to 0.1 mA/cm^2, where the rate of charge was usually set to be one-half that for discharge. The voltage windows used varied, but a typical range was 3.5 to 3.0 V.

Periodically, impedance spectroscopy at various states of charge and discharge and at different temperatures was done during cycling. The cycle was interupted for a only a short time while a spectrum was collected. After a cell had lost capacity the components were then either examined using SEM or Auger spectroscopy. Chemical analyses on the cathodes were also done to check the amounts of lithium inserted and the capacity of the cathode material used.

Fig. 3.1 Schematic diagram of the single-cell lithium battery in a sealed glass container under argon atmosphere.

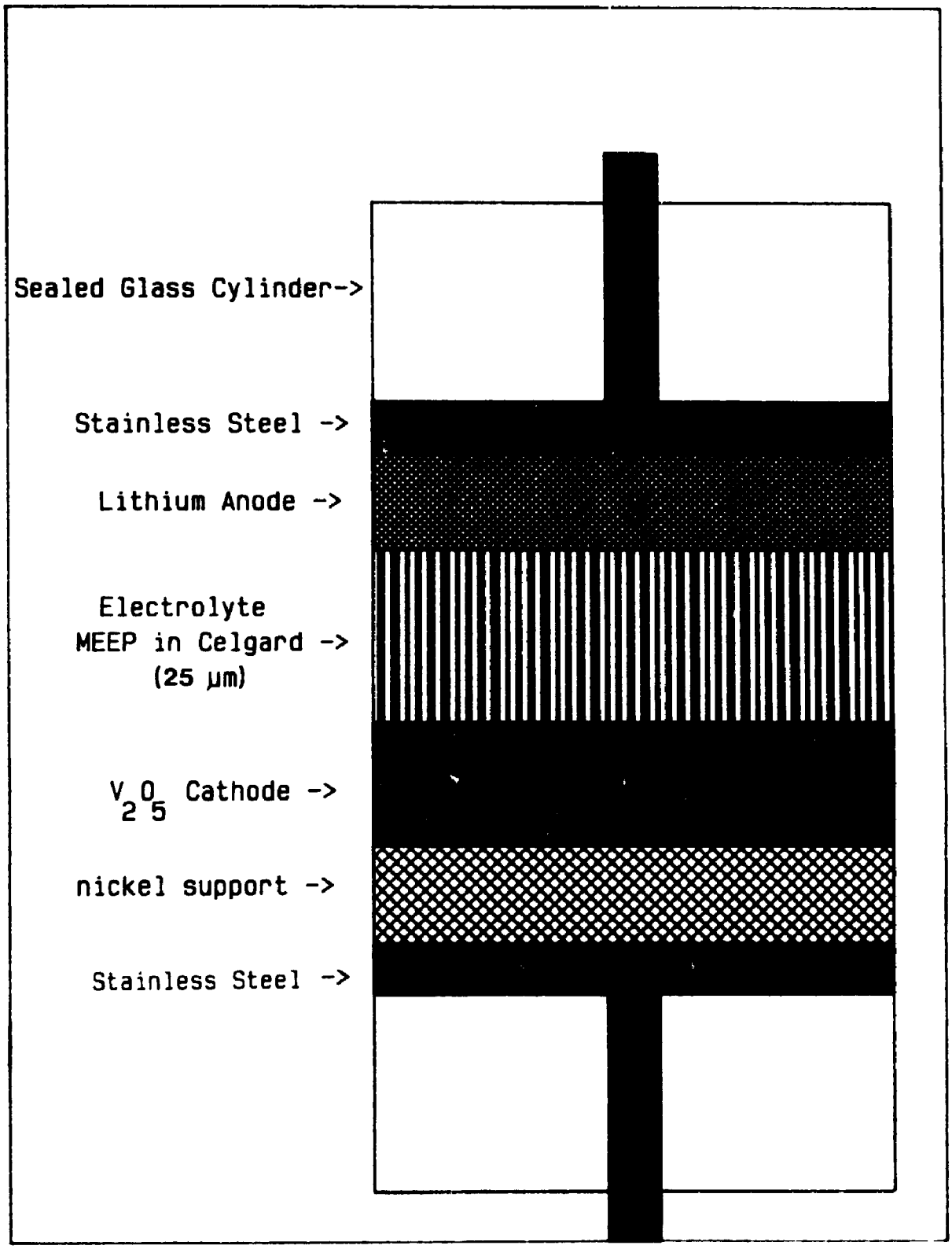
Sealed Glass Cylinder->
Stainless Steel ->
Lithium Anode ->
Electrolyte
MEEP in Celgard ->
(25 μm)
V_2O_5 Cathode ->
nickel support ->
Stainless Steel ->

CHAPTER 4

RESULTS ON THE ANODIC DEPOSITION OF VANADATES

4.1 Introduction

As mentioned in chapter one, most of the previous work on electrodeposition of vanadium oxides was done by A.S. Goncharenko and co-workers in the late 60's. However, their deposits were highly hydrated and non-stoichiometric [19]. Anodic deposits of potassium hexavanadate monohydrate were formed by Goncharenko [20] but are of no practical use for cathode materials. Ptitsyn *et al* [22] did report making V_2O_5 films on a steel substrate, and that lithium could be inserted into these films. However, the nature, mechanism of formation and detailed electrode performance of the films were not examined, leaving many questions about their use as practical electrodes. The experiments described in this chapter allowed for careful control of the conditions of deposition, which enabled determination of the mechanism of formation and the exact nature of the deposit. The mechanism of formation and the insertion of alkali cations and protons into this electrode will also be discussed.

4.2 Results

The success of the electrochemical preparation of thick, uniform deposits of vanadium oxide depends on observing certain experimental conditions. Analysis of these deposits could then be made routinely by methods discussed in chapter 3.

4.2.1 Formation of Deposits

All deposits for analysis and for insertion experiments were prepared under galvanostatic conditions with a current density between 0.1 and 1 mA/cm². Current densities of about 10 mA/cm² caused oxygen evolution on the electrode at a rate sufficiently vigorous to impede uniform deposit formation of the oxide. Deposits can be formed at current densities of 0.1 mA/cm², but the time taken becomes greater than 24 h. The temperature of the electrolyte was also found to be important for good deposit formation, largely because of the increased solubility of NH_4VO_3: about 0.05 mol/L at 25°C and 0.11 mol/L at 40°C and 0.26 mol/L at 70°C [7]. Best results were obtained for electrolyte temperatures in the range of 40-60°C.

Under these conditions, a bright orange-red deposit forms on the SnO_2 glass anode over a period of several hours. The deposit starts at the top of the electrode and spreads downwards. After some time, there is evidence of nucleation and growth over the entire electrode. Eventually the entire surface becomes covered with a thick crystalline deposit. The deposit tends to be slightly thicker at the top. The same type of deposit was also found to form under potentiostatic conditions; a potential in the range of +2.0 to +3.0 V (SCE) gave the best results. The uniformity of the deposit appears to be a result of its conductivity, which is lower than that of the substrate, and to gradients of pH due to convection along the surface of the electrode. As the first deposit forms, the pH is highest at the top of the electrode, and the current density decreases over the area of the deposit, and increases over the remaining area of the electrode. The increase in current density causes a slow rise in potential under galvanostatic conditions (fig. 4.1). On shorter electrodes, the

deposits tend to be more uniform than on SnO_2 glass, probably because the pH gradients are smaller.

These deposits have also been formed on numerous other conducting substrates, including stainless steel, platinum, nickel, glassy carbon, graphite, and woven carbon cloth.

4.2.2 Nature of Deposits

The deposits formed on the SnO_2-coated glass were typically grown to a thickness of 100 μm and a density of about 10 mg/cm^2 of SnO_2 surface. The rate of deposition was about 0.5 mg/C at 1 mA/cm^2. At the anode, not all the vanadium oxide deposits on the electrode; most remains in the aqueous solution. Chemical analysis confirms that the fresh deposit corresponds closely to diammonium hexavanadate monohydrate, $(NH_4)_2V_6O_{16}\cdot H_2O$, or, equivalently, $2NH_3\cdot 3V_2O_5\cdot 2H_2O$ where the calculated values for NH_3, V, H_2O are: 5.53, 49.64, 5.85 mass %; found, 5.64±0.10, 49.59±0.28, 5.78±0.21 mass % with ranges of ±1 standard deviation. The mole ratio $y = (NH_3+H_2O)/V_2O_5$ is a function of the conditions of drying the deposit as seen in table 4.1. For example, for $(NH_4)_2V_6O_{16}\cdot H_2O$, $y = 4/3$. After heating the deposit at 105°C for 24 h to remove any surface water, chemical analysis gives $y \approx 1.3$. Thus, under these conditions it was possible that the ammonium-containing analogue of the K-containing species of Goncharenko [20] had been made. An SEM photograph of the fresh deposit, plate 1(a) and 1(b), shows highly oriented crystals of uniform size (about 50 x 5 μm) and shape.

The X-ray powder diffraction pattern for $(NH_4)_2V_6O_{16}\cdot H_2O$, where y is approximately 1.3, is shown in fig. 4.2(a). It shows clearly that the fresh deposit is crystalline with no amorphous component. The

pattern could not be matched exactly with any known pattern in the ASTM index that describe a hydrated V_2O_5 system [46]. The closest match is the ASTM pattern for $V_2O_5 \cdot H_2O$ [46,47]; except for a very prominent peak at 0.786 nm, $\theta = 5.6^{\circ}$, most other peaks seem to be consistent with this structure. This was because of the improper assignment of this pattern by the authors [47] to a hydrated oxide rather than to one containing at least some NH_4^+ ion. The fact that there really is no true crystalline monohydrated phase of V_2O_5 has been pointed out by Levanto [25].

The same pattern, with only minor shifts in the cell dimensions, is obtained when the deposit is heated at 200-250°C for several hours (table 4.2 and table 4.3). Water is completly removed to yield pure $(NH_4)_2V_6O_{16}$ (see DTA results, chapter 6, section 6.2.1.1). As seen in table 4.2 the match to the work of Kelmers [48] and Levanto [25] is extremely good. There were only slight differences in the major peaks of the electrodeposited $(NH_4)_2V_6O_{16} \cdot H_2O$ (fig. 2b), and the values for $(NH_4)_2V_3O_8$ given by Levanto, as seen in fig. 4.2. The cell dimensions are summarized in table 4.3 for the hydrated and dehydrated diammonium hexavanadate for comparison with values reported by Kelmers and the recalculation of the cell dimensions from the d-spacings reported by Levanto. The assignment by Levanto [25] of the 0.8656 nm peak as [*010*] is incorrect. Its presence may be due to impurities present in the sample, since it could not be identified with any reasonable *hkl* value for the hexavanadate structure. Values of our cell dimensions are within one standard deviation of those reported by Kelmers [48].

The differences in X-ray peak intensities, figure 4.2, for electrodeposited diammonium hexavanadate compared to Levanto's [25] results are believed to be caused by the high orientation of the

crystals of our electrodeposit grown on the substrate. Plate 1(a) shows the general regular crystal form of the freshly deposited $(NH_4)_2V_6O_{16}$ hydrate on SnO_2 glass. Plate 1(b), at higher magnification, shows the uniform size, shape and orientation of the crystals, which are about 50 μm wide and 5 μm thick. It is believed that the large flat surface is the (*100*) plane. Thus the relative intensity of a peak such as [*010*] compared to the [*100*] could be reduced, compared to that expected from a true powder pattern, to the point where it became indistinguishable from the background of the spectrum. This, in general, causes our intensities to differ from those in Levanto's spectrum, which is a true powder pattern. This phenomenon will be seen again later in discussions of other electrochemical deposits in chapters 5 and 6.

4.2.3 Mechanism of Formation

Changes in pH accompany the formation of deposits. Using a two compartment cell, with saturated aqueous NH_4VO_3, pH 6.5, at 50°C in both compartments, a constant current of density 10 mA/cm^2 was passed. The pH in the anode compartment dropped significantly to the range 2 to 3, while the pH in the cathode compartment increased to about 9. This phenomenon was also reported by Goncharenko [49], who observed a decrease in pH in the anodic compartment and an increase in the cathodic compartment of a two-compartment cell during the formation of anodic deposits of potassium hexavanadate. In galvanostatic experiments deposition did not begin until the potential increased to the point at which the oxygen evolution reaction had commenced. This can be seen in a galvanostatic potential-time plot, fig. 4.1.

These observations suggest the following mechanism. When a

constant current is applied, the potential of O_2 evolution is reached quickly, and the pH decreases at the anode because of the formation of protons by the oxygen evolution reaction:

$$H_2O = 1/2\ O_2 + 2H^+ + 2e^-$$

The decreased pH results in the formation of a fresh V_2O_5 sol, some of which deposits immediately on the SnO_2 anode. Because there is no oxidation of vanadium, the sol must be deposited on the anode by electrophoresis. The sol particles are oriented in the electric field with their long axes parallel to the field. Thus the deposited crystals are strongly oriented in a direction perpendicular to the surface of the electrode, but are randomly oriented in a direction parallel to the electrode.

Support for this mechanism is found from the predominance diagram for ionic species in vanadium (V) solutions [50]. The starting pH of the ammonium vanadate solution is close to 7, where the predominant species for the stoichiometric concentrations of vanadium of interest are the polynuclear anions $V_4O_{12}^{4-}$ and $V_3O_9^{3-}$. As the pH decreases near the electrode, the species in solution are, progressively, $V_{10}O_{28}^{6-}$ and $V_{10}O_{27}(OH)_2^{4-}$, until at about pH 3 the solubility curve for V_2O_5 is reached. Our observations show that the actual solid formed on the electrode is not V_2O_5, however, but a hydrated ammonium vanadate whose anion may form by protonation of the hydrated polyanion $V_{10}O_{27}(OH)_2^{6-}$:

$$3V_{10}O_{27}(OH)_2^{6-} + 8H^+ = 5\ V_6O_{16}^{2-} + 7\ H_2O,$$

where the formula of the anion has been written as a possibly more probable hexavanadate. It is assumed that the sol particles contain the

charged polyanion $V_6O_{16}^{2-}$ and mobile ammonium counterions, and are related to sols produced from ammonium-free solutions. It is known that acidification of hypovanadate solutions by passage through a cation exchange column in the H^+ form produces a hydrated V_2O_5 sol [51]. We have found that sols prepared in this way show strong streaming birefringence, indicating that the sol particles can be oriented easily in a hydrodynamic field. Orientation of V_2O_5 sols in both hydrodynamic and electric fields has been known since 1916 (see [52]). Attempts at direct observation of birefringence of the sol near the anode during deposition proved to be technically difficult and inconclusive; however, we believe that orientation in the electric field during electrophoretic deposition is the cause of the high degree of orientation of the crystalline deposits.

4.2.4 Insertion Into Deposits: Ion Selectivity

Insertion of various alkali metal ions was attempted on electrodes formed using electrodeposits on SnO_2 substrates with no special drying other than above 100°C to remove surface water. Lithium ions, presumably unhydrated, inserted into the deposit in aqueous and non-aqueous solutions of propylene carbonate and dimethylforamide to give a lithium vanadium bronze. This cathodic reaction is given by :

$$xLi^+ + xe^- + (NH_4)_2V_6O_{16} = Li_x(NH_4)_2V_6O_{16}$$

The charge injected was measured by passing a measured constant current for a known time. A typical galvanostatic insertion curve is shown in fig. 4.3. The final value of x always corresponded to a point on the final plateau of the charging curve which continues for long times. Random drifting up and down in potential usually occurred after

this plateau had been reached, which indicated an end to the insertion of lithium. The bronze was analyzed for lithium by atomic absorption and for V(IV) by chemical analysis (See chap. 6, table 6.4). From the amount of charge passed, it was possible to plot a potential against x curve for the charging process, as shown in fig. 4.3. Chemical analysis of the amount of V(IV) (shown by arrow on curve) confirmed the value of charge passed to within 1 %.

The presence of ammonia and water between the crystal layers in the deposit has a definite influence on the amount of alkali cation that can be inserted into the structure. The maximum value of x in $Li_x(NH_4)_2V_6O_{16}$ was about 1.44 (i.e. ratio of Li/V = 0.24). Insertion of H^+ occurred in 0.1 mol/L aqueous $HClO_4$ solutions, with maximum values of x = 1.50 (Li/V = 0.25) for these deposits. However, the electrode was affected by the dissolution of the diammonium hexavanadate in this solution; in fact, acid solutions are used to dissolve hexavanadates for chemical analysis. Using a non-aqueous electrolyte with small concentrations of $HClO_4$ the value increases to a maximum of x = 3.0 (H/V = 0.5). X-ray diffraction patterns for the H^+ bronzes showed little or no change in crystal structure. However, as discussed in more detail for the decomposed deposits of V_2O_5 in Chapter 7, the line corresponding to the (*100*) plane shifts, showing a linear expansion perpendicular to the (*100*) with the amount of Li inserted: 0.7830 nm for the diammonium hexavanadate (x = 0) to 0.7893 at x = 0.50 and 0.7930 nm at x = 0.79. Two phase changes occur when Li was inserted into a hexavanadate electrode; see fig. 4.3. The two phases are centered at about x = 0.15 and 0.45 and correspond to similar phase changes seen for lithium insertion into V_2O_5 (see chapter 7, sec. 7.2). However, because of the

presence of ammonia and water between the crystal layers of the deposit, the phase changes in the Li bronze, $Li_x(NH_4)_2V_6O_{16}$, occurred at much smaller values of x than for the Li bronze, $Li_xV_2O_5$.

The electrochromic behaviour of these deposits was quite apparent. Starting from the orange-red deposit, insertion of Li^+ or H^+ causes a gradual colour change from light to dark green to almost black as the limit to insertion is approached. This was also found to be a reversible process: starting with a greenish bronze, removal of Li^+ and electrons leaves an electrode with the same bright orange-red colour. As the amount of inserted Li increases in the electrodeposit, there is a corresponding reduction of V(V) to V(IV), as expected for the reaction given above. Lithium, therefore, can be inserted into this deposit with a minor change in structure (expansion of inter-layer lattice spacing perpendicular to the [*100*] direction). However, only about half as much lithium can be inserted compared to other vanadium oxide electrodes such as vanadium pentoxide (V_2O_5), and the reversibility of such an electrode for secondary battery purposes is limited to much smaller values of Li/V, with the complete removal of lithium w. ' /steresis for $x \leqslant 0.15$. On comparing the insertion of lithium into the undecomposed hexavanadate (figure 4.3) and into vanadium pentoxide (figure 5.6), it was noted that the potential of the hexavanadate was seen to drop quite rapidly, while the pure V_2O_5 had definite "flat" portions in its insertion curve (seen later, section 6.2.3).

Potassium and sodium ions could not be inserted in detectable amounts into these electrodes in non-aqueous solutions, probably because of their larger diameters. This was confirmed by the X-ray diffraction patterns, where no change in structure from the original pattern was

observed. Actually, an electrode of this type was found to be a good check for the presence of any trace water present in the non-aqueous solutions containing the K^+ or Na^+ salts. Hydrogen would effectively insert into the electrode until a large voltage drop (> 1V) to a new plateau indicated that the traces of water had all been used to form the hydrogen bronze, $H_x(NH_4)_2V_6O_{16}$. From the charge used an estimate of the amount of water present could be made. However, for our purposes the amount was so small as to be virtually undetectable when proper drying procedures were later employed for non-aqueous electrolytes.

4.2.5 Mechanism of Insertion and Removal

By the direct deposition of the hexavanadate on to a glassy carbon rotating disk electrode (RDE), potential sweep experiments were done on the initial insertion of lithium to form a lithium hexavanadate bronze at various rotation speeds. By use of a supporting electrolyte of $NaClO_4$ with smaller concentration of $LiClO_4$ (ionic strength of solution 0.525 mol/dm^3) the transport number of the lithium was made negligible ($t_{Li^+} = 0.016$) to eliminate migration effects. The transport number was determined from the equation;

$$t_{Li^+} = c_{Li}\,\lambda_{Li} \,/\, (c_{Li}\,\lambda_{Li} + c_{ClO_4}\,\lambda_{ClO_4})$$

where the ionic strength of the solution was 0.53 mol/dm^3 and λ_i is the limiting molar conductivity of ion i.

By determining the mass transport-limited currents at the RDE it is possible to calculate the diffusion coefficient in solution. Once a recording of the current during a potential sweep is made at various rotation speeds a plot of the limiting current at a fixed potential in the sweep vs. $\omega^{1/2}$ was made. This plot should be linear and the

intercept is equal to the charging current which passes in to the electrode due to the potential scan (see table 4.4 and figure 4.4). The charging current is independent of rotation speed and the slope of the plot I_L vs. $\omega^{1/2}$ should be independent of the scan rate. The diffusion coefficient of the electroactive species can be calcuated from the slope of the plot I_L vs. $\omega^{1/2}$ which is given by:

$$dI_L / d\omega^{1/2} = 0.62\ nFAD^{2/3}\ \nu^{-1/6}\ C^b \qquad (4.1)$$

where $A = \pi R^2$ and the kinematic viscosity, ν, depends on the bulk solution. From the equation, the overall diffusion coefficient could be estimated and was found to be 2.5×10^{-6} cm^2/s. This value of D is rather qualitative but is of the correct order of magnitude for diffusion in solution: the Nernst-Einstein value for Li^+ in aqueous solution at 25°C is $D = 1.26 \times 10^{-5}$ cm^2 s^{-1} [53].

The charge transfer current in an electrode is described by the Butler-Volmer equation:

$$I = I_0 [\exp(\alpha_a nF\eta/RT) - \exp(-\alpha_c nF\eta/RT)] \qquad (4.2)$$

where α_a and α_c are constants between 0 and 1 called transfer coefficients for the anodic and cathodic reactions respectively ($\alpha_a + \alpha_c = 1$). The overpotential, η, is defined as the deviation of the potential from its equilibrium value. This equation is the basis from which a theoretical description of an electrode process can be made. A Tafel equation can be derived from equation (4.2) for high negative overpotentials. This equation for a cathodic current density is given by:

$$\ln(I) = \ln(I_o) - \alpha nF\eta/RT \qquad (4.3)$$

A plot of the inverse of the limiting current at various potentials against the inverse square root of the rotation speed is shown in figure 4.4 and the values of the slope and intercept at the various potentials are summarized in table 4.4. As can be seen in figure 4.4 the first and second rotation speeds of 400 and 900 rpm give erratic results as well as the last point at the highest rotation speed for reasons discussed later. Thus, these points where not used in the calculation of the slope for figure 4.4. The transfer coefficient, α, may be found by equating the slope of a plot of over-potential against $\ln(I)$ to $RT/\alpha F$, which yields a value of 0.07, assuming a one-electron change. The value of I_o obtained from the intercept of this plot was 1.25 mA/cm^2. The standard rate constant, k^0 , was then obtained by using the equation;

$$k^0 = I_o / nF\,(c_O^{\sigma})^{\alpha}a\,(c_R^{\sigma})^{\alpha}c \qquad (4.4)$$

and was found to be 1.0×10^{-5} cm s^{-1}. Under steady state conditions, electron transfer processes with a rate constant less than 5×10^{-3} cm s^{-1} are irreversible because the rate of electron transfer is not fast enough to maintain Nernstian equilibrium at the electrode surface. This appears to be the case for our electrode system. The value for the rate constant for the reduction of the V(V) to V(IV) in the hexavanadate appears to be quite reasonable and has a value close to that for electron tranfer in other systems such as for the oxidation of species $V(H_2O)_6^{3+}$ and $Cr(H_2O)_6^{3+}$ which have rate constants of 4×10^{-3} and 1.4×10^{-5} cm s^{-1}, respectively [54]. Thus, for our irreversible system the electrode kinetics are slow compared to diffusion.

There are a few problems in performing RDE experiments by direct deposition of the hexavanadate on a glassy carbon electrode. These include frequent and sometimes severe flaking of the electrodeposit from the substrate during the experiment. Also, the hexavanadate will always flake off the electrode when the rotation speed reaches a value above 4900 rpm. No solution to these problems could be found. However, careful deposition of the hexavanadate to only a minimal thickness (20-30 μm) helped substantially. Unfortunately, there is a limit to how thin a deposit could be made without "bare spots" being visible on the glassy carbon substrate. Another problem is the large surface roughness of the hexavanadate electrode, as evident in the SEM photos, which may have an influence on the kinetic measurements. This is because the RDE technique employs convective diffusion, and surface roughness may influence the hydrodynamics at the RDE. Since the kinetic parameters calculated are about what would be expected for this system (within an order of magnitude), this effect was probably less important than was originally thought, but does have some influence on the results as will be discussed for similar experiments with cathodic deposits (chapter 5).

The study of the initial insertion of lithium or protons, followed by their removal from this diammonium hexavanadate will be discussed in chapter 7 because of the very similar behaviour of the potential step insertion and removal curves to those of the decomposed pure V_2O_5 electrodes (chapter 6).

4.3 Conclusions

Thick, uniform, crystalline, highly oriented deposits of hydrated V_2O_5 can be formed readily on SnO_2-coated glass anodes or any other suitable conducting metal substrate such as Pt, from saturated aqueous NH_4VO_3 at 40 - 60°C using a constant current density of 0.1 - 1 mA/cm^2. The mechanism of formation involves a decrease in pH at the anode accompanying evolution of oxygen, which causes formation of a V_2O_5 sol. The microcrystalline sol particles then orient in the electric field and deposit on the anode by electrophoresis. A uniform crystalline deposit of stoichiometric diammonium hexavanadate monohydrate is formed under these conditions. The water of hydration was removed by mild heating for several hours at 200°C.

Insertion of H^+ and Li^+ into these deposits gives a dark green bronze, with maximum values of 0.24 for Li/V and 0.5 for H/V. The removal of these two ions regenerates the orange-red colour of the original electrodeposit. Anodes made from this material are of limited use because of the low reversible capacity of lithium (Li/V) in the hexavanadate, caused by the presence of ammonia and water in the inter-layer spacings of the vanadium-oxygen lattice.

Plate 1(a) SEM photo of hydrated ammonium hexavanadate on SnO_2 coated glass; X300, bar length 33 μm.

1(b) SEM photo of hydrated ammonium hexavanadate on SnO_2 coated glass; X1210, bar length 8.3 μm.


2KX

Table 4.1 Chemical analysis of anodic electodeposits made using current density of 1mA/cm², from aqueous NH_4VO_3, 0.2 mol/L.

temp. of heating /°C (time of heating/h)	mass % NH_4^+ ± 0.10	mass % V ± 0.28	mass % H_2O ± 0.21	$y = (NH_3+H_2O)/V_2O_5$	formula of deposit from chemic l analysis
air dry (1)	5.85	49.34	3.52	1.40	$(NH_4)_2V_6O_{16}\cdot 1.2H_2O$
105 (24)	5.91	49.59	2.89	1.33	$(NH_4)_2V_6O_{16}\cdot H_2O$
R.T. vacuur (3)	5.90	50.84	1.50	1.17	$(NH_4)_2V_6O_{16}\cdot 0.5H_2O$
200 (24)	5.88	50.89	0.0	0.98	$(NH_4)_{1.95}V_6O_{16}$
350 (3)	0.0	56.15	0.0	0.00	V_2O_5*

* See discussion in chapter 6.

Table 4.2 X-ray diffraction of anodic electrodeposit of composition $(NH_4)_2V_6O_{16}$ (heated at 250°C to remove H_2O), in comparison to Kelmers [48] and Levanto [25].

hkl	this work			Kelmers [48][a]		Levanto [25]		
	rel. intensity	d/nm obs.	calc.	rel. intensity	d /nm calc.	rel. intensity	d /nm obs.	calc.[b]
010						20	0.8656	0.8090[c]
100	100	0.7830	0.7822	vs	0.784	90	0.7830	0.7858
110	39	0.5756	0.5732	s	0.575	51	0.5735	0.5637
001	7	0.4965	0.4974	w	0.498	3	0.4983	0.4960
101						2	0.4439	0.4390
020				w	0.421			
200	19	0.3912	0.3911	m	0.391	90	0.3910	0.3929
210	65	0.3546	0.3547	s	0.355	90	0.3551	0.3534
201	23	0.3256	0.3259	m	0.326	12	0.3255	0.3235
021	42	0.3213	0.3214	m	0.321	11	0.3215	0.3135
211	6	0.3037	0.3040	w	0.304	4	0.3039	0.3004
-201	12	0.2913	0.2918	m	0.292	11	0.2915	0.2945
-121	27	0.2898	0.2899	m	0.290			
220	21	0.2865	0.2866	m	0.287	19	0.2870	0.2818
-211	4	0.2757	0.2757					
130	6	0.2642	0.2643			2	0.2652	0.2551
300	6	0.2577	0.2607			12	0.2604	0.2619
002	6	0.2483	0.2487	w	0.249	7	0.2488	0.2480
102	5	0.2443	0.2452			1	0.2454	0.2433
301	3	0.2419	0.2425			3	0.2426	0.2414
-221	8	0.2396	0.2398	w	0.240	3	0.2409	0.2381
112	3	0.2368	0.2354			2	0.2352	0.2330
311	4	0.2324	0.2331			4	0.2326	0.2313
-102	4	0.2276	0.2296					
-112	24	0.2208	0.2215			15	0.2213	0.2214
-311	6	0.2139	0.2136					
-231	23	0.2023	0.2023			10	0.2025	0.1989
400	7	0.1954	0.1956			10	0.1957	0.1965
330	8	0.1906	0.1911			4	0.1913	0.1879
401	6	0.1891	0.1895			8	0.1892	0.1890
132	6	0.1845	0.1847			7	0.1845	0.1807
-222	5	0.1803	0.1806	w	0.180			
-401	12	0.1771	0.1753			8	0.1753	0.1769
421	3	0.1737	0.1728					
-411	3	0.1709	0.1717			5	0.1717	0.1728
402	3	0.1625	0.1630					
412	8	0.1602	0.1600			12	0.1604	0.1586
213	3	0.1564	0.1565			10	0.1564	0.1550
123	5	0.1551	0.1545			8	0.1542	0.1528
023						6	0.1538	0.1531

cont'd next page

Table 4.2 (cont'd)

hkl	this work		Kelmers [48][a]		Levanto [25]		
	rel intensity	d/nm obs.	calc.	rel. intensity	d /nm calc.	rel. intensity	d /nm obs. calc.[b]
-203						11	0.1465 0.1474
233						5	0.1296 0.1363
004						11	0.1245 0.1240
204						8	0.1227 0.1217

[a] Composition of salt: $(NH_4)_2V_6O_{16}$, only major lines were given.
[b] Re-indexed by us to estimate cell dimensions of Levanto's crystalline diammonium hexavanadate [25].
[c] Incorrectly indexed, probably impurity.

Table 4.3 Unit cell dimensions for monoclinic $(NH_4)_2V_6O_{16}$

	a/nm	b/nm	c/nm	β	X-ray sample
$(NH_4)_2V_6O_{16}\cdot H_2O$					
	0.7883	0.8317	0.5037	84.029°	polycrystalline electrodeposit
	± 0.0034	± 0.0074	± 0.0027	± 0.357	
$(NH_4)_2V_6O_{16}$					
this work[a]	0.7873	0.8424	0.5006	83.483°	polycrystalline electrodeposit
	± 0.0011	±0.0026	± 0.0008	± 0.094	
Kelmers[b] [48]	0.787	0.843	0.497	96.75°	precipitate
Levanto[c]	0.7895	0.8090	0.4983	84.171°	precipitate
[25]	± 0.0071	± 0.0140	± 0.0026	± 0.541	

[a] Indexed after heating at 250°C to remove water.
Error limits are ±1 std. dev in each of these cases.
[b] Levanto [25] used the same cell dimensions as Kelmers for calculation of d-spacings.
[c] Re-indexed by us to estimate cell dimensions of Levanto's crystalline diammonium hexavanadate [25].

Table 4.4 Summary of the insertion of lithium into diammonium hexavanadate on a glassy carbon rotating disk electrode.

Potential /V	Slope /$mA^{-1}min^{1/2}$ ± 4.2	Intercept /mA^{-1} ± 0.20	ln(I/mA)
-0.050	11.3	6.066	-1.803
-0.100	76.5	3.171	-1.154
-0.150	109.7	1.941	-0.663
-0.200	109.6	1.766	-0.569
-0.250	118.3	1.318	-0.276
-0.300	108.9	1.100	-0.095
-0.350	105.1	0.957	0 044
-0.400	103.1	0.962	0.039
-0.450	100.2	0.884	0.124
-0.500	101.2	0.756	0.280

Fig. 4.1 Potential-time plot during galvanostatic anodic deposition of diammonium hexavanadate on SnO_2 glass; current density 0.6 mA/cm^2.

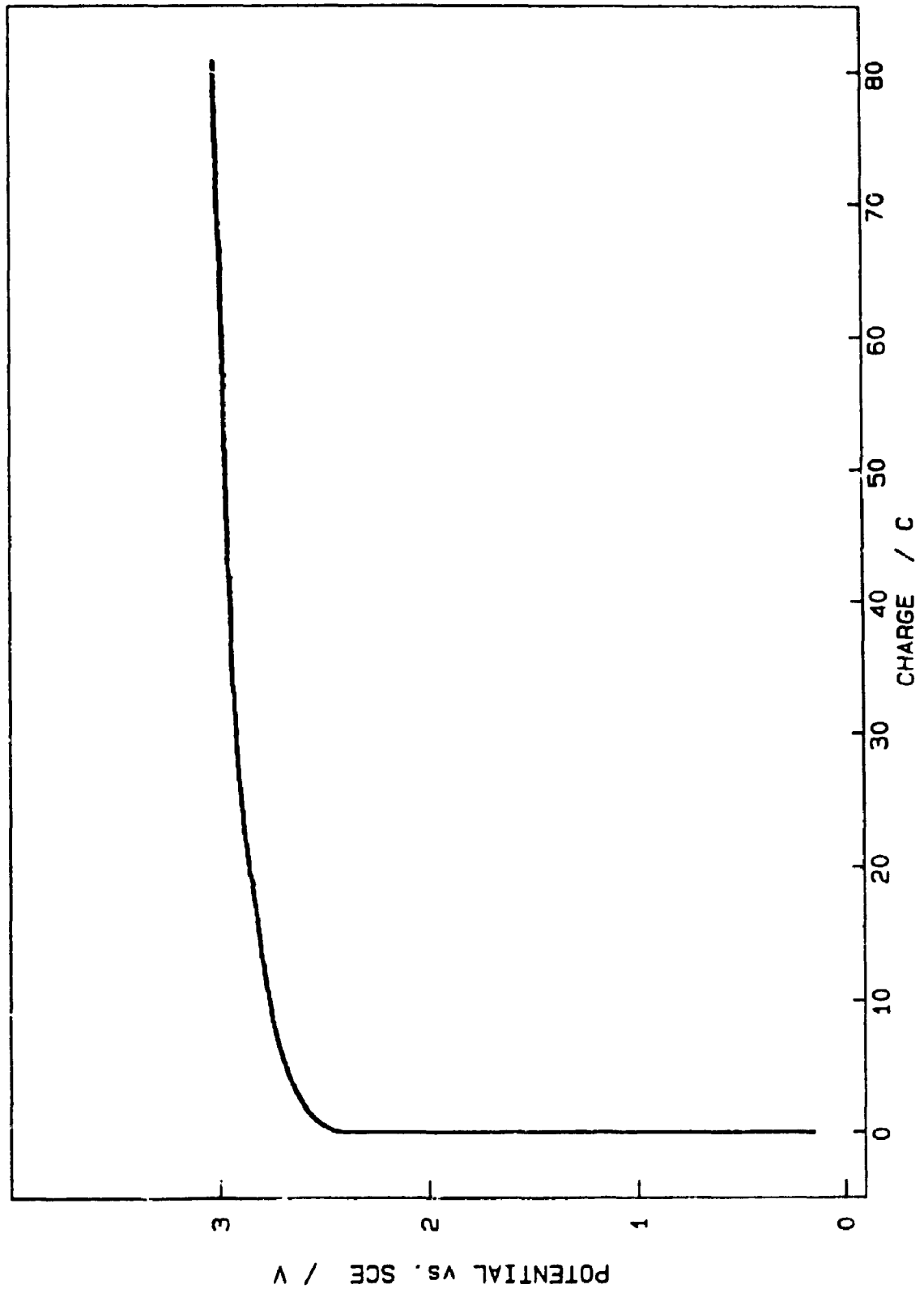
POTENTIAL vs. SCE / V
0
1
2
3
CHARGE / C
0
10
20
30
40
50
60
70
80

Fig. 4.2(a) X-ray diffraction of hydrated diammonium hexavanadate deposit.

Fig. 4.2(b) X-ray diffraction stick diagram of diammonium heaxavanadate, after Levanto [25].

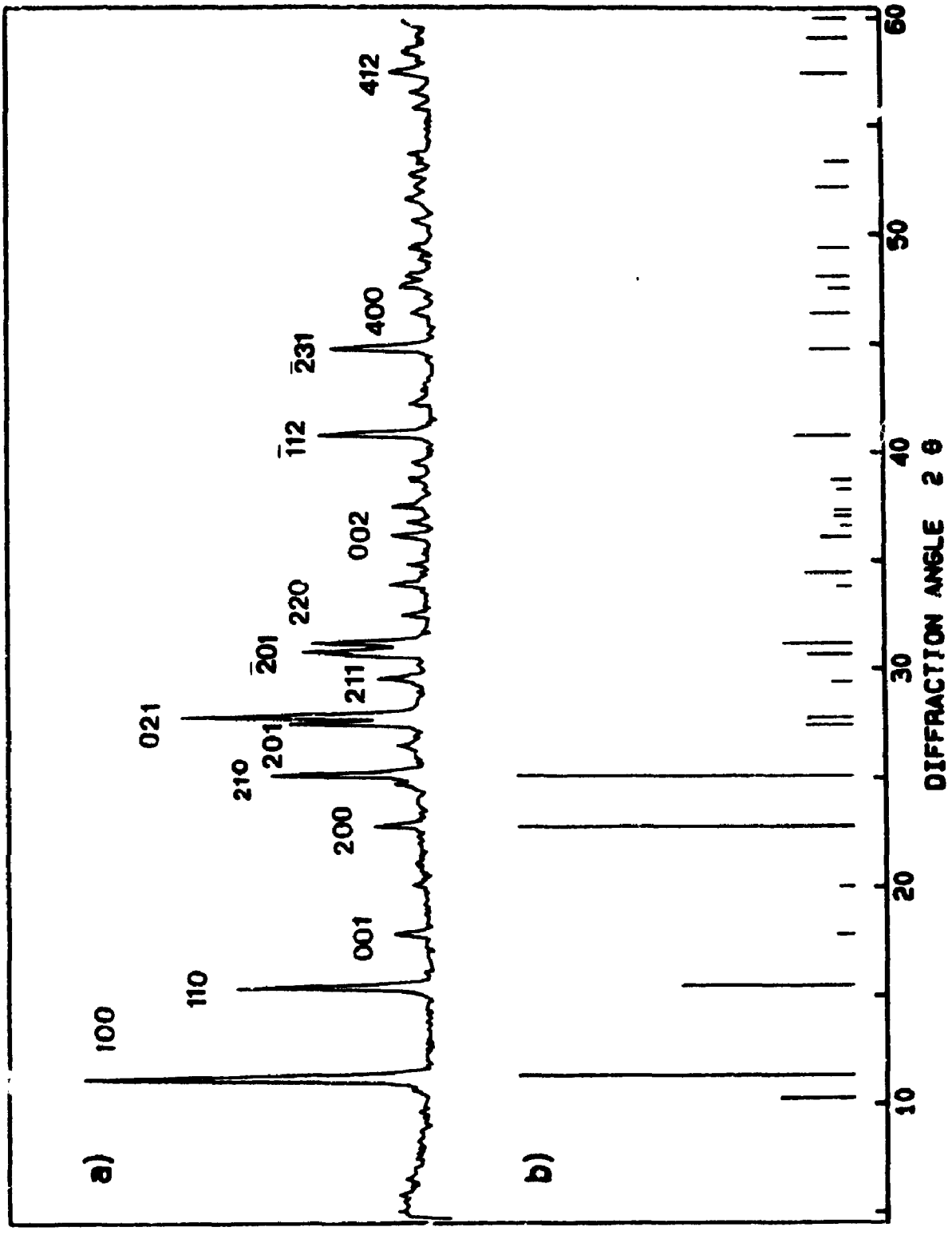
a)
b)
100
110
001
200
210
201
021
$\bar{2}01$
211
220
002
$\bar{1}12$
$\bar{2}31$
400
412
10
20
30
40
50
60
DIFFRACTION ANGLE 2 θ
INTENSITY

Fig. 4.3 Potential as a function of lithium inserted into hydrated diammonium hexavanadate on SnO_2 glass from 0.1*M* $LiClO_4$ in propylene carbonate; current density 0.8 mA/cm².

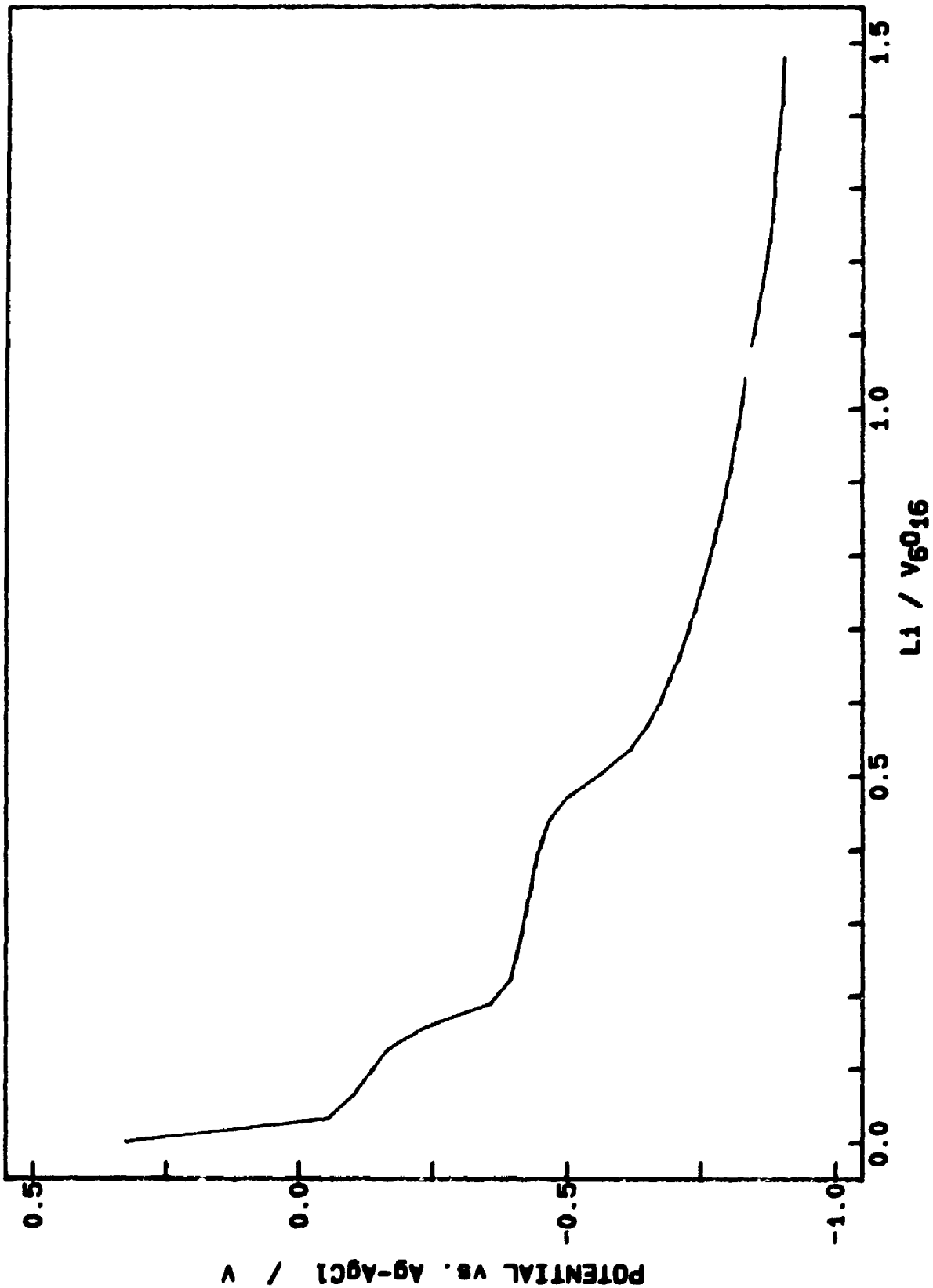
POTENTIAL vs. Ag-AgCl / V
0.5
0.0
-0.5
-1.0
0.0
0.5
1.0
1.5
Li / V6O16

Fig. 4.4 Inverse of limiting current I_l against the inverse square root of the rotation speed, $\omega^{-1/2}$, for a solution of $NaClO_4$ + $LiClO_4$ (t_{Li^+} = 0.01).

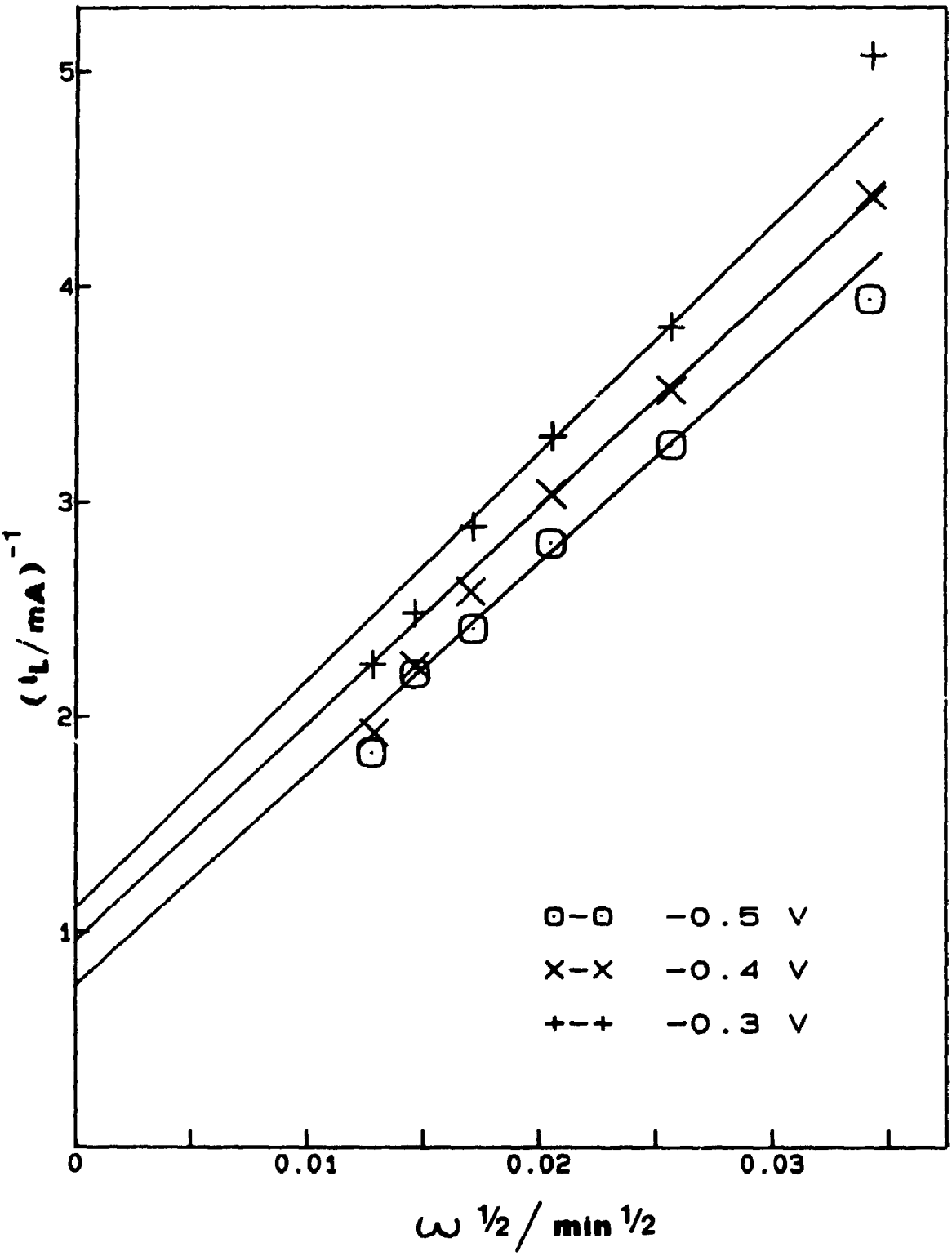
5
4
3
2
1
$(i_L/mA)^{-1}$
0
0.01
0.02
0.03
$\omega^{1/2}$ / $min^{1/2}$
⊙–⊙ −0.5 V
X–X −0.4 V
+–+ −0.3 V

CHAPTER 5

RESULTS OF THE CATHODIC ELECTRODEPOSITION OF VANADATES

5.1 Introduction

The formation of a stoichiometric anodic deposit from aqueous vanadate solutions suggested that careful experimental control could yield useful electrode materials. During the formation of an anodic deposit, it was observed that over a long period of time a black cathodic deposit formed. Goncharenko [19,21] made the original observation, and studies on these deposits using potassium vanadate solutions yielded a non-stoichiometric oxide with approximate composition $3K_2O \cdot 2VO_2 \cdot 5V_2O_5 \cdot 15H_2O$. However, a careful study of the nature of this material was not done.

In this chapter, a detailed study of the electrochemical formation of new stoichiometric phases as well as numerous mixed phases will be given, including a suggested mechanism of formation. The potential of these materials as insertion electrodes will also be discussed.

5.2 Results

The formation of the cathodic deposits used a number of electrochemical techniques. The analysis of these deposits follows the same general method employed in chapter 4 for the anodic deposits. However, A.A. analysis for Li was not done since it had been established that the amount of reduced V(IV) was equal, within experimental error, to the amount of Li inserted (see table 6.4). Included in this chapter, however, are results from using other techniques, including gravimetric

and EDAX analysis to help determine the stoichiometry of the deposit and to identify any alkali cations such as K, Rb, and Cs present in the cathodic electrodeposit.

5.2.1 Formation of Deposits

As with anodic deposition certain important experimental conditions must be observed if formation of a cathodic deposit is to occur. For reasons given in chapter 4, temperatures in the range of 40-60°C again gave the best results for the various vanadate solutions. Cathodic deposits were formed on a conducting substrate by galvanostatic or potentiostatic electrolysis, or by cyclic voltammetry in a saturated NH_4VO_3 solution at 40°C. For galvanostatic deposition, a current density of 0.1 - 1 mA/cm² caused formation of an anodic deposit during the early part of the experiment, as mentioned in chapter 4. A uniformly thick, black deposit on the Pt cathode then formed over longer times (24 h). Similar deposits were formed using constant potentials of -0.5 to -2.0 V vs. SCE. It was found that much higher current densities or potentials resulted in such vigorous evolution of hydrogen that formation of deposits was hindered. Deposits have been made on various conducting substrates including platinum, nickel, stainless steel and carbon cloth.

Cyclic voltammetry (scan rate 50 mV/s, potentials +0.2 to -0.5 V (SCE)) also produced a thick black deposit after about 2000 cycles. During cycling experiments there was a gradual colour change of the electrolyte over many hours from yellow-orange to dark green, with the darkest region around the cathode. At times dark streams of solution originating from the cathode could be seen flowing slowly in all

directions, eventually spreading throughout the solution. This colour change in the solution was also seen over a long time when forming the deposits under galvanostatic or potentiostatic conditions. Again, as with the anodic growth of hydrated $(NH_4)_2V_6O_{16}$ crystals, deposition at the cathode appears to begin at several nucleation sites, spreading until the entire electrode is covered with a thick and uniform black deposit.

A deposit formed using other salts mixed with NH_4VO_3, such as $MClO_4$ and M_2SO_4, where M = Li, Na or K, in varying concentrations from 0.05 to 1 mol/L. For example, black crystalline deposits were made from saturated NH_4VO_3 containing 0.05 to 0.6 mol/L K_2SO_4 at 40°C, using various substrates and over 1000 cycles between 0.2 and -0.5 V (SCE) at 50 mV/s. The rate of deposition was about 3.5 mg/C, which roughly corresponds to an effective utilization of the charge passed of about 95% relative to amount of V(IV) present in the deposit formed assuming that all the charge passed (in mol e^-) would reduce V(V) to V(IV) (see analysis of deposit in 5.2.2). Deposits were also formed in various solutions containing K^+, Cs^+, Rb^+ and NH_4^+ vanadates, either as a single solution or as a mixture of two different vanadate solutions. However, Li and Na vanadate solutions yielded no deposit under the same conditions for the other vanadates and the reasons for this will be discussed shortly.

The rate of deposition depends on the method of formation. For example, under galvanostatic deposition from a solution containing saturated NH_4VO_3 at 40°C, the rate of deposition was 0.02 mg/C at current density 1 mA/cm² and 2.0 mg/C at 0.1 mA/cm² (an effective utilization of charge of about 60%); at the higher current density, much

of the product does not adhere to the electrode. From cyclic voltammetry, 1.8 mg of deposit formed per coulomb of total reducing charge passed in each cycle (corresponding to a utilization of charge of about 55%).

5.2.2 Nature of Deposits

There are many similarities in both the morphological and crystalline structure of these cathodic deposits compared to the deposit made anodically. However, there are very important differences in the mechanism of formation, stoichiometry and use as an insertion electrode which make it a more interesting, yet more complicated study. None of these deposits act as usable cathodes, at least in the stoichiometric form that they are in when first deposited. However, either by decomposition of the ammonia-containing deposits or by constant current cycles of reduction ollowed by oxidation, their lithium inserion capabilities can be greatly increased, which makes their study worthwhile. The insertion ability of these cathodes for redox cycles will be discussed in section 5.2.6 and the possibility of forming a wide range of vanadium oxides by thermal decomposition will be discussed in chapter 6.

All deposits formed on a conducting substrate such as platinum were uniform, crystalline and black in colour and were usually grown to thicknesses up to 100-200 μm, with a surface density of 10-20 mg/cm^2. The crystals show a preferred orientation and are typically 50 μm long and 5-50 μm thick.

5.2.2.1 Pure Phases

All crystals are of relatively similar size and shape for deposits from the same vanadate solutions. However, there are some notable differences between different vanadate solutions as seen in the SEM photographs of plates 2 and 3. These deposits were made in various solutions of MVO_3, where M = K, NH_4, Rb or Cs. For NH_4VO_3 the formation of a highly-oriented deposit is shown in plate 2(a) where the crystals are very uniform in size (about 50 x 5 μm) and shape. The form and orientation of the crystals appears to be the same as for anodic electrodeposits (plate 1), but the packing density is much higher. The deposit shown in plate 2(a) is 40-50 μm thick; the platinum substrate can be seen in the cavity in the lower left of the photograph. For KVO_3, deposits with very high packing density (plate 2(b)) are formed. There is an underlying deposit similar to that shown in plate 2(a), and overlying rosette-shaped crystalline masses which appear to arise from secondary nucleation and growth at long electrolysis times. The $RbVO_3$ solutions tend to give crystals (plate 2(c) and 3(a) and (b)) that are much thicker but vary from sizes similar to those in plate 2(a) to some crystals in plate 3(b) which are almost perfectly square (50 x 50 μm). Plate 2(c) again shows the range of thickness from 5-50 μm where the platinum substrate can be seen in the cavity in the lower left of the photograph. Under similar conditions, another $RbVO_3$ solution yields crystals of uniform cubes of various sizes (plate 3(b)). For the $CsVO_3$ solution, formation of a highly-oriented deposit is shown in plate 3(c), where the crystals are uniform in size (about 100 x 5 μm) and shape with a sheet-like layering effect seen much more clearly than with the other deposits.

The chemical analysis of the deposits formed in NH_4VO_3 solutions

indicated that a mixed-valence vanadium oxide containing NH_4^+ was formed, with about one-third of the vanadium present as V(IV) (table 5.1). The formula of the freshly made deposit corresponds to $(NH_4)_4V_6O_{16+\delta} \cdot yH_2O$, where $0.00 \leq \delta < 0.04$ and $0.0 \leq y \leq 1.0$ depending on the method and amount of drying. Deposits made at a constant current density of 1.0 mA/cm^2 tended to contain more water than those made at lower current densities or by cyclic voltammetry (table 5.1). Heating the highly hydrated deposits at about 200°C for a short time (< 10 min) effectively removes all the water (see the DTA results in fig. 6.3 and table 5.1).

The chemical analyses show that the deposits correspond to $M_4V_6O_{16+\delta}$ where M = K, NH_4, Rb or Cs, where $0.00 \leq \delta < 0.04$, for the four vanadate solutions of K, NH_4, Rb and Cs respectively. Details of the chemical and gravimetric analyses are shown in table 5.2. The electrodeposits are remarkably stoichiometric according to the analysis. Since the gravimetric analysis could not distinguish between the alkali ions of K, Rb or Cs, EDAX was used to confirm their presence. For these pure phases, traces of any other contaminants such as other alkali metals were not detected by EDAX and although this was only a semi-quantitative method, with an accuracy of no better than ± 10%, it did confirm the gravimetric analysis.

Cyclic voltammetry of solutions of NH_4VO_3 with lithium or sodium salts also yields black deposits on the cathode. A black deposit could be made by cycling for longer times (4000 cycles) from 0.0 to -0.5 V (SCE) at 50 mV/s in a solution containing 0.9 mol/L $LiClO_4$ or Li_2SO_4 and saturated with NH_4VO_3 at 40°C. The rate of depositon was 2.6 mg/C (about 80% utilization of charge). Chemical analysis and experiments on

loss of mass on heating indicate again the formula $(NH_4)_4V_6O_{16+\delta}\cdot yH_2O$ where $0.00 \leq \delta \leq 0.04$ and $y \approx 0.1$ (table 5.1). SEM photographs of a deposit made in aqueous vanadate solutions with $LiClO_4$ or Li_2SO_4 as the added salt are shown in plates 4(a) and 4(b). They show crystals with a high packing density, but the crystal morphology and orientation are similar to deposits made with only NH_4VO_3, plate 2(a). Similar results were obtained by cycling under the same conditions, but replacing the Li salt with a Na salt. Chemical analysis confirmed that the deposit had similar δ values but $0.2 < y < 1.0$ (table 5.1). EDAX revealed only vanadium and no Na in this deposit. The rate of deposition for the solutions containing Na was 0.9 mg/C (about 30% efficiency), lower than for any other solution, and suggesting that the sodium salt was merely a supporting electrolyte. SEM (plate 4(c)) shows crystals that are smaller and thinner, with much secondary growth in the form of thin octagonal plates.

Use of Na or Li vanadate solutions does not yield electrodeposits containing these two ions. That the ions of Li^+ and Na^+ are not incorporated in the deposits is well known for the formation of K^+, NH_4^+ Cs^+ and Rb^+ hexavanadates containing V(V) [48] and for precipitates of V_2O_5 formed by acidification of the appropriate NH_4^+ or alkali metal vanadate solution [25]. While the salts of Li and Na do not form deposits containing these cations, they do have some effect on the orientation of the crystals of $(NH_4)_4V_6O_{16}$ as seen in the SEM photographs.

The X-ray diffraction data (tables 5.3 and 5.4) of the deposits made by cyclic voltammetry or galvanostatically in NH_4VO_3 solutions gave lattice spacings which can be compared to those reported by Bernard *et*

al. [24,55] for materials with compositions in the range $(NH_4)_{3.56}V_6O_{15.18}\cdot zH_2O$ to $(NH_4)_{3.16}V_6O_{15.58}\cdot zH_2O$, with $0.23 \leq z \leq 1.07$, prepared by reduction of V_2O_5 by tin in a solution of NH_4Cl; the material has not been identified correctly in the ASTM index [57,58]. Subsequently, Theobald *et al.* [26] determined the X-ray crystallographic structure of a single crystal of a similar material, but with the composition $(NH_4)_4V_6O_{16}$, as determined from the complete structural analysis. They confirmed the conclusion of Bernard *et al.* [24,55] that the unit cell was tetragonal, and assigned the space group P4bm. Our material was almost stoichiometric, with the ratio (total V)/NH_4 = 1.5 within experimental error, but with a V(IV)/V(V) ratio which was generally slightly less than the value of 1/2 required for perfect stoichiometry. Table 5.3 compares our observed lattice spacings with those of Bernard *et al.* [24], and also includes the results of iterative least-squares analyses of our data and those of Bernard based on a tetragonal unit cell. Of the 38 different spacings observed in the two studies, 24 matched well, although ours were 0.01 to 0.001 nm larger that the corresponding ones given by Bernard *et al.* [24], the larger differences occurring at the smaller diffraction angles. Three spacings of Bernard were outside the range of our measurements, and five were not observed, while we observed six lines not given by Bernard, but of such low intensity as to be unimportant for comparative purposes. The lines not observed by us may arise from impurities, possibly $(NH_4)_2V_6O_{16}$, although data for confirmation of this are limited [48]. Statistical tests indicate that the unit cell dimensions found by us are indistinguishable, at a 95% confidence level, from those derived from the single-crystal data of Theobald *et al.* [26] (table 5.4).

The diffraction patterns of the deposit made in KVO_3 are compared with those of Lukàcs *et al.* [56], in table 5.5, along with the results of iterative least-squares fitting of the data to a tetragonal unit cell. Of the 35 different observed spacings in the two studies, 12 match well, six of ours have intensities too small to be apparent in the spectrum given in [56], eight are outside the range of our measurements, two of ours belong to the unit cell, but appear to arise from solid solutions with $(NH_4)_4V_6O_{16}$, three appear to arise from other impurities, and the remaining four are unidentified, but also appear to arise from impurities. The unit cell dimensions found from this study and from the data of Lukàcs *et al.* [56] (omitting the reflections at 0.707 and 0.235 nm, which could not be indexed, and are presumed to be due to impurities), along with those given by Pouchard *et al.* [27] and by Galy and Carpy for a single crystal [30], are given in table 5.4. Our lattice parameters agree with those derived from single-crystal data within 95% confidence limits; the overall agreement among the four sets is good, with the set derived from the data in Lukàcs *et al.* [56] the least reliable.

Similarly, the X-ray patterns of the two new phases $Rb_4V_6O_{16}$ and $Cs_4V_6O_{16}$ are listed and fitted in table 5.6 and 5.7 respectively. The possibility of a monoclinic system has not been ruled out, but the angle β must be sufficiently close to 90° to make deviations from a tetragonal lattice negligible. As with the corresponding K and NH_4 compounds, assumption of a tetragonal lattice leads to successful indexing of these two compounds. Of 35 observed lines, there are 19 matches between Rb and Cs compounds; note the interchange in *d*-spacing between the [*312*] and [*411*] reflections (fig. 5.2). The X-ray patterns for the four pure

phases are summarized in tables 5.3 to 5.9, and are also shown in figures 5.1 and 5.2.

Once the unit cell dimensions have been determined it is possible to calculate the density of the crystal. This is done by first calculating the unit cell volume, which for an orthogonal system is simply the product of the unit cell dimensions, a, b, c ($V = abc$). The density can then be determined from the equation

$$d = F_u M_S / V N_A$$

where F is the number of formula units per unit cell, M_S is the molar mass of the salt and N_A is Avogadro's constant. Comparisons with the experimental density determination are shown in table 5.9 for the four pure phases analyzed. A problem with the experimental measurements of density was "wetting" of the deposits in the toluene buoyancy liquid. This was particularly severe with the potassium-containing hexavanadate and, to a lesser extent, the tetrammonium hexavanadate. Use of a wetting agent (Triton X-100^R) and waiting for at least 15 minutes before taking the "in liquid" weight helped the situation, although the density value obtained for $K_4V_6O_{16}$ is still lower than the density calculation from the unit cell dimensions.

5.2.2.2 Mixed Phases

Chemical analyses of several deposits formed at varying ratios of K^+ to NH_4^+ are given in table 5.10(a) and for Cs^+ to NH_4^+ in table 5.10(b). Varying the concentration of K^+ in solution produces a continuous series of mixed crystals of formula $(NH_4)_xK_{4-x}V_6O_{16+\delta}$, where $0.00 \leq \delta < 0.06$ and $0.0 \leq x \leq 4.0$. This is also true for the phases $(NH_4)_xCs_{4-x}V_6O_{16+\delta}$ as well as phases with the combinations of K, Rb and Cs. The results

show that deposits of mixed-valence vanadates can be made with the formula $M_xN_{4-x}V_6O_{16+\delta}$ where M and N = K, NH_4, Rb or Cs, and M ≠ N. Again δ varies over the small range from 0.00 to 0.10 with a mean value for all analysis of 0.04. If only NH_4VO_3 is present, tetrammonium hexavanadate is formed, but as the amount of N = K^+, Rb^+, or Cs^+ in the solution increases, the value of x decreases; i.e., the amount of N in the solid increases, until in a NVO_3 solution the value $x = 4$ is reached, corresponding to $N_4V_6O_{16}$. The amounts of K, Rb, and Cs were not determined because of interference from NH_4^+ and its presence as a common contaminant; the value $(4 - x)$ was therefore found by difference between the amount of ammonium (x) determined in the NH_4^+ containing deposits and the theoretical value of 4. However, semi-quantitative estimation of the ratio of these ions to total vanadium in the deposits can be obtained from EDAX analysis of the deposits. In the $(NH_4)_xK_{4-x}V_6O_{16+\delta}$ system the error is quite large (> 10%), but it does confirm the presence of K^+ and shows the same trend as the chemical analysis if we fix $x = 0$ for the deposit from KVO_3 solution (i.e., $K_4V_6O_{16}$) with better than 2% agreement for the three intermediate mixed cation phases analyzed (table 5.10(a)). For the two phases $(NH_4)_xCs_{4-x}V_6O_{16+\delta}$ in table 5.10(b), EDAX confirms the presence of Cs^+; the agreement is poorer, but still acceptable. The large size of the Cs^+ ion makes analysis of NH_4^+ and V less accurate for a given sample size.

Thus, the combination of different vanadate solutions results in the formation of a range of mixed-valence vanadium oxides with the amount of each cation depending on the ratio of their amounts in solution. It is therefore possible to electrodeposit crystals with

several different ratios and combinations of two cations in a continuous mixture $M_xN_{4-x}V_6O_{16+\delta}$, where x may vary continuously over the range from 0 to 4.

There are some interesting morphological differences in the crystals, depending on the alkali cations present in solution. In the SEM photographs of plate 5(a) and (b), where a large amount of secondary nucleation and growth is evident as overlying rosette-shaped crystalline masses, the underlying layer appears similar to that of the previous pure phases of the two alkali components. The change in ratio of K/Rb from 1/2 to 2 in plate 5(a) and 5(b) has little effect on the overall crystal form. Both have a high packing density and similar orientation. However, as can be seen in plate 5(c) and (d) there is a noticeable change in the crystal morphology when the ratio of K/Cs changes from 1 to 1/2. The presence of more Cs in the hexavanadate (plate 5(d)), causes the crystals to become much thinner, splitting into a more layered structure, along the preferred plane, (*001*), perpendicular to the larger crystal face.

To our knowledge no X-ray diffraction pattern for vanadium oxide phases containing a mixture of the cations K^+ or Cs^+ and NH_4^+ or any of the other combinations has been reported. Because the value of x is continuous, only a few X-ray patterns with detailed chemical analysis will be shown for comparison. Tables 5.10(a) and 5.10(b) show phases that have been analyzed by EDAX, X-ray and chemical methods. The X-ray pattern for the system $(NH_4)_xK_{4-x}V_3O_8$, where x = 0.000, 0.744, 2.214, 2.820 and 3.990 and also the system $(NH_4)_xCs_{4-x}V_6O_{16}$ with x = 0.00, 1.92 and 3.990 are shown in figure 5.1 and 5.2 respectively. The d-spacings and cell dimensions are given in tables 5.8 and 5.11. The tetrarubidium

hexavanadate, $Rb_4V_6O_{16}$, is also shown in figure 5.2 below the X-ray pattern for $(NH_4)_4V_6O_{16}$.

The progression from one of these phases to the other is seen as the NH_4^+ is replaced by K^+ or *vice versa* (figure 5.1). All major peaks in the one phase can be seen in the other with only minor shifts in their diffraction angles. Dotted lines in the figure identify the splitting or shifts of a few major peaks for these five phases. A progression from one phase to the next can be seen in these two figures as the amount of the cation with the larger ionic radius increases in the deposit. The same shifting can be seen in fig. 5.2 when NH_4^+ is replaced by Cs^+ or *vice versa*.

The values for the ionic radii of Cs^+, NH_4^+, Rb^+ and K^+ are 0.166, 0.146, 0.149 and 0.134 nm, respectively. These values were obtained for consistency by the subtraction of the Pauling radius for Cl^- (0.181 nm) from the interionic distances in alkali metal or ammonium chloride crystals with the NaCl structure [59]. The expansion of the lattice to accommodate the larger cation can be seen in fig. 5.3 where plots of the *a* lattice dimension and the volume a^2c of the unit cell are linear in the ionic radius, but the dimension *c* (the V-O layers lie in the (*001*) plane) increases more rapidly at smaller ionic radii. The lattice dimensions *a*, *b*, *c* and the volume for the monoclinic diammonium hexavanadate, $M_2V_6O_{16}$, [48] are given for comparison: for these, the V-O layers lie in the (*100*) plane. Thus, as expected, the expansion on adding larger cations is mainly in a direction perpendicular to the interplanar spacing between sheets of V and O atoms for both di- and tetrametalhexavanadates. Also as expected, for a particular insertion cation, the volumes of the unit cells for $M_4V_6O_{16}$ are larger than those

for $M_2V_6O_{16}$, the difference increasing slightly as the cation becomes larger.

Plots of the lattice parameters and volume are almost linear with x in the system $M_{4-x}(NH_4)_xV_6O_{16}$ as shown in figure 5.4. The phases show a very uniform almost linear progression as the concentration of the cation with the larger radius increases, although there is a suggestion of a very small excess volume of mixing above the linear behaviour which is to be expected for completely random mixing of the two different ions on their lattice sites.

The formation of solid mixed crystalline phases is not unique; however, this is an example that such crystalline mixed hexavanadate phases can be formed electrochemically under near room temperature conditions. This careful electrochemical control of the deposition yields a stoichiometric mixed-ion hexavanadate, with its stoichiometry determined by chemical and X-ray analysis. The relative concentrations of the alkali and/or ammonium ions present in the vanadate solution determine the relative amounts of these ions in the mixed phase hexavanadate. However, the amount of alkali metal and/or ammonium ion present in the hexavanadate deposits does not follow precisely the concentrations of these ions in solution. It appears that there is some preferential deposition of NH_4^+ compared to the alkali metals, and the smaller radius ion is preferred to some extent to the larger ions in a mixture of vanadates. The effect is not large, but noticeable, so that if a certain mixed phase is desired some correction must be made to account for this effect.

5.2.3 Relation To Other Vanadate Phases

Pouchard *et al.* [27] have plotted a composition diagram for the solid phases in the ternary system $V_2O_5 \cdot VO_2 \cdot K_2O$. They studied phases of the form $K_{2-x}V_{3+2x}O_{8+2x}$, where $K_2V_3O_8$ ($x = 0$) corresponds to the minimum of compacticity (minimum density) for the system with the V(IV) atoms occupying unique positions in the structure. They also interpreted precision density measurements on a series of compounds in terms of the above formula, which implies a double non-stoichiometry involving replacement of K^+ with $(VO)_2$ units, starting with the phase $K_4V_6O_{16}$. Bernard and Theobald [24] have extended this diagram to include $(NH_4)_4V_6O_{16}$ made by precipitation near room temperature. This is isomorphous with the Φ-$K_2V_3O_8$ and also contains variable proportions of V(IV) and V(V). They have generalized the diagram of Pouchard *et al.* [27] to $V_2O_5 \cdot VO_2 \cdot M_2O$ where M = K or NH_4.

Our results extend this 2-D phase diagram even further to include the mixed crystals described in this thesis, which have been prepared electrochemically and contain both NH_4^+ and K^+. The quaternary system is plotted in a tetrahedral diagram with vertices $(NH_4)_2O$, V_2O_4, K_2O and V_2O_5 (figure 5.5). The mixed crystals are stoichiometric in the M/V(total) ratio, but not in the V(IV)/V(V) ratio, and thus exhibit a different stoichiometry than the compounds described by Pouchard *et al.* [27] and by Bernard and Theobald [24]. Their compositions lie on a narrow surface bounded by the line *bb'* (on the plane $(NH_4)_2O$-*c*-K_2O) and a corresponding line on the plane $(NH_4)_2O$-*c'*-K_2O, where *b* = $(NH_4)_4V_6O_{16}$, *b'* = $K_4V_6O_{16}$, c = V_6O_{14} = $2V_2O_5 \cdot V_2O_4$. All other observed data lie on the two front faces of the tetrahedron. The V(V) hexavanadates *a*, *a'*, the Φ-phases of Pouchard *et al.* [26], the phases of Bernard and Theobald

[24] and the single phase *d* reported by Goncharenko and Suvorova [19] are also shown, along with a number of characteristic compositions for the system. The phase reported in [19] probably contains ammonium, so that its position is questionable. It may be possible to extend the range of solids to include a much broader region by removal of NH_4^+ from the system by mild heating (see chapter 6), but, for clarity, this was not shown on the figure. As seen later the thermal decomposition would include several other phases which exist over small composition ranges in the V_2O_5-rich part of the K_2O - V_2O_5 - V_2O_4 system. In principle, it is possible to make a total of six pseudo-ternary mixed crystal phases $M_xN_{4-x}V_6O_{16}$, M,N = K, Rb, Cs, NH_4, four pseudo-quaternary phases $L_xM_yN_{4-x-y}V_6O_{16}$, and one pseudo-quinary mixed crystal phase $L_xM_yN_zQ_{4-x-y-z}V_6O_{16}$, each with an average oxidation state 14/3, or V(V)/V(IV) mole ratio 2.

5.2.4 Analysis For Ammonia

Previous work on diammonium hexavanadate did not confirm unambiguously whether ammonium ion or the ammonia ligand occurred in the structure, i.e., whether the formula is $(NH_4)_2V_6O_{16}$ or $(NH_3)_2V_6O_{15}\cdot H_2O$. Raman spectra of the $(NH_4)_4V_6O_{16}$ deposit (fig. 5.6) show the frequencies for N-H stretching as ν_1 = 3100 cm^{-1} and for the N-H bending as ν_2 = 1420 cm^{-1} which are characterisitic of ammonium ion. With polarization of the incident beam along the length of the crystals (plate 2(a) - parallel to flat face), the ν(N-H) bands were not seen and considerable radiation damage was observed. These single-crystal Raman results confirm coordination of the ammonium ion, which is to be expected for a layered vanadium oxide structure. The new bands (fig. 5.6) that appear

in the Raman spectrum at 924 and 453 cm^{-1}, compared to crystalline V_2O_5 [60], presumably arise from the presence of VO^{2+}.

5.2.5 Mechanism of formation

The mechanism of formation of anodic deposits from aqueous NH_4VO_3 solutions has been discussed in chapter 4 in terms of electrophoretic deposition of colloidal hydrated $(NH_4)_2V_6O_{16}$ in an acidic pH gradient near the anode. Some of this colloid is not deposited, but spreads by convection, migration and diffusion farther into the solution.

Formation of cathodic deposits is a more complicated process, and is sensitive to the conditions of formation. A basic gradient of pH occurs at the cathode (chapter 4), and the V(IV) species may be $VO(OH)^+$, although the charge on the particles is not known with certainty; recently it has been reported that colloidal V_2O_5 in pure water has a negative zeta potential, and deposits cathodically to form a thin film [61]. Recent work [41] has confirmed the deposition of V_2O_5 gel from colloidal V_2O_5 which deposited cathodically to form a thin film containing a large amount of V(IV). The SEM photographs shown in plates 2 to 4 show evidence that nucleation and growth is occurring, so that a possible mechanism involves adhesion of the colloid particles to the electrode, where they act as nucleation sites.

By performing cyclic voltammetry using a saturated solution of NH_4VO_3 at different temperatures and pH's (table 5.12(a) and (b)) it is possible to suggest what process is occurring during deposition. Figure 5.7 shows the cyclic voltammograms of a solution of ammonium metavanadate at a platinum cathode after the first and 1000^{th} cycles. The average of the cathodic and anodic diffusion-limited peaks is E -

-0.15 V (SCE), which appears to correspond to the process

$$\textit{in acid} \quad 4\,H^+ + HV_2O_7^{3-} + 2\,e^- = HV_2O_5^- + 2\,H_2O \qquad (5.1)$$

$$\textit{in base} \quad 2\,H_2O + HV_2O_7^{3-} + 2\,e^- = HV_2O_5^- + 4\,OH^-$$

For the process in (5.1) for which $E^o(298.15\ K) = 0.991$ V (NHE), as calculated from the Gibbs energies tabulated by Post and Robins [52] the reduction potential is:

$$E = E^o - (RT/2F)\ln(\gamma_- m_-/\gamma_{3-} m_{3-}) - (2RT\ln 10/F)pH \qquad (5.2)$$

where subscripts - and 3- refer to $HV_2O_5^-$ and $HV_2O_7^{3-}$, respectively. The activity coefficients can be estimated roughly from the equation

$$\ln\gamma = -z^2 A I^{1/2}/(1+I^{1/2}) \qquad (5.3)$$

where $A = 1.173\ dm^{3/2}mol^{-1/2}$ is the Debye-Hückel parameter at 25°C and I the ionic strength:

$$I = 1/2\{m(NH_4^+) + m(H^+) + m(HV_2O_5^-) + 9m(HV_2O_7^{3-})\} \qquad (5.4)$$

At 25°C and $pH = 7$, the average of the cathodic and anodic peak potentials is -0.151 V (SCE) = +0.093 V (NHE), as estimated from a plot of the average E against T, which is linear between 10 and 40°C (table 5.12a). For saturated NH_4VO_3, $m(NH_4^+) = 0.1$ mol kg^{-1}. Substitution of these values into eqn. (5.2) indicates that the ratio m_-/m_{3-} must be

large, so that only the first and third terms in eqn. (5.2) are significant. Correction for the activity coefficients then gives, finally, $m_-/m_{3-} = 24$, approximately; *i.e.*, at p*H* = 7 and $m(NH_4^+) = 0.1$ mol kg^{-1}, the predominant anionic species in solution is $HV_2O_5^-$. This prediction is what would be expected from the *E* - p*H* diagram given by Post and Robins [62]. Thus, most of the vanadium in solution is present as V(IV) species at the cathode surface during cyclic voltammetry, if the potential is in the neighbourhood of the reversible potential for the process (5.1). It follows that any colloidal material which reaches the cathode surface will either be at least partially reduced, or will incorporate V(IV) species through dissolution and precipitation. The almost constant ratio of V(IV) to V(V) in the deposits suggests strongly that direct reduction is the predominant mechanism for formation of V(IV) from colloidal particles containing predominantly V(V).

Vanadium (IV) on the surface of the collodial crystallites can probably bind ions like K^+ or NH_4^+, and thereby decrease the negative surface charge, so that cathodic deposition by electrophoresis can again occur. However, ions of Li^+ and Na^+ are not incorporated in the deposits. This phenomenon is well known for the formation of K^+, NH_4^+, Cs^+ and Rb^+ hexavanadates [48] and for precipitates of V_2O_5 formed by acidification of the appropriate NH_4^+ or alkali metal vanadate solution [25]. The fact that K^+ and NH_4^+ have been found to induce phase changes in vanadium bronzes more readily than Na^+ [29] is related to differences in structure, probably arising from differences in the polarizabilities of the ions.

It is possible to make a few more comments on the mechanism by performing cyclic voltammetry using a saturated solution of NH_4VO_3 at

different scan rates. The following is a brief summary of the equations needed for analysis of the CV curves obtained in aqueous vanadate solutions [37]. Assume that we are dealing with a reduction process:

$$O + n\,e^- = R \qquad (5.5)$$

The equation for a potential sweep begins with Fick's 2nd Law. Assuming only O present initially in solution, $D_O = D_R = D$, and applying certain initial conditions [37], it can be shown that for planar diffusion an expression known as the Randles-Sevcik equation [31,32] can be derived which at 25°C is:

$$I_p = -(2.69 \times 10^5)\, n^{3/2}\, c_0^{\infty}\, D^{1/2}\, \nu^{1/2} \qquad (5.6)$$

where I_p is the peak current density. The peak current density is proportional to the concentration of the electroactive species and to the square root of the sweep rate and the diffusion coefficient.

Irreversible systems are found when an inefficient rate of electron transfer occurs. Surface equilibrium is not maintained and the shape of the CV changes. A totally irreversible system can usually be recognized by a total absence of a reverse peak. Solution of the equations as in the reversible case gives the equation for peak current density as [37]:

$$I_p = -(2.99\times10^{-5})\, n\, (\alpha_c n_\alpha)^{1/2}\, c_0^{\infty}\, D_0^{1/2}\, \nu^{1/2} \qquad (5.7)$$

For the reversible case E_p^c (fig. 2.1b) is independent of sweep rate but for an irreversible case it varies as shown below (2.4):

$$E_p^c = K - [2.3\, RT / 2\, \alpha_c\, n_\alpha\, F]\, log\, \nu \qquad (5.8)$$

where

$$K = E_e^0 - RT/\alpha_c n_\alpha F \, [0.78 - 2.3/2 \log (\alpha_c n_\alpha FD/k^{0\,2}RT)] \quad (5.9)$$

It is also possible that, depending on sweep rate, a system that is reversible becomes irreversible with a quasi-reversible intermediate region being present. Some diagnostic tests for this state would include [37]:

1) $|I_p|$ increases with $\nu^{1/2}$ but is not proportional to it
2) $|I_p^A I_p^C| = 1$ provided $\alpha_C = \alpha_A = 0.5$
3) ΔE_p is greater than $59/n$ mV and increases with increasing ν at 25°C
4) E_p^C shifts negatively with increasing ν

By looking at the dependence of the maximum current at the cathodic peak, I_p^C, on the sweep rate a crude determination of the reversibility of the reaction at the electrode in the vanadate solution can be made. Such a plot is shown in figure 5.8(a) for NH_4VO_3 and is expected to be linear for a reversible system. As can be seen from the figure, two straight lines can be drawn and there is a definite small kink in the plot, which indicates a diffusion region and a kinetic region, with mixed control occurring in the region of the bend. Thus, it appears that the reaction is quasi-reversible and can be matched quite well with the criteria for such a case as summarized above.

Assuming that we are dealing with an *ec* reaction process [37]:

$$O + n\,e^- = R$$

$$R \underset{k_{-1}}{\overset{k_1}{=}} Y \qquad (5.10)$$

the cyclic voltammogram observed depends on the relative rates of the two steps. An *ec* reaction scheme implies an electron transfer step followed by a chemical step. Two possible steps for this type of mechanism could be:

I $\quad 4H_2O + HV_2O_7^{3-} + 2e^- = 2VO^{2+} + 9OH^-$

II $\quad 2VO^{2+} + 3H_2O + 5OH^- = HV_2O_5^- + 5H_2O$

where the overall reaction is the process in (5.1).

The simplest case is where the electron transfer is totally irreversible and thus the presence of a chemical reaction has no effect on the voltammogram obtained, (no kinetic data related to the chemical reaction are obtained) giving the properties discussed in chapter 2 for irreversible systems. Similar behaviour is seen to occur when the rate of the electron transfer step is relatively fast if the rate constant for the chemical reaction is very large. However, such does not to appear to be the case in this situation, and a first assumption is that the electron transfer is reversible and the chemical reaction irreversible, although other possibilities may have to be considered. Certain diagnostic tests for these *ec* mechanisms are the following [37]:

1) $|I_p^A/I_p^C|$ is less than unity but tends to unity as ν is increased
2) $I_p^C/\nu^{1/2}$ decreases slightly with increasing ν
3) E_p^C is positive of the value for the reversible case
4) E_p^C shifts negatively with increasing ν, and in kinetic region by 30/n mV per 10 fold increase in ν.

For the region where a reverse peak is seen and $I_p^A/I_p^C < 1$, kinetic data can be obtained (ie., the region where $5 > \lambda > 0.1$, where $\lambda = k(RT/nF)\nu$). A plot of I_p^C against log ν is shown in figure 5.8(b) and from this the rate constant can be estimated to lie in a range centred at about $k = 1.5\ s^{-1}$. Interpretation of cyclic voltammograms is often difficult, so an attempt to obtain information using RDE was also done on aqueous vanadate solutions. Unfortunately the results found by this method were erratic and inconclusive, and hence could not be used to corroborate the rough approximation for the rate constant made from the CV results.

5.2.6 Insertion Into Deposits

Insertion of lithium ions into electrodes of the various cathodic deposits has been observed. Lithium insertion into the unheated deposit of general formula $M_xN_{4-x}V_6O_{16}$ was extremely small (<1% Li/V), which was to be expected because NH_4^+ ions or the alkali cations K^+, Rb^+ or Cs^+ are present between the layers of the hexavanadate structure. Previously, anodic deposits of $(NH_4)_2V_6O_{16}$ were found to insert Li up to $x = 1.44$ in $Li_x(NH_4)_2V_6O_{16}$ (chapter 4). These anodic deposits contain half as much NH_4^+ as the cathodic deposits of $(NH_4)_4V_6O_{16}$, therefore insertion into cathodic deposits would be expected to be less than anodic deposits. This was seen for the insertion of lithium ions into several electrodes of these various hexavanadate phases. Lithium insertion into an unheated deposit of $(NH_4)_4V_6O_{16}$ was very small, and occurs only in the α phase for lithium vandium bronzes where the value of x in $Li_x(NH_4)_4V_6O_{16}$ was 0.050; see figure 5.9. Figure 5.10 also shows that all the deposits containing K^+ insert very little lithium, with $x = 0.025$ for $K_4V_6O_{16}$. Mixed potassium and ammonium phases have

values also in this range. Results identical to this are also seen for other mixed phases and pure phases of $Cs_4V_6O_{16}$ and $Rb_4V_6O_{16}$ with values of x of about 0.05. As shown in figure 5.9 and 5.10, the initial insertion of lithium into all hexavanadates shows a sharp drop in open circuit potential for the extremely small amounts of Li inserted. This small amount is caused by the large amount of ammonium or alkali metal present in the hexavanadate and as a result very little lithium can be inserted. A plateau at an open circuit value of about -2.9 V is reached and no further lithium is inserted into the hexavanadate structure. At this point the only reaction probably occuring is the plating of lithium on to electrode via the reaction $Li^+ + e^- = Li$. This is because although the open circuit value is smaller than the value of -3.2 V (vs. NHE) a potential of about -3.5 V is observed just prior to swithching off the current to make an open circuit measurement. The potential of the Ag-AgCl reference electrode was 3.55 V for this electrolyte against Li^+/Li at 25°C.

Repetitive oxidation and reduction of the deposit leads to further lithium insertion. On cycling between oxidation and reduction several times, the amount of reduction increases. This was because of the removal of small amounts of NH_4^+ or K^+ in the hexavanadate during the oxidation step, as confirmed by chemical analysis and EDAX. After only a few such cycles, as seen in figures 5.9 and 5.10, plateaus can be seen beginning to form indicating that phase changes are taking place as the lithium was inserted. By the 10^{th} cycle, the insertion of lithium clearly takes place in two steps, the first step involving the insertion of lithium to replace the Cs^+, Rb^+, NH_4^+ or K^+ removed from the previous oxidation of the electrode to the general formula

$(2-x)M_2O\cdot(2-x)V_2O_5\cdot(1-x)V_2O_4$, where M = K, NH_4, Rb or Cs, with increase of the V(V)/V(IV) ratio to above its initial value of 2. The second step occurs after a large drop in potential and involves insertion of lithium past this formula to reduce the V(V)/V(IV) ratio to less than 2. This can be summarized by the following:

$$(2-x)M_2O\cdot(2-x)V_2O_5\cdot(1-x)V_2O_4 \xrightarrow{+\,2x\,Li^+ + 2\,e^-} (2-x)M_2O\cdot xLi_2O\cdot 2V_2O_5\cdot V_2O_4$$

$$\xrightarrow{+\,2y\,Li^+ + 2\,e^-} (2-x)M_2O\cdot(x+y)Li_2O\cdot(2-y)V_2O_5\cdot(1+y)V_2O_4$$

or, using salt formulas, as:

$$M_{4-2x}V_6O_{16} \xrightarrow{+\,2x\,Li^+ + 2\,e^-} M_{4-2x}Li_{2x}V_6O_{16} \xrightarrow{+\,2y\,Li^+ + 2\,e^-} M_{4-2x}Li_{2(x+y)}V_6O_{16}$$

In tables 5.13 and 5.14 the values for x + y have been determined by chemical analysis of several reduction-oxidation experiments and these agree very well with the actual charge passed to 1%; the difference can be attributed to double layer charging. The $K_4V_6O_{16}$ electrodes seem to be the most resistant to the oxidation-reduction process. This was most likely due to fact that K^+ is much smaller than NH_4^+, which both are smaller than Cs^+ (see section 5.2.2.2), making removal from the layered hexavanadate structure more difficult.

5.2.7 Mechanism of Insertion

The insertion of lithium in tetrammonium hexavanadate was also attempted by direct deposition on a Pt RDE. Potential sweep experiments were done on the insertion of lithium at various rotation speeds. As with the anodic deposit, a supporting electrolyte of $NaClO_4$ with a smaller concentration of $LiClO_4$ (ionic strength of solution 1.01 mol/L) made the transport number of the lithium negligible (t_{Li^+} = 0.00325).

The transport number was estimated as shown in chapter 4.

Again, as with the anodic deposit, by determining the mass transport-limited currents at the RDE it was possible to calculate the diffusion coefficient in solution. The charging current again should be independent of rotation speed and the slope of the plot of I_L vs. $\omega^{1/2}$ should be independent of the scan rate. The diffusion coefficient of the electroactive species can be calculated from the slope of the plot $I_{l,d}$ vs. $\omega^{1/2}$ given in chapter 4, equation 4.1. From that equation, the overall diffusion coefficient can be estimated and was found to be about 1.0×10^{-5} cm^2/s. This rough value of D describes diffusion of the lithium ion in the aqueous solution and yields no information about diffusion in the solid. Therefore, we can only say again that diffusion of Li^+ in solution was what was expected.

By using the Butler-Volmer equation, an equation can be derived from the equation for high negative overpotentials and the cathodic current density found. A similar plot of the inverse of the limiting current at various potentials versus the inverse square root of the rotation speed was made, resembling that of the anodic deposit which was shown in figure 4.5. The values of the slope and intercept at the various potentials are summarized in table 5.15. The transfer coefficient, α, was found to be approximately 0.086, in fairly close agreement with that for the anodic deposit in chapter 4. The value of I_o was obtained from extrapolation by plotting ln(I) against the potential, and was found to be about 1.59 mA/cm^2. The standard rate constant, k^0 , was then calculated and found to be 2.4×10^{-5} cm s^{-1}, which was also in close agreement with the value for the anodic deposit. Thus, for the reduction process of Li insertion into the hexavanadate structure, the

electrode kinetics appear to be similar for the anodic and cathodic deposits. The low value for the transfer coefficient indicated that possibly something can be said about the kinetics of lithium diffusion in the electrode. A value of about 0.15 had been obtained for the lithium insertion into a composite TiS_2 and $TiSe_2$ electrodes using chronoamperometry by vanSchalkwijk [63]. Thus, it may be possible to obtain more quantitative kinetic data for pure vanadium oxide electrodes by careful design of a RDE experiment.

There are a few problems in performing RDE experiments by direct deposition of the hexavanadate on a platinum electrode. Severe flaking occurs if the deposit is too thick, and flaking of the electrode will occur consistently when the rotation speed reaches values above 4900 rpm. The deposits made on the RDE were often very thick (100μm) to ensure uniformity. Thus, the deposit protruded significantly below the insulating sheath, and may have interfered with the normal flow pattern. Also, the deposit as seen in the SEM photos has a very rough surface and this may also have some influence on the experiments. The rotation speed also effects the results, as evidenced by significant increased deviations from linearity occurring with lower rotation speeds, as seen in figure 4.5. A problem again occurs with rotation speeds greater than 4900 rpm since some or most of the sample was lost because of flaking. At intermediate rotation speeds, the behaviour approached what would be expected, and when only these points were used a diffusion coefficient of the order of 1×10^{-5} cm^2/s was obtained. Because of the difficulties with reproducibility in the starting samples and the problems with adherence of the electrodeposit no further information could be obtained from the use of the RDE technique.

5.3 Conclusions

An electrochemical preparation of stoichiometric ammonium and alkali metal hexavanadates, of formula $M_4V_6O_{16}$, has been achieved. Also, several new phases of Rb and Cs hexavanadate and several mixed oxides of these pure phases were synthesized electrochemically near room temperature. Several discrepancies in the literature have been clarified, as well as some of the work of previous researchers such as Bernard *et al.* [24,55]. The substitution of one or more of the alkali metal cations K^+, Rb^+ or Cs^+, was found to occur in a continuous fashion from $x = 0$ to 4 with stoichiometry $N_xM_{4-x}V_6O_{16}$. A composition diagram for these phases was made, and extends that of Pouchard *et al.* [27] and Hagenmuller [29]. Thus, the electrochemical method to produce deposits, which are stoichiometric with respect to the ratio of vanadium to alkali metal or ammonium (6:4) and the ratio of V(IV) to V(V) (1:2), is advantangeous to other methods of synthesis used in the past [24,27].

Insertion of lithium into these materials proved to be very limited owing to the presence of a large amount of ammonia or alkali ion. Thus, insertion past the α-phase (see chapter 8) was not possible and these electrodes are of no practical use as battery cathodes. By continuous insertion and removal the capacity of the electrode was improved, but this was caused by the gradual electrochemical removal of ammonia and any alkali cations present. Therefore, the practical use of these materials as reversible cathodes for lithium batteries is doubtful. However, much has been learned about the mechanism of formation, and the nature of these deposits. Because of their stable nature and ease of formation, their possible use as catalysts for other processes for which other vanadium oxides are presently being used is of interest.

Plate 2(a) SEM photograph of fresh, unheated $(NH_4)_4V_6O_{16}$. Magnification X610, bar length 16 μm.

(b) SEM photograph of deposit made by cyclic voltammetry in KVO_3. Magnification X410, bar length 24 μm.

(c) SEM photograph of deposit made by cyclic voltammetry in $RbVO_3$. Magnification X380, bar length 26 μm.

Plate 3(a) SEM photograph of deposit made by cyclic voltammetry in $RbVO_3$. Magnification X240, bar length 42 μm.

3(b) SEM photograph of deposit made by cyclic voltammetry in $RbVO_3$. Magnification X225, bar length 44 μm.

3(c) SEM photograph of deposit made by cyclic voltammetry in $CsVO_3$. Magnification X242, bar length 41 μm.

Plate 4(a) SEM photograph of deposit made by cyclic voltammetry in $LiClO_4$ + NH_4VO_3. Magnification X120, bar length 84 μm.

4(b) SEM photograph of deposit made by cyclic voltammetry in Li_2SO_4 + NH_4VO_3. Magnification X520, bar length 19 μm.

4(c) SEM photograph of deposit made by cyclic voltammetry in Na_2SO_4 + NH_4VO_3. Magnification X227, bar length 44 μm.

Plate 5(a) SEM photograph of deposit made by cyclic voltammetry, $K_{2.66}Rb_{1.33}V_6O_{16}$. Magnification X273, bar length 37 μm.

5(b) SEM photograph of deposit made by cyclic voltammetry in $K_{1.33}Rb_{2.66}V_6O_{16}$. Magnification X242, bar length 41 μm.

5(c) SEM photograph of deposit made by cyclic voltammetry in $K_2Cs_2V_6O_{16}$. Magnification X224, bar length 45 μm.

5(d) SEM photograph of deposit made by cyclic voltammetry in $K_{1.33}Cs_{2.66}V_6O_{16}$. Magnification X192, bar length 44 μm.


C
D
A
B

Table 5.1 Chemical analysis of deposits made by cyclic voltammetry from 0.0 to -0.5 V (SCE) at 50mV/s from aqueous NH_4VO_3, 0.2 mol/L.

temp. of heating /°C (time of heating/h)	V(IV) /10^{-5} mol	total V /10^{-4} mol	mass /mg	mole ratio V(IV)/V(V)	formula of deposit from chemical analysis
air-dried (3)	8.14	2.465	26.27	0.493	$(NH_4)_4V_6O_{16}\cdot 0.31H_2O$
air-dried (1yr)	19.83	6.139	64.80	0.477	$(NH_4)_4V_6O_{16}$
vacuum (12)	12.61	3.816	40.52	0.494	$(NH_4)_4V_6O_{16}\cdot 0.18H_2O$
125 (4.0)	14.00	4.421	46.99	0.464	$(NH_4)_4V_6O_{16}\cdot 0.22H_2O$
180 (2.0)	7.83	2.463	26.00	0.466	$(NH_4)_4V_6O_{16}$
200 (1/2)	11.94	3.602	37.34	0.496	$(NH_4)_{3.6}V_6O_{15.8}$
with Li_2SO_4 (1.0 mol/L) added to NH_4VO_3					
air-dried	10.06	3.048	32.30	0.493	$(NH_4)_4V_6O_{16}\cdot 0.1H_2O$
with Na_2SO_4 (0.8 mol/L) added to NH_4VO_3					
air-dried	10.41	3.179	34.35	0.487	$(NH_4)_4V_6O_{16}\cdot 0.84H_2O$
with K_2SO_4 (0.6 mol/L) added to NH_4VO_3*					
air-dried	9.857	3.061	36.78	0.475	$(NH_4)_{0.7}K_{3.3}V_6O_{16}\cdot 0.1H_2O$

* See table 5.10(a) for other combinations, with EDAX and X-ray analysis.

Table 5.2 Chemical and gravimetric analysis of deposits made by constant current ($0.1 mA/cm^2$) at the Pt cathode from saturated aqueous vanadate solutions at 40°C.

solut on (mass/mg sample)	EDAX analysis	mass % of ion	mole ratio V(IV)/V(V)	mass % total V	formula of deposit from analysis
NH_4VO_3	no elements	11.385 (11.35)[a]	0.4771	48.30	$(NH_4)_4V_6O_{16.03}$
KVO_3	K only	21.78	0.4728	42.52	$K_4V_6O_{16.04}$
$RbVO_3$	Rb only	37.84	0.4535	33.75	$Rb_4V_6O_{16.07}$
$CsVO_3$[b]	Cs only	48.70	0.4948	30.1	$Cs_4V_6O_{16.02}$

[a] analyzed by Kjeldahl method

[b] small sample size (15.9mg) and large molar mass of Cs makes the V analysis in error by up to 5%.

Table 5.3 X-ray diffraction data for $(NH_4)_4V_6O_{16}$

hkl	this work[a]			Bernard *et al.* [24][b]		
	rel. intensity	d/nm obs.	d/nm calc.	rel. intensity	d /nm obs.	d /nm calc.
001	100	0.564	0.5587	90	0.556	0.555
200	11	0.450	0.4458	30	0.4446	0.4428
111	3	0.4226	0.4181			
210	76	0.4019	0.3988	90	0.3972	0.3960
201	9	0.3506	0.3485	50	0.3471	0.3462
211	53	0.3264	0.3246	100	0.3229	0.3225
220	16	0.3173	0.3173	30	0.3137	0.3131
310	45	0.2829	0.2820	60	0.2807	0.2800
002	33	0.2803	0.2793	40	0.2781	0.2778
221	3	0.2758	0.2746	20	0.2731	0.2728
311	19	0.2525	0.2517	50	0.2503	0.2501
320	6	0.2479	0.2473	20	0.2456	0.2456
212	4	0.2291	0.2288	30	0.2275	0.2274
321	5	0.2267	0.2256	30	0.2249	0.2246
400	5	0.2234	0.2229	20	0.2217	0.2214
410	3	0.2168	0.2163			
330	4	0.2102	0.2102	10	0.2087	0.2087
401	2	0.2075	0.270			
411	3	0.2018	0.2017			
420	10	0.1993	0.1994	40	0.1983	0.1980
312				30	0.1974	0.1972
331				20	0.1936	0.1954
421	6	0.1881	0.1878	40	0.1867	0.1865
003	5	0.1862	0.1862	10	0.1851	0.1852
322				10	0.1840	0.1840[c]
510	5	0.1749	0.1749	40	0.1739	0.1737
213	4	0.1689	0.1687	40	0.1677	0.1677
332	10	0.1670	0.1679			
511	7	0.1658	0.1669	40	0.1660	0.1658
520				40	0.1646	0.1644
422	2	0.1625	0.1623	30	0.1615	0.1612
521	7	0.1589	0.1588	40	0.1580	0.1577
303	8	0.1577	0.1574			
440				40	0.1567	0.1565
313	5	0.1554	0.1554	40	0.1545	0.1545
441				40	0.1507	0.1507
323				30	0.1478	0.1479
531				30	0.1458	0.1465

a Composition of salt: $(NH_4)_4V_6O_{16.02}$
b Composition of salt: see text; authors' intensities multiplied by 10 to compare with our values.
c hkl incorrectly given as *330* in [24]

Table 5.4 Unit cell dimensions for tetragonal $K_4V_6O_{16}$ and $(NH_4)_4V_6O_{16}$

	a/nm	c/nm	X-ray sample
$(NH_4)_4V_6O_{16}$			
this work[a]	0.8917±0.0007	0.5587±0.0007	polycrystalline electrodeposit
Theobald *et al.* [76]	0.8891±0.0004	0.5582±0.0002	single crystal
Bernard *et al.* [24][b]	0.8855±0.0005	0.5555±0.0006	powder
$K_4V_6O_{16}$			
this work[a]	0.8878±0.0005	0.5227±0.0006	polycrystalline electrodeposit
Caly and Carpy [29]	0.8870±0.0006	0.5215±0.0005	single crystal
Lukács *et al.* [56][a]	0.884±0.002	0.527±0.001	powder
Pouchard *et al.* [26]	0.8897±0.0001	0.5246±0.0002	powder

[a] Indexing new. [b] Indexing recalculated for this paper. Error limits are ±1 std. dev.

Table 5.5 X-ray diffraction data for $K_4V_6O_{16}$

hkl	this work[a] rel. intensity	d/nm obs.	calc.	Lukàcs *et al.* [56][b] rel. intensity	d /nm obs.	calc.
				med.	0.707[c]	
	6	0.565[d]				
001	63	0.523	0.5227	strong	0.530	0.5269
200	6	0.444	0.4439			
210	24	0.397	0.3971	medium	0.402	0.3953
201	12	0.339	0.3384	weak	0.341	0.3386
211	45	0.3160	0.3162	v. strong	0.317	0.3162
310	100	0.2801	0.2808	strong	0.280	0.2795
002	34	0.2617	0.2614	strong	0.262	0.2634
311	11	0.2471	0.2473	medium	0.248	0.2469
320	7	0.2456	0.2462			
				weak	0.235[c]	0.2450
400	21	0.2213	0.2220	medium	0.224	0.2210
410	18	0.2149	0.2153			
330	5	0.2088	0.2093			
222				strong	0.200	0.2014
420	21	0.1981[e]	0.1985			
312	6	0.1914	0.1913	strong	0.192	0.1917
421	5	0.1855	0.1856	weak	0.182	0.1851
510	4	0.1749	0.1741			
003	10	0.1739	0.1742	medium	0.175	0.1756
402	2	0.1695	0.1692			
412				medium	0.166	0.1663
520	13	0.1649[e]	0.1649			
213				strong	0.160	0.1605
422	3	0.1583	0.1581			
440	15	0.1568	0.1570	strong	0.157	0.1563
313				strong	0.148	0.1487
601				weak	0.142	0.1419
621				strong	0.135	0.1351
423				medium	0.131	0.1313
631				medium	0.128	0.1278
513				medium	0.123	0.1234
314				strong	0.119	0.1192
324				medium	0.117	0.1160

[a] Composition of salt: $K_4V_6O_{16.04}$
[b] Composition of salt: $K_4V_{5.94}O_{15.88}$
[c] Apparantly impurity; possibly a K-salt of a V(V) vanadate.
[d] Probably admixed $(NH_4)V_6O_{16}$
[e] Probably solid solution with $(NH_4)_4V_6O_{16}$

Table 5.6 Summary of X-ray diffraction of electrodeposit with chemical formula $Rb_4V_6O_{16.02}$

θ /degree	*h k l*	layer spacing d_{obs} / nm	layer spacing d_{calc} / nm	relative intensity
9.99	*2 0 0*	0.444	0.4452	4
12.84	*2 0 1*	0.347	0.3480	19
13.795	*2 1 1*	0.3230	0.3242	38
14.175	*2 2 0*	0.3145	0.3148	10
15.91	*3 1 0*	0.2810	0.2816	100
16.19	*2 2 1*	0.2763	0.2742	7
17.885	*3 1 1*	0.2508	0.2514	4
18.18	*3 2 0*	0.2469	0.2470	4
18.73	*2 1 2*	0.2310	0.2285	1
19.86	*3 2 1*	0.2267	0.2258	3
20.255	*4 0 0*	0.2225	0.2226	25
20.905	*4 1 0*	0.2159	0.2160	40
21.54	*3 3 0*	0.2098	0.2099	22
22.21	*3 0 2*	0.2038	0.2033	7
22.49	*4 1 1*	0.2014	0.2014	23
22.765	*4 2 0*	0.1991	0.1991	44
22.96	*3 1 2*	0.1975	0.1982	5
23.09	*3 3 1*	0.1964	0.1964	9
24.245	*4 2 1*	0.1876	0.1875	2
26.14	*5 1 0*	0.1748	0.1746	4
26.88	*4 1 2*	0.1704	0.1708	5
27.395	*3 3 2*	0.1674	0.1677	5
27.51	*5 1 1*	0.1668	0.1667	12
28.415	*4 2 2*	0.1619	0.1621	2
29.50	*5 2 1*	0.1584	0.1585	30
29.265	*4 4 0*	0.1576	0.1574	6

Table 5.7 Summary of X-ray diffraction of electrodeposit with chemical formula $Cs_4V_6O_{16.04}$.

θ /degree	*h k l*	layer spacing d_{obs} / nm	layer spacing d_{calc} / nm	relative intensity
10.235	*1 1 1*	0.4335	0.4337	11
11.145	*2 1 0*	0.3985	0.3998	12
12.475	*2 0 1*	0.3566	0.3576	60
13.44	*2 1 1*	0.3314	0.3321	100
14.16	*2 2 0*	0.3149	0.3161	12
14.93	*3 0 0*	0.2990	0.2980	42
15.85	*3 1 0*	0.2820	0.2827	45
16.04	*2 2 1*	0.2788	0.2793	4
16.52	*1 1 2*	0.2709	0.2697	7
16.755	*3 0 1*	0.2672	0.2666	5
17.555	*3 1 1*	0.2554	0.2554	8
18.065	*3 2 0*	0.2484	0.2480	19
18.75	*2 1 2*	0.2396	0.2390	31
20.165	*4 0 0*	0.2234	0.2235	6
20.82	*4 1 0*	0.2167	0.2168	23
21.455	*3 3 0*	0.2106	0.2107	18
22.01	*3 1 2*	0.2055	0.2052	27
22.205	*4 1 1*	0.2038	0.2038	24
22.67	*4 2 0*	0.1998	0.1999	19
22.82	*0 0 3*	0.1986	0.1988	19
25.015	*2 0 3*	0.1822	0.1815	6
25.55	*4 0 2*	0.1786	0.1788	46
26.01	*5 1 0*	0.1756	0.1753	19
26.58	*3 3 2*	0.1721	0.1721	17
27.29	*5 1 1*	0.1680	0.1682	9
27.65	*4 2 2*	0.1660	0.1660	5
28.82	*5 2 1*	0.1598	0.1599	19
29.12	*4 4 0*	0.1583	0.1580	4

Table 5.8 Unit cell dimensions for tetragonal $Rb_4V_6O_{16}$, $Cs_4V_6O_{16}$ and mixed phases $(NH_4)_xK_{4-x}V_6O_{16}$ and $(NH_4)_xCs_{4-x}V_6O_{16}$.

	a/nm	c/nm	X-ray sample
$Rb_4V_6O_{16}$			
this work[a]	0.8904 ± 0.0006	0.5581 ± 0.0012	polycrystalline electrodeposit
Pouchard [27]	0.8891	0.5542	high temperature synthesis
$Cs_4V_6O_{16}$			
this work[a]	0.8940 ± 0.0003	0.5964 ± 0.0006	polycrystalline electrodeposit
$(NH_4)_xK_{4-x}V_6O_{16}$ [a]			
x = 2.82	0.8908 ± 0.0005	0.5492 ± 0.0007	polycrystalline electrodeposit
x = 2.22	0.8904 ± 0.0006	0.5453 ± 0.0008	polycrystalline electrodeposit
x = 0.74	0.8872 ± 0.0016	0.5369 ± 0.0018	polycrystalline electrodeposit
$(NH_4)_xCs_{4-x}V_6O_{16}$ [a]			
x = 1.92	0.8905 ± 0.0007	0.5849 ± 0.0060	polycrystalline electrodeposit

[a] Indexing new. Error limits are ±1 std. dev. in each of these cases.

Table 5.9 Comparison of the density calculated experimentally and from the unit cell (tables 5.4 and 5.8) of deposits made by constant current (0.1 mA/cm^2) at the Pt cathode from saturated aqueous vanadate solutions at 40°C.

formula of deposit from analysis	Measured Density d / g cm^{-3}	Calculated Density from unit cell dimensions d / g cm^{-3}
$(NH_4)_2V_6O_{16.04}$	3.024 ± 0.040	3.067 ± 0.010+
$(NH_4)_4V_6O_{16.04}$	2.328 ± 0.022	2.369 ± 0.006
$K_4V_6O_{16.04}$	2.772 ± 0.039*	2.893 ± 0.007
$Rb_4V_6O_{16.07}$	3.360 ± 0.017	3.388 ± 0.014
$Cs_4V_6O_{16.02}$	3.777 ± 0.027	3.815 ± 0.011

* see section 5.2.2.2 for comments on the experimental density value.
+ from cell dimensions of table 4.3

Table 5.10(a) Chemical analysis of deposits made galvanostatically at a current density of 0.1 mA/cm² from a solution of NH_4VO_3 (0.2 mol/L, 40°C) + specified concentrations of K_2SO_4

Solution of 0.2 *M* NH_4VO_3 + K_2SO_4/(mol/L)	mass % NH_4^+	mass % V(IV)	mass % total V	$(NH_4)_xK_{4-x}V_6O_{16+\delta}$ values in formula for the value x	δ	EDAX 4-x
No K_2SO_4	11.33	15.6	48.3	3.990	0.028	0.02
0.048	7.71	15.2	46.2	2.820	0.010	0.22
0.096	5.94	14.9	45.4	2.214	0.012	1.78
0.57	1.90	13.9	43.3	0.744	0.036	3.20
KVO_3 only	0.00	13.3	42.3	0.000	0.056	*4.00

* The value of x for the deposit from KVO_3 solution was fixed at $x = 0$ for comparison with chemical analysis (see section 5.2.2.2).

Table 5.10(b) Chemical analysis of deposits made galvanostatically at a current density of 0.1 mA/cm² from a solution of NH_4VO_3 and $CsVO_3$ (about 0.2 mol/L, 40°C).

Solution of 0.1 *M* NH_4VO_3 + $CsVO_3$ (mol/L)	mass % NH_4^+	mass % V(IV)	mass % total V	$(NH_4)_xCs_{4-x}V_6O_{16+\delta}$ values in formula for x	δ	EDAX value 4-x
No $CsVO_3$	11.33	15.6	48.3	3.99	0.028	0.00
0.1 *M* $CsVO_3$	3.99	10.1	34.8	1.92	0.130	2.18
0.2 *M* $CsVO_3$	2.45	10.95	33.5	1.28	0.020	2.84
$CsVO_3$ only	0.00	9.98	30.3	0.00	0.014	*4.00
$RbVO_3$ only	0.27	10.36	33.9	0.12	0.082	only Rb present

* The value of x for the deposit from $CsVO_3$ solution was fixed at $x = 0$ for comparison with chemical analysis (see section 5.2.2.2).

Table 5.11 X-ray patterns *d*-spacing of three mixed phase K-NH_4 hexavanadates and one Cs-NH_4 hexavanadate.

	$(NH_4)_xK_{4-x}V_6O_{16}$						$(NH_4)_{1.92}Cs_{1.08}V_6O_{16}$					
	$x = 2.82$			$x = 2.22$			$x = 0.74$					
hkl	θ /deg	spacing d/nm	intensity	θ /deg	spacing d/nm	intensity	θ /deg	spacing d/nm	intensity	θ /deg	spacing d/nm	intensity
001	8.01	0.553	76	8.12	0.544	45	8.37	0.529	51			
200	9.91	0.448	3	9.93	0.447	6	9.96	0.445	6			
210	11.10	0.400	40	11.12	0.399	36	11.16	0.398	41			
201	12.85	0.346	26	12.88	0.346	22	13.09	0.340	30			
211	13.80	0.323	100	13.83	0.322	100	14.03	0.318	100	13.53	0.3292	40
220	14.10	0.316	11	14.11	0.316	15				14.16	0.3149	35
310	15.83	0.2824	45	15.83	0.2824	58	15.89	0.2813	96	15.87	0.2817	100
002	16.30	0.2744	30	16.42	0.2725	23	16.98	0.2638	31			
311	17.87	0.2510	20	17.92	0.2503	20	18.09	0.2481	18			
320	18.10	0.2479	7							18.16	0.2471	25
212	19.83	0.2271	6	19.85	0.2268	16						
321	20.01	0.2251	12	20.02	0.2250	22	20.26	0.2224	18			
400	20.19	0.2232	8	20.20	0.2231	13				20.25	0.2227	20
410	20.84	0.2165	6	20.84	0.2165	9	20.93	0.2156	15	20.91	0.2158	35
330				21.43	0.2108	4	21.56	0.2096	5	21.65	0.2088	42
401				21.92	0.2063	4						
420	22.72	0.1994	16	22.72	0.1994	25	22.81	0.1987	12	22.76	0.1991	39
312	23.09	0.1964	14	23.15	0.1959	24	23.61	0.1923	11	22.31	0.2029	19
421	24.31	0.1871	8	24.32	0.1870	11	24.46	0.1860	6			
003	24.88	0.1831	10	25.08	0.1817	6	25.31	0.1802	2	22.95	0.1975	15
510	26.15	0.1748	9	26.15	0.1748	13	26.21	0.1744	9	26.10	0.1751	9
402	26.47	0.1728	4	26.56	0.1723	5	26.96	0.1699	3			
213	27.15	0.1688	16									
511				27.70	0.1657	22	27.76	0.1654	17	27.36	0.1676	23
422	28.57	0.1611	6	28.67	0.1605	5	28.61	0.1609	7			
521	29.16	0.1581	12	29.18	0.1580	20	29.31	0.1573	16	29.02	0.1588	27
303	29.24	0.1577	10									
440										29.28	0.1575	22

Table 5.12(a) Cyclic voltammetry of an aqueous ammonium vanadate solution as a function of temperature of the solution; scan rate 50 mV/s from 0.25 to 0.75 V.

Temperature / °C	Potential of Reduction Peak / V	Average of Potential Reduction and Oxidation Peaks / V
55	-0.158	-0.115
40	-0.227	-0.125
26	-0.260	-0.156
10	-0.314	-0.194

Table 5.12(b) Cyclic voltammetry of an aqueous ammonium vanadate solution as a function of pH of the solution, saturated at 25°C; scan rate 50 mV/s from 0.25 to 0.75 V, with addition of 8.33 mol/L KOH to change pH.

Ionic Strength / mol/L	pH	Potential of Reduction Peak / V	0.05916log(I)
0.05	6.86	-0.216	0.0770
0.0506	7.14	-0.213	0.0767
0.0524	7.50	-0.224	0.0758
0.0536	7.73	-0.234	0.0752
0.0545	7.84	-0.239	0.0748
0.0554	7.92	-0.245	0.0743
0.0567	8.05	-0.253	0.0737
0.0583	8.11	-0.261	0.0730
0.0595	8.23	-0.267	0.0725
0.0610	8.32	-0.273	0.0719

Table 5.13 Chemical analysis of deposits after lithium insertion into pure tetrammonium and potassium hexavanadates, during electrochemical reduction-oxidation experiments.

ammonium present /10^{-4} mol	V(IV) /10^{-4} mol	total V /10^{-4} mol	mass /mg	moles e^- analysis (charge) /10^{-5} mol	formula from analysis (before Li^+)	Li^+ that inserted Li/V_6O_{16}
$(NH_4)_4V_6O_{16}$ electrode initial reduction						
3.69	2.02	6.04	64.4	0.47 (0.50)	$(NH_4)_4V_6O_{16}$	0.05
$(NH_4)_4V_6O_{16}$ electrode 5th scan[1]						
1.26*	NA	1.95	20.79	2.02* (1.98)[1]	$(NH_4)_{3.8}V_6O_{16}$	0.28
$(NH_4)_4V_6O_{16}$ electrode 5th scan (final oxidation)						
1.20	0.577	1.953	20.79	1.30 (1.55)[1]	$(NH_4)_{3.6}V_6O_{16}$	NA
$(NH_4)_4V_6O_{16}$ after 10 red-ox scans (about 4 Q oxidation)						
4.22	2.96	8.02	82.70	14.4 (14.6)[1]	$(NH_4)_{3.15}V_6O_{16}$	1.10
$(NH_4)_4V_6O_{16}$ electrode after 6.7 Q oxidation (6.6 Q from analysis)[2]						
2.14	1.795	4.21	44.27	10.35 (10.47)[2]	$(NH_4)_3V_6O_{16}$	1.48
$(NH_4)_4V_6O_{16}$ after 6 deep red-ox scans (followed by final insertion)						
1.68	1.263	3.91	40.51	-	$(NH_4)_{2.5}V_6O_{16}$	~ 1.47

* based on estimate from chemical analysis of oxidation product (5th scan), figure 5.9, third entry above.
[1] see figures 5.9, reduction curves labelled a for scans 1, 5 and 10.
[2] see figures 5.9, solid oxidation curve, b, reduction curve, c.

Table 5.14 Chemical analysis of deposits after lithium insertion into pure tetrammonium and potassium hexavanadates, during electrochemical reduction-oxidation experiments.

EDAX analysis ion/V_6O_{16}	V(IV) /10^{-4} mol	total V /10^{-4} mol	mass /mg	moles e^- analysis (charge)* /10^{-5} mol	formula from analysis (before Li^+)	Li^+ that inserted Li/V_6O_{16}
$K_4V_6O_{16}$ electrode after initial reduction						
3.99	5.965	1.804	192.45	0.269 (0.573)*	$K_4V_6O_{16}$	0.025 [1]
$K_4V_6O_{16}$ electrode after oxidation of 3.7 Q						
3.852	1.96	6.33	78.68	1.50 (3.68)*	$K_{3.852}V_6O_{16}$	0.077 [1]
$K_4V_6O_{16}$ electrode after oxidation of about 12 Q						
3.66	0.996	3.65	43.19	2.07 (12.44)*	$K_{3.66}V_6O_{16}$	0.733 [1]
$(NH_4)_{2.67}K_{1.33}V_6O_{16}$ electrode after five redox scans						
K - 1.234 NH_4-2.20	1.19	3.59	38.82	(7.33)*	$(NH_4)_{2.2}K_{1.23}V_6O_{16}$	1.21 [2]

* Number based on actual oxidation charge passed compared to analysis
[1] See figure 5.10, reduction curves labelled a for scans 1, 5 and 10.
[2] see figures 5.10, solid reduction curve, b. Based on reduction charge passed minus 1% double layer charging in figure 5.10

Table 5.15 Summary of the insertion of lithium into tetrammonium hexavanadate on a platinum rotating disc electrode.

Potential /V	Slope /$mA^{-1}min^{1/2}$ ± 5.5	Intercept /mA^{-1} ± 0.03	ln(I/mA)
0.100	56.62	0.273	-1.299
0.000	48.14	0.291	-1.235
-0.100	40.73	0.296	-1.218
-0.200	36.91	0.266	-1.324
-0.300	40.74	0.139	-1.974
-0.400	54.36	0.040	-3.218

Fig. 5.1 X-ray diffraction pattern for $(NH_4)_xK_{4-x}V_6O_{16}$ at x = 3.99, 2.82, 2.21, 0.74 and 0.00, with principal reflections identified. The large shifts with x of the 001 reflections are apparent. For x = 0.74, sample is sufficiently thin to show lines from the Pt substrate. All intensities are relative to the most intense line in each pattern.

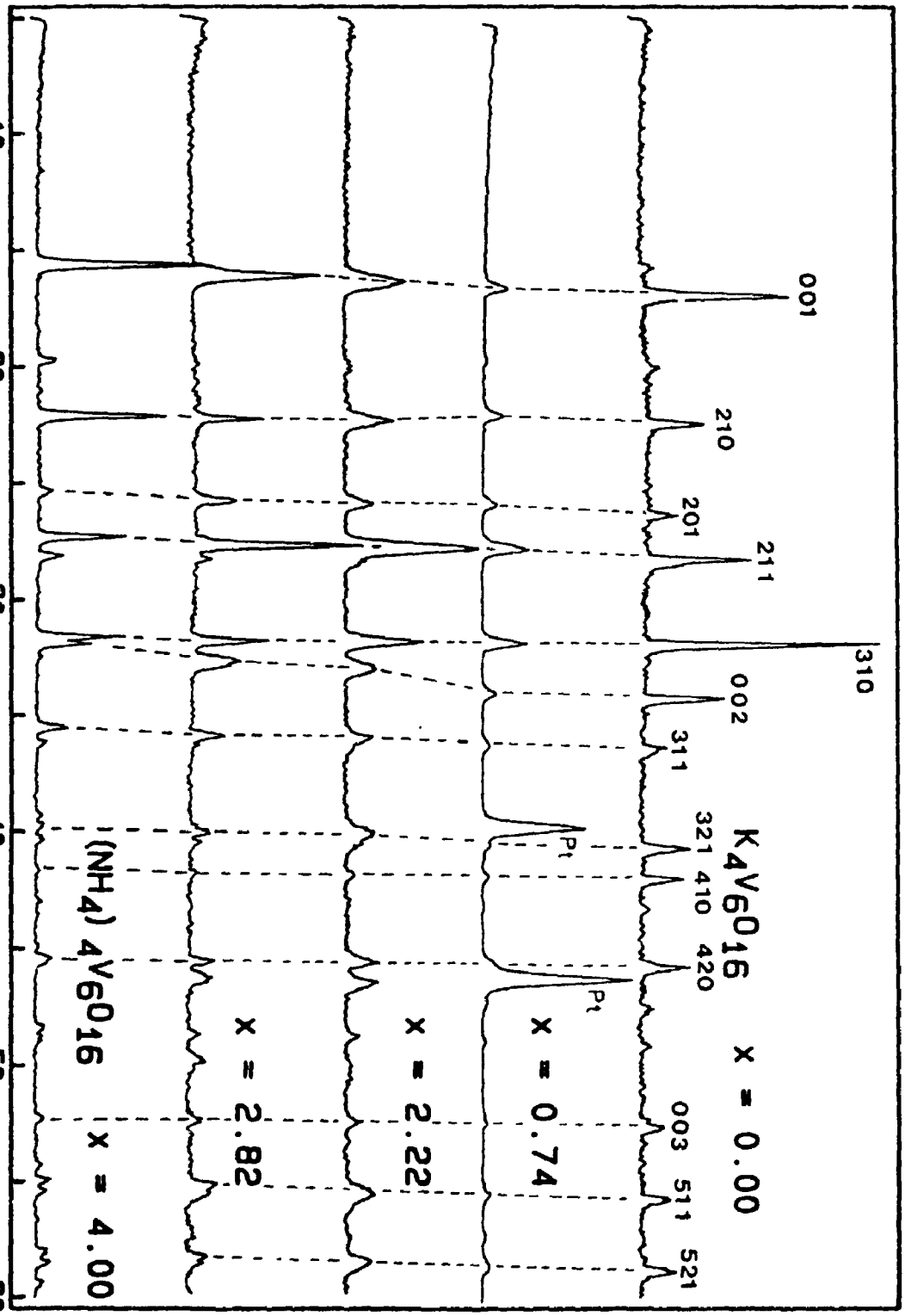
RELATIVE PEAK INTENSITY
001
210
201
211
310
002
311
321 410 420
003 511 521
Pt
Pt
$K_4V_6O_{16}$ x = 0.00
x = 0.74
x = 2.22
x = 2.82
$(NH_4)_4V_6O_{16}$ x = 4.00
10
20
30
40
50
60
DIFFRACTION ANGLE 2 θ

Fig. 5.2 X-ray powder diffraction pattern for $(NH_4)_xCs_{4-x}V_6O_{16}$ at $x = 3.99$, 1.92 and 0.00, and $Rb_4V_6O_{16}$, with principal reflections identified.

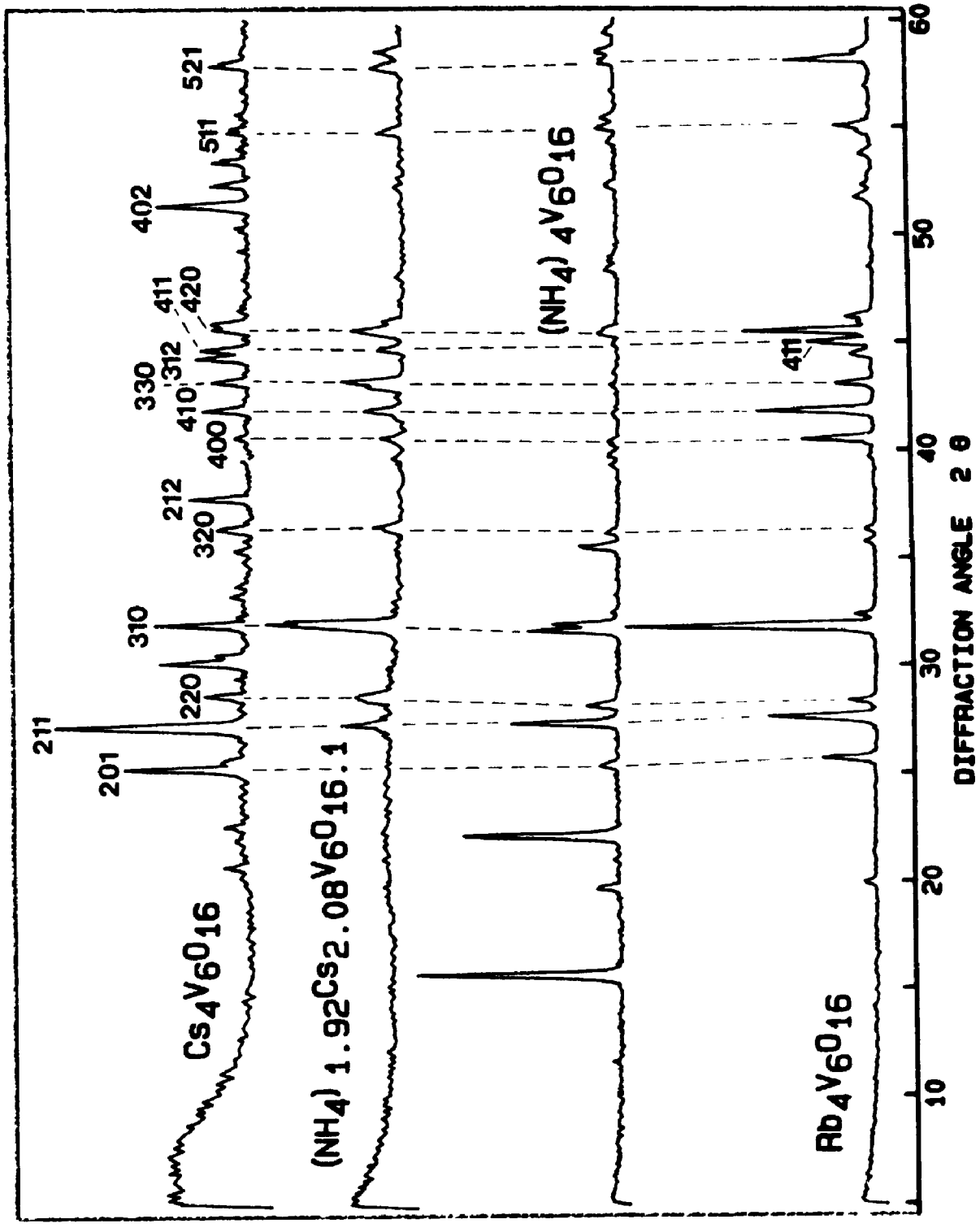
RELATIVE PEAK INTENSITY
DIFFRACTION ANGLE 2 θ
10
20
30
40
50
60
$Cs_4V_6O_{16}$
$(NH_4)_{1.92}Cs_{2.08}V_6O_{16}\cdot 1$
$(NH_4)_4V_6O_{16}$
$Rb_4V_6O_{16}$
211
201
220
310
320
212
400
410
330
312
411
420
402
511
521
411

Fig. 5.3 Dependence of the lattice parameter *l* and volume *V* on the ionic radius r_+ in $M_2V_6O_{16}$ [48] (closed circles; parameters *a*, *b*, *c*) and in $M_4V_6O_{16}$ (open circles; *a*, *c*).

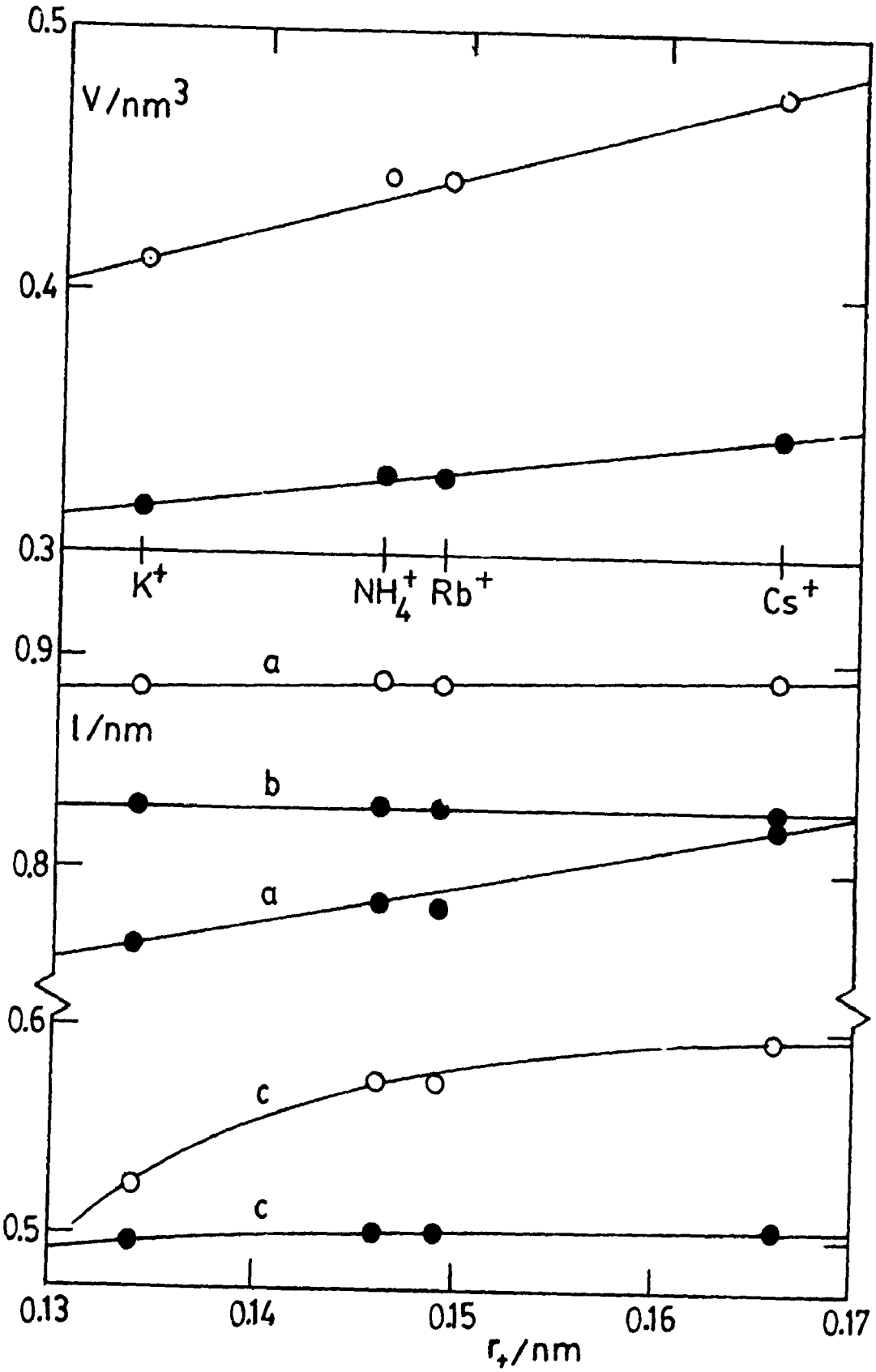
0.5
V/nm3
0.4
0.3
K+
NH4+
Rb+
Cs+
0.9
a
l/nm
b
0.8
a
0.6
c
c
0.5
0.13
0.14
0.15
0.16
0.17
r+/nm

Fig. 5.4 Dependence of the lattice parameter l and volume V of unit cells in $(NH_4)_xM_{4-x}V_6O_{16}$ on x for M = K (open circles), M = Cs (closed circles).

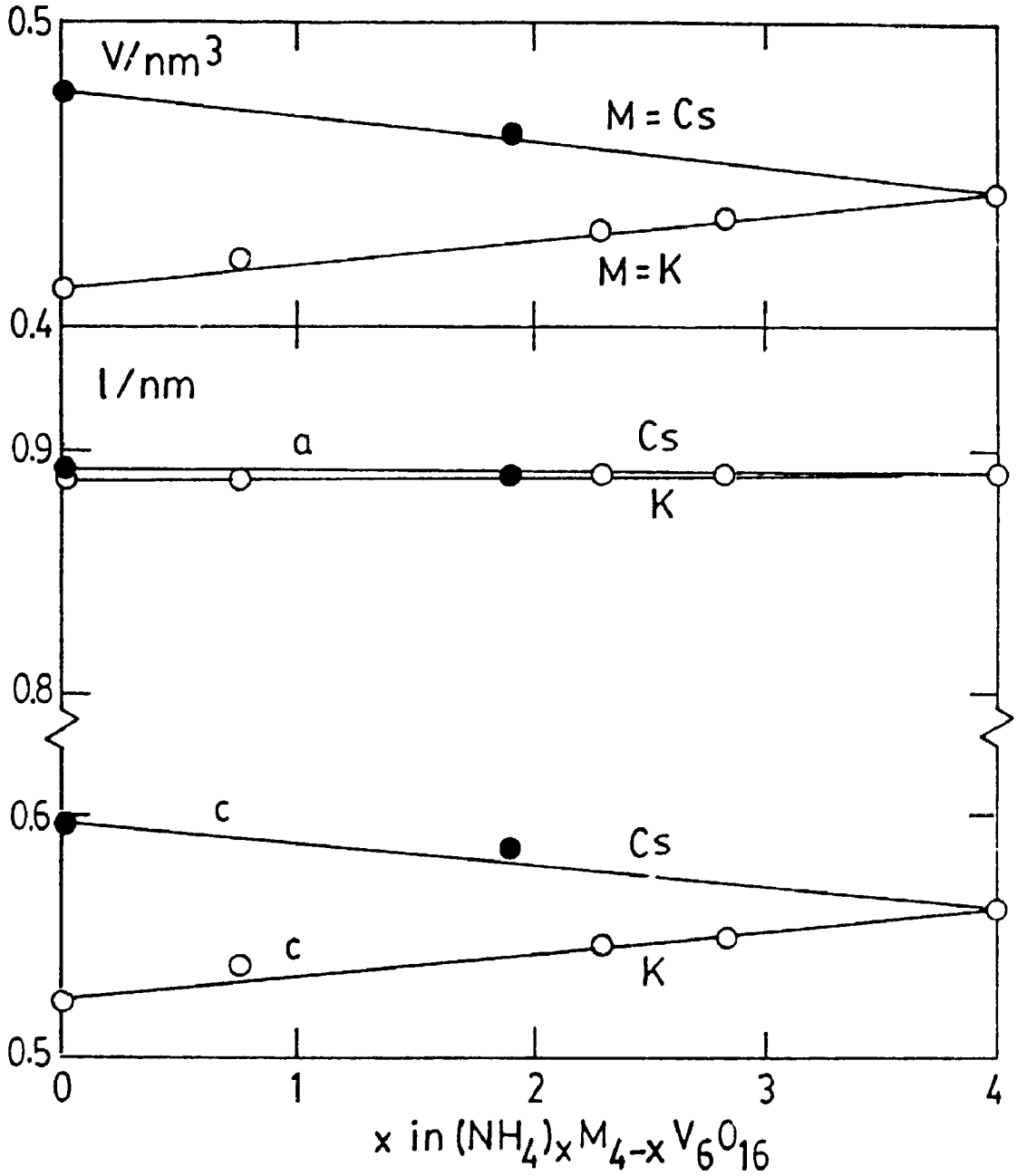
0.5
V/nm3
M = Cs
M = K
0.4
l/nm
0.9
a
Cs
K
0.8
0.6
c
Cs
c
K
0.5
0
1
2
3
4
x in (NH4)x M4-x V6 O16

Fig. 5.5 Compositions of homogeneous phases in the quaternary system K_2O - $(NH_4)_2O$ - V_2O_4 - V_2O_5. *a*, *a'* - $(NH_4)_2V_6O_{16}$, $K_2V_6O_{16}$; *b*, *b'* - $(NH_4)_4V_6O_{16}$, $K_4V_6O_{16}$ [59]; *c* - V_3O_7; *d* - $3K_2O \cdot 5V_2O_5 \cdot V_2O_4$; *e* - $K_2V_8O_{17}$; *f* - $K_2V_6O_{13}$; *g* - $K_4V_3O_7$; *h*, *h'* - NH_4VO_3, KVO_3; *j* - $(NH_4)_2V_3O_7$. Solid area: results of [27]; diagonal hatching: results of [24]; vertical hatching: this thesis.

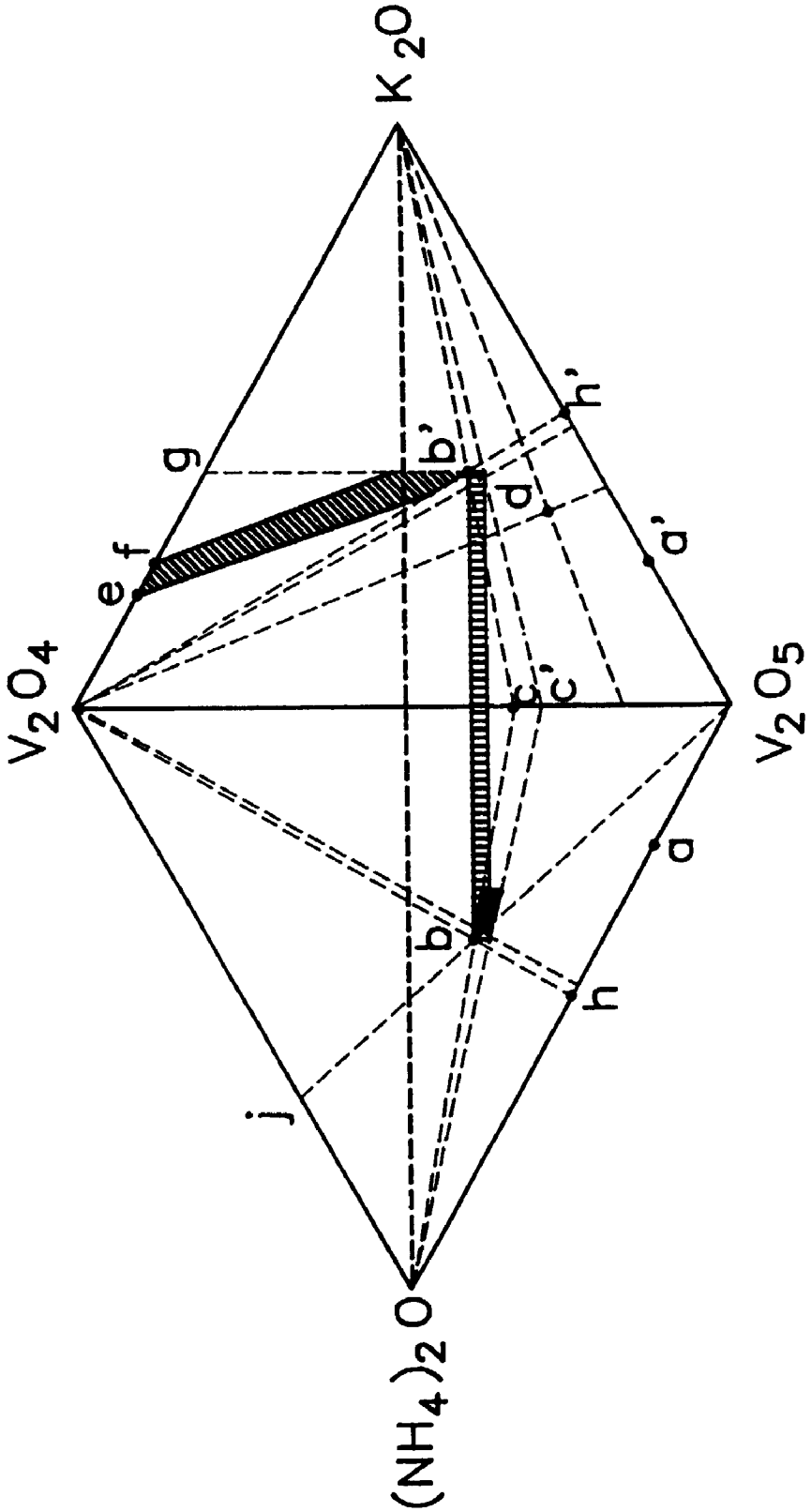
K2O
V2O4
V2O5
(NH4)2O
g
b'
h'
d
a'
e
f
c'
a
b
h
j

Fig. 5.6 Raman spectrum for $(NH_4)_4V_6O_{16}$ electrodeposit on Pt substrate; green excitation, power 3 mW.

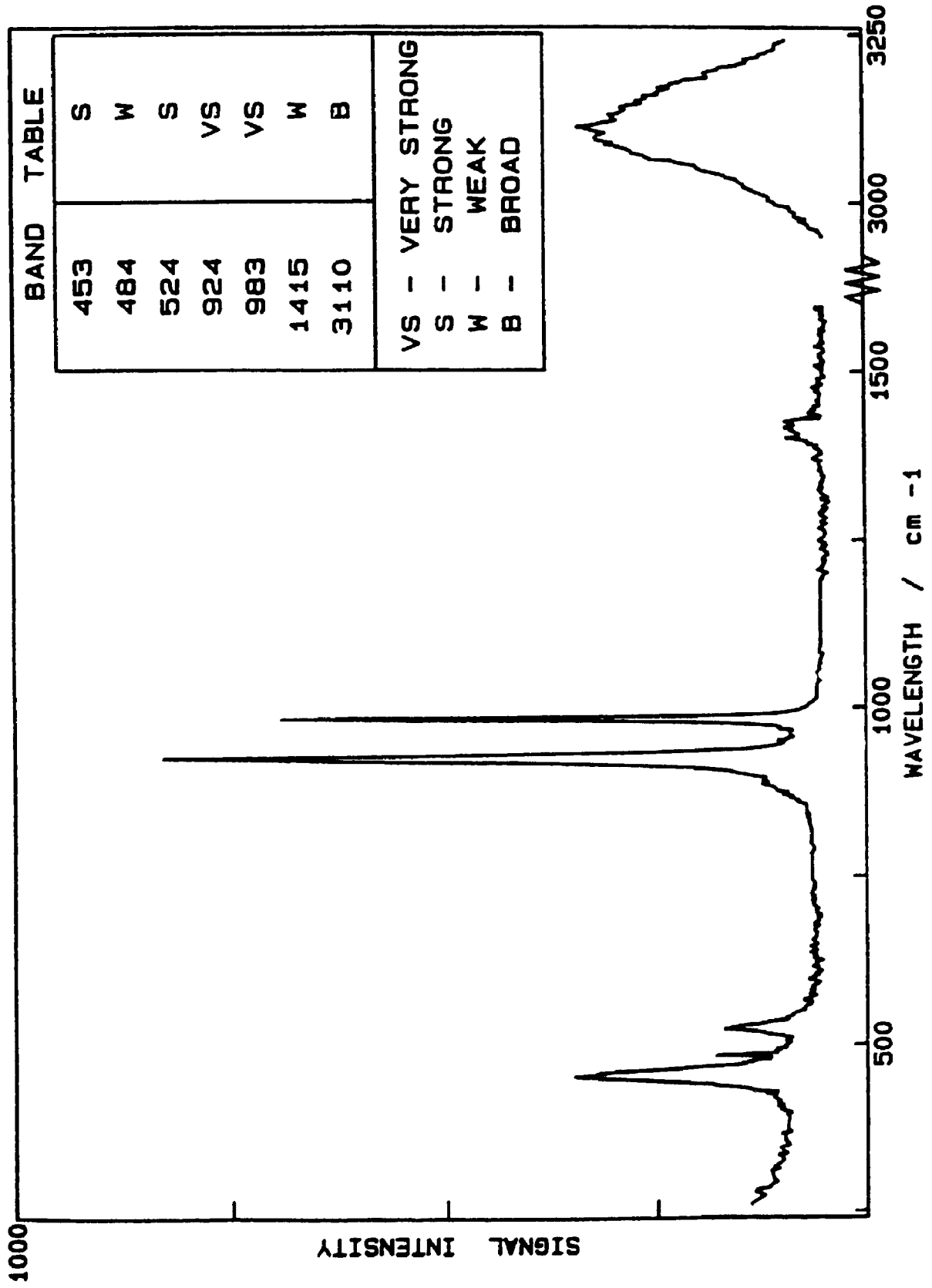
BAND TABLE
453 S
484 W
524 S
924 VS
983 VS
1415 W
3110 B
VS - VERY STRONG
S - STRONG
W - WEAK
B - BROAD
1000
SIGNAL INTENSITY
500
1000
1500
3000
3250
WAVELENGTH / cm -1

Fig. 5.7 Cyclic voltammogram of Pt cathode in sat. aq. NH_4VO_3 solution at 40°C; after first (- - -) and 1000th (——) cycles.

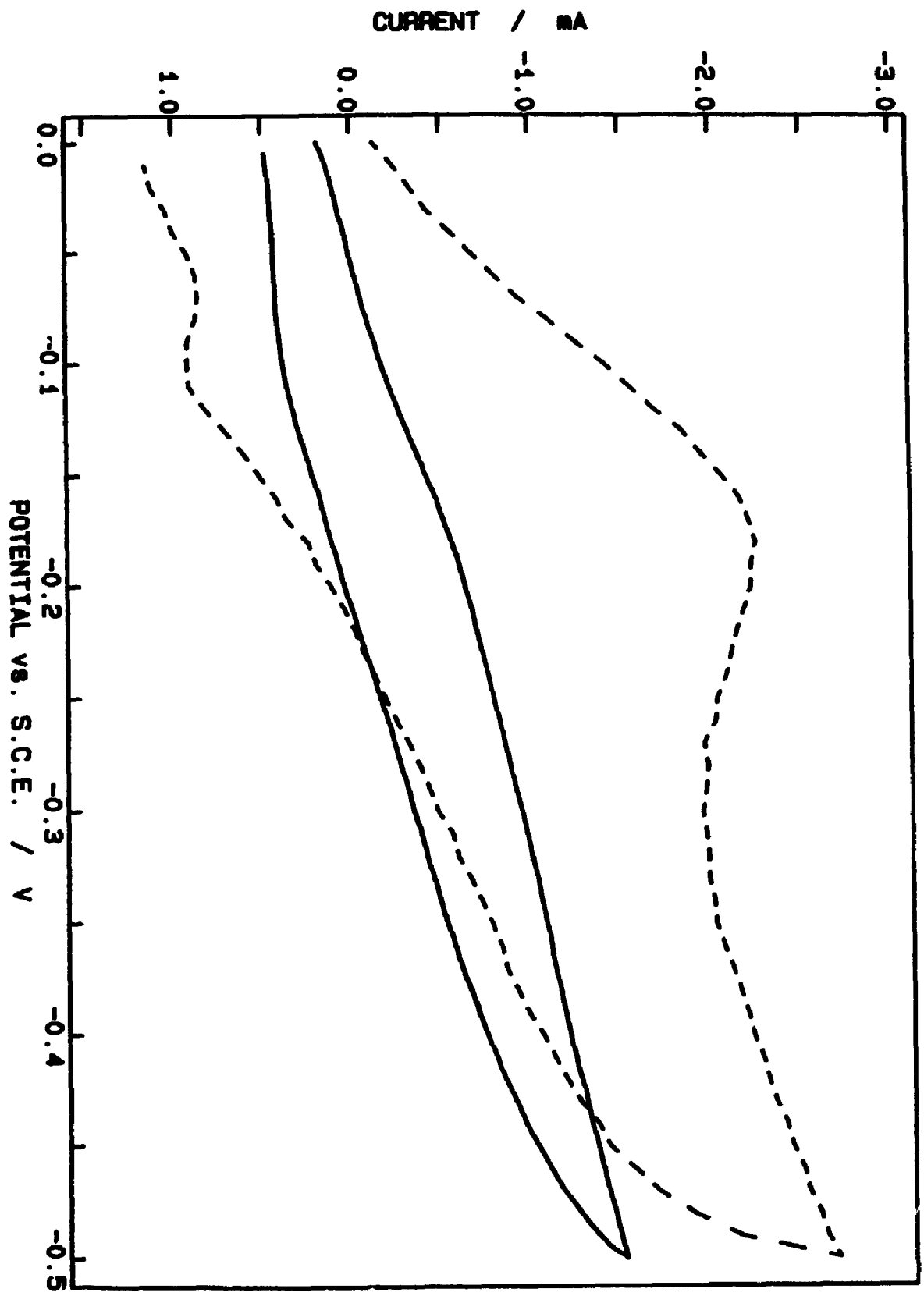
CURRENT / mA
1.0
0.0
-1.0
-2.0
-3.0
0.0
-0.1
-0.2
-0.3
-0.4
-0.5
POTENTIAL vs. S.C.E. / V

Fig. 5.8(a) Plot of current at cathodic peak vs. sweep rate for an RDE experiment.

Fig. 5.8(b) Plot of cathodic peak potential, E_p^c, vs. log sweep rate for an RDE experiment.

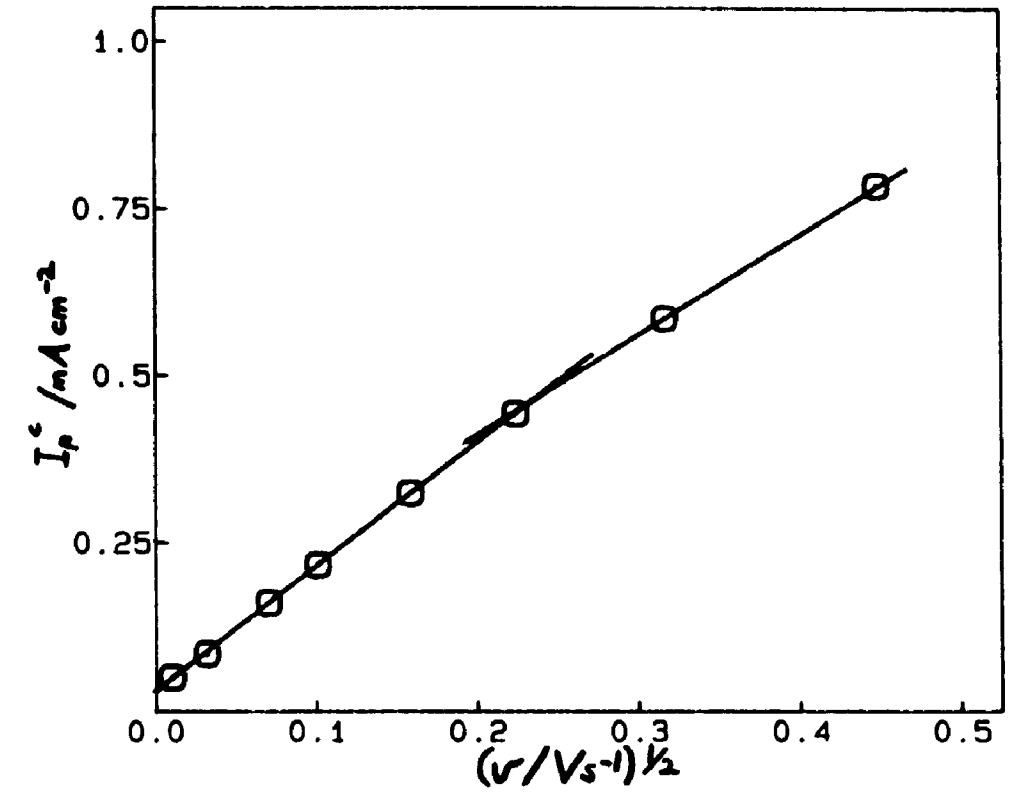
1.0
0.75
0.5
0.25
I_p^c /mA cm^{-2}
0.0
0.1
0.2
0.3
0.4
0.5
$(v/Vs^{-1})^{1/2}$

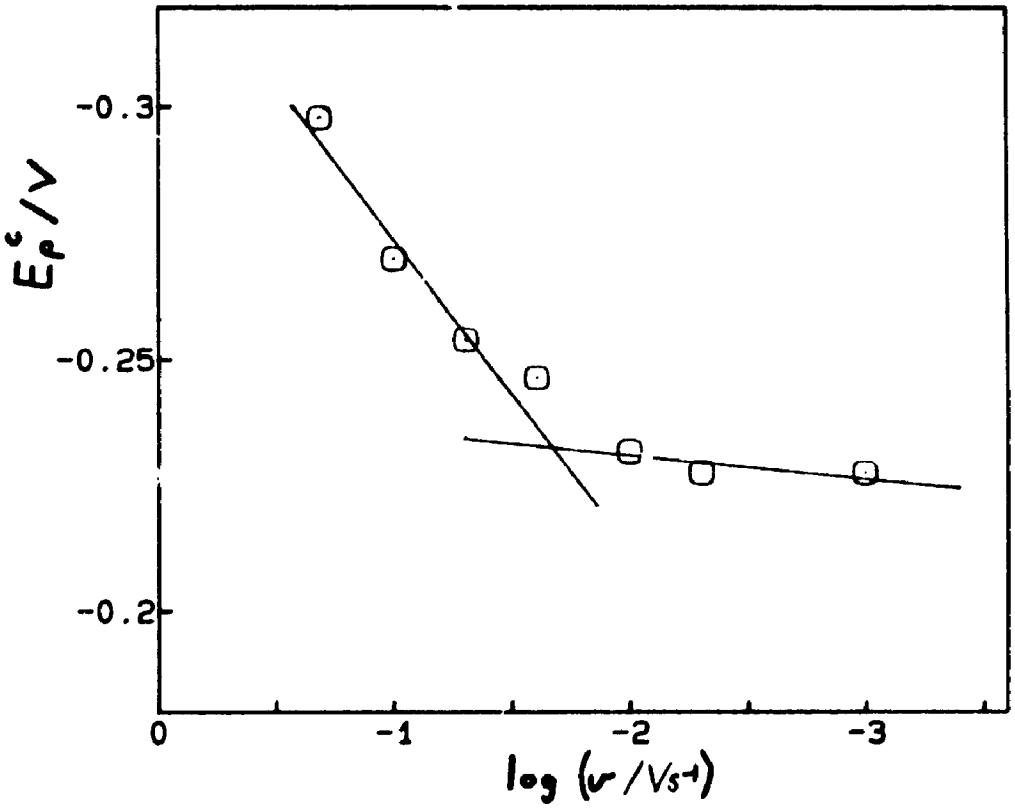
-0.3
-0.25
-0.2
E_p^c /V
0
-1
-2
-3
log (v/Vs^{-1})

Fig. 5.9 Open circuit potentials for insertion of lithium into $(NH_4)_4V_6O_{16}$; (a) not oxidized; (b) after electro-oxidation by 6.7 C of charge; (c) subsequent insertion of Li. Numbers are cycles of insertion and removal. Compositions given for end of insertion process (arrows) and analyses given in table 5.13.

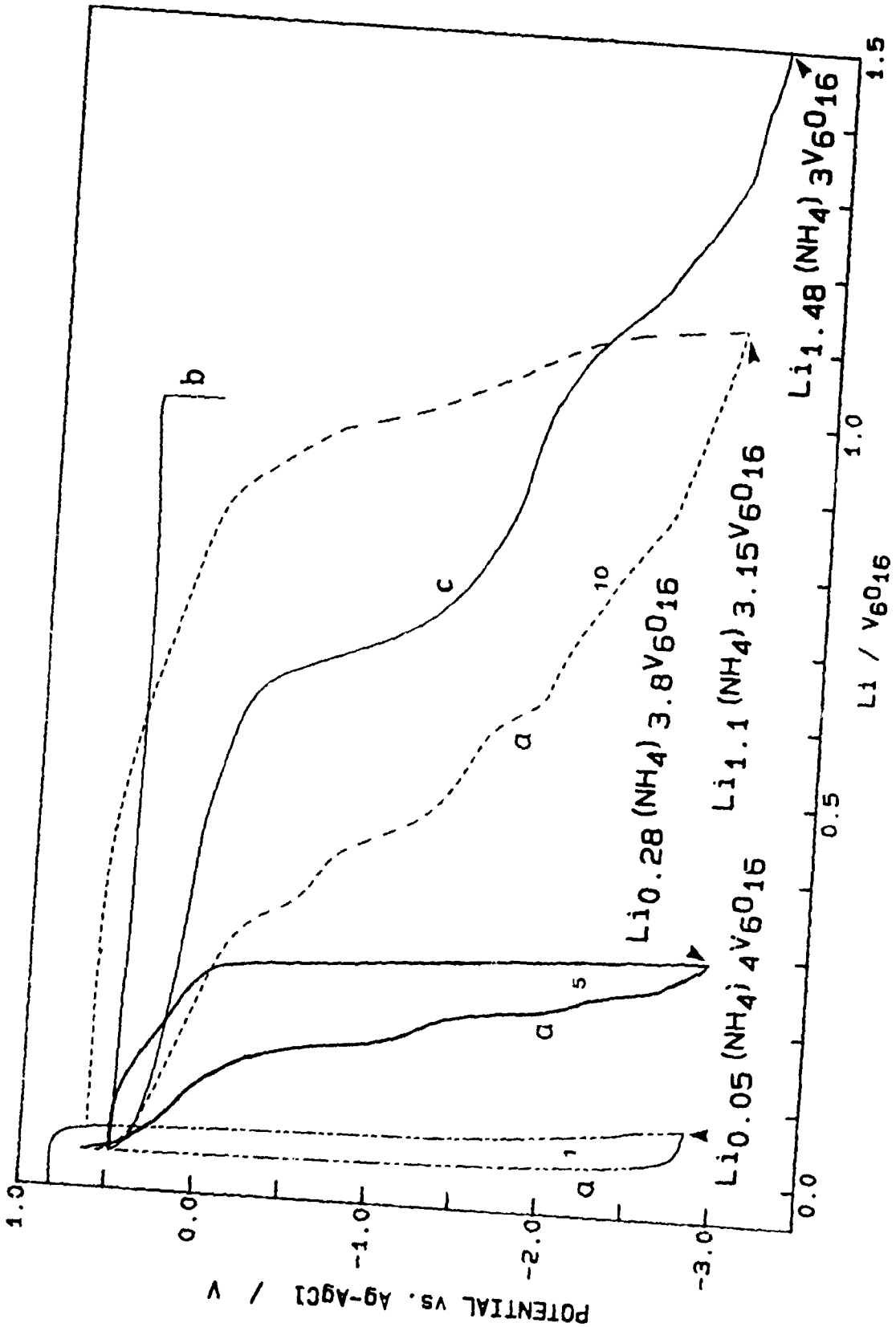
POTENTIAL vs. Ag-AgCl / V
1.0
0.0
-1.0
-2.0
-3.0
0.0
0.5
1.0
1.5
Li / V6O16
Li1.48 (NH4) 3V6O16
Li1.1 (NH4) 3.15V6O16
Li0.28 (NH4) 3.8V6O16
Li0.05 (NH4) 4V6O16
a
b
c
a
a
1
5
10

Fig. 5.10 Open circuit potentials for insertion of lithium into (a) $K_4V_6O_{16}$; (b) $(NH_4)_{2.67}K_{1.33}V_6O_{16}$. Numbers are cycles of insertion and removal. Compositions given for end of insertion process (arrows) and analyses given in table 5.14.

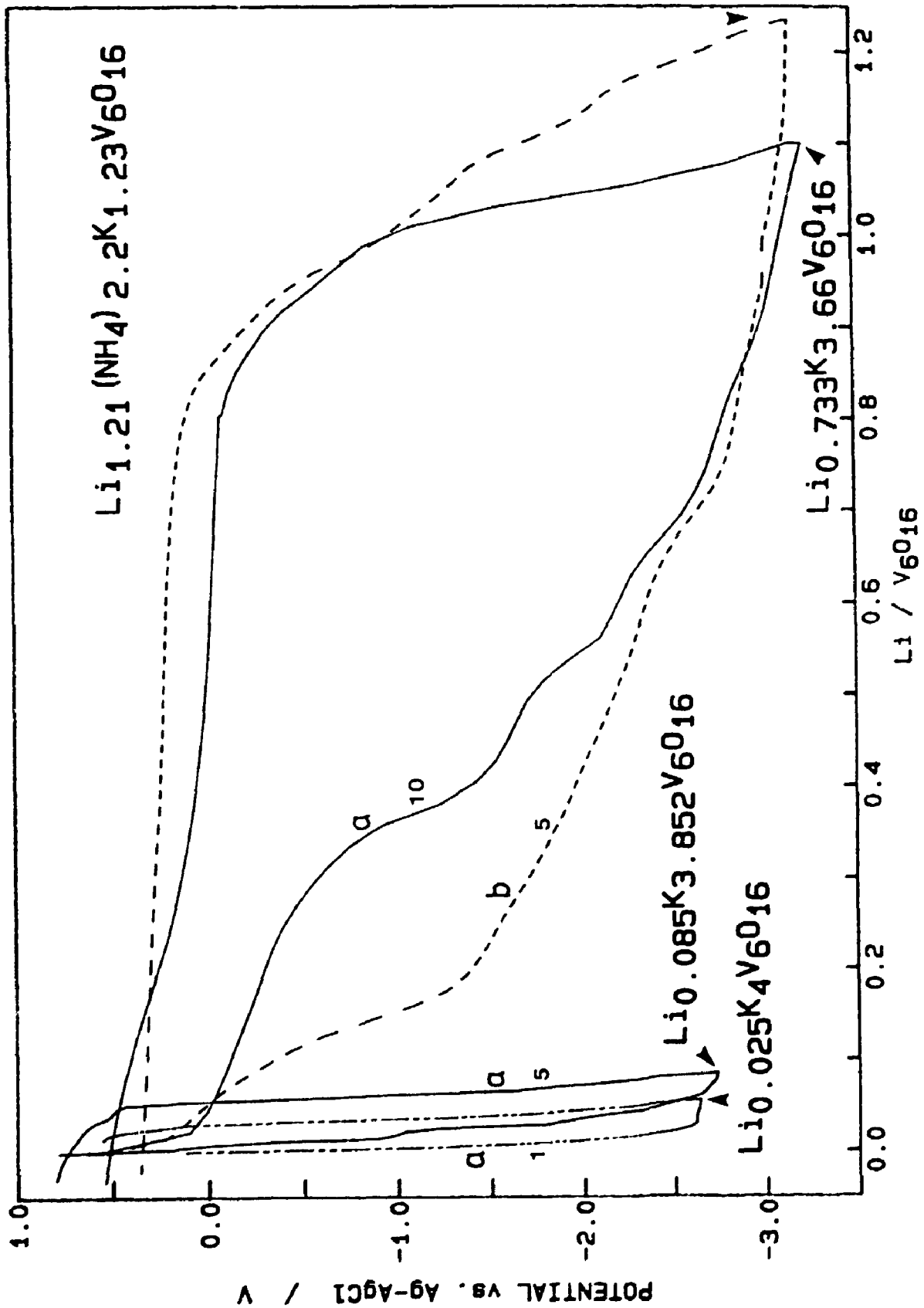
Li1.21 (NH4) 2.2K1.23V6O16
Li0.733K3.66V6O16
Li0.085K3.852V6O16
Li0.025K4V6O16
a 10
b 5
a 5
a 1
POTENTIAL vs. Ag-AgCl / V
Li / V6O16
1.0
0.0
-1.0
-2.0
-3.0
0.0
0.2
0.4
0.6
0.8
1.0
1.2

CHAPTER 6

RESULTS OF THE THERMAL DECOMPOSITION OF HEXAVANADATES

6.1 Introduction

The electrodes made by the electrodeposition methods described in chapters 4 and 5 contain either ammonium or some other alkali metal (K, Rb, Cs) in the hexavanadate structure. In this form, these electrodes show poor capacity for insertion of hydrogen or lithium which makes them unusable in their present form as cathodes for secondary lithium batteries. However, by mild thermal treatment of the ammonia-containing deposits, decomposition to more favourable products has been achieved and the formation, nature and use of these products as insertion electrodes will be discussed in this chapter.

6.2 Results

Vanadium oxides have in the past have always been made by high temperature synthesis. Cathodes for lithium batteries are then made by mixing the oxide with a binder and conducting material. Some recent work has examined the thermal decomposition of NH_4VO_3, which, under a flow of inert gas, forms oxides in the composition range from V_2O_3 to V_2O_5 [64]. Other researchers have used this process to produce non-stoichiometric V_6O_{13} [16,65]. This thesis reports a method of obtaining a range of pure vanadium oxides on a conducting support from the decomposition of ammonium hexavanadates. The decomposition of $(NH_4)_4V_6O_{16}$ to form V_6O_{13} is known to occur for hydrated hexavanadates as discussed by Bernard *et al.* [24].

6.2.1 Formation and Nature of Pure Vanadium Oxides

The decomposition of ammonium hexavanadates to a "pure" vanadium oxide, i.e., with only vanadium and oxygen present, occurs for both the anodic and cathodic deposits containing only NH_4^+. There are some differences in the final product and the mechanism of decomposition will be discussed in section 6.2.2.

6.2.1.1 Decomposition of the Anodic Deposit

Earlier it was mentioned that mole ratio $y = (NH_3+H_2O)/V_2O_5$ was a function of the temperature of drying, where the initial deposit has a value of $y \approx 1.3$. Heating the deposit above 300°C for 24h gives (by chemical analysis) a product with $y = 0$, i.e., pure vanadium pentoxide (table 4.1). This was confirmed by X-ray diffraction, with checks from the pattern of a known V_2O_5 powder (Fisher Certified) and with the ASTM powder diffraction pattern of orthorhombic V_2O_5 [66]. The differences in the peak intensities of the decomposed V_2O_5 and the ASTM values [66,67] can be accounted for by the highly oriented, crystalline structure of the deposit. Heating at 350°C speeds up the process and decomposition is complete within 1h. A SEM photograph of the heated deposit in plate 6(a) shows that heating the deposit causes the crystals to split into many layers, but leaves the overall shape and orientation of the crystals intact.

A problem with the choice of axes used to describe a particular direction in the unit cell has been observed in the literature. For example, Bachman *et al.* [68] and Wyckoff [69] as well as some recent authors, including Murphy *et al.* [9,10], interchange the b and c axes

given in [66] and [67]. However, both these choices are not crystallographically correct for the orthorhombic system since the choice of axis should follow the general rule that $b > a > c$ [59]. In order to compare our decomposed oxides to X-ray patterns given in the ASTM index, the convention used in the NBS X-ray tables [59] will be used (see table 6.2 and figure 6.1).

An X-ray diffraction pattern for the decomposed anodic deposit is shown in figure 6.1. Comparison of the peak intensities with the observed crystal morphology and the crystal structure of a true X-ray powder pattern for orthorhombic V_2O_5 [66,67] indicates that the *bc* plane of the crystals lies predominantly in a direction perpendicular to the electrode surface, while the *a* axis, which is perpendicular to the largest crystal face, is predominantly parallel to the electrode. Thus, for example, reflections from the [*220*] plane at 22.2°, the [*160*] plane at 26.0° and the [*240*] plane at 26.3° are missing (fig. 6.1). The unit cell dimensions for our thermally composed V_2O_5 was compared in table 6.2 with good agreement with the ASTM pattern [66,67] and the results of Bachman *et al.* [68].

The evidence from electron microscopy and from X-ray diffraction indicates that the hexavanadate has a structure similar to that of orthorhombic V_2O_5; otherwise, the crystals would not retain their overall shape on decomposition, and at the same time give the X-ray pattern for orthorhombic V_2O_5. The NH_3 and H_2O present in the hexavanadate probably lie between the vanadium-oxygen layers in the crystal and this can be seen from the increase in the *d*-spacings of the hexavanadate for (*001*) plane compared to the (*100*) of V_2O_5. This structure has been suggested by Aldebert *et al.* [70] for amorphous V_2O_5

gels, which do not contain extraneous ions, except perhaps H^+. It has also been observed that propylene carbonate, DMSO, DMF and other solvents of high polarity can replace inter-layer water in V_2O_5 gels [41,71,72]. This effect was not observed for decomposed deposits indicating that the cavities of sufficient size are not available once the ammonia and water have been removed.

6.2.1.2 Decomposition of Cathodic Deposits $(NH_4)_4V_6O_{16}$

Heating at 300°C in air for several hours caused the black deposit to change to a brown-orange colour. Chemical analysis gave less than 0.5 mol% V(IV) and 28.6 mol% V(V), corresponding to V_2O_5 (table 6.1). Comparison of laser Raman spectra for the deposit with single-crystal Raman data [60] confirmed that the deposit was V_2O_5. The X-ray diffraction pattern matches the ASTM file for orthorhombic V_2O_5 [66,67] except for changes in the peak intensities, which again result from the high degree of orientation of the deposit. The small differences between the peak intensities of the anodic and cathodic heated deposits can be attributed to a higher packing density of the crystals for the cathodic deposits. Heated deposits show no major changes in the structure or orientation of the crystals (plate 6(b)), and no splitting of the crystals as seen for decomposition of hydrated ammonium hexavanadates, due in part to the milder and more gradual heating conditions used in their decomposition (table 6.1). These conditions also greatly reduced the amount of flaking off of the sample during heating, leaving an improved electrode for electrochemical measurements.

On heating the tetrammonium hexavanadate under reduced oxygen

partial pressure, either using argon (see section 6.2.2.3) or under a vacuum of about 1 x 10^{-3} torr, non-stoichiometric V_6O_{13} was formed (table 6.3). The temperatures used were again about 300°C, but the times needed were longer, in the range of 3 to 24 hours. This was confirmed by both chemical analysis and X-ray diffraction. Heating under these conditions again caused no change in the crystal morphology (plate 6(c)), although the X-ray pattern did change dramatically. A typical X-ray pattern in shown in figure 6.1, in which the peaks are much broader than for the orthorhombic V_2O_5, possibly due to some non-crystallinity in this oxide. These peaks that are present in our case match well with those for V_6O_{13} [66,73]. However, many minor peaks cannot be seen because of the greater than normal noise of the spectrum. The unit cell dimensions for a monoclinic unit cell have been calculated for a few of these oxides under different decomposition conditions (figure 6.1) given in table 6.3. The errors in the unit cell dimensions were very large because of the broadness of the few peaks that could be indexed. Both the X-ray pattern and unit cell dimensions of the air-decomposed anodic diammonium and cathodic tetrammonium hexavanadate agree with the ASTM results [66,67] (table 6.2). This was also true for the non-stoichiometric V_6O_{13} compared to the V_6O_{13} ASTM pattern [66,73].

The broadness of these peaks for vacuum-decomposed hexavanadate indicates some non-crystallinity and non-uniformity to the oxide stoichiometry, which in fact was confirmed by the chemical analysis of the decomposed deposit. The analysis corresponds to a non-stoichiometric $V_6O_{13+\delta}$, where δ has a range depending predominantly on the time of decomposition; see table 6.2. The value of δ has been

found to range from almost 0.0 to 1.0, indicating that a broad range of oxides from V_3O_7 to V_6O_{13} can be made, all with the apparent structure of orthorhombic V_6O_{13}. The formation of a broad range of non-stoichiometric oxides of V_6O_{13} has been observed by other workers [16,65] by thermal decomposition of NH_4VO_3. They found the desired stoichiometry of the final product hard to obtain, possibly because of lack of control of such factors as the heating rate and the flow rate of inert gas.

6.2.1.3 Decomposition of Cathodic Deposits With Alkali Metals

The stability of alkali metal hexavanadates upon heating up to over 400°C is very good, i.e., there was very little change in the amount of vanadium present or of the alkali cation, with extremely small amounts of oxidation occurring during a time equal to that taken to decompose ammonium hexavanadates. The heating of mixed-phase hexavanadates which contained the ammonium ion do show thermal decomposition of the original sample. The loss in weight and increase in the amount of vanadium in the sample agree within experimental error with the loss of ammonia and water, as summarized for the mixed phase $(NH_4)_{0.8}K_{3.2}V_6O_{16}$ in table 6.4. The mechanism of decomposition will be discussed later in section 6.2.2.4. Only when ammonium ion is present in the hexavanadate do noticeable structural changes take place in the hexavanadate at the mild heating temperatures used to give non-stoichiometric alkali-metal hexavanadates.

6.2.2 Mechanism of Decomposition

The decomposition of tetrammonium hexavanadates differs slightly

from the diammonium hexavanadate, because of the presence of V(IV) in the deposit. The partial pressure of oxygen influences the mechanism of decomposition.

6.2.2.1 Anodic Deposits

Simultaneous DTA, DTG and TGA traces on the hydrated diammonium hexavanadate, $(NH_4)_2V_6O_{16}$, are shown in figure 6.2. The anodic deposit shows three endothermic DTA peaks at 235, 345, 400°C, respectively, and an exothermic peak at 470°C (scan rate 25 K/min). The total loss in weight over the whole temperature range by chemical analyses and X-ray diffraction corresponds to the net reaction

$$(NH_4)_2V_6O_{16}\cdot H_2O \longrightarrow 3\ V_2O_5 + 2NH_3 + 2H_2O \qquad (6.1)$$

for which the loss is 11.38 % or 9.24 mg on an 81.2 mg sample; the observed value is 9.2 mg.

The monohydrate contains 2.93 % H_2O, loss of which on heating corresponds to 2.4 mg on 81.2 mg; this is indicated by region I in fig. 6.2. The first two endothermi TA peaks appear to be roughly equal in area, span region I, and thus correspond to loss of hydrated water in two equal steps each of 0.5 H_2O per mole anhydrous salt. The next endothermic peak is postulated to result from partial reduction of V(V) to V(IV) and release of NH_3 and H_2O, a process which begins before dehydration is complete (regions II plus III, fig. 6.2). The reducing agent is presumably ammonia, so that some nitrogen is also formed:

$$(NH_4)_2V_6O_{16} \longrightarrow 3V_2O_{5-\delta} + \delta N_2 + (1+3\delta)H_2O + 2(1-\delta)NH_3 \qquad (6.2)$$

(The non-stoichiometric V_2O_5 corresponds to V_3O_7 if $\delta = 1/3$, and to V_6O_{13} if $\delta = 2/3$).

Bernard and Theobald [55] were the first to establish that compounds similar to $(NH_4)_4V_6O_{16}\cdot xH_2O$ prepared by reaction of V_2O_5 with zinc and aqueous NH_4Cl actually contained ammonia. They observed the reduction of V(V) during heating, and attributed this to the liberated ammonia. Deschanvres *et al.* [74] made similar claims for the thermal decomposition of diammonium hexavanadate. Von Sacken and Dahn [64], using a quadrupole mass spectrometer for gas analysis, actually detected small amounts of nitrogen during the thermal decompostion of ammonium metavanadate. Possible production of nitrogen in our experiments was checked by mass spectrometry on a sample of diammonium hexavanadate placed directly on the hot probe inside the mass spectrometer. The probe was heated over the temperature range 50 to 500°C, with monitoring of masses 17, 18 and 28 (NH_3, H_2O and N_2 respectively). Release of NH_3 and H_2O at temperatures indicated by the DTA results was observed, but detection of N_2 was inconclusive because of the high background of this gas in the apparatus. With V_2O_5 gels dried at various temperatures [72,75], it was found that V(IV) was oxidized to V(V) by oxygen between 300 and 360°C, so that spontaneous partial reduction is improbable, even in the presence of large concentrations of ammonia and water vapour at the surface, where the partial pressure of oxygen is lowered below that of the surrounding air.

In region III, the small increase in weight corresponds to re-oxidation of V(IV) to V(V), as with V_2O_5 gels [41,75], but at a higher temperature:

$$V_2O_{5-\delta} + \delta/2\ O_2 \longrightarrow V_2O_5 \qquad (6.3)$$

a process which, along with recrystallization, gives rise to the large exothermic peak. It is not possible to separate the decomposition-reduction and re-oxidation processes, which clearly overlap over a range of about 30 K. In DSC, only a large endothermic peak at 360°C (10 K/min) was seen because of difficulties in obtaining a good baseline and the upper temperature limit imposed by the calorimeter (700 K).

6.2.2.2 Cathodic Deposits in Air

Simultaneous DTA, DTG and TGA traces on the cathodic deposit of hydrated tetrammonium hexavanadate, $(NH_4)_4V_6O_{16}\cdot yH_2O$, are shown in figure 6.3. DTA (scan rate 10 K/min) reveals four endothermic peaks at 195, 218, 268, and 332°C, respectively, and two exothermic peaks at 310 and 365°C (figure 6.3). DSC confirms the DTA results. The overall loss in weight by chemical analyses and X-ray diffraction corresponds to the reaction

$$(NH_4)_4V_6O_{16}\cdot yH_2O + 1/2\ O_2 \longrightarrow 3V_2O_5 + 4NH_3 + (y+2)H_2O \qquad (6.4)$$

for which the net loss is 16.29 % if $y = 1.0$; the observed value is 15.6 mg on 103.0 mg sample, or 15.1 %, suggesting that some slight dehydration of the initial product (to $y = 0.50$) in air drying occurred, as in the first entry of table 6.3. Region I in fig 6.3 marks the loss of this amount of water: 1.40 % or 1.44 mg on 103.0 mg.

The large endothermic DTA peak corresponds, as with $(NH_4)_2V_6O_{16}$, to

the start of decomposition with the loss of ammonia and water. The second and third entries in table 6.1 indicate that, for long heating times, the reaction

$$1/2\ O_2 + (NH_4)_4V_6O_{16} \longrightarrow (NH_4)_2V_6O_{16} + H_2O + 2NH_3 \qquad (6.5)$$

may occur, with solids containing fractions 0.8 and 0.2 of $(NH_4)_4V_6O_{16}$ for the two successive entries. For the fourth entry, all $(NH_4)_2V_6O_{16}$ has disappeared, and decomposition has occured to a mixture of $(NH_4)_2V_6O_{16}$ and $V_2O_{5-\delta}$, in mole ratio 7:3 for $\delta = 0$ (or 17:3 for $\delta = 1/3$, 9:1 for $\delta = 2/3$) according to eqn (6.2) above. Thus, decomposition appears to occur in two stages. That described by eqn (6.5) has almost reached completion in the DTA experiment at 300°C; the DTA curve rises towards the baseline, and the rate of loss of weight decreases. Decomposition according to eqn (6.2) then begins (at a somewhat lower temperature than for pure $(NH_4)_2V_6O_{16}$, consistent with the lower scan rate), and the DTA curve decreases again, giving rise to the maximum at 332°C. Finally, decomposition is complete, and oxidation occurs according to eqn (6.3).

Thus, thermal decomposition proceeds via similar mechanisms for both $(NH_4)_2V_6O_{16}$ and $(NH_4)_4V_6O_{16}$. The differences arise from the larger initial content of V(IV) in the latter, and probably a resulting lower Gibbs energy change for reaction (6.5) compared to (6.2) which, in turn, makes decomposition of the tetrammonium salt easier than that of the diammonium salt at a given temperature.

Decomposition of diammonium hexavanadates to form V_2O_5 has been reported before [76], but there has been no mention of the formation of V_2O_5 from tetrammonium hexavanadates.

6.2.2.3 Cathodic Deposits in Argon

Simultaneous DTA, DTG and TGA traces on the cathodic deposit of hydrated tetrammonium hexavanadate, $(NH_4)_4V_6O_{16}\cdot yH_2O$, are shown in figure 6.4 when decomposed under an argon atmosphere. DTA (scan rate 10 K/min) reveals three endothermic peaks at 193, 215, and 268°C, respectively, and one exothermic peak at 382°C (figure 6.4). The overall loss in weight by chemical analyses corresponds to the reaction

$$(NH_4)_4V_6O_{16}\cdot 0.5H_2O \longrightarrow V_6O_{13.77} + 4NH_3 + 2.5H_2O + 0.115\ O_2 \quad (6.6)$$

for which the net loss is 18.23 %; the observed value is 18.3 mg on 100.4 mg sample, or 18.20 %. Region I in fig 6.4 marks the loss of this amount of water: 1.41 % or 1.40 mg on 100.4 mg.

The large endothermic DTA peak corresponds, as with $(NH_4)_4V_6O_{16}$ decomposed in air, to the start of decomposition with the loss of ammonia and water. However, as shown in eqn (6.5) for air decomposition this reaction would not occur since a reduced species is formed under these conditions (40% V(IV) of total V - chemical analysis) after decomposition is complete. Decomposition occurs only in a similar manner to eqn (6.2). The large endothermic peak was postulated to result from the partial reduction of V(V) to V(IV) and release of NH_3 and H_2O, a process which begins before dehydration was complete (regions II & III fig. 6.4). The reducing agent was presumably ammonia, so that some nitrogen was also formed:

$$(NH_4)_4V_6O_{16}\cdot yH_2O \longrightarrow V_6O_{13+\delta} + (4-2/3\delta)NH_3 + \delta/3N_2 + (2+y+\delta)H_2O \quad (6.7)$$

(The non-stoichiometric V_2O_5 corresponds to V_3O_7 if δ = 1/3, and to V_6O_{13} if δ = 2/3). It was presumed in this case that in the first step of the bulk decomposition that δ = 1/3.

In region III, the continued loss of weight corresponds to further reduction of V(V) to V(IV) as given by:

$$V_3O_7 \longrightarrow V_3O_{7-\delta} + \delta/2\ O_2 \quad (6.8)$$

where now the value of δ can range from 0.0 to 0.5; for this specific example, δ = 0.385. With large bulk recrystallization occurring at this point, only a very small exothermic peak is seen compared to the large one which is principally due to the oxidation process that occurs during decompostion in air. Again it is not possible to separate the decomposition-reduction processes, which clearly overlap over a range of about 30 K.

Thus, thermal decomposition proceeds via different mechanisms for $(NH_4)_4V_6O_{16}$ decomposed in air and in argon. The differences arise from the absence of the reaction occurring in eqn (6.5) and the inclusion of the reduction reaction shown in eqn (6.8). Decomposition of tetrammonium hexavanadates to form V_6O_{13} has been seen by other researchers and confirmed using X-ray analysis [24]. DTA and chemical analysis has helped confirm that thermal decomposition yields a non-stoichiometric oxide with the X-ray diffraction pattern matching V_6O_{13} [16,65]. Thus, Bernard *et al.* [24] probably formed a non-stoichiometric form of V_6O_{13} that cannot be distinguished from pure V_6O_{13} as seen in this thesis and by other researchers [16,65].

6.2.2.4 Decomposition of Cathodic Deposits With Alkali Metals

Simultaneous DTA, DTG and TGA traces on the cathodic deposit of the mixed phase of tetrammonium and potassium hexavanadate with stoichiometry $(NH_4)_{0.8}K_{3.2}V_6O_{16}$ are shown in figure 6.5. DTA (scan rate 10 K/min) reveals a single endothermic peak at 286.6 °C and a single exothermic peak at 376.9 °C (figure 6.5). The overall loss in weight by chemical analyses corresponds to the following reaction (table 6.4);

$$(NH_4)_{0.9}K_{3.1}V_6O_{16} + 0.105O_2 \longrightarrow K_{3.1}V_6O_{15.75} + 0.9NH_3 + 0.45H_2O \quad (6.9)$$

for which the net loss is 2.87 % ; the observed value is 1.6 mg on 55.27 mg sample, or 2.89 %, in very good agreement, and suggesting that the initial product is unhydrated (table 6.4).

The large endothermic DTA peak corresponds, as with $(NH_4)_2V_6O_{16}$, to the start of decomposition with the loss of ammonia and water. Here, as with the tetrammonium hexavanadate the decomposition appears to occur in two stages. That described by eqn (6.5) has almost reached completion in the DTA experiment at 300°C; the DTA curve remains steady for a while and the rate of loss of weight decreases dramatically. Decomposition according to eqn (6.2) then begins, and the DTA curve decreases again, giving rise to the maximum at 376.9°C. Finally, decomposition is complete, and oxidation occurs according to eqn (6.3).

Thus, thermal decomposition proceeds via similar mechanisms to $(NH_4)_4V_6O_{16}$ with the endothermic and exothermic peaks corresponding to the same temperatures, when the different scan rates are taken into account.

6.2.3 Insertion of Ions

6.2.3.1 V_2O_5 from Diammonium Hexavanadate

Insertion of various alkali metal ions was attempted on electrodes of these decomposed electrodeposits on SnO_2, Pt and Ni subtrates. Lithium ions inserted into the V_2O_5 electrodes in both aqueous and non-aqueous solutions of propylene carbonate and dimethylformamide to give a lithium vanadium bronze. This cathodic reaction is [77]

$$xLi^+ + xe^- + V_2O_5 = Li_xV_2O_5$$

The charge injected was measured by passing a measured constant current for a known time. A typical galvanostatic charging curve is shown in fig. 6.6 for a V_2O_5 electrode made from an anodic deposit. The initial times were found from the intersection of the extrapolated double layer charging portions and the plateau portions of these curves, as shown in the figure. The final time always corresponded to a point on the plateau of the charging curve. Lithium was measured by atomic absorption and the V(IV) in the bronze by chemical analysis. For atomic absorption a blank was used, which consisted of a V_2O_5 electrode placed in the same solution for the same length of time as the electrode actually being reduced. This compensated, at least partially, for any traces of lithium remaining from incomplete removal of solution.

The results of these analyses are given in table 6.5. The analyses for Li by AA may be in error by as much as 10 %, while the chemical analyses for V(IV) are precise to about 1 %, or 2 % on samples as small as 10 mg. The total amount of vanadium could be determined with a precision of about 0.5 %. Thus the data in table 6.5 show that the

charge injected corresponds, within experimental error, to the amount of lithium inserted and to the amount of V(IV) formed, and provide strong evidence that the inserted lithium was present as ions rather than as lithium atoms.

There are small discrepancies between the charge injected and the amount of V(IV). In some cases, these could be accounted for by the finite solubility of V(IV) species which was detected by the colour changes in aqueous solutions. Systematic investigation of the error due to solubility was not carried out, and one example will suffice. For an injected charge of 2.059×10^{-5} mol, the amount of V(IV) on the electrode was 1.74×10^{-5} mol, while 0.31×10^{-5} mol V(IV) was found in solution, giving a total of 2.05×10^{-5} mol V(IV) by chemical analysis, in good agreement with the coulometric value. The solubility of vanadium (IV) in water appears to be somewhat greater than that of V(V). This phenomenon, since published [78], has been confirmed by other researchers [79] studying ion insertion reactions at a vanadium pentoxide cathode. The discrepancy due to solubility between the charge injected and the amount of V(IV) or Li^+ on the electrode is smaller in non-aqueous solutions (table 6.5). In other cases, part of the decomposed deposits tended to flake off the substrate, making reliable analyses difficult. This was especially true for other substrates such as platinum or stainless steel. Once it was verified that Li does indeed insert via the chemical reaction given above, chemical analysis for V(IV) in the bronze was the primary method used to derive values of x.

The electrochromic behaviour of these deposits was quite apparent. Starting from the orange-red of V_2O_5, insertion of Li^+ or H^+ causes a

gradual colour change from light to dark green to almost black as the limit to insertion is approached. This was also found to be a reversible process: starting with a greenish bronze, removal of Li^+ and electrons leaves an electrode with the same orange-red colour of V_2O_5. As the amount of inserted Li increases in electrodeposited V_2O_5, there is a corresponding reduction of V(V) to V(IV), as expected for the reaction given above. Lithium, therefore, can be readily inserted into this pure V_2O_5 electrode forming a ternary phase [77] with little change in structure.

6.2.3.2 X-ray Photoelectron Spectroscopy of $Li_xV_2O_5$

Figure 6.7 shows X-ray photoelectron spectra for deposits into which lithium has been inserted. The spectra are characterized by two peaks, with average binding energies 516.6 eV for V(IV) and 517.9 eV for V(V). The XPS binding energies, (B.E.), for the pure V_2O_5 electrode agree with that of Larsson and Folkesson [80]. The growth of the peak due to V(IV) with increasing amounts of lithium is apparent, and confirms the conclusion from chemical analysis that vanadium (IV) is present, and therefore that the inserted lithium is in ionic form. The binding energies for vanadium and oxygen are summarized in table 6.6 and apparently show small shifts with x. These shifts appear to correlate more or less with the phase changes occurring in the bronze and are shown in figure 6.8. From the figure, the binding energy for V(IV) and V(V) shifts are small, but noticeable between the three phases of $Li_xV_2O_5$, with a linear portion in the central ϵ-phase region of the bronze (see chapter 7 for discussion on bronze structure). The value for V(IV) at $x = 0$ is result of the curve fitting process for XPS which

gives a value of 3% V(IV) present although chemical analysis gives < 0.5%. This type of behaviour has not been reported before for phase changes in intercalation oxides. However, an attempt at interpreting the spectra quantitatively was complicated by the small value of these shifts and the small separation between the binding energy of V(IV) and V(V) (about 1.2 eV). Furthermore, quantitative correlation of the values of x from chemical analysis and from XPS was difficult because of the possibility of a significant amount of reduction of V(V) to V(IV) in the electron beam. This phenomenon has been observed in a few electron beam experiments for pure vanadium pentoxide; for example, Curelaru *et al.* [81] observed a change over long times in the chemical composition from V_2O_5 to V_6O_{13} using APS and XPS. It was felt that over the time of the experiment this effect should be almost negligible and values from XPS for the ratio V(IV)/V(V) can be larger than expected from chemical analyses since XPS yields only a semi-quantitative number.

6.2.3.3 Insertion of Ions: Ion Selectivity

Electrodes of V_2O_5 prepared by decomposition of ammonium hexavanadate deposits on various conducting substrates appear to behave identically with composite V_2C_5 electrodes in terms of insertion of lithium. The presence of ammonia and water between the crystal layers in the hexavanadates has a definite influence on the amount of Li that can be inserted. The maximum value of x in $Li_xV_2O_5$ found for the diammonium hexavanadate was about $x = 0.48$, while for etrammonium hexavanadate it was less than $x = 0.1$. Insertion curves for a V_2O_5 electrode on a platinum substrate and on a thinner sample of 10-20 μm on a nickel substrate (fig. 6.9) show maximum values for V_2O_5 of $x = 1.75$

for Pt substrates and $x = 2.01$ for Ni in $Li_xV_2O_5$. The mid-point between the two plateaus in fig. 6.9 corresponds to a charge which is about 1 per cent higher than the value given by chemical analysis (table 6.5). This small difference probably arises from double layer charging, which is included in the total charge passed. The maximum value found for the insertion of H^+ from trace $HClO_4$ in non-aqueous propylene carbonate solutions was found to be $x = 4.4$. The insertion of protons is much higher compared to Li because of its relatively small size. It is for this reason also that very little change in the X-ray diffraction pattern is seen for the $H_xV_2O_5$ bronzes compared to the insertion of similar amounts of lithium. The insertion of other ions such as Na^+ and K^+ did not occur in any detectable amounts, probably because of their larger diameters. Lack of insertion was confirmed by chemical analysis and by the X-ray diffraction patterns, where no change in structure from the original V_2O_5 electrode was found.

Although it is possible to insert large amounts of lithium into these V_2O_5 electrodes, their optimum use as reversible cathodes in batteries may require insertion of less lithium. Figure 6.10 shows the changes in potential during several insertion-removal cycles up to various values of x in $Li_xV_2O_5$. For cycles up to the maximum x (i.e., past the second plateau) a definite hysteresis occurs between the insertion and removal curves suggesting irreversibility. However, the results for $x < 1.2$ show much better reversibility. This finding supports earlier suggestions that additional lithium at $x > 1$ causes disproportionation into V_2O_3 and $LiVO_3$ [29]. A phase change at $x = 1.33$ has been observed, indicating low stability of $LiVO_3$ and formation of more V_2O_3 as well as Li_3VO_4 [82].

The insertion of lithium into non-stoichiometric $V_6O_{13+\delta}$, where δ lies in the range of about 0.9 to 0.08, was done for thermally decomposed tetrammonium hexavanadate (table 6.3). Insertion curves for the potential versus value of x are shown in figure 6.11 for three values of δ. There was a sharp drop in potential for the thicker electrodes (100 to 200 μm) of greater than 1 V when a value of Li/V of about 0.35 was reached. This was largely attributed to the loss of electrical contact between the vanadium oxide insertion electrode, electrochemically deposited and thermally decomposed, on the conducting substrate of either Pt or Ni. However, depositing thinner tetrammonium hexavanadate (50μm) at lower current density (0.1 mA/cm^2) reduced this problem to yield thermally decomposed electrodes that could insert lithium up to 0.8 lithium per vanadium (fig. 6.11). For the case where δ = 0.276 in figure 6.11, the insertion curve was very similar to that for composite V_6O_{13} electrodes of other researchers [16,65]. The insertion was stopped at this value to compare the actual charge passed with the amount of change in V(IV) content by chemical analysis before loss of contact of the oxide to its conducting was lost.

6.2.4 Electrochemical Impedance Results

Electrochemical impedance spectroscopy can be a powerful tool in examining electrochemical systems. Results for the impedance analysis for the symmetric cell:

$$V_2O_5 \ / \ \text{Tetraglyme} + LiClO_4 \ (O/Li = 12:1) \ / \ V_2O_5$$

are given in fig. 6.12 for 40 and 21°C. As the theory in Chapter 2

explains, it is possible to fit the data to a theoretical equivalent circuit. For this symmetric case the circuit is shown in figure 6.13(b). This circuit consists of a resistor (R_1) in series with a constant phase element (CPE2) in parallel with a second constant phase element (CPE1) and resistor (R_2). The constant phase element (CPE) is responsible for the low frequency shape in the impedance plane. The parameters for the equivalent circuits are given in table 6.7 where n is the power of the frequency in the equation:

$$Z = A\,(j\omega)^{-n}$$

When n = 1 we have a capacitor, with $n = 0.5$, a Warburg impedance and with n = 0, a resistor. As shown in table 6.7, the value of n is close to about 0.78 indicating an almost capacitor-like behaviour. Thus, the fitting of the circuit was good, although theoretically for an ideal blocking situation a low frequency spur of 90° would be expected [38]. In our case the value was approximately 70° and can be explained qualitatively by the complicated morphology of the cathode itself. A fractal model for the effect of a rough surface on the impedance spectroscopy has been proposed by Liu [83] and Liu *et al.* [84]. They have found that the constant phase element angle was directly related to the fractal nature of the interface. Thus, the exponent n is closely related to the roughness of the interface, where the interface becomes smoother as n approaches 1. As seen in the SEM photos, the V_2O_5 electrodes provide a rough surface and therefore the impedance results obtained for this V_2O_5 blocking electrode and a tetraglyme-$LiClO_4$ electrolyte seems consistent with this type of model.

The temperature dependance of the conductivity of the TEGDME + $LiClO_4$ (O/Li = 12) between V_2O_5 electrodes for different temperatures is

shown in figure 6.12. The curve was fitted using the Vogel-Tammann-Fulcher (VTF) equation

$$\sigma = (A/\sqrt{T}) \exp [-E/k(T-T_o)]$$

where least-squares parameters A = 0.063 S cm^{-1} $s^{1/2}$, E = 0.022 eV and T_o = 215 K. The fitting of these four points to the equation was good and the electrolyte-V_2O_5 electrode interface appears to make good contact and was stable in the temperature range over which measurements were made.

6.3 Conclusions

Decomposition of ammonium hexavanadates, under mild heating at about 300°C for 1h, results in the formation of an electrode containing essentially pure crystalline orthorhombic V_2O_5. No major changes occur in crystal morphology as NH_3 and H_2O leave the inter-layer positions between vanadium and oxygen. By decomposition of tetrammonium hexavanadates under low O_2 partial pressure (argon or vacuum atmosphere), a non-stoichiometric $V_6O_{13+\delta}$ is formed where δ varies from 0 to 0.9. The mechanism of decomposition depends on the method used and the presence of V(IV) and the amount of ammonia in the sample.

Reversible insertion of protons and Li^+ occurs in amounts seen by other researchers studying vanadium pentoxide composite electrodes. The structural changes that are seen on insertion of these ions into the vanadium pentoxide structure will be discussed in the next chapter. The use of these electrodes in a lithium single cell battery will be discussed in chapter 8.

Plate 6(a) SEM photo of decomposed diammonium hexavanadate on SnO_2 coated glass; X1220, bar length 8.2 μm.

6(b) SEM photo of decomposed tetrammonium hexavanadate on a Pt substrate; X245, bar length 41 μm.

6(c) SEM photo of decomposed tetrammonium hexavanadate on a Ni substrate under reduced O_2 partial pressure, heated 350°C for 20 h; X500, bar length 20 μm.


3
1.0
1.1
1.25
1.4
1.6
1.8
2.0
2.2
2.8
3.2
3.6
4.0
MicroD

Table 6.1. Chemical analysis of deposits made by cyclic voltammetry from 0.0 to -0.5 V (SCE) at 50 mV/s from aqueous NH_4VO_3, 0.2 mol/L followed by thermal decomposition.

temp. of heating /°C (time of heating/h)	V(IV) /10^{-5} mol	total V /10^{-4} mol	mass /mg	Mole ratio V(VI)/V(V)	formula of deposit from chemical analysis
180 (2.0)	7.83	2.463	26.00	0.466	$(NH_4)_4V_6O_{16.04}$
200 (0.5)	11.94	3.602	37.34	0 496	$(NH_4)_{3.6}V_6O_{15.8}$
200 (2.0)	4.22	1.747	17.50	0.318	$(NH_4)_{2.4}V_6O_{15.5}$
250 (16)	7.39	10.019	99.46	0.080	$(NH_4)_{1.75}V_6O_{15.7}$
300 (10)	1.85	10.877	100.51	0.017	$V_2O_{4.98}$
350 (12)	0.28	4.606	42.20	0.006	$V_2O_{5.00}$
DTA*	0.52	9.653	88.37	0.005	$V_2O_{5.00}$

* After DTA experiment, see section 6.2.2.2.

Table 6.2(a) Unit cell dimensions for orthorhombic V_2O_5

a/nm	b/nm	c/nm	X-ray sample
anodically this work[a]			
0.4379±0.0002	1.1503±0.0004	0.3565±0.0002	polycrystalline electrodeposit
cathodically this work[a]			
0.4370±0.0004	1.149±0.001	0.3567±0.0004	polycrystalline electrodeposit
ASTM Pattern 9 - 387 [66,67]			
0.4372±0.0001	1.1516±0.0003	0.3559±0.0001	single crystal
Bachmann *et al.* [68]			
0.4373±0.0002	1.1519±0.0006	0.3564±0.0002	single crystal

Table 6.2(b) Unit cell dimensions for monoclinic V_6O_{13}

a/nm	b/nm	c/nm	β	X-ray sample
Heated 355°C (13h)[a], δ = 0.311				
1.201 ±0.006	0.369 ±0.006	0.999 ±0.002	103.8° ±0.8	polycrystalline electrodeposit
Heated 350°C (20h)[a], δ = 0.215				
1.195 ±0.009	0.369 ±0.006	0.996 ±0.002	103° ±2	polycrystalline electrodeposit
K. Wilhelmi *et al.* [66,73]				
1.1922 ±0.0002	0.3680 ±0.0001	1.0138 ±0.0002	100.87° ±0.02	single crystal

[a] Indexing new, see table 6.3. Error limits are ±1 std. dev. in each of these cases.

Table 6.3 Chemical analysis of deposits made by heating under vacuum for diammonium and tetrammonium hexavanadate.

temp. of heating /°C (time of heating/h)	V(IV) /10^{-4} mol	total V /10^{-4} mol	mass /mg	value of δ from analysis for $V_6O_{13+\delta}$ δ	amount of x Li^+ that inserted $Li_xV_6O_{16+\delta}$
diammonium hexavanadate					
350 (2)	0.3663	4.336	39.15	1.754	NA
350 (4)	0.0770	4.381	39.63	1.947	NA
350 (6)	0.3204	8.683	78.78	1.889	NA
tetrammonium hexavanadate					
300 (10)	0.2031	0.688	6.40	1.115	2.462
300 (20)*	1.7629	4.490	42.63	0.822	2.22
350 (1.5)	1.814	3.758	32.96	0.552	NA
355 (5.0)	2.039	3.855	33.90	0.413	NA
355 (13)	2.934	5.213	46.95	0.311+	2.12
355 (16)	2.150	3.784	32.96	0.295	NA
350 (20)	3.176	5.337	47.25	0.215+	3.06
355 (23)	2.337	3.658	31.83	0.083	3.21
325 (20)	0.8455	1.471	12.73	0.276	4.74

* with Na_2SO_4 (0.8 mol/L) added to NH_4VO_3

+ X-ray pattern given with cell dimensions in table 6.2(b)

Table 6.4 Chemical analysis of thermally decomposed deposits of a mixed-phase hexavanadate containing the ammonium ion as one of the cations.

temp. of heating /°C (time of heating/h)	V(IV) /10^{-5} mol	total V /10^{-4} mol	mass /mg	Mole ratio V(IV)/V(V)	formula of deposit from chemical analysis
100 (1)	9.86	3.061	36.78	0.475	$(NH_4)_{0.6}K_{3.2}V_6O_{16}$
vacuum(no heat)	9.51	2.927	35.00	0.481	$(NH_4)_{0.8}K_{3.2}V_6O_{16}$
345 (1) (vacuum)	8.58	2.770	32.23	0.450	$(NH_4)_{0.6}K_{3.2}V_6O_{16.07}$
350 (14)	6.23	3.524	40.58	0.215	$K_{3.2}V_6O_{16.07}$
350 (28)	0.93	2.994	36.00	0.032	$K_{3.2}V_6O_{16.51}$
350 (100)	0.56	4.356	52.18	0.013	$K_{3.2}V_6O_{16.56}$
400 (DTA)*	10.54	3.980	43.60	0.360	$K_{3.1}V_6O_{15.76}$

* see section 7.2.2.4 for discussion of DTA results.

Table 6.5 Analysis of reduction of V_2O_5 electrode in contact with 1.0 mol/L $LiClO_4$ solution.

charge Li in passed /10^{-5} mol	deposit (by AA) /10^{-5} mol	V(IV) in deposit (by chemical analysis) /10^{-5} mol	total vanadium /10^{-4} mol	Mole ratio V(IV)/V(V)	value of x in $Li_xV_2O_5$
Blank					
0.000	0.03	0.0	2.173	0.00	0.0
Aqueous solution					
0.514	0.34	0.43	1.037	0.043	0.096
2.059	1.70	1.74	1.135	0.181	0.307
amounts in solution		0.31	0.100	0.449	0.62
totals and average *x*		2.05	1.235	0.199	0.332
9.098	8.42	8.48	2.615	0.480	0.648
Propylene carbonate solution					
1.489		1.48	0.897	0.198	0.330
5.875		5.67	2.245	0.338	0.505
2.990		2.94	0.633	0.867	0.930
13.990		13.67	2.749	0.989	0.994
Diammonium Hexavanadate in propylene carbonate solution					
3.005		2.995	1.590	0.232	0.377

Table 6.6 Binding energies of the vanadium and oxygen states present in the bronze $Li_xV_2O_5$ where x = 0.0, 0.10, 0.28, 0.53 and 0.93.

x in $Li_xV_2O_5$	B.E. V(V)	B.E. V(IV)	B.E. O^{531}	B.E. O^{530}	B.E. O^{532}	Ratio (XPS) O^{530}/O^{531}	Ratio (XPS) V(IV)/V(V)
0.00*	517.76	516.43	531.38	530.55			
0.00	517.75	516.46	531.94	530.54	533.53	9.45	0.033
0.10	518.12	516.68	531.77	530.82	533.09	5.98	0.233
0.26	518.01	516.55	531.43	530.60	532.33	3.35	0.466
0.53	517.75	516.42	531.75	530.40	533.05	2.81	0.915
0.93	517.96	516.79	531.79	530.80	532.95	2.14	1.197

* Binding energies from Larsson and Folkesson [80]

Table 6.7 The parameters of the equivalent circuit (figure 6.12) of the cell V_2O_5/tetraglyme-$LiClO_4$/V_2O_5 as a function of temperature.

Temperature / °C	R_1 / Ω	R_2 / Ω	CPE1 $Y_0 \cdot 10^2$ / S	n	CPE2 $Y_0 \cdot 10^4$ / S	n
55	3.43	6.33	4.80	0.77	7.43	0.71
40	4.45	10.80	3.90	0.78	5.05	0.71
29	6.76	16.46	3.16	0.79	5.62	0.70
21	8.34	21.16	2.95	0.78	5.28	0.69

Fig. 6.1 X-ray pattern for thermally decomposed ammonium hexavanadates to yield V_2O_5 or non-stoichiometric V_6O_{13}.

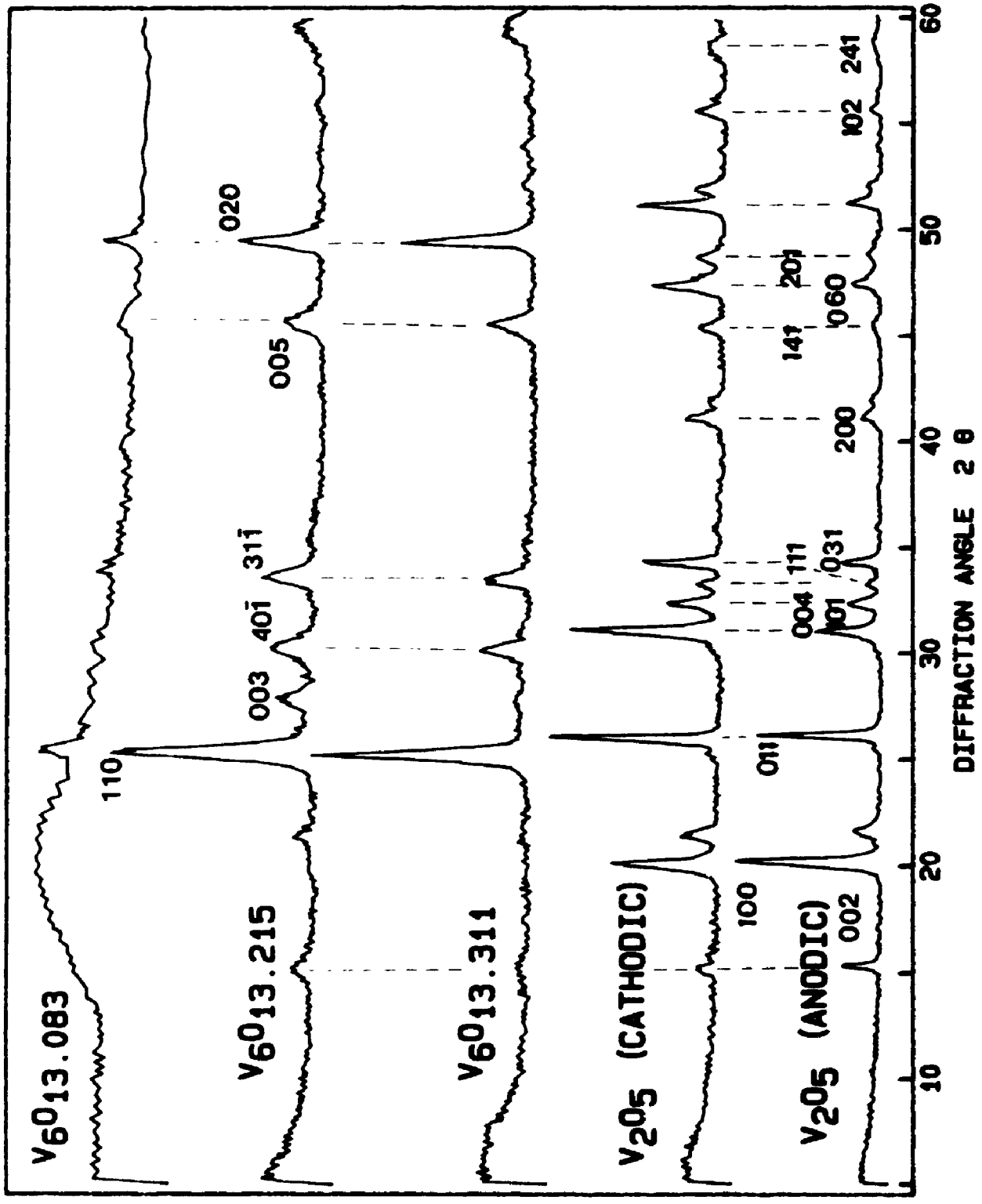
V_6O_{13}.083
V_6O_{13}.215
V_6O_{13}.311
V_2O_5 (CATHODIC)
V_2O_5 (ANODIC)
110
003
40$\bar{1}$
31$\bar{1}$
020
005
011
100
002
004
111
031
101
200
141
201
060
102
241
10
20
30
40
50
60
DIFFRACTION ANGLE 2 θ
RELATIVE PEAK INTENSITY

Fig. 6.2 TGA, DTA and DTG of anodic deposits $(NH_4)_2V_6O_{16}$. Scan rate 25 K/min. sample mass 81 mg. Base line for DTA is approximate. For explanation of regions I-III see text.

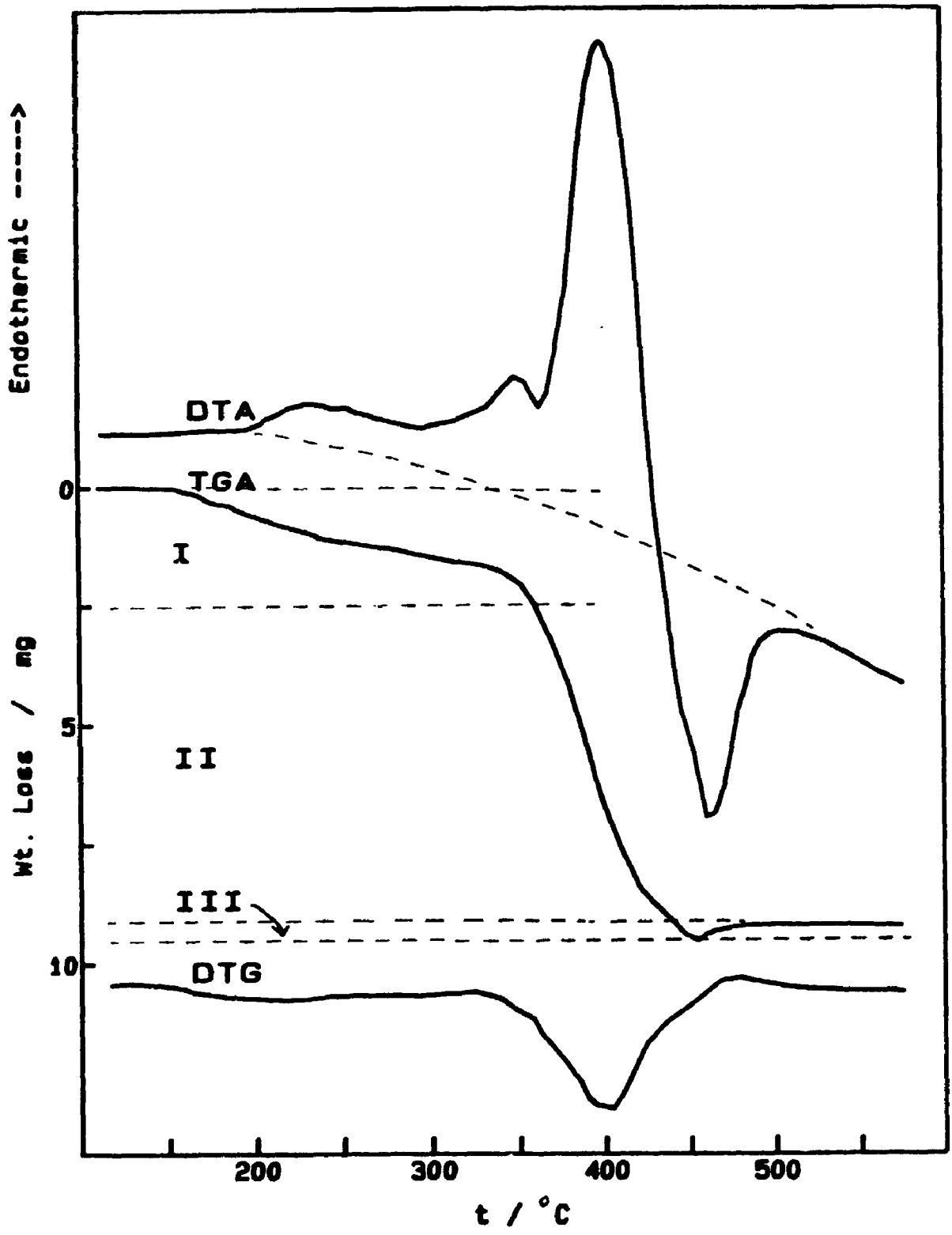
Endothermic ------>
DTA
TGA
0
I
II
III
5
10
DTG
Wt. Loss / mg
200
300
400
500
t / °C

Fig. 6.3 TGA, DTA and DTG of cathodic deposits $(NH_4)_4V_6O_{16}$ in air atmosphere. Scan rate 10 K/min. sample mass 103 mg.

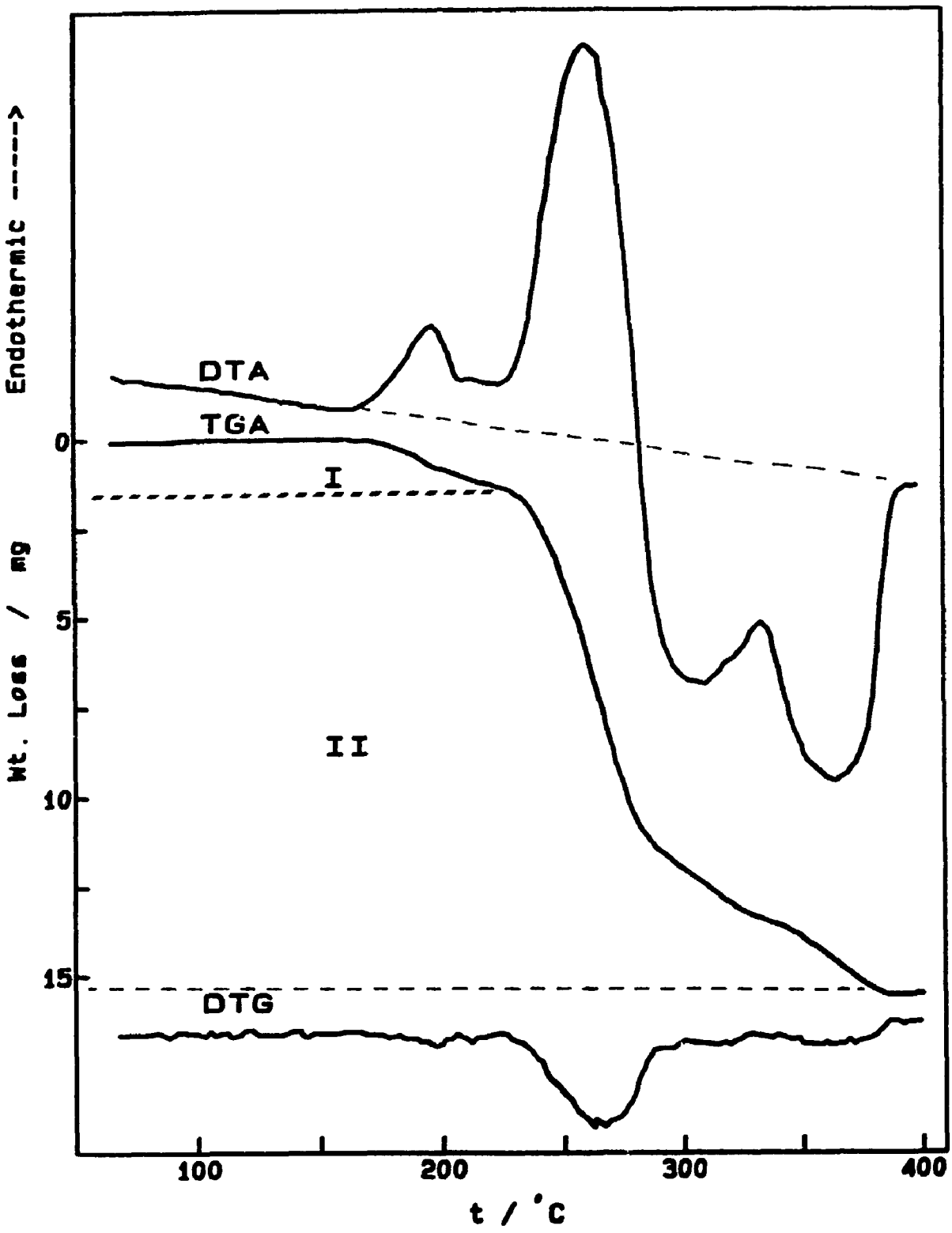
Endothermic ------>
DTA
TGA
0
I
5
II
10
15
DTG
Wt. Loss / mg
100
200
300
400
t / °C

Fig. 6.4 TGA, DTA and DTG of cathodic deposits, $(NH_4)_4V_6O_{16}$ in argon atmosphere. Scan rate 10 K/min. sample mass 100 mg.

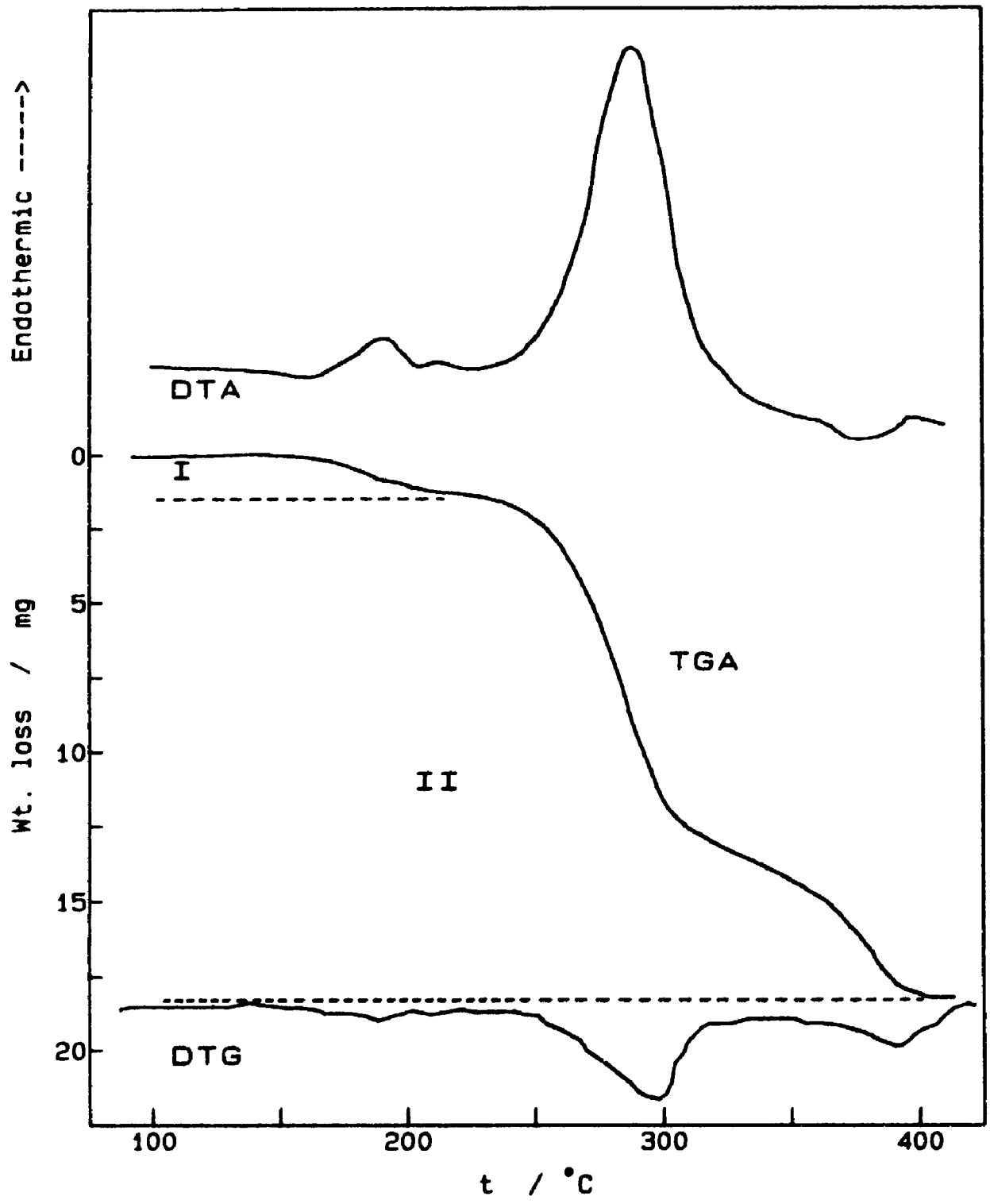
Endothermic ----->
DTA
0
I
5
TGA
10
II
15
DTG
20
Wt. loss / mg
100
200
300
400
t / °C

Fig. 6.5 TGA, DTA and DTG of cathodic deposits, of mixed phase $(NH_4)_{0.9}K_{3.1}V_6O_{16}$ in argon atmosphere. Scan rate 10 K/min. sample mass 55 mg.

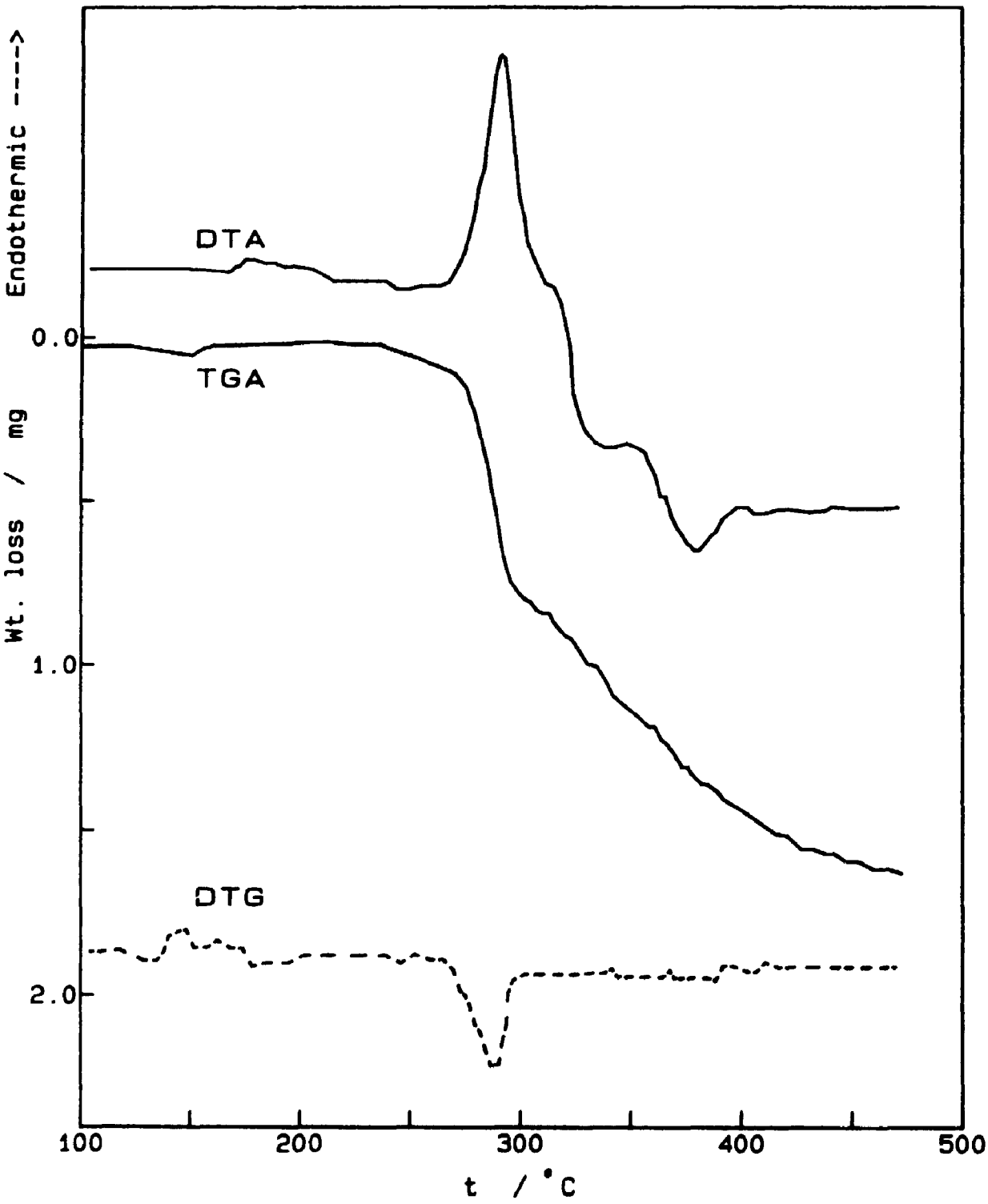
Endothermic ---->
DTA
0.0
TGA
Wt. loss / mg
1.0
DTG
2.0
100
200
300
400
500
t / °C

Fig. 6.6 Galvanostatic charging curve for Li insertion into dehydrated V_2O_5 on SnO_2 glass from 0.1 mol/L $LiClO_4$ in propylene carbonate; current density 0.8 mA/cm^2.

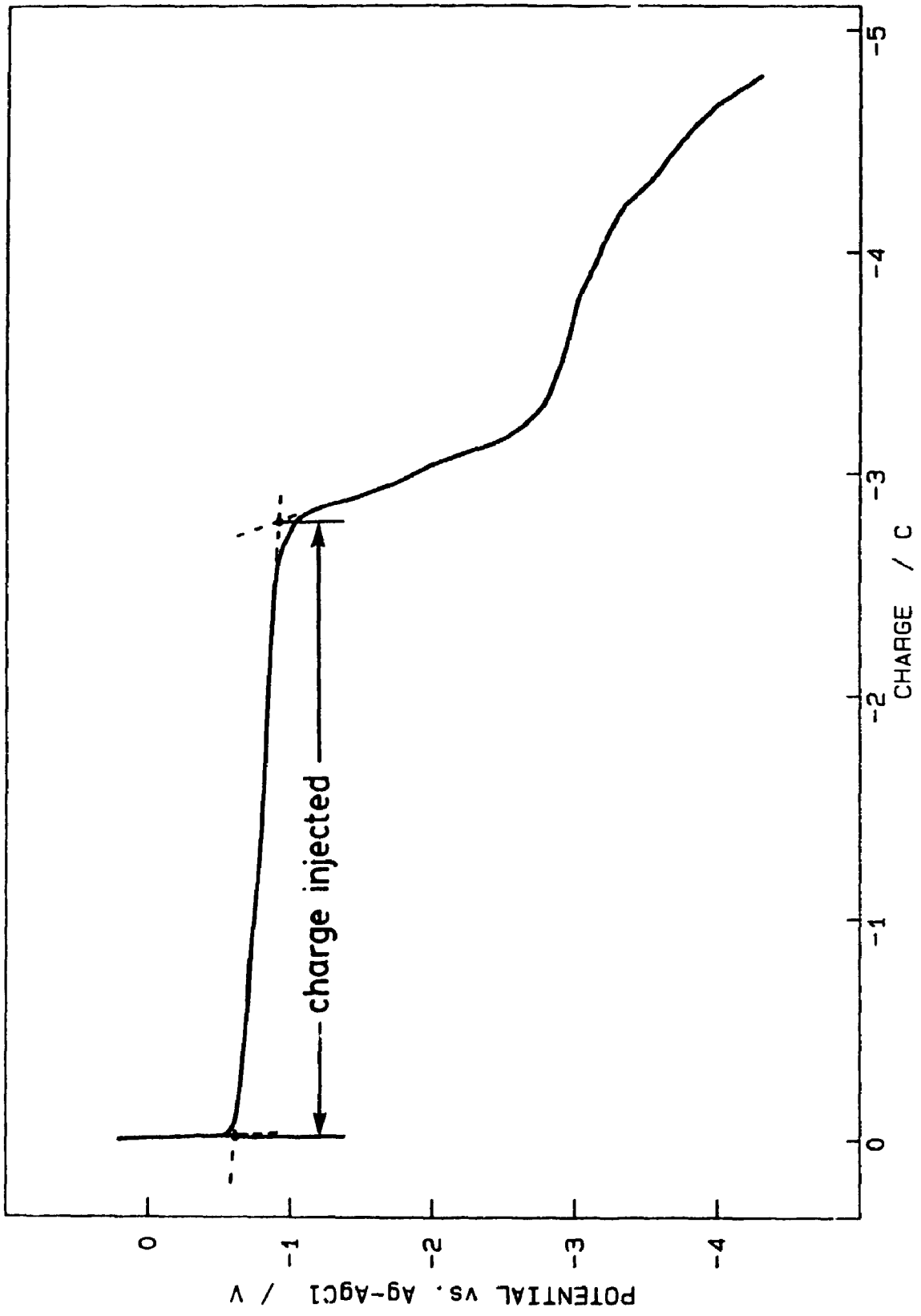
charge injected
CHARGE / C
0
-1
-2
-3
-4
-5
POTENTIAL vs. Ag-AgCl / V
0
-1
-2
-3
-4

Fig. 6.7 PES of electrochemically prepared V_2O_5 for $Li_xV_2O_5$ at x = 0.0, 0.10, 0.51 and 0.93.

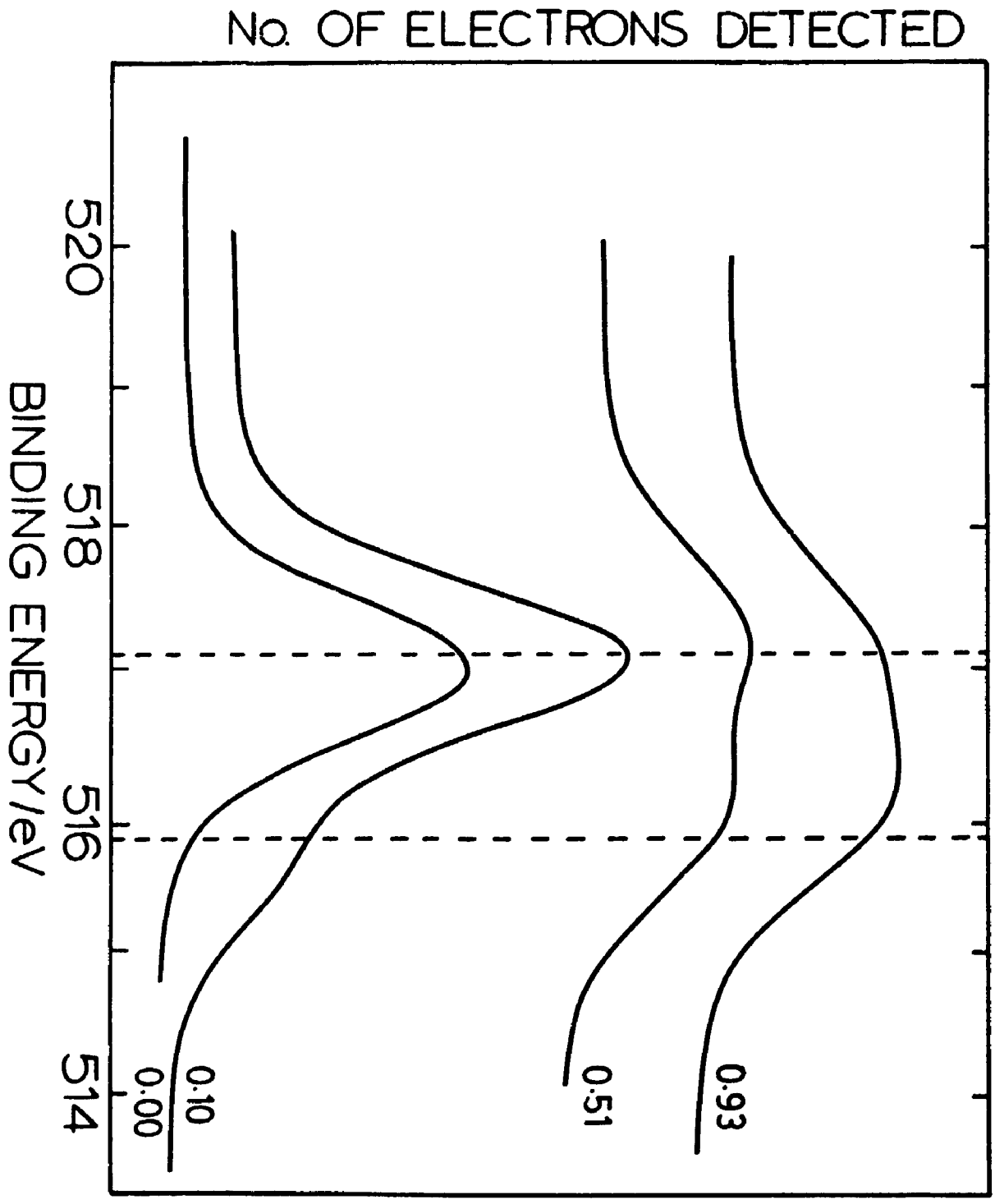
No. OF ELECTRONS DETECTED
BINDING ENERGY/eV
520
518
516
514
0.00
0.10
0.51
0.93

Fig. 6.8 Binding energies for V(IV), V(V), O(530), O(531) against x in $Li_xV_2O_5$.

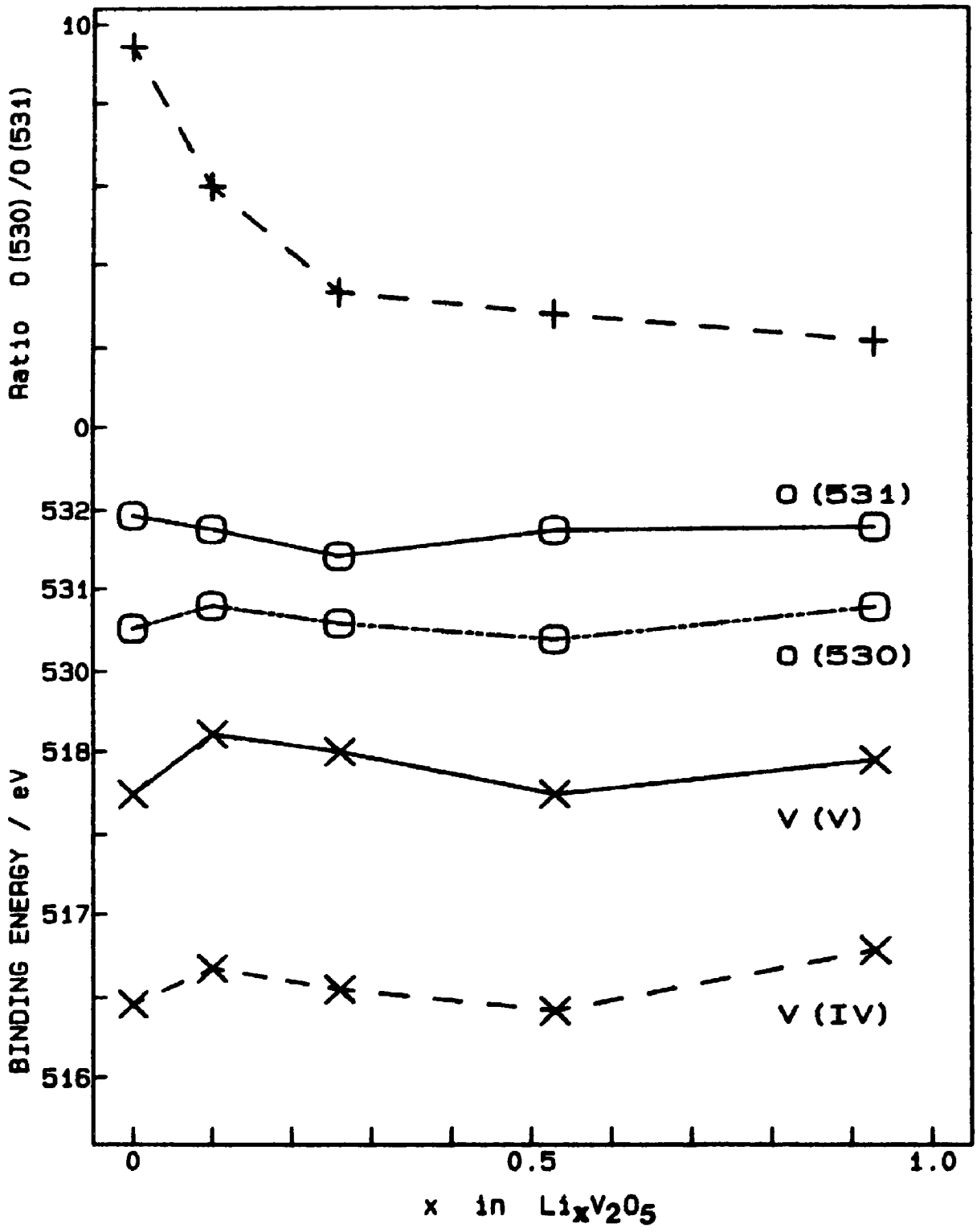
10
0
Ratio O(530)/O(531)
532
531
530
518
517
516
BINDING ENERGY / eV
O (531)
O (530)
V (V)
V (IV)
0
0.5
1.0
x in $Li_xV_2O_5$

Fig. 6.9 Lithium insertion curves of V_2O_5 prepared by heating tetrammonium hexavanadate as dependance of x and dx/dE in $Li_xV_2O_5$ on potential E. On Pt (——); on Ni (- - -). Electrolyte: 0.25 mol/L $LiClO_4$ in propylene carbonate; current density 0.1 mA/cm². (Add 3.550 V to obtain potentials versus Li^+/Li in this electrolyte at 25°C.

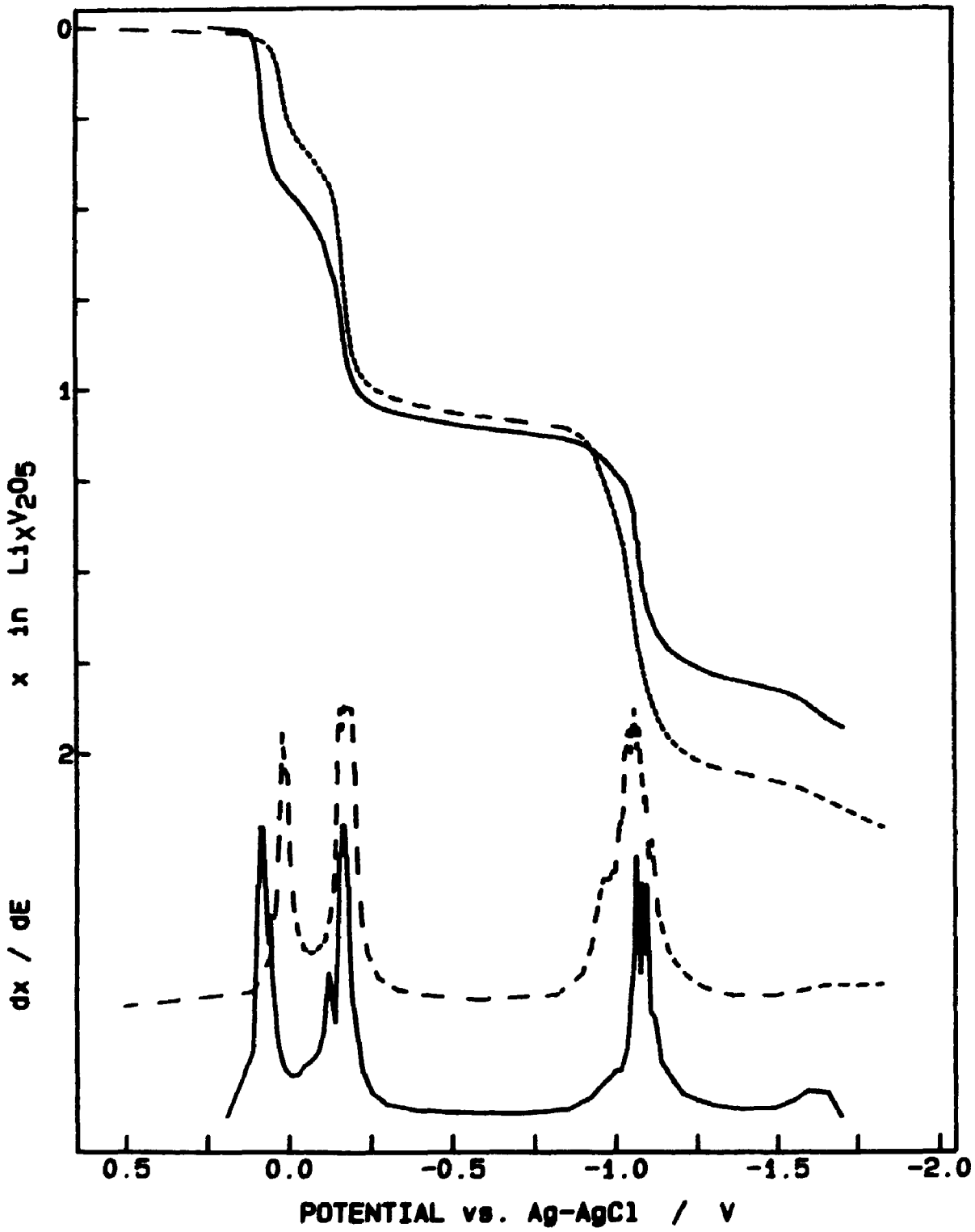
0
1
2
x in LixV2O5
dx / dE
0.5
0.0
-0.5
-1.0
-1.5
-2.0
POTENTIAL vs. Ag-AgCl / V

Fig. 6.10 Insertion and removal of lithium from V_2O_5 electrode on Pt substrate at current density of 0.2 mA/cm², showing increasing hysterysis with increase in total insertion of Li. Max. $x = 0.8$ (——); max. $x = 1.1$(····): max. $x = 1.45$ (- - -).

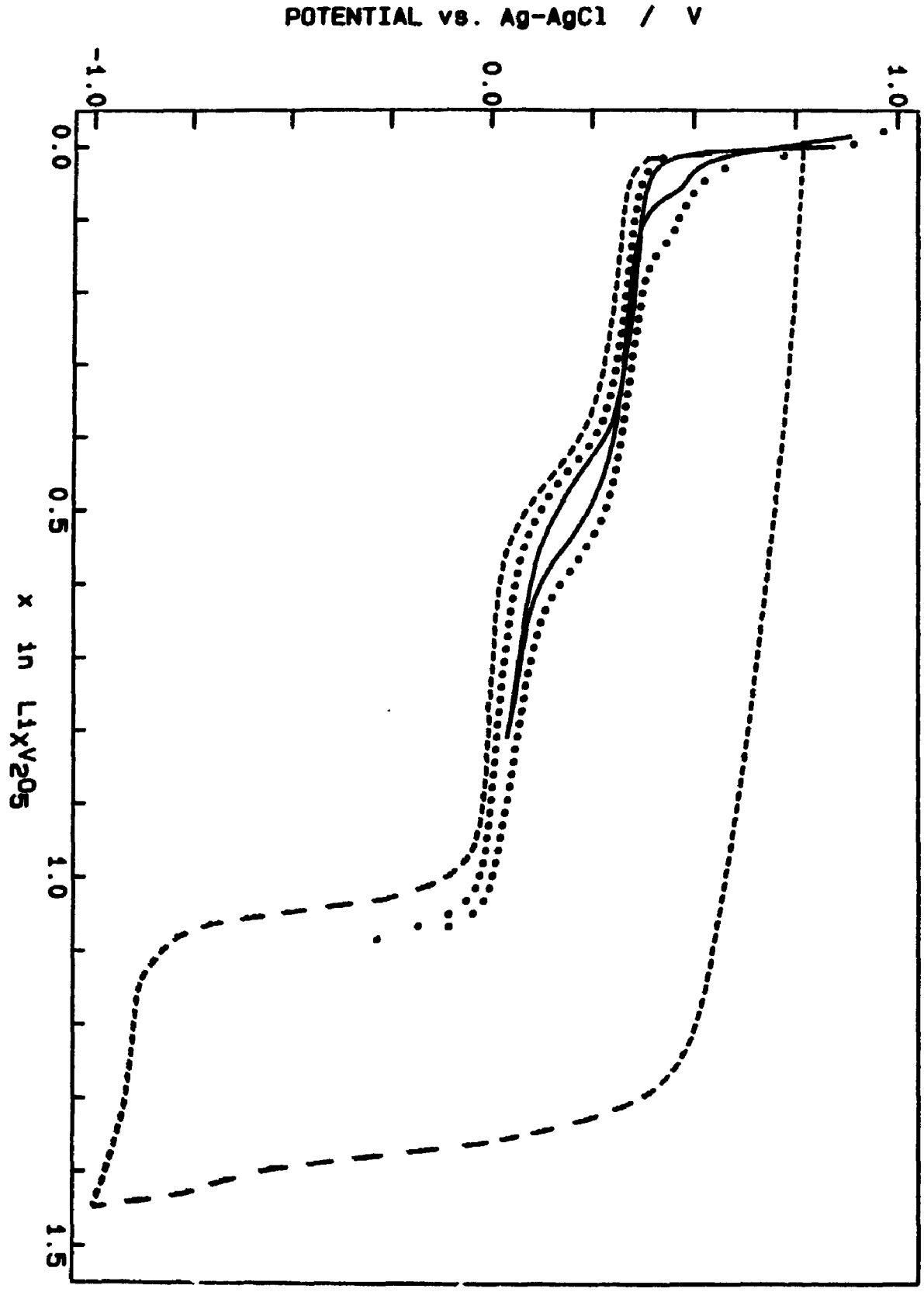
POTENTIAL vs. Ag-AgCl / V
-1.0
0.0
1.0
0.0
0.5
1.0
1.5
x in LixV2O5

Fig. 6.11 Lithium insertion into $Li_xV_6O_{13}$ at 25°C for various values of δ made by heating tetrammonium hexavanadate under vacuum ($1x10^{-3}$ torr); —— $\delta = 1.115$, - - - $\delta = 0.311$ and ···· $\delta = 0.276$.

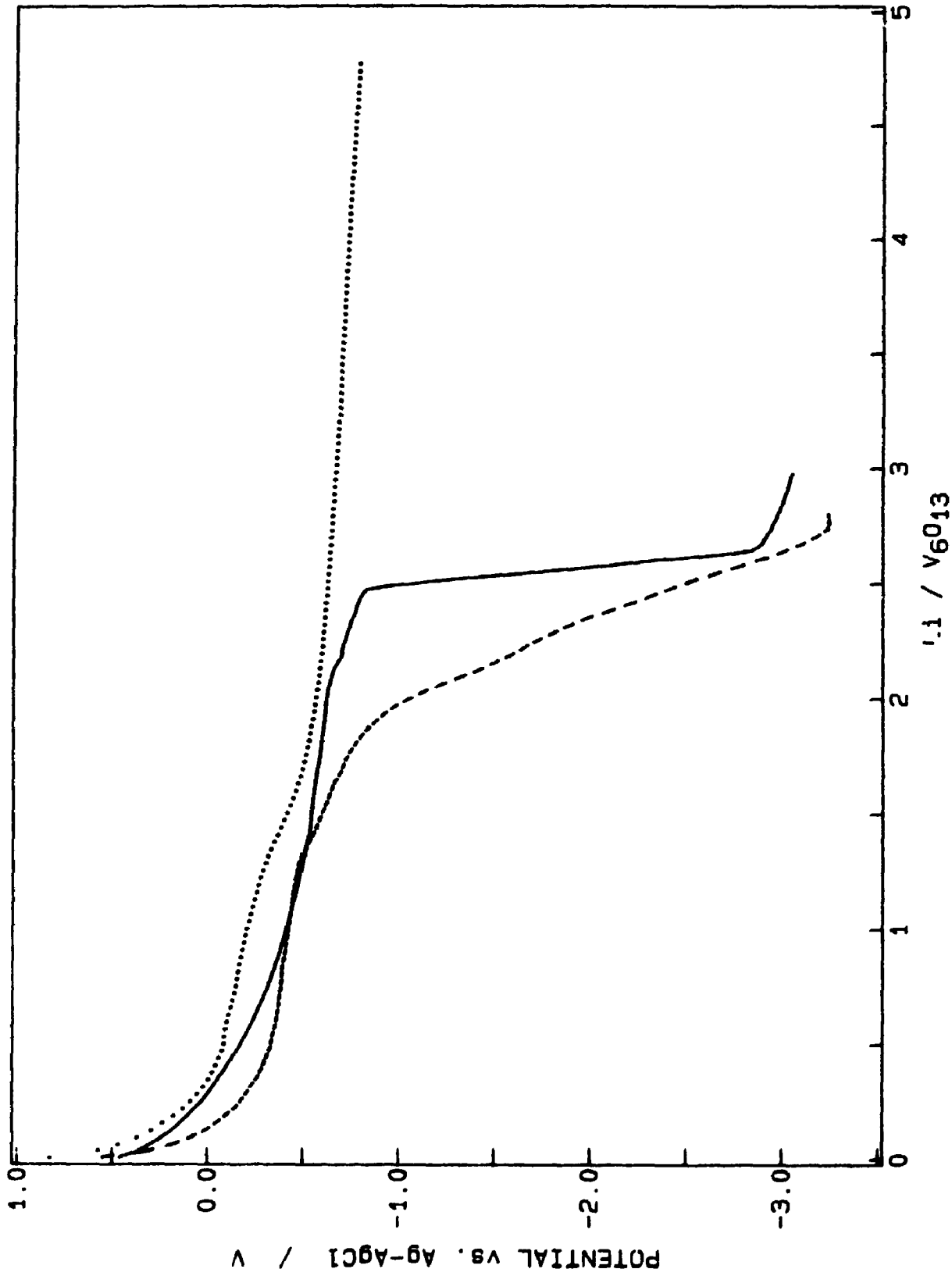
POTENTIAL vs. Ag-AgCl / V
1.0
0.0
-1.0
-2.0
-3.0
0
1
2
3
4
5
i / V6013

Fig. 6.12 Impedance spectrum of symmetric V_2O_5 blc ..ng electrodes with tetraglyme-$LiClO_4$ electrolyte; a) 1 40 and b) 21°C.

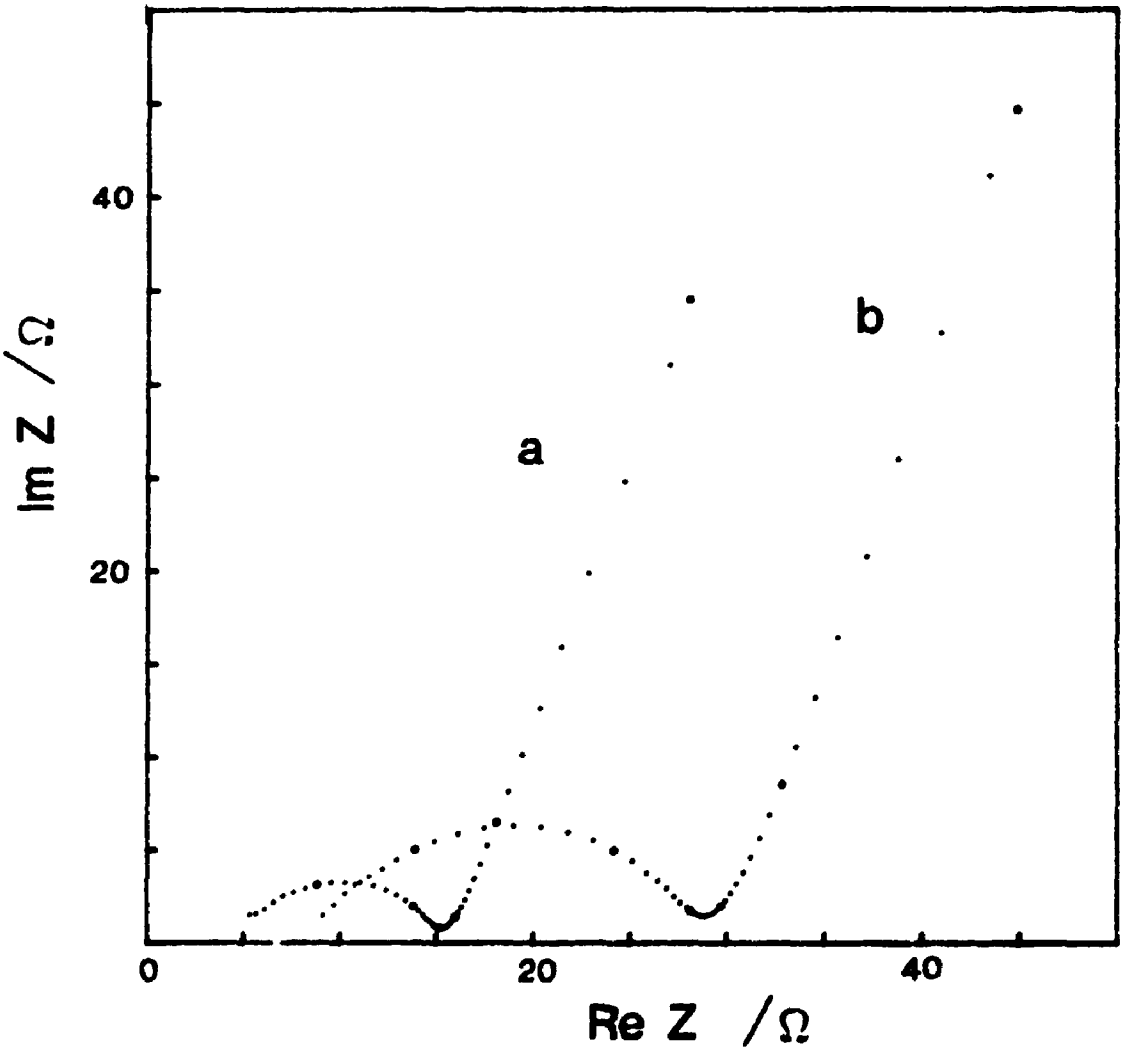
40
20
0
20
40
Im Z /Ω
Re Z /Ω
a
b

Fig. 6.13(a) VTF equation fit to data at various temperatures.

Fig. 6.13(b) Equivalent circuit for fitting impedance spectrum of figure 6.12.

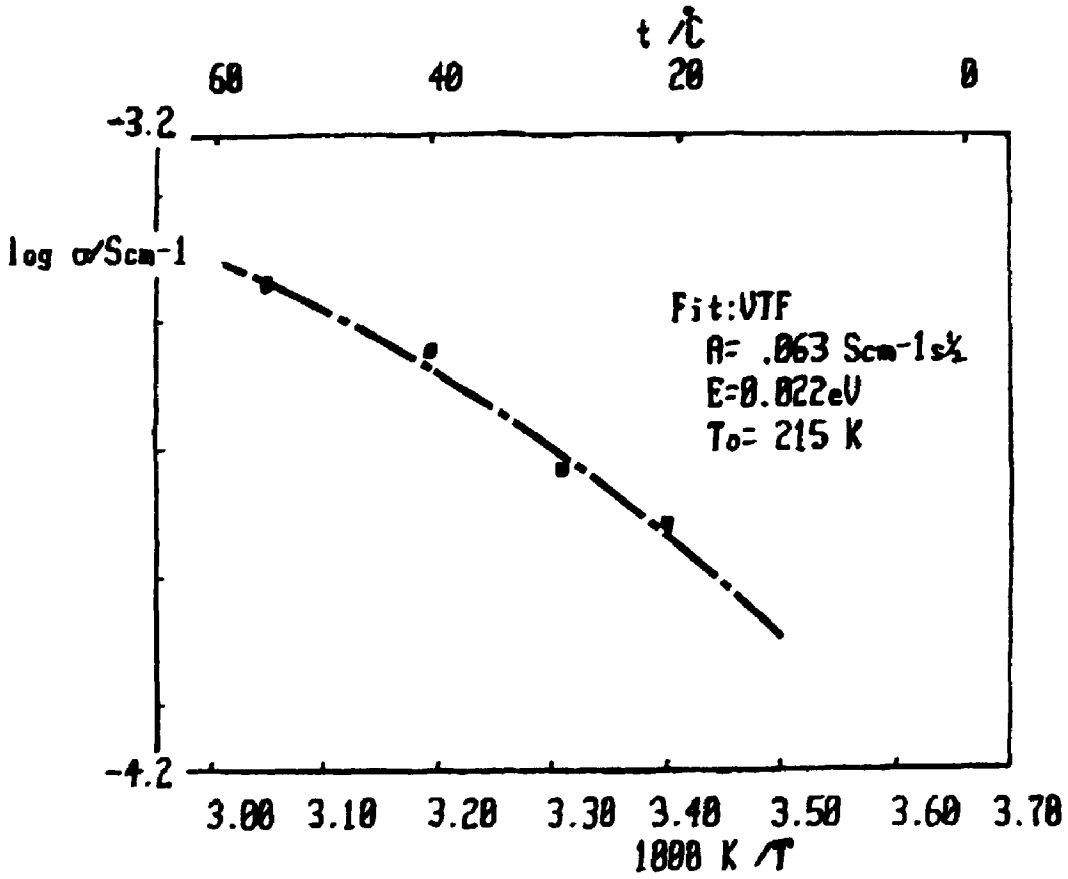
t /℃
60
40
20
0
-3.2
log σ/Scm-1
-4.2
Fit:VTF
A= .063 Scm-1s½
E=0.822eV
To= 215 K
3.00
3.10
3.20
3.30
3.40
3.50
3.60
3.70
1000 K /T

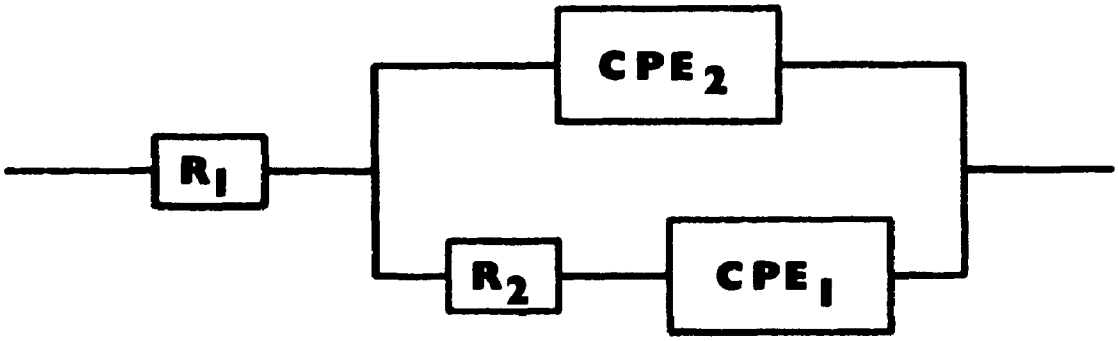
CPE2
R1
R2
CPE1

CHAPTER 7

STRUCTURAL EFFECTS OF LITHIUM INSERTION AND THE LATTICE-GAS MODEL FOR VANADIUM PENTOXIDE

7.1 Introduction

The system that results when lithium is inserted into vanadium pentoxide to form the bronze $Li_xV_2O_5$ is a rather complicated one. This chapter will cover three areas of the V_2O_5 electrodes prepared as described in chapter 6: (1) a comparison of the structure of lithium vanadium pentoxide bronzes; (2) a discussion of work on the mechanism of insertion and removal of lithium in other systems such as WO_3; and (3) the use of a simple lattice-gas model to describe the insertion behaviour of the electrode.

7.2 Results

7.2.1 Structure of Electrodeposited Lithium Bronzes

There have been several studies showing the presence of three phases when lithium is inserted into V_2O_5 using chemical and electrochemical synthesis [5,9,85,86]. These agree that the ranges of stoichiometry of $Li_xV_2O_5$ are: α-phase: $0.05 \leq x \leq 0.1$; ϵ-phase, $0.35 \leq x \leq 0.70$; δ-phase, $0.9 \leq x \leq 1.0$. The insertion curve for the open circuit potential plotted against x for a V_2O_5 electrode made by either decomposition from a diammonium or tetrammonium hexavanadate is shown in fig. 6.9. The plateaus on the potential-x plot indicate two-phase regions. The sharp drop in potential of about 1.0 V in the region of $Li_1V_2O_5$ has been observed by several authors [5,82,85,87] for composite V_2O_5 electrodes. It is quite apparent that insertion into V_2O_5

electrodes made from the decomposition of either tetrammonium or diammonium hexavanadate is identical. Both products are V_2O_5 by analysis and, from SEM photos, their morphologies are similar. However, depending on the conducting support used, the maximum amount of insertion is different, as seen from figure 6.9 (Pt; $x = 1.5$ and Ni; $x = 2.01$) This effect arises entirely from adhesion and thickness of the deposit. As discussed earlier, since reversibility is limited to $x \leq 1$ (before the large potential drop) the V_2O_5 electrode shows identical phase changes upon lithium insertion, independent of the conducting substrate. Also, the electrochemical method (C.V., galvanostatic or potentiostatic) for deposition of the di- or tetrammonium hexavanadate gave slightly different crystalline morphologies, but had no influence on insertion behaviour.

The X-ray diffraction patterns show no sharp change from one phase to another. For the V_2O_5 electrode, X-ray diffraction gives similar results to those obtained by others using chemically-prepared V_2O_5 [8,10,88,89]. Cava *et al.* [88] synthesized δ-LiV_2O_5, and found that, for unhydrated vanadium bronzes, no change in structure was observed in the first (α) phase; in the second (ϵ) phase, the c-dimension of the unit cell expanded to accommodate the lithium, while in the third (δ) phase, the crystal structure began to break down as more lithium cations were added. This expansion of the (*100*) plane in the X-ray pattern, shown in fig. 7.1, is linear in x in the region of the ϵ-phase. Also shown in the figure are data from Ptitsyn *et al.* [89] for electrochemical insertion of lithium into composite V_2O_5 electrodes and chemically prepared bronzes. Since the [*011*] peak in the X-ray diffraction pattern showed only small random shifts from pure V_2O_5 in

the α and ϵ-phase, its value was fixed at 0.340 nm and was used as an internal reference in calculating the *c* expansion. The results of Ptitsyn *et al.* [89] were recalculated on the same basis for these regions. However the two points at $Li_1V_2O_5$ are the values obtained with no internal reference since the [*011*] peak shifts noticeably as the V_2O_5 structure breaks down in the δ-phase. Our value for the [*011*] peak was found to be 0.327 nm for this phase.

Little change, if any, could be detected in the structure when lithium was inserted into either an ammonium or alkali metal hexavanadate electrode including all mixed phase hexavanadates examined using X-ray powder diffraction. This was because of the very small initial amount of lithium inserted into the hexavanadate structure (see table 5.15, 5.16; $Li/V < 0.01$). There is, however, a noticeable expansion of the diammonium hexavanadate structure for the (*100*) plane from an initial value of 0.783 to 0.793 nm when the ratio of Li/V_6O_{16} was 0.79 (section 4.2.4).

Insertion of hydrogen into diammonium hexavanadate gave no noticeable change to the X-ray pattern. This was also true for V_2O_5 electrodes, where the expansion of the lattice containing the H^+ is undetectable within experimental error compared to that containing an equal amount of Li^+.

7.2.2 Mechanism of Insertion and Removal

Chronoamperometry is a potential step technique where the potential of the working electrode is changed almost instantaneously and the current-time response is recorded. We assume as before for CV that only the species O in equation 5.5 is present and the initial potential, E_1,

is such that no reduction of O occurs at t = 0 the potential is stepped to E_2, where the reduction of O occurs at a diffusion controlled rate (see figure 2.1).

Fick's 2nd Law with the appropriate boundary conditions gives the Cottrell equation:

$$|I| = nFD^{1/2} c_O^{\infty} / \Pi^{1/2} t^{1/2} \quad . \qquad (7.1)$$

Notice that the current falls as $t^{-1/2}$ and a plot of I vs $t^{-1/2}$ should be linear and pass through the origin (test for diffusion control). The diffusion coefficient can be found from the slope (or from the value of $It^{1/2}$ which should be independent of t) (see [37] for more details).

A great deal of effort has gone towards trying to interpret the kinetic mechanism of the insertion of ions into several chalcogenides. Honders and Broers [90,91] have studied this in great detail and corrected values obtained by Atlung *et al.* [92] for insertion of Li into TiS_2. However, to date all the emphasis has been on the insertion mechanism and little, if any, has been said about the removal mechanism.

A model based on a space-charge limited diffusion mechanism has been described for the bleaching (oxidation) of WO_3 electrochromic films by Faughnan *et al.* [93,94]. When electrons were extracted at one contact and cations at another, Faughnan *et al.* [93,94] verified their theoretical prediction that the current decays as $t^{-3/4}$ over long times for these amorphous thin WO_3 films.

Colouring (insertion) and bleaching (removal) experiments, using both Li^+ and H^+, have been performed on the diammonium hexavanadate and V_2O_5 (thermally decomposed diammonium hexavanadate electrodeposits) in

aqueous 0.1*M* solutions of $HClO_4$ and $LiClO_4$. Insertion and removal of H^+ into an electrode of diammonium hexavanadate is shown in figure 7.2. The cell potential was held at -3.0 V versus SCE for 10 s, then the potential was stepped to a positive value of +3.0 V. A Pt electrode was used as a counter electrode. Very similar results were found for insertion and removal of Li^+ into diammonium hexavanadate and the pure V_2O_5 electrode.

As shown in figure 7.2 the insertion curve is almost flat for short times, and probably indicates rapid attainment of a steady state in the solution phase before any significant diffusion has occurred in the solid electrode [92,93]. The removal curve in fig. 7.2 suggests a complex mechanism compared to that for insertion. A ln (current) vs. ln (time) plot is shown in figure 7.3 for the removal curve. The middle portion of this curve has a slope close to -3/4, which is the value found by Faughnan *et al.* [93,94] for their thin vapour-deposited WO_3 films. Therefore, for a small portion of the removal of lithium from thick V_2O_5 electrodes there may be a similar mechanism seen by Faughnan *et al.* [93,94], but the reproducibility of this exact slope of -3/4 in our results and to some extent for those of Faughnan *et al.* [93] makes further comment on the mechanism impossible.

However, these preliminary experiments on initial removal of lithium from a thick V_2O_5 electrode suggest that a phenomenon similar to that found on insertion of lithium into TiS_2 by Vaccaro *et al.* [95] is occurring. For TiS_2, the chronoamperometric lithium insertion curves from Vaccaro *et al.* [95] and vanSchalkwijk [63] have a similar shape to the removal curve for V_2O_5 (fig. 7.3).

7.2.3 Lattice-gas Model

To account for the dependence of the potential on the amount of lithium inserted, a theoretical calculation of the potential was made on the basis of a Bragg-Williams model (see chapter 2 for details). As shown earlier the addition of eqn. (2.13) and (2.21) gives eqn. (2.23) for the cell potential

$$\begin{aligned} E &= -(RT/F)\ln[\alpha x^2/(2 - x)(2 - \alpha x)] + a + bx \\ &= E_{cf} + a + bx \end{aligned} \qquad (7.2)$$

where α is the number of lithium sites per vanadium atom.

In practice, a pseudo-reference electrode is used instead of a reversible lithium electrode; the only change introduced is in the significance of the constant a. This equation is analogous to those developed by Crandall *et al.* [96] and by Armand (see [12]), who used a slightly different derivation which was limited to $\alpha = 1$. Dahn and McKinnon [2] demonstrated that the fitting of such an expression to data for the system $Li_xMo_6Se_8$ with $x < 1$ and for Li_xTaS_2 with $x < 1$ can closely describe the potential vs. x behaviour.

According to the equation above (7.2), a plot of $Q = E - E_{cf}$ should be linear in x for a given value of α. Since V_2O_5 has a framework structure containing cavities in which inserted lithium ions have 4 nearest-neighbour V atoms, then each of these V atoms is shared with a neighbouring cavity, so that $\alpha = 2$.

The plot of Q against Li/V in figure 7.4 for the diammonium hexavanadate, $(NH_4)_2V_6O_{16}$, shows that the configurational contribution to the potential is small, and that the Q function shows two roughly linear portions centred about Li/V = 0.07 ($x = 0.14$) and starting from

Li/V = 0.10 (x = 0.2). For small values of x, the configurational contribution was very sensitive to errors in x, so an initial sharp rise or drop in a plot of the Q function against x was of questionable significance. The use of the Q function for this hexavanadate was justified if it was assumed that the coordination of Li^+ and V(IV) are the same in the structure of the hexavanadate as they are in orthorhombic vanadium pentoxide. The plot in figure 7.4 for the tetrammonium hexavanadate, $(NH_4)_4V_6O_{16}$, also shows the configurational contribution to the potential was also small, and that the Q function shows a linear portion with a very large slope centred about Li/V = 0.02.

Similarly, in figure 7.4, a decomposed anodic deposit (V_2O_5) or a decomposed cathodic deposit in air, again shows a relatively small contribution from the configurational term. The Q function shows linear portions between the approximate values Li/V = 0.05 and 0.15, and Li/V = 0.25 and 0.5; the Q function was undefined for Li/V > 0.5 (i.e., x > 1).

The slope of the Q plot for V_2O_5 electrodes was much smaller than for the hexavanadate electrodes, with the tetramonium hexavanadate having the largest slope. This suggests that ion-ammonia-water interactions are more important than ion-ion interactions between Li ions and V(IV) ions on the lattice.

Similar results to the tetrammonium hexavanadate were obtained for the insertion of lithium into other alkali metal hexavanadates with Rb, Cs, and K and mixed phases.

This simple model proved inadequate in describing the potential-x curves of insertion of lithium into vanadium pentoxide electrodes. A

more complicated potential-x curve is seen for V_2O_5 than other insertion electrodes, such as TiS_2 and Mo_6Se_8 [1,2,39,40]. Thus, a more involved model is necessary to account for the sharper phase transitions in $Li_xV_2O_5$. Some of the details of this extension of the lattice-gas model to include distinct phase equilibria and strong interactions have been discussed by McKinnon and Haering [1]. To date, little or no progress in modelling the potential-x behaviour of vanadium oxides has been made by other researchers.

7.3 Conclusions

For insertion of Li into the V_2O_5 electrode, X-ray diffraction gives similar results to those obtained by others using chemically-prepared V_2O_5 where no change in structure was observed in the first (α) phase; in the second (ϵ) phase, the *a*-direction of the crystal lattice expanded to accommodate the lithium, while in the third (δ) phase, the crystal structure began to break down as more lithium cations were added. This expansion perpendicular to the (*100*) plane in the X-ray pattern is linear in x in the region of the ϵ-phase. The mechanism of removal is important in investigating the reversibility of V_2O_5 electrodes. Results suggests a complex mechanism with part of the removal (bleaching) step showing similar behaviour for bleaching curves using a potential step technique for thin WO_3 films. Results from fitting the potential-x curves to a simple lattice-gas model suggest that ion-ammonia-water interactions are more important than ion-ion interactions.

Fig. 7.1 Spacing between *100* planes in nm vs. x in $Li_xV_2O_5$ using the *011* reflection at 0.340 nm as an internal reference.

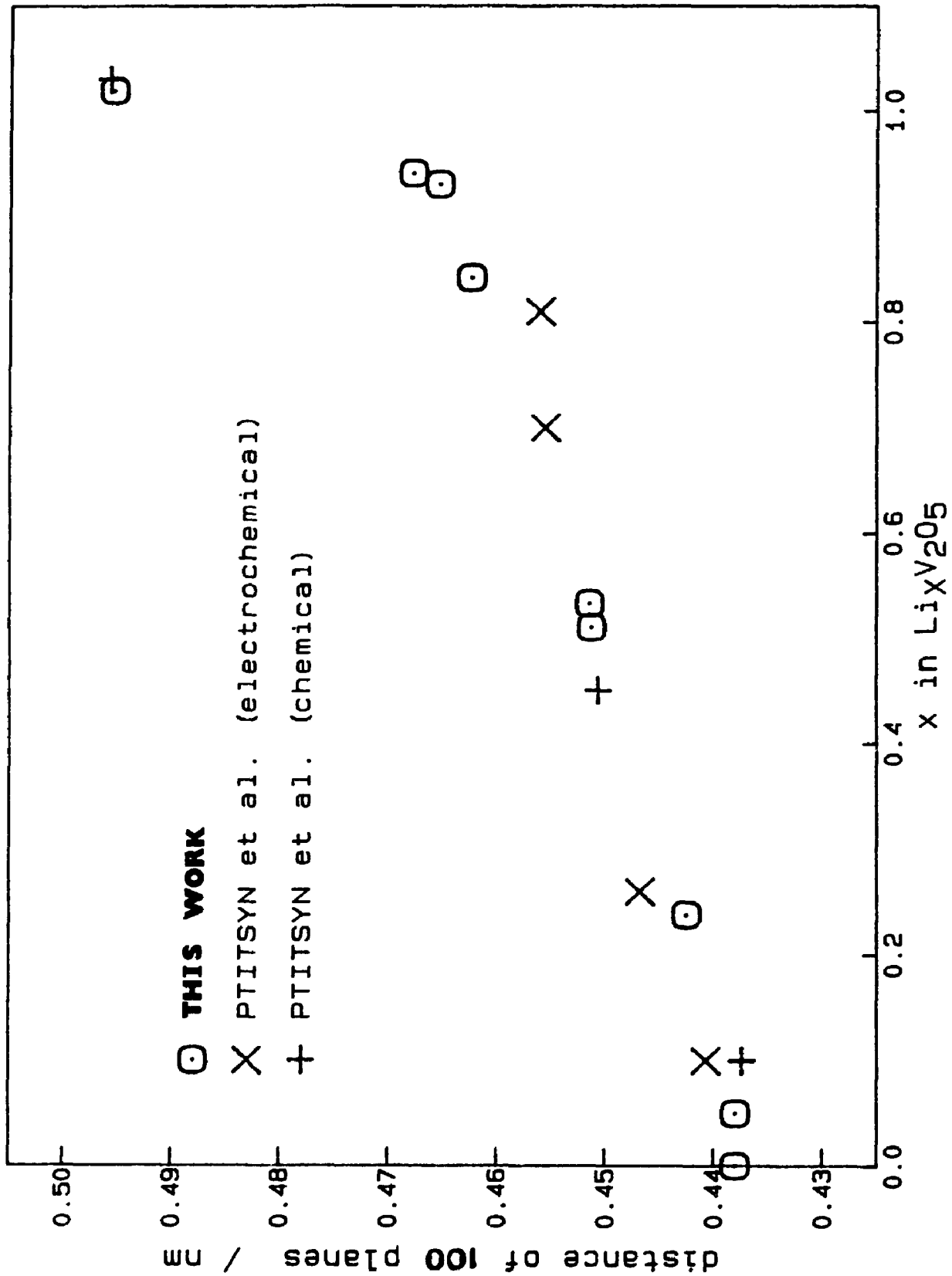
distance of 100 planes / nm
0.50
0.49
0.48
0.47
0.46
0.45
0.44
0.43
0.0
0.2
0.4
0.6
0.8
1.0
x in $Li_xV_2O_5$
THIS WORK
PTITSYN et al. (electrochemical)
PTITSYN et al. (chemical)

Fig. 7.2 H^+ insertion and removal for a decomposed V_2O_5 electrode in 0.1 mol/L aqueous $HClO_4$; —— for insertion, - - - for removal.

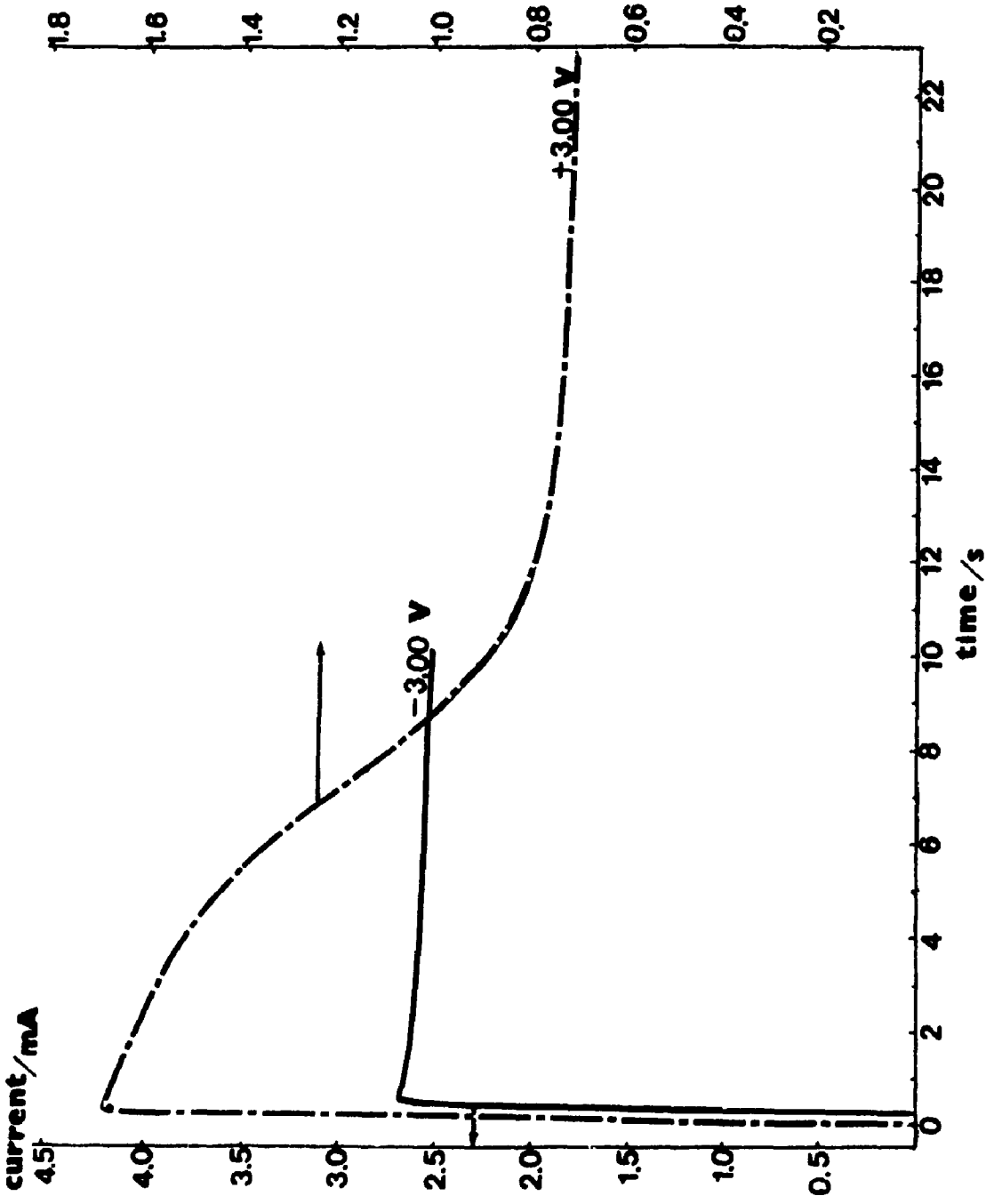
current/mA
4.5
4.0
3.5
3.0
2.5
2.0
1.5
1.0
0.5
0
2
4
6
8
10
12
14
16
18
20
22
time/s
1.8
1.6
1.4
1.2
1.0
0.8
0.6
0.4
0.2
+3.00 V
-3.00 V

Fig. 7.3 Ln(current) vs. ln(time) for the bleaching curve for the dehydrated V_2O_5 electrode.

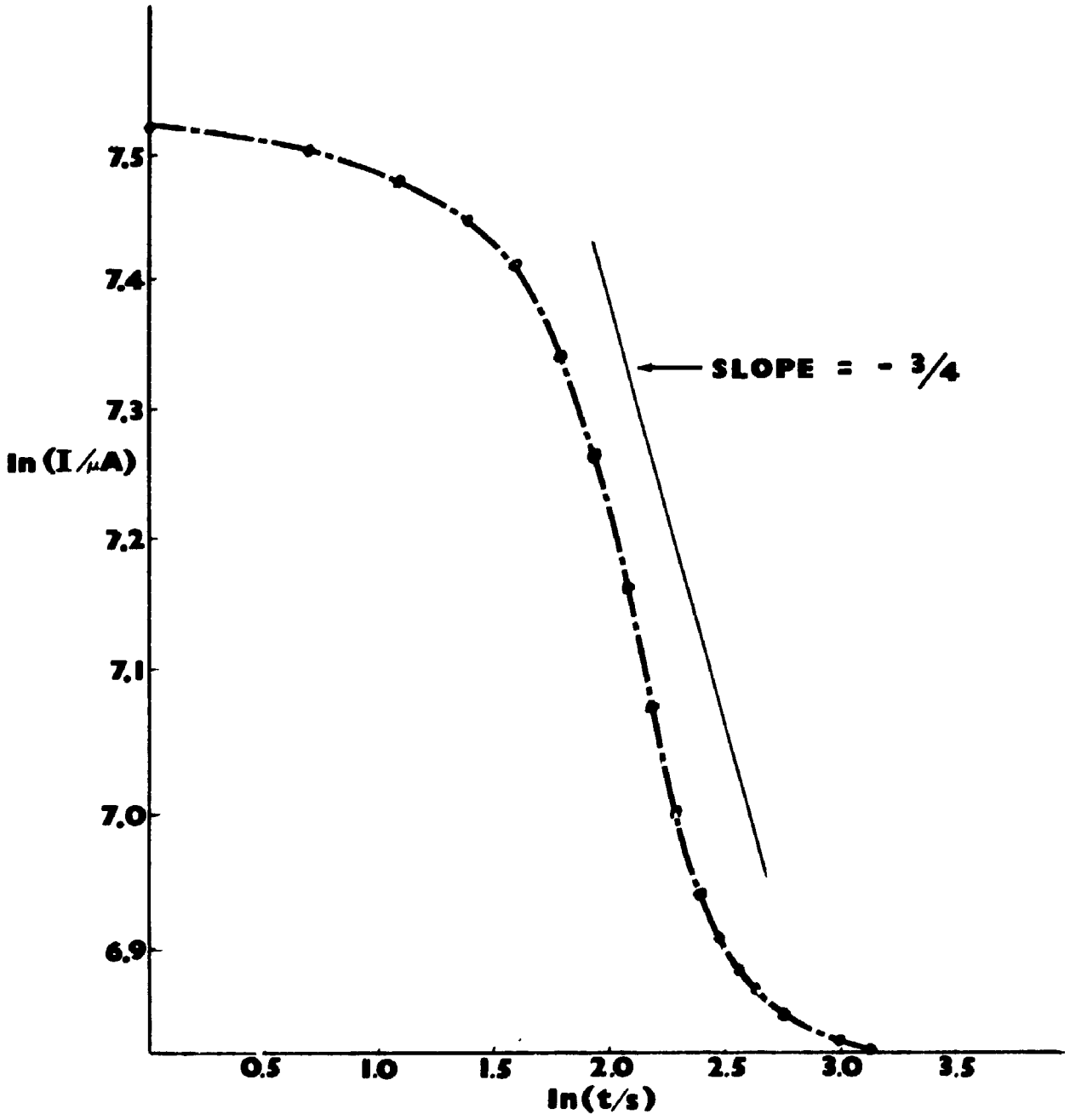
7.5
7.4
7.3
7.2
7.1
7.0
6.9
ln (I/μA)
SLOPE = - 3/4
0.5
1.0
1.5
2.0
2.5
3.0
3.5
ln(t/s)

Fig. 7.4 Q - function for diammonium hexavanadate (····), tetrammonium hexavanadate (----) and V_2O_5 (thermally decomposed tetrammonium hexavanadate) (——).

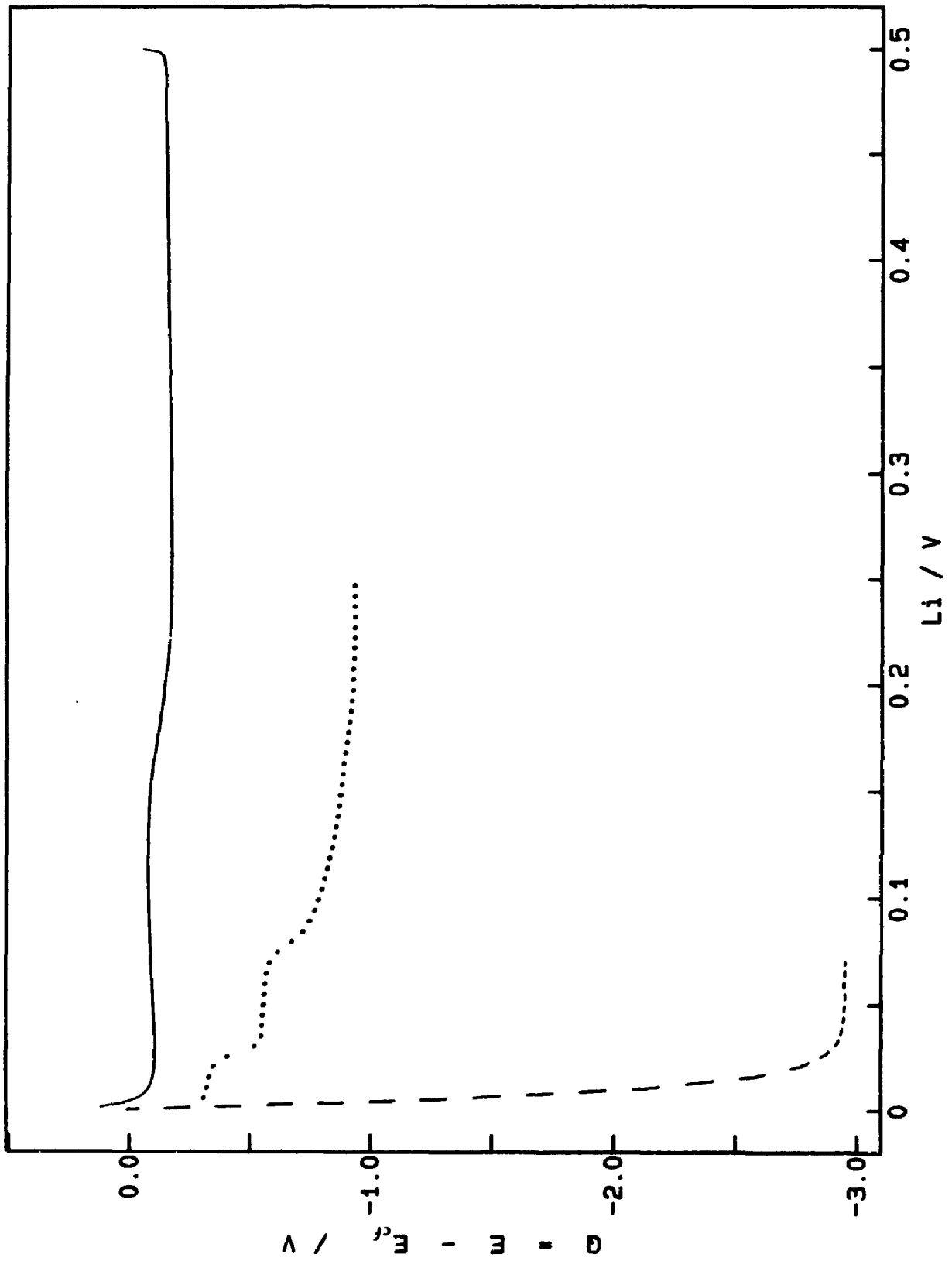
0.0
-1.0
-2.0
-3.0
0
0.1
0.2
0.3
0.4
0.5
Li / V
Q = E - E_cf / V

CHAPTER 8

SINGLE CELL BATTERIES

8.1 Introduction

Several rechargeable lithium batteries in the past have used layered chalcogenides such as TiS_2 and MoS_2 as cathode materials. However, V_2O_5 cathode materials have several advantages including a higher theoretical specific energy (about 500 W h/kg), a lower sensitivity to moisture and air, a greater resistance to solvent intercalation, a higher Gibbs energy of reaction and theoretically a high potential (3.2 V vs. Li). The theoretical specific energy was calculated using the reaction, $xLi + V_2O_5 = Li_xV_2O_5$ and $x = 1$. It has been mentioned that one disadvantage of V_2O_5 is its low electronic conductivity which decreases with the amount of lithium inserted. This phenomenon will be examined by using pure V_2O_5 cathodes prepared by decomposition of electrodeposits.

8.2 Results

This chapter is concerned with the fabrication and the electrochemical properties of a single cell battery system. Long term charge-discharge cycles were performed at various current densities. Impedance spectroscopy at various cycle numbers and at different states of discharge was also done.

8.2.1 Choice of Materials

All the cells studied used cathodes that were prepared electrochemically on circular Ni or Pt foils and decomposed to V_2O_5 as

described in chapter 4 and 5. The anode was a lithium foil or electrochemically-prepared LiAl alloys. The formation of LiAl anodes will be discussed in a following section. To date most lithium batteries on the market use a non-aqueous electrolyte such as propylene carbonate with a lithium salt. Recent research has focussed on the use of various polymer electrolytes such as PEO with Li salts [97], MEEP [98,99] and many others in the literature. Discussion of these polymers will be limited to how they apply to the topic of this thesis and further details on their specific nature can be obtained from the respective references.

PEO and MEEP with Li salts could be cast directly on the V_2O_5 cathode with a thickness of about 1-5 μm. To give a thicker electrolyte coating several castings were required. A picture of this is shown in plate 7(a) for the MEEP-$LiClO_4$ electrolyte where it was obvious that some problems will occur when a smooth surface of lithium is pressed on top to form a cell. Puncturing of the polymer by crystalline V_2O_5 and consequent shorting of the lithium anode did occur in cells using this type of casting method. Problems with the capacity of the cathode occur because of insufficient "wetting" of the cathode by the electrolyte. Also, conductivity and phase problems that are well known for PEO electrolyte systems [97,100] led to abandoning this electrolyte. MEEP electrolytes, being less viscous, were used with Celgard 2500, a porous polypropylene film, as shown in plate 7(b). The electrolyte made good contact with the cathode, and it has been found that the MEEP + $LiClO_4$ system (O/Li = 12) had a conductivity of about 1×10^{-4} S cm^{-1} [98]. A few cells have been made and cycled using this electrolyte with favourable results [99]. Cells were made with cycle lives greater than

500 and good utilization of the cathode (> 90%). However, because of the better conductivity of the tetraglyme electrolyte system only cells with this solvent will be discussed in this chapter since the behaviour of the cathode material is identical. Celgard 2500 was used with this low viscosity solvent as a support. As shown in plate 7(b) this inert material has a porosity of about 50% and from SEM examination, the electrolyte penetrates the Celgard completely.

The only use of tetraglyme by past researchers for lithium batteries has been as a plasticiser for a PEO electrolyte such as for example NaSCN-PEO_8 complex [101]. Recently, Bruce and Krok [102] reported the conductivity of tetraglyme-$LiCF_3SO_3$ using impedance spectroscopy. Tetraglyme is a material that consists of four monomer units of ethylene oxide capped with methyl groups, and is an oligomer of end-capped PEO. The conductivity of tetraglyme with $LiClO_4$ (O/Li = 12) was determined by impedance spectroscopy between symmetric Pt, Li or V_2O_5 electrodes. The case of symmetric V_2O_5 electrodes was discussed in chapter 6. The conductivity of tetraglyme-$LiClO_4$ mixtures was of the order of 1.7 x 10^{-3} S cm^{-1} at 298 K [103], which was about an order of magnitude higher than that of the MEEP-$LiClO_4$ electrolyte. Electrolyte decomposition on Pt occurred only at a voltage greater than 5.1 V (vs. Li), inside this voltage window the electrolyte was unreactive to the highly reactive lithium electrode. Tetraglyme + $LiClO_4$ (O/Li = 12), because of its high conductivity and stability, was found to be the most suitable system to study the V_2O_5 cathode in a single cell.

8.2.2 Influence of Cathode

Since it is felt by most researchers working on lithium batteries that the electrolyte / lithium interface is the interface that is the hardest problem to resolve, the choice of a proper electrolyte may help overcome this difficulty. Tetraglyme has a relatively low viscosity at room temperature, making it necessary to use a porous support (Celgard 2500) to hold the electrolyte between the electrodes. Cathodes of vanadium pentoxide made by thermal decomposition of electrochemically-prepared ammonium hexavandates have a oriented, crystalline structure, and the low viscosity of the tetraglyme electrolyte allows for good contact with these cathodes. It fills the cavities between crystals effectively and thus takes full advantage of the larger available surface area.

Complete discharge of the cell (electrode area 2 cm^2), at 0.25 mA/cm^2 constant current, gives the potential-time plot shown in figure 8.1. Notice that the phase changes are similar to that seen for V_2O_5 in other electrolytes such as PC in earlier chapters and by other researchers using composite electrodes. The initial voltage of about 3.3 V is lower than that for an electrode in a non-aqueous electrolyte (fig. 6.9) due in part to the *iR* drop of the cell and the Ag-AgCl reference electrode used in fig. 6.9. The phase changes in the V_2O_5 are clearly evident: a large potential drop of almost 1 V occurs at about $x = 1.0$ (δ-phase), by chemical analysis. At this point additional lithium causes disproportionation into V_2O_3 and $LiVO_3$ [29]. Another phase change is seen at about $x = 1.5$, which has been associated with further disproportionation of the V_2O_5, i.e., the lowering of the stability of $LiVO_3$, with further formation of more V_2O_3 as well as Li_3VO_4 [82].

However, the reversibility of the discharge is limited to cycling the battery no further than $x = 1.0$. Therefore, since the cell discharge in figure 8.1 and the insertion curves for V_2O_5 electrodes in figure 6.9 are identical, it was the cathode material that largely determined the voltage characteristics of the cell. The overall reversible capacity of the cell for insertion of lithium also depended on the cathode, where the anode had a large excess of lithium.

8.2.3 Cycling of Single Cell Batteries

Since discharge past $Li/V_2O_5 = 1.0$ results in non-reversible behaviour and hysteresis (chapter 6) it is important to set carefully the upper and lower voltage limits for battery cycling. These values were chosen to be 3.5 and 3.0 V respectively, with a constant current density applied to the cell. Thus, the voltage window was about 0.5 V; narrower windows were also used. Segments of the record of charge-discharge cycles for a cell are shown in figure 8.2 for various cycle numbers and temperatures from 50 to 92 °C. The charging times are much longer than the discharging time because of the different currents being used. The cell was charged at 0.125 mA and discharged at a high rate of 0.5 mA. The phase changes are clearly seen in the cycling cell. Also, a noticeable IR drop of about 0.05 V occurs when switching from charge to discharge and vice versa. The cell was capable of cycling up to 1000X. However, there was a gradual drop from the initial capacity of the cell, with about 50% of the starting capacity at about 200 cycles, dropping to about 25% at about 400-500 cycles and finally to less than 10 to 15% at 1000 cycles. The actual starting capacity was close to the theoretical value for the mass of crystalline V_2O_5 used as

a cathode (>90% utilization assuming discharge is to x = 0.9 in $Li_xV_2O_5$). The utilization of the cathode was good compared to earlier batteries reported by other researchers using TiS_2 where 80% utilization of the active material in a composite cathode was acceptable [4].

By remaining in the ϵ-phase of the V_2O_5 (ratio of Li/V_2O_5 between about 0.05 to 0.85) these longer cycle lifetimes were obtained. However, by increasing the voltage window to include cycling in the δ-phase region resulted in a dramatic decrease of cycle life to almost 10% (about 100 cycles). The cell was cycled at a charge/discharge current density of 0.05 to 0.50 mA/cm^2. Cycle lifetimes were only slightly better at lower discharge currents but the overall utilization of the cathode did improve noticeably (better than 95%). By cycling in a narrower window of 0.2V from 3.5 to 3.3 V (in the range x = 0.05 to 0.45), using the start of the second plateau at slightly lower potential as a switch point, phase changes in the V_2O_5 cathode could be avoided, which increased the cycle lifetime marginally but the estimated cathode utilization improved only if low charge-discharge rates were used. The importance of phase changes on the overall internal resistance will be seen in the impedance analysis discussed below.

8.2.4 Impedance Spectroscopy

The impedance spectrum of a cell, consisting of a lithium anode and thermally decomposed tetrammonium hexavanadate (V_2O_5) as a cathode, as a function of cycle number is shown in figure 8.3 and the parameters are summarized in table 8.1 for the equivalent circuit shown below the table. This circuit consists of a resistor (R_1) in series with a capacitor (C) which is in series with a Warburg impedance, both in

parallel to two other elements; a second resistor (R_2) and a constant phase element (CPE). The impedance spectra (figures 8.3, 8.4 and 8.5) for the cell:

$$\underset{\text{(anode)}}{Li} \;/\; \underset{\text{(in Celgard 25}\mu\text{m)}}{\text{tetraglyme} + LiClO_4\ (O/Li = 12:1)} \;/\; \underset{\text{(cathode)}}{V_2O_5}$$

have broad semicircles and non-vertical spikes similar to polymer electrolyte systems discussed by Bruce [38] (Chapter 2).

In figure 8.3 and table 8.1 the charging current was 0.125 mA and the discharging current was 0.25 mA for a voltage window of 0.2V (3.5 to 3.3V) for cycling in the range x = 0.05 to 0.5 for $Li_xV_2O_5$ at room temperature. There was a noticeable drop in the overall resistance (R_2) to a minimum at around 25 cycles of 64 ohms for the charged state. This lowering of the resistance can be attributed to the improved contact between the anode-electrolyte-cathode interfaces as the cell sits between two spring-loaded stainless steel contacts. The cell resistance gradually increases slowly with cycle number up to about 70 ohms at 75 cycles. Furthermore, the difference between the overall resistance between the charged and discharged states decreases with cycle number and by 75 cycles the resistance was equal. This shows that during each charge-discharge cycle a very small portion of the capacity of the V_2O_5 cathode was lost. In other words, some of the lithium vanadium bronze, $Li_xV_2O_5$, formed on discharge (reduction) was not recovered. Thus, as more and more of the cathode remains in the reduced bronze form, the overall resistance becomes an average of the fully charged and discharged values. This can also be seen in the change of the constant phase element (CPE) value, *n*, which decreases over cycle number for the charged state (table 8.1). Thus, the cell becomes more resistive as it

is repeatedly cycled.

Some further evidence that the cathode provided the major contribution to the increased overall resistance comes from studying the change in the resistance at various stages of discharge (or charge); see table 8.2. The voltage window was 0.45 V (3.5 to 3.05V) for charge and discharge currents of 0.125 and 0.25 mA, respectively, at 50°C. As seen in table 8.2, the data were again fitted to the equivalent circuit shown below the table. The resistance (R_2) increases with the amount of lithium inserted into the V_2O_5 cathode from 20.2 ohms when fully charged to 32.9 ohms when fully discharged at x = 1 for $Li_xV_2O_5$. The value of R_1 remains constant within experimental error at about 9.8 ohms.

The effect of temperature on the impedance spectrum is shown in figure 8.4(a) for the 35th cycle at 21 and 45°C and for figure 8.4(b) for the 59th cycle at 45 and 58°C. As the temperature increases both R_1 and R_2 decrease dramatically. Temperatures higher than 60°C gave erratic impedance measurements, which was attributed to leakage of electrolyte from between the two electrodes. Therefore, the optimum temperature for these single cell batteries in terms of the measured resistance was in the range of 50 to 60°C.

8.2.5 Post-Mortem of Cell

Once the single cell battery had lost essentially all its capacity (i.e., ceased to deliver a reasonable cycle time, less than 1% of original capacity (time of discharge), see figure 8.2) it was disassembled and the individual components examined. By visual inspection, the electrolyte showed no degradation on contact with lithium or the V_2O_5 electrodes. The V_2O_5 cathode maintained good

contact with the support and the electrolyte. It had a blackish colour, indicating the δ-phase, and this was confirmed by chemical analysis, which gave $x = 0.9$ to 1.0. As shown in plate 7(c) no change in morphology occurred for the V_2O_5 cathode upon reduction to the δ-phase. However, areas of the lithium anode had lost their metallic lustre, especially around the edge of the circular electrode which appeared whitish in colour, indicating perhaps the formation of either Li_2O or LiOH. The problem was acute when exposure to a moist environment was not avoided in earlier work. Even with the use of a glass jacket flushed with argon, a small amount of oxidation on the edge of the lithium anode was evident over long cycle times (cell cycling about 3 weeks). The cell lifetimes did improve by periodic flushing with argon. However, the eventual failure (loss of capacity) of the cell could not be accounted for only by oxidation of the lithium.

Preliminary results indicate the major reason for the decay of the battery was dendritic growth occurring at the highly reactive Li anode. Some evidence that this was occurring can be seen in the SEM photograph in plate 7(d). Here the interface between the lithium metal and electrolyte contains many large Li metal clusters which penetrate the Celgard. These large clusters contact the lithium metal poorly, and would effectively "block" lithium from the metal surface in making contact with the electrolyte and eventually, with sufficient build-up, could short-circuit the cell. Using another electrolyte, such as MEEP + lithium triflate ($LiCF_3SO_3$), passivation of the Li anode from reaction with the electrolyte was observed. The single cell battery with this electrolyte lost capacity after 300 cycles and upon SEM examination a passivating film was found on the lithium anode which by Auger and PES

spectroscopy was found to contain F and sulfate compounds from decomposition of the electrolyte. Passivation was not found to occur for the tetraglyme + $LiClO_4$ electrolyte. Thus, at the lithium anode, only the phenomenon of poor adhesion of the deposited lithium occurred (plate 7(d)). The replacement of lithium with LiAl alloy was ineffective, due to inherent problems with the fabrication of the alloy itself (see below).

8.2.6 LiAl Alloys

Several cells were cycled using an electrochemically-prepared LiAl alloy. An alloy was made under a constant current density of 0.1 to 1 mA/cm^2 in a propylene carbonate solution containing about 0.5 to 1.0 mol/L $LiClO_4$. The substrate was an aluminum foil cut to the correct dimension to be used in the single cell assembly for lithium cells. LiAl alloys formed in this way gave a uniform grayish metallic colour to the substrate surface. The amount of current used to form the alloy was approximately an order of magnitude larger compared to the theoretical amount needed for the complete reduction of the cathode in a single cell battery. Initially, the behaviour of these cells were identical to lithium, giving the same starting open circuit potential for the single cell battery. However, rapid loss in capacity with a complete breakdown of cyclability occurred after about 20 cycles (i.e., less than 1% total capacity of the initial cycle by 20^{th} cycle).

There are several reasons for this poor performance that have been observed by other researchers with LiAl alloys [104,105]. The most probable explanation in our case was that during formation of LiAl, dendritic growth of Li on the aluminum occurs after a "saturation" of

LiAl on the substrate to a certain depth has occurred. Thus, some lithium metal also forms near the surface, as well as LiAl. Evidence for this comes from X-ray diffraction studies of the surface. From the X-ray patterns, a combination of the spectra for lithium, lithium-aluminum alloy and lithium oxide (Li_2O) could be identified. Li_2O was present because of unavoidable exposure of the sample to room atmosphere before and during the X-ray scan.

As a result, once assembled in the cell and cycling has begun, further dendrite formation was quickly promoted, accelerating the breakdown at this interface. Further evidence that this was a problem came from the replacement of the LiAl anode, after the cell failed to deliver any normal cycle, with a fresh lithium anode keeping the same electrolyte and cathode. The cell upon reassembly immediately returned to its usual cycling behaviour (90% utilization of cathode) with several hundred cycle numbers and the gradual loss of capacity as was seen for other lithium single cells. However, further work on alloys is very important in battery research because of the advantages in stability compared to the highly reactive lithium.

8.3 Conclusions

Reversible single cells using electrochemically-made V_2O_5 cathodes have a very good lifetime of 500+ cycles. The initial utilization of the cathode was good (>90%) with a half-life (when capacity of cell drops to half its initial value) of 200 cycles. The tetraglyme-$LiClO_4$ electrolyte does not seem to react with the cathode and good contact was achieved. The advantage for electrochemical analysis is that we are studying a pure V_2O_5 electrode with no extraneous material.

The problems in the loss of capacity and eventual death of the cell lie primarily with the Li anode-electrolyte interface because of formation of dendrites. Also the small non-reversible nature of the cathode in which some lithium was not removed during cell charging appears to occur. This was seen in impedance spectroscopy by the eventual decrease in the difference of the overall resistance between charge and discharge and that capacity of the cathode was lost with cycle number. Attempts at replacing the lithium metal with a electrochemically-made LiAl alloy proved less successful, since complete failure occurred after only 20 cycles. This was due to extensive dendrite formation during alloy formation which probably accelerated the loss of capacity of the cell.

Plate 7(a) SEM photo of thin film of MEEP on V_2O_5 cathode; X720, bar length 7 μm.

7(b) SEM photo of celgard (2500) porous membrane; X10100, bar length 1 μm.

7(c) SEM photo of vandium pentoxide bronze after continuous cycling in single cell battery; X250, bar length 41 μm.

7(d) SEM photo of disassembled single cell showing dendrite formation of lithium on the anode side of the electrolyte; X2010, bar length 5 μm.

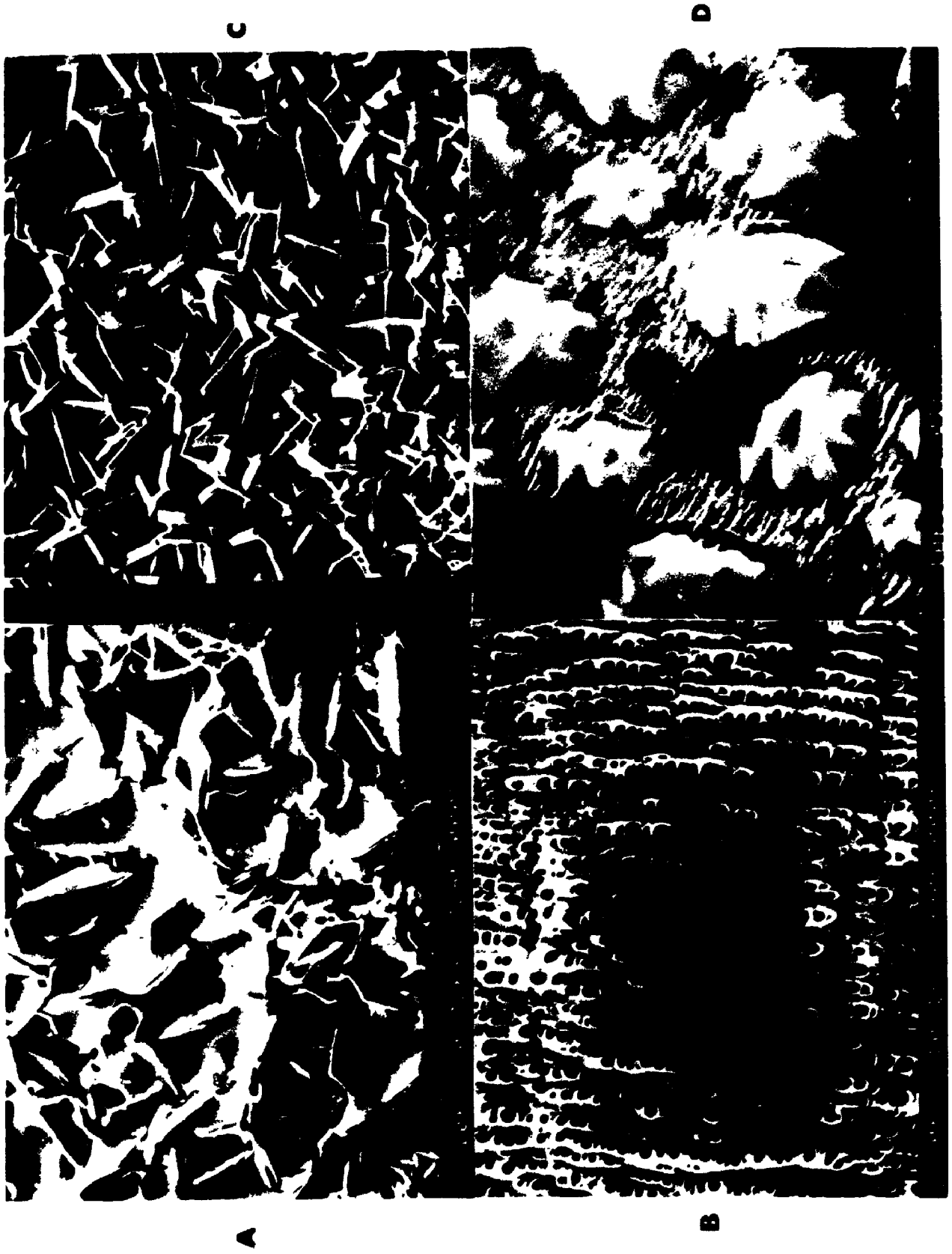
C
D
A
B

Table 8.1 Parameters of the equivalent circuit for impedance results as a function of cycle number of the cell Li/tetraglyme-$LiClO_4$/V_2O_5; T = 27°C.

Battery state	Cycle number	R_1 / Ω	R_2 / Ω	CPE $Y_0 \cdot 10^2$ / S	n	C /μF	W $Y_0 \cdot 10^4$ /S
1 *h* after assembling	-	25.0	96.5	4.22	0.64	6.09	2.30
charged	7-8	18.0	84.0	3.90	0.29	6.57	2.77
discharged	7-8	16.8	122.0	3.38	0.11	6.21	2.39
charged	25-26	19.0	63.9	5.72	0.37	4.80	2.46
discharged	25-26	20.7	72.9	1.42	0.07	4.25	2.62
charged	72-73	20.9	70.0	3.00	0.31	4.31	1.63
discharged	72-73	23.7	70.0	1.80	0.13	3.29	2.17

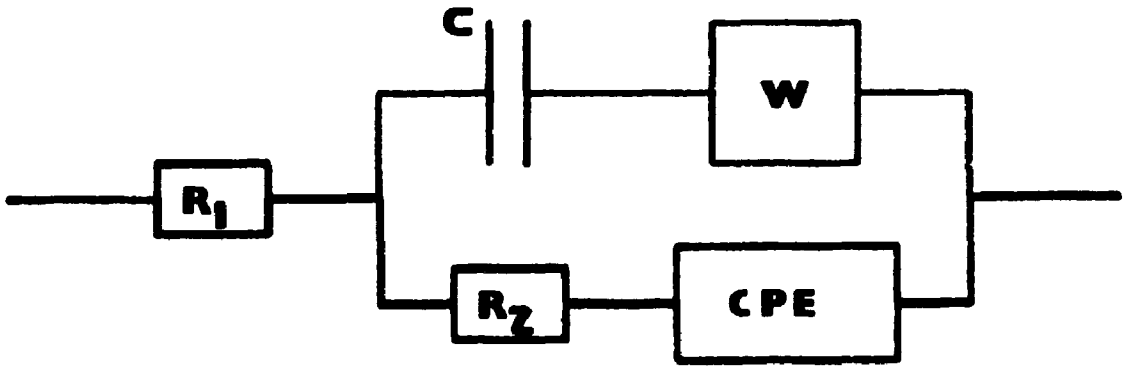

Table 8.2 Parameters of the equivalent circuit for impedance results as a function of the state of charge/discharge of the cell Li/tetraglyme-$LiClO_4$/V_2O_5; T = 50°C.

Battery state	R_1 / Ω	R_2 / Ω	CPE $Y_0 \cdot 10^2$ / S	n	C /μF	W $Y_0 \cdot 10^4$ /S
Full charge	9.8	20.2	6.78	0.22	1.94	6.00
Discharged 1st step	9.8	28.5	5.18	0.21	1.76	4.76
Discharged 2nd step	9.8	32.9	5.65	0.23	1.72	3.23
Charged 1st step	9.7	22.0	6.67	0.26	1.94	5.43

Fig. 8.1 Complete discharge of a single cell battery.

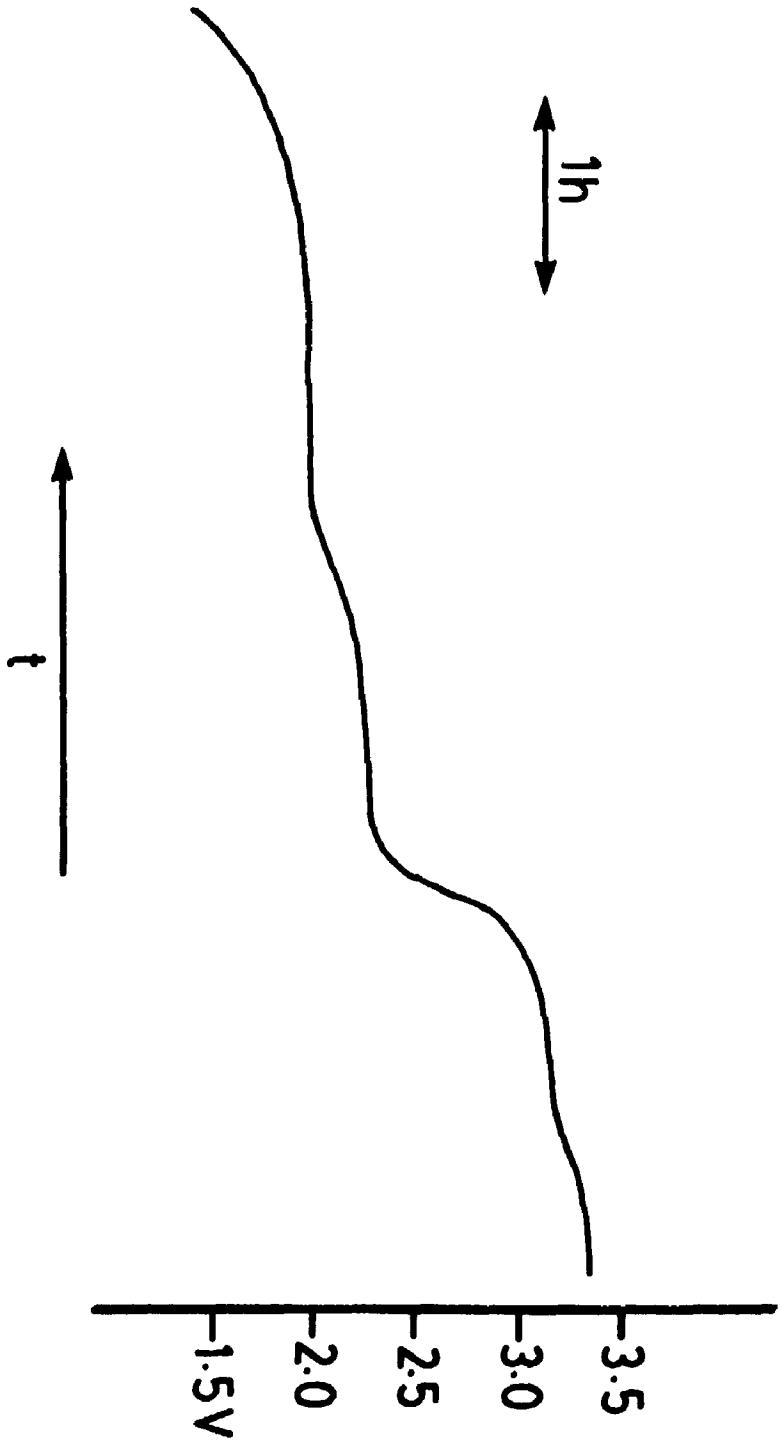
1h
t
1.5V
2.0
2.5
3.0
3.5

Fig. 8.2 Charge-discharge segments for single cell batteries for various temperatures for T = 50, 72 and 92°C , charge 0.125 mA and discharge of 0.5 mA.

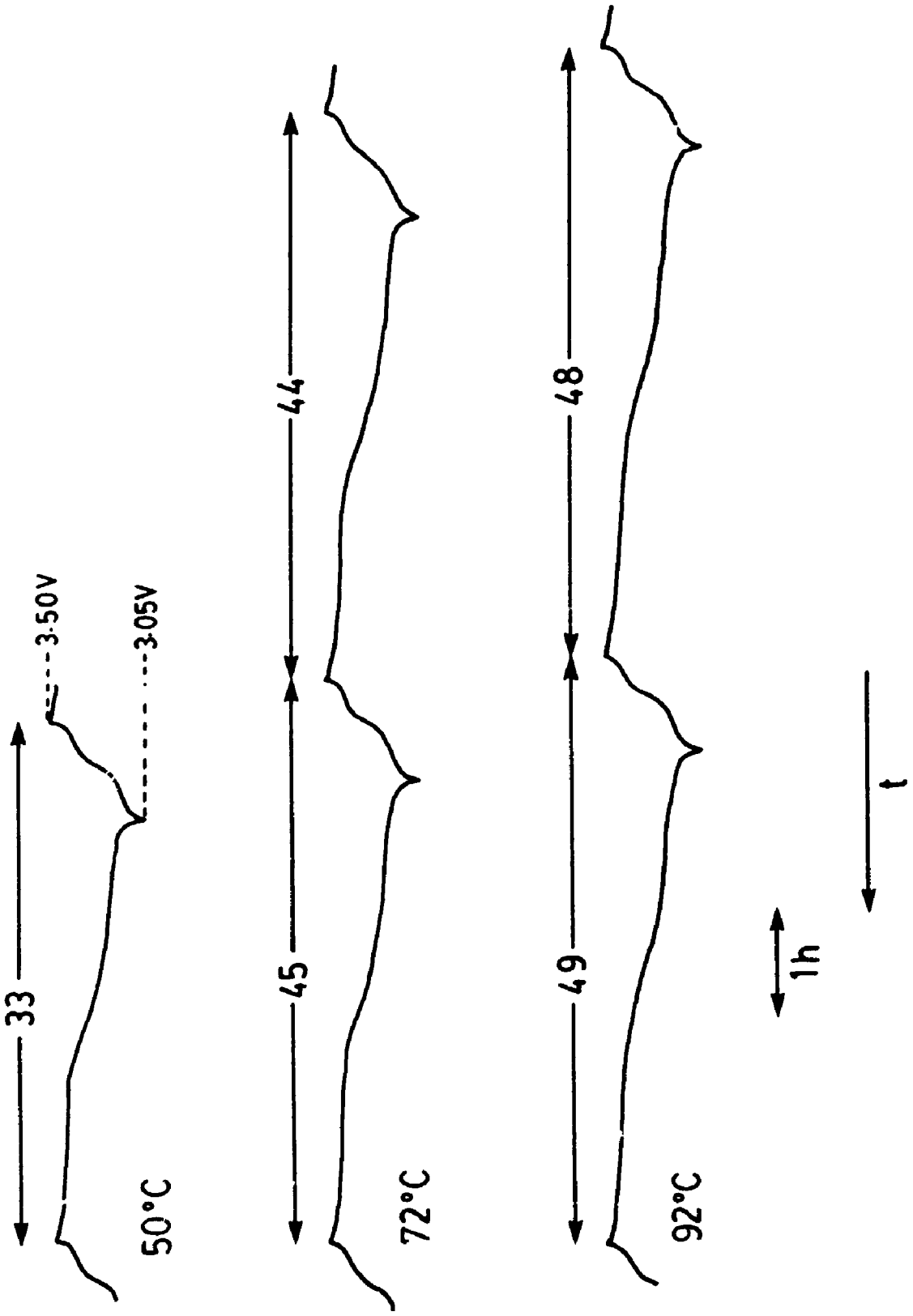
3·50V
3·05V
33
50°C
44
45
72°C
48
49
92°C
1h
t

Fig. 8.3(a) Impedance spectrum as a function of cycle number of a single cell battery in the charged state; a) initial cycle, b) cycle number 7. c) cycle number 25 and d) cycle number 72.

Fig. 8.3(b) Impedance spectrum as a function of cycle number of a single cell battery in the discharged state; a) cycle number 7, b) cycle number 25 and c) cycle number 72.

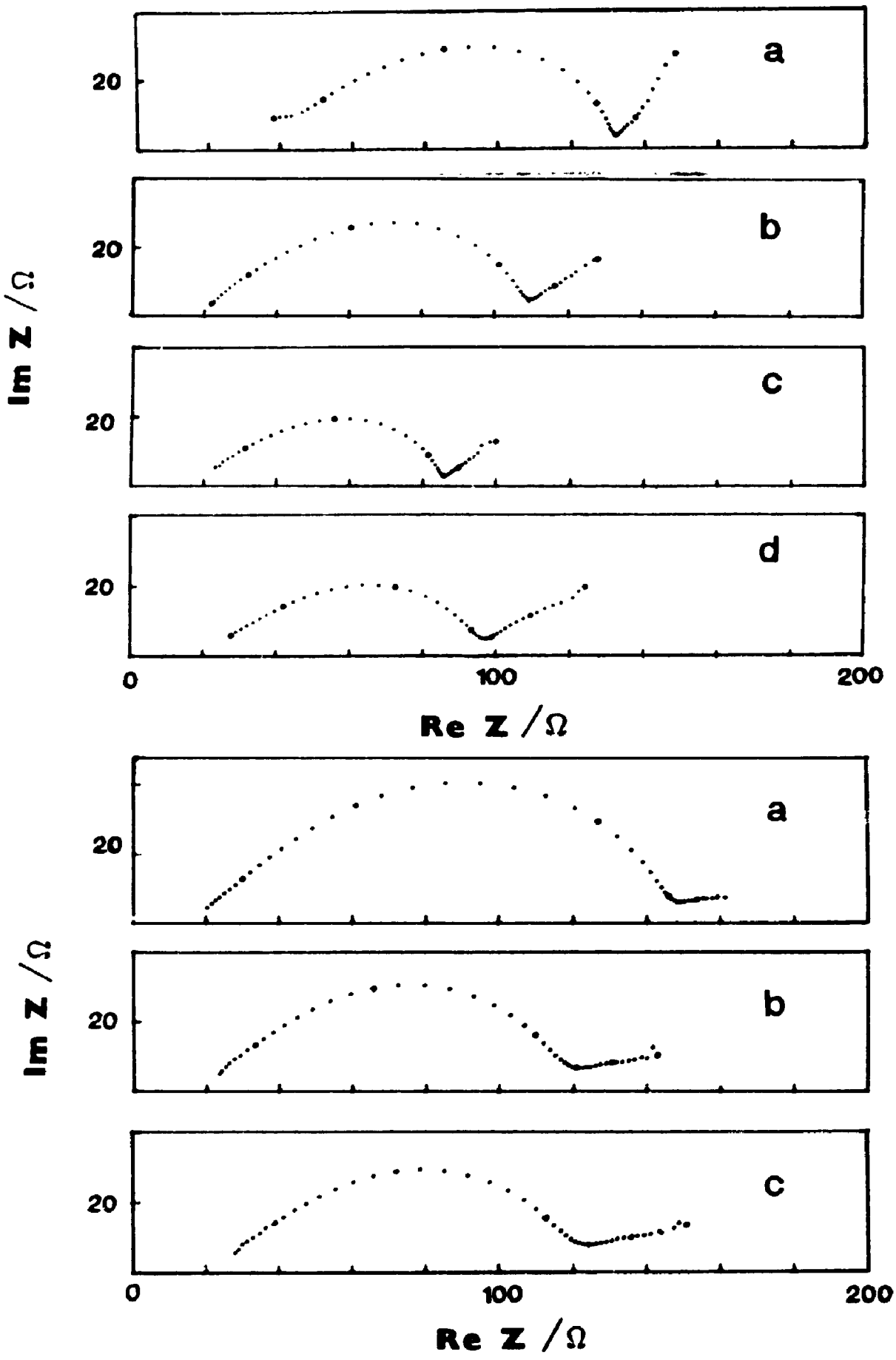
a
b
c
d
20
20
20
20
Im Z /Ω
0
100
200
Re Z /Ω
a
b
c
20
20
20
Im Z /Ω
0
100
200
Re Z /Ω

species may be $VO(OH)^+$, although the charge on the particles was not known. It has been reported that colloidal V_2O_5 in pure water has a negative zeta potential [61]. The SEM photographs show that nucleation and growth occurs, so a mechanism which involves the adhesion of the colloid particles to the electrode was possible, where they then act as nucleation sites.

Formation of the cathodic species appears to be described by the process

$$4\ H^+ + HV_2O_7^{3-} + 2\ e^- = HV_2O_5^- + 2\ H_2O$$

where from cyclic voltammetry the cathodic and anodic diffusion-limited peak at E = -0.15 V (SCE). It was estimated that pH = 8 would be required to reach this potential at 40°C, which was a not unreasonable value based on the calculations shown in chapter 5.

9.2 Cathode materials and batteries

Decomposition of ammonium hexavanadates, under mild heating conditions of about 300°C for about 1h, results in the formation of an electrode containing essentially pure crystalline orthorhombic V_2O_5. Upon heating no major changes occur in crystal morphology as NH_3 and H_2O leave from their inter-layer positions between vanadium and oxygen. By decomposition of tetrammonium hexavanadates under low O_2 partial pressures (argon or vacuum atmosphere) non-stoichiometric $V_6O_{13+\delta}$ was formed where δ ranges from 0 to 0.8. The mechanism of decomposition depends on the method used and the presence of V(IV) and the amount of ammonium in the sample. The reversible insertion of protons and Li^+, in amounts seen by other researchers, has been observed in these electrodes

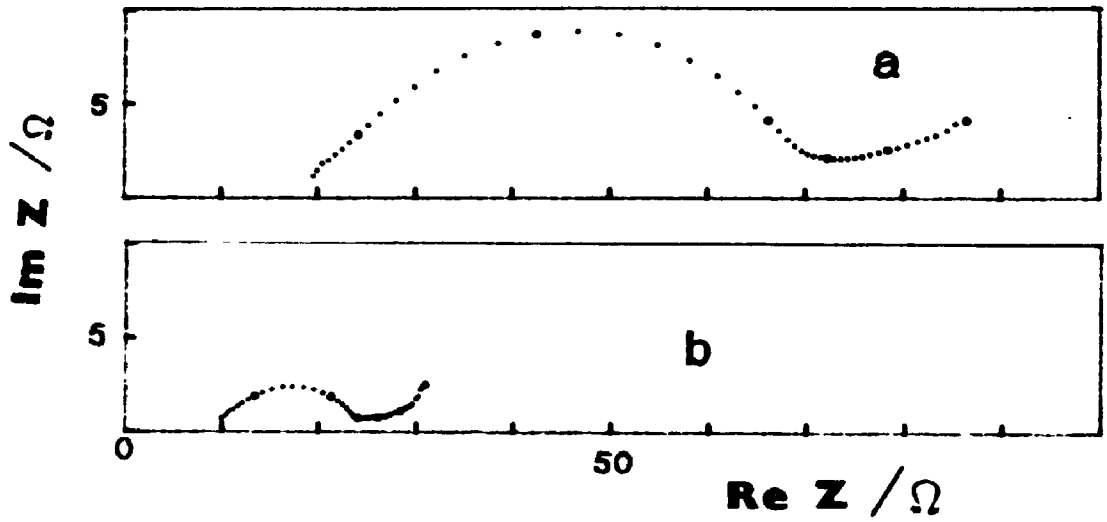
a
b
5
5
0
50
Im Z /Ω
Re Z /Ω

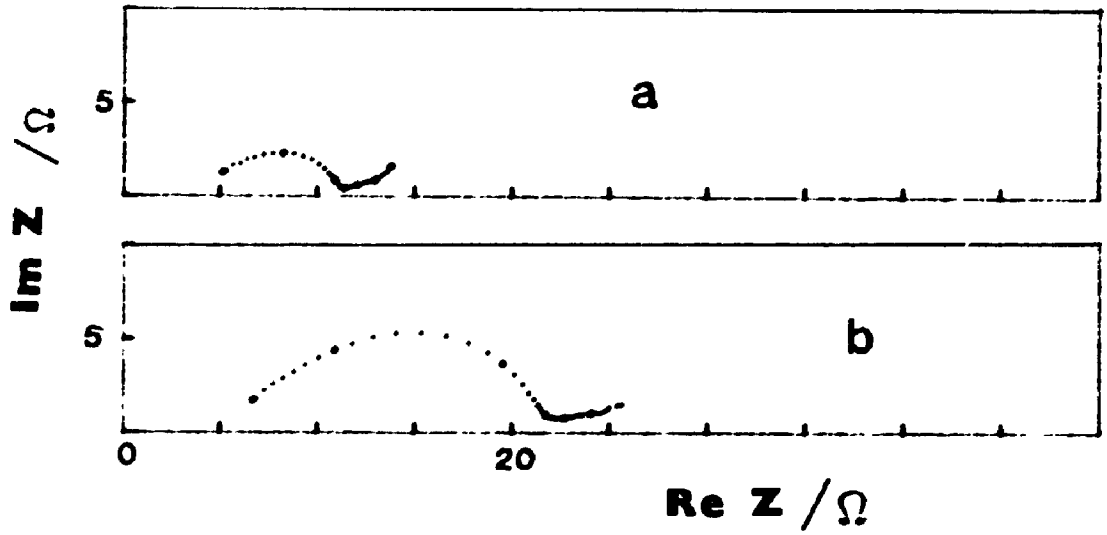
a
b
5
5
0
20
Im Z /Ω
Re Z /Ω

Fig. 8.5 Impedance spectrum as a function of the state of charge/discharge of the single cell battery. a) fully charged, b) discharged 1st step, c) discharged 2nd step and d) charged 1st step.

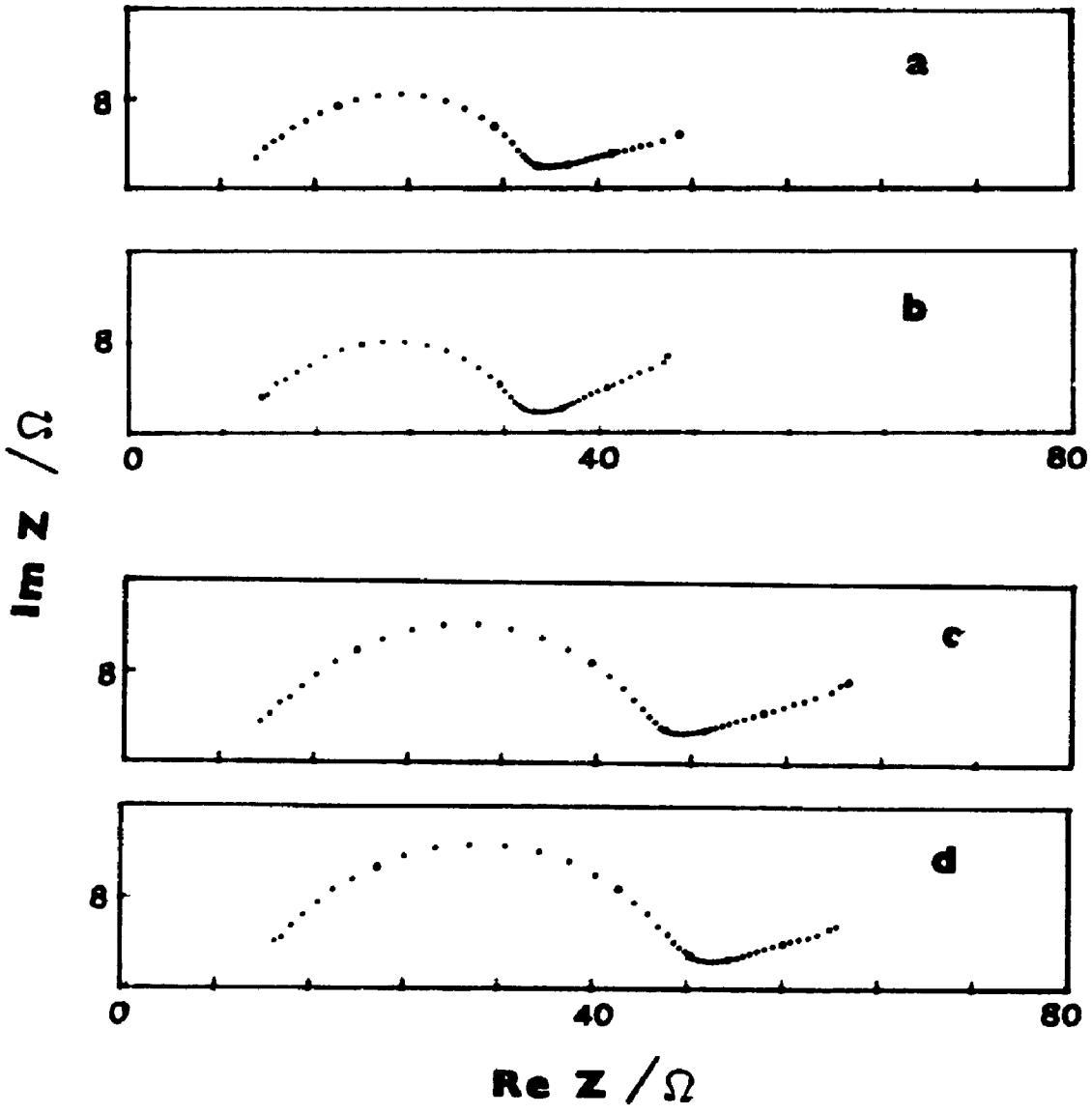
a
b
c
d
8
8
8
8
0
40
80
0
40
80
Im Z /Ω
Re Z /Ω

CHAPTER 9

SUMMARY AND CONCLUSIONS

9.1 Electrodeposition

The conditions of formation of useful insertion electrodes by electrodeposition have been found to be very important. Optimum formation of uniform, crystalline deposits of hexavanadates depended on both the electrochemical technique used and on the nature of the solution, including the concentration of vanadate, VO_3^-, and cation species present. Thick, uniform, crystalline, highly oriented anodic deposits of hydrated diammonium hexavanadate, $(NH_4)_2V_6O_{16}\cdot H_2O$, can be galvanostatically formed on various conducting substrates anodes from saturated aqueous NH_4VO_3 at 40°C. By heating this deposit at about 200°C the water was removed to give a pure phase of $(NH_4)_2V_6O_{16}$. The X-ray pattern for this deposit matches well with similar material made by the precipitation method [25,48].

The mechanism of formation involves a decrease in pH at the anode accompanying evolution of oxygen, which causes formation of V_2O_5 sol. The microcrystalline sol particles then orient in the electric field and deposit on the anode by electrophoresis. Only insertion of unhydrated H^+ and Li^+ occurs for an electrode of diammonium hexavanadate. The potassium and sodium ion do not insert into the structure to form a bronze because of their larger ionic radii compared to lithium. Insertion gives a dark green colour to the bronze, while removal regenerates the original bright orange-red colour. Phase changes for the hexavanadate are very distinct corresponding to similar phase changes in pure V_2O_5, only at lower Li/V ratios. The presence of

ammonia and water in the layered hexavanadate framework limits the maximum amount of lithium or hydrogen that can be inserted (Li/V = 0.24). Use as a reversible cathode material was possible; however, because of the limited amount of lithium that can be inserted and removed, it is doubtful if this compound is a suitable cathode material for lithium batteries.

An electrochemical preparation of stoichiometric tetrammonium and alkali metal hexavanadates of the form $M_4V_6O_{16}$, where M = NH_4, K, Rb, or Cs, has been reported. Two of these new phases, Rb and Cs hexavanadate, have never been synthesized before. Their x-ray patterns have been measured and analyzed. Also, several mixed hexavanadates of these pure phases were synthesized electrochemically. The substitution of one or more of the alkali metal cations was found to occur in a continuous fashion from x = 0 to 4 with stoichiometry $N_xM_{4-x}V_6O_{16}$, where M,N = NH_4, K, Rb, or Cs and M ≠ N. An extension to the composition diagram of Pouchard for $K_2V_3O_8$ [26] has been made to include the new pure and mixed phases. The electrochemical method seems to offer much better control of the stoichiometry of the crystalline material deposited compared to other methods used in the past for making ammonium or potassium hexavanadates.

These materials proved to be poor insertion electrodes for lithium because of the large amount of ammonium or alkali metal ion that they contained. Insertion past the ratio Li/V = 0.05 was not possible and these electrodes did not display any reversibility at all. Therefore, potential use of the materials in this form as reversible cathodes for lithium batteries was not possible. Formation of cathodic deposits occurs by creating a gradient of basic pH at the cathode. The V(IV)

species may be $VO(OH)^+$, although the charge on the particles was not known. It has been reported that colloidal V_2O_5 in pure water has a negative zeta potential [61]. The SEM photographs show that nucleation and growth occurs, so a mechanism which involves the adhesion of the colloid particles to the electrode was possible, where they then act as nucleation sites.

Formation of the cathodic species appears to be described by the process

$$4\ H^+ + HV_2O_7^{3-} + 2\ e^- = HV_2O_5^- + 2\ H_2O$$

where from cyclic voltammetry the cathodic and anodic diffusion-limited peak at E = -0.15 V (SCE). It was estimated that pH = 8 would be required to reach this potential at 40°C, which was a not unreasonable value based on the calculations shown in chapter 5.

9.2 Cathode materials and batteries

Decomposition of ammonium hexavanadates, under mild heating conditions of about 300°C for about 1h, results in the formation of an electrode containing essentially pure crystalline orthorhombic V_2O_5. Upon heating no major changes occur in crystal morphology as NH_3 and H_2O leave from their inter-layer positions between vanadium and oxygen. By decomposition of tetrammonium hexavanadates under low O_2 partial pressures (argon or vacuum atmosphere) non-stoichiometric $V_6O_{13+\delta}$ was formed where δ ranges from 0 to 0.8. The mechanism of decomposition depends on the method used and the presence of V(IV) and the amount of ammonium in the sample. The reversible insertion of protons and Li^+, in amounts seen by other researchers, has been observed in these electrodes

with the three phases α, ϵ, and δ clearly visible experimentally in the ranges expected for a V_2O_5 bronze.

In an attempt to account for the shape of the potential - x curves, a theoretical equation for the potential was developed on the basis of a Bragg-Williams model. Both the insertion into ammonium hexavanadates and pure V_2O_5 electrodes show a relatively small contribution from the configurational term. The Q function (eqn. 2.9) (shows linear portions where the slopes of the Q plot for V_2O_5 are much smaller than for the hexavanadate electrodes, with the tetrammonium steeper than the diammonium hexavanadate (contains more ammonia and water). This suggests that the lithium ion-ammonium-water interactions are more important than ion-ion interactions between the lithium ions and the V(IV) ions on the lattice.

A reversible single cell using an electrochemically-made V_2O_5 cathode has a good lifetime of 500+ cycles. The initial utilization of the cathode was good (>90%), using reasonable discharge values of about 0.125 mA/cm^2. Cells typically have a half-life of about 200 cycles for the capacity of the cathode material from the initial cathode utilization. No reaction occurs at the interface between the tetraglyme-$LiClO_4$ electrolyte and the cathode, and the contact was good owing to the low viscosity of the polymer at the temperatures of interest. This lower viscosity of the electrolyte allowed the cell to make better use of the larger surface area of the crystalline pure V_2O_5 cathode. Futhermore, the tetraglyme-$LiClO_4$ electrolyte system has a better conductivity than PEO or MEEP as well as a better electrochemical stability [103].

An advantage of using thermally decomposed electrodeposits over

composite electrodes used by other researchers, especially for fundamental electrochemical experiments, was that only pure V_2O_5 electrodes with no extraneous materials were used. Cells show an initial decrease in the overall resistance (which reached a minimum at 25 cycles of about 64 ohms) followed by a gradual increase with cycle number. Increasing the temperature from 25°C improved the electrolyte and overall cell resistance with the best results in the temperature range of 50-60°C. The cell resistance, and more specifically that of the V_2O_5 cathode, was affected by the state of charge or discharge, i.e., the phase of the $Li_xV_2O_5$ bronze. Generally, the resistance increased with the amount of lithium inserted, with large changes occuring in the range of $x = 0.8$ to 1.0 for the δ-phase of the bronze.

The problems in the loss of capacity and eventual death of the cell lie primarily with the Li anode-electrolyte interface because of formation of dendrites. Attempts at replacing the pure lithium metal with a electrochemically-made LiAl alloy proved even less successful since complete failure occurred after only 20 cycles. This was probably due to extensive dendrite formation during the alloy formation which speeds up the eventual death of the battery.

Appendix I(a)

```
10 PRINT:INPUT "TYPE - P - IF YOU WISH TO PLOT A FILE ALREADY STORED : ";P$
20 IF P$="P" GOTO 1110
30 FOR J=1 TO 500:NEXT J
40 FOR J=1 TO 100:NEXT J:SCREEN 2,0:WIDTH 80:CLS 2
50 LINE(1,1)-(800,400),1,B
60 LINE(266,35)-(266,400):LINE(532,35)-(532,400)
70 LOCATE 2,22:PRINT "PAR 273 COMMAND FILES AVAILABLE"
80 LINE(120,1)-(690,35),1,B
90 LOCATE 4,12:PRINT "CV":LOCATE 4,39:PRINT "CP":LOCATE 4,66:PRINT "CC"
100 REM ---- ------- ----------------------------------------------------------
110 LOCATE 6,28:PRINT "COMTST(3000,200 pt,.01s)"
120 LOCATE 7,28:PRINT "COMTST2(3000,200 pt,.01s)"
130 LOCATE 8,28:PRINT "COMTST3(3000,200 pt,.01s)"
140 LOCATE 9,1:PRINT "REDRAMP(0to-.7V(50mV/s))"
150 LOCATE 6,1:PRINT "LV#2(1.0TO-1.0V(50mV/s))"
160 LOCATE 10,1:PRINT"REDRAMP2(0to-.7V(50mV/s))"
170 LOCATE 11,1:PRINT"REDRAMP3(.5to-0.7(50mV/s))"
180 LOCATE 12,1:PRINT"REDRAMP5(.5to-1.0(50mV/s))"
190 LOCATE 9,28:PRINT "PS-700(10step(1000to-700)"
  0 LOCATE 10,28:PRINT "COLBLE1(-1.00Vto+1.00V step)"
210 LOCATE 11,28:PRINT "COLBLE2(-2.0Vto+2.0V step)"
220 LOCATE 12,28:PRINT "COLBLE3(-3.0Vto+3.0V step)"
230 LOCATE 12,28:PRINT "COLBLER(-0.5Vto+0.5V step)"
240 LOCATE 6,55:PRINT "CCV205(1000pt.10mA 100Q)"
250 LOCATE 7,56:PRINT "CC#1(200pt,1s,1mA)"
260 LOCATE 8,55:PRINT "CCINSERT(2000pt.10mA 20Q)"
270 LOCATE 9,56:PRINT "CC#2(1000pt,2+hr,1mA)"
280 LOCATE 11,56:PRINT "CC#3(1000pt,27+hr,.1mA)"
290 LOCATE 13,54:PRINT "CC#4(500pt,13+hr,.1mA,5.0Q)"
300 LOCATE 15,54:PRINT "CC#5(6000pt-s .1mA,.60Q)"
310 LOCATE 17,54:PRINT "CC#6(2500pt-s .1mA .25Q)"
320 LOCATE 19,54:PRINT "CC#7(6000pt-s 100mA,600Q)"
330 LOCATE 21,58:PRINT    00(DC 0 500 COMMAND)"
340 LOCATE 23,57:PRI      0(DC 0 1000 COMMAND)"
350 REM ---- ------ -----    -- ----------------------------------------------------
360 BEEP:LOCATE 24,1:INPUT "ENTER COM FILE YOU WISH TO EXECUTE - ";CO$
370 SCREEN 2,0:WIDTH 80:CLS 2
380 PS$="N"
390 FIL$="A:"+CO$
395  OPEN  FIL$ FOR INPUT AS #1
400 LINE INPUT #1,LIN$:PRINT LIN$:PRINT
410 LINE INPUT #1,LIN$:NUM=VAL(LIN$):PRINT NUM;" # COMMAND LINES"
420 M$="CELL "
430   FOR I=1 TO NUM-1
440     LINE INPUT #1,LIN$:PRINT LIN$
450       IF NOT LIN$="CELL 1" GOTO 470
460       BEEP:PRINT "CELL IS NOW ON ! ! !"
470       IF NOT LIN$="TC" GOTO 490
480       BEEP:PRINT "- - - - - - CURVE AQUISTION IS NOW IN PROGRESS ! ! ! - - - -
490        GOSUB 6090
500        OPEN"COM1:"
510        TERMIN,2:TERMOUT,2
```

```
520 FOR J=1 TO 50:NEXT J
530       LAG,10:OUTBUS,LIN$:UNLISTEN
540 FOR J=1 TO 50:NEXT J
550       CLOSE488
560 NEXT I
570 PRINT:PRINT "COM FILE HAS BEEN EXECUTED !":BEEP:PRINT
580 PRINT "TYPE - COM - TO RUN ANOTHER COMMAND FILE"
590 PRINT "      - SAVE - TO SAVE DATA IN A FILE AND SEE DATA ON SCREEN"
600 PRINT "     -  SA  - TO SAVE DATA ONLY ! ! !
610 INPUT "      -  Q  - TO QUIT NOW      - - ENTER CHOICE - - ";Q$
620 IF Q$="COM" THEN CLOSE#1
630 IF Q$="COM" THEN GOTO 40
640 IF Q$="SAVE" GOTO 690
650 IF Q$="SA" GOTO 700
660 IF Q$="Q" GOTO 680
670 GOTO 580
680 END
690 DIM LN(3004),Z(3004)
700 PRINT:PRINT "DATA COLLECTION TO FLOPPY DISK B"
710 LINE INPUT #1,DC$:PRINT DC$
720 LINE INPUT #1,LIN$:NUBB=VAL(LIN$):PRINT "FIRST PT.";NUBB
730 LINE INPUT #1,LIN$:NUMB=VAL(LIN$):PRINT "LAST PT. ";NUMB
740 PRINT:INPUT "ENTER THE FILENAME YOU WISH TO STORE THE DATA UNDER  ";DAT$
750 PRINT "ENTER EXPERIMENTAL CONDITIONS (stored 1st line of file)"
760 INPUT "                -    - ";FL$
770 HEAD$=FL$
780 FLA$="NO"
790 INPUT "MORE CONDITIONS or type NO - ";FLA$
800 IF FLA$="NO" THEN HEA$=" "
810 IF NOT FLA$="NO" THEN HEA$=FLA$
820 FI$="B:"+DAT$
830 OPEN "O",#2,FI$
840 PRINT #2,FL$
850  PRINT#2,HEA$
860 GOSUB 6090
870 OPEN488
880 TERMIN,2:TERMOUT,2
890 LAG,10:OUTBUS,DC$:UNLISTEN
900 TAG,10
910   FOR I=NUBB TO NUMB-1
920     X$=STRING$(5," "):Y$=STRING$(5," ")
930     INBUS,X$
940     INBUS,Y$
950     X=VAL(X$):PRINT #2,X
960     IF Q$="SA" GOTO 980
970     R=1+I:LN(R)=-X
980    NEXT I
990  NPOINTS=R
1000 UNTALK
1010 CLOSE488
1020 CLOSE #2
1030 PS$="N"
1040 BEEP:INPUT "  IF COLOUR-BLEACH EXP. TO STORE BLEACH FILE ENTER  ";
1050 IF PS$="Y" GOTO 700
```

```
1060 CLOSE #1
1070 PRINT:BEEP:FOR J=1 TO 100:NEXT J
1080 PRINT "FILE HAS BEEN MADE IN DRIVE B - filename= ";FILE$:PRINT
1090 INPUT "TO QUIT NOW TYPE -- Q -  ";FIN$
1100 IF NOT FIN$="Q" GOTO 1110
1110 IF Q$="SAVE" GOTO 1130
1120 DIM Z(3004),LN(3004)
1130 SCREEN 2,0:WIDTH 80:CLS 2
1140 PRINT "WHAT TYPE OF EXPERIMENT WAS RUN ?"
1150 PRINT "      TYPE  CC  - FOR CONSTANT CURRENT"
1160 PRINT "            CP  - FOR CONSTANT POTENTIAL"
1170 PRINT "            CV  - FOR CYCLIC VOLTAMMETRY"
1180 INPUT "MAKE CHOICE";EXPER$
1190 PRINT " "
1200 IF Q$="SAVE" GOTO 1420
1210 INPUT "TYPE NAME OF DATA FILE TO CONVERT";DATA$
1220 FILE$="B:"+DATA$
1230 OPEN FILE$ FOR INPUT AS #1
1240 LINE INPUT #1,LN$
1250 HEAD$=LN$
1260 LINE INPUT #1,LN$
1270 HEA$=LN$
1280 I=1:YTINY=0:YBIG=0:Y=0
1290 WHILE NOT EOF(1)
1300 LINE INPUT #1,LN$
1310 IF NOT EXPER$="CC" GOTO 1340
1320 I=I+1:Y=VAL(LN$)
1330 GOTO 1350
1340 LN(I)= VAL(LN$)
1350 Y=LN(I)
1360 IF I=1 THEN YBIG=Y
1370 IF Y>YBIG THEN YBIG=Y
1380 IF I=1 THEN YTINY=Y
1390 IF Y<YTINY THEN YTINY=Y
1400 I=I+1
1410 WEND:NPOINTS=I-1:CLOSE #1
1420 PRINT "NO. POINTS = ";NPOINTS
1430 BEEP
1440 PRINT " "
1450 PRINT "PROGRAM ASSUMES 1 SAMPLE/POINT ie. averaging done,only POINTS"
1460 PRINT " "
1470 IF NOT EXPER$="CV" GOTO 2010
1480 PRINT "CONDITIONS : ";HEAD$,HEA$
1490 INPUT "ENTER STARTING POTENTIAL OF SWEEP IN mV:";XMININ
1500 INPUT "END POTENTIAL OF INITIAL SWEEP IN mV:",XMAXFOR
1510 INPUT "WHAT WAS THE SWEEP RATE IN mV/SEC";RATE
1520 IF XMININ<XMAXFOR THEN DIR=1:PRINT DIR;"--"
1530 IF XMININ>XMAXFOR THEN DIR=-1:PRINT DIR;"--"
1540 PRINT "SWEEP IN ONE DIRECTION TAKES ";T;" SEC"
1550 I=0
1560 FOR I=1 TO NPOINTS-2
1570 NEXT I:PRINT NPOINTS
1580 DELTAV=T/NPOINTS
1590 FOR I=1 TO NPOINTS
```

```
1610    IF B>ABS(LN(I)) GOTO 1630
1620    B=ABS(LN(I))
1630 Z(I)=T
1640  T=T + DELTAT
1650 NEXT I
1660 PRINT "HALF WAY  ";NPTS
1670 NPTSS=NPTS+1
1680 FOR I=NPTSS TO NPOINTS
1690    IF B>ABS(LN(I)) GOTO 1710
1700    B=ABS(LN(I))
1710 Z(I)=T
1720  T=T-DELTAT
1730 NEXT I
1740 IF NOT NPTS*5 GOTO 1780
1750 FOR I=(NPTS-3) TO (NPTS+3)
1760 PRINT I,Z(I),LN(I)
1770 NEXT I
1780 XMAX=Z(NPTS):XMIN=Z(1)
175   YMIN=0:YMAX=B
1800  APRED = 0   :   APR = 0   :   APOX   =   0   :   APO   =   0
1810      FOR   I = 2   TO NPOINTS   STEP   2
1820        B = I-1
1830        C = I
1840        D = I+1
1850     Y0   =   LN(B)
1860     Y1   =   LN(C)
1870     Y2   =   LN(D)
1880   IF   Y1 > 0   GOTO   1920
1890        APRED =   DELTAT / 3 * (Y0 + 4*Y1 + Y2)
1900          APR   =   APR +   APRED
1910   GOTO 1940
1920        APOX   =   DELTAT / 3 * (Y0 + 4*Y1 + Y2)
1930          APO   =   APO +   APOX
1940   NEXT I
1950        PRINT:PRINT "AREA UNDER REDUCTION PEAK  =  ";APR;" arb. units"
1960        PRINT:PRINT "AREA UNDER OXIDATION PEAK  =  ";APO;" arb. units"
1970    ARRAT =   APR/APO
1980        PRINT:PRINT "RATIO OF RED/OX PEAKS   =  ";ARRAT;"arb. units"
1990   PRINT:PRINT
2000 GOTO 2500
2010 BEEP
2020 INPUT "WHAT WAS TIMEBASE USED IN microseconds: ";TBASE
2030 INPUT "WHAT WAS SAMPLES/POINT SETTING FOR Data: ";SP
2040 DELTAT=SP*TBASE/1000000
2050 T=0
2060 B=0
2070 FOR I=1 TO NPOINTS
2080 Z(I)=T
2090    T=T + DELTAT
2100 NEXT I
2110 XMAX=Z(NPOINTS)
2120 XMIN=Z(1)
2130 PRINT
```

```
2140 IF EXPER$="CC" GOTO 2170
2150 INPUT "ENTER VALUE OF CONSTANT POTENTIAL USED IN mV - ";CST:BEEP
2160 GOTO 2180
2170 INPUT "ENTER THE VALUE OF CONSTANT CURRENT USED IN mA - ";CST
2180 PRINT " "
2190 GOTO 2500
2200 IF NOT LOGP$="Y" GOTO 2260
2210 FOR I= XMPT TO XMAPT STEP NTH
2220 Z(I)=(Z(I) - 300)/XDIV
2230 LN(I)=(330 - LN(I))/YDIV
2240 NEXT I
2250 GOTO 2330
2260 FOR I = 1 TO NPOINTS STEP NTH
2270 Z(I)=(Z(I)  - 300)/XDIV
2280 IF NOT EXPER$="CV" GOTO 2310
2290 LN(I)=(180 - LN(I))/YDIV
2300 GOTO 2320
2310 LN(I)=(330 +YMIN*YDIV-LN(I))/YDIV
2320 NEXT I
2330 IF YEA$="Y" GOTO 3770
2340 FACT=1000
2350 IF NOT LOGP$="Y" GOTO 2500
2360 INPUT "ENTER DATA PT. YOU WISH AS X-MIN: ";XMPT
2370 PRINT NPOINTS;" # OF PTS."
2380 INPUT "ENTER DATA PT. YOU WISH AS X-MAX: ";XMAPT
2390 CONV=2.302585#
2400 XMIN=Z(XMPT):YMIN=LN(XMPT):XMAX=Z(XMAPT):YMAX=LN(XMAPT)
2410 XMIN=LOG(XMIN)/CONV:XLIMIT=LOG(XMAX)/CONV
2420 YMIN=ABS(YMIN):YMAX=ABS(YMAX)
2430 YLIMIT=LOG(YMIN)/CONV:YMIN=LOG(YMAX)/CONV
2440 PRINT "YMIN",YMIN,"YLIMIT",YLIMIT
2450  FOR I= XMPT TO XMAPT
2460   Z(I)=LOG(Z(I))/CONV
2470   LN(I)=ABS(LN(I)):LN(I)=LOG(LN(I))/CONV
2480  NEXT I
2490  GOTO 2670
2500 PRINT "SET THE FILE TO THE PROPER UNITS ie. not yet corrected"
2510 PRINT "CONDITIONS - ";HEAD$:BEEP
2520 INPUT "TYPE - Y  ";OK$
2530 FACT=1000
2540 IF NOT OK$="Y" GOTO 2570
2550 PRINT "FORM IS:  FILE/1000 * CURRENT RANGE"
2560 INPUT "ENTER CURRENT RANGE :";FACT
2570 PRINT "XMAX IS:";XMAX,"XMIN IS:";XMIN
2580 INPUT "WHAT DO YOU WISH AS X-LIMIT OF X-AXIS";XLIMIT
2590 PRINT " "
2600 PRINT "FROM FILE (not changed in any way)"
2610 PRINT "ABSLOUTE YMAX IS: ";YBIG,"YMIN IS: ";YTINY
2620 INPUT "WHAT DO YOU WISH AS UPPER Y OF Y AXIS";YLIMIT
2630 INPUT "WHAT DO YOU WISH AS LOWER Y OF Y AXIS";YMIN
2640 PRINT " "
2650 NTH=1
2660 PRINT "THERE ARE ";NPOINTS;" POINTS"
2670 INPUT "ENTER HOW MANY PTS. TO PLOT BY PLOTTING THE N'TH PT. - ";NTH
```

```
2680 PRINT " "
2690 XDIV=450/XLIMIT
2700 IF NOT EXPER$="CV" GOTO 2730
2710 YDIV=150/YLIMIT
2720 GOTO 2740
2730 YDIV=300/(YLIMIT - YMIN)
2740 YEA$="N"
2750 YL=YLIMIT/1000*FACT
2760 PRINT " "
2770 IF EXPER$="CC" GOTO 2820
2780 PRINT " "
2790 PRINT "ENTER UNITS OF CURRENT AS - uA, mA, or A"
2800 INPUT "MAKE CHOICE:";CUR$
2810 GOTO 2850
2820 PRINT " "
2830 PRINT "ENTER UNITS OF POTENTIAL AS - uV, mV, or V"
2840 INPUT "MAKE CHOICE:";POT$
2850 PRINT " "
2860 SCREEN 2,0
2870 WIDTH 80
2880 CLS 2
2890 IF NOT EXPER$="CV" GOTO 3190
2900 LINE (295,25)-(295,330)
2910 LINE (300,180)-(755,180)
2920 DRAW " bm 295,360"
2930 FOR I=0 TO 10
2940 DRAW " u 30;br 5;l 5"
2950 NEXT I
2960 DRAW " bm 300,180"
2970 DRAW "bu 2; d 2"
2980 FOR I=0 TO 9
2990 DRAW " r 45; bu 2;d 2"
3000 NEXT I
3010 LOCATE 12,28:PRINT "0"
3020 LOCATE 5,16:PRINT "CURRENT/";CUR$
3030 LOCATE 1,1:PRINT "A C.V. EXPERIMENT"
3040 LOCATE 2,1:PRINT "from ";XMINPOT;" to ";XMAXPOT;" mV"
3050 LOCATE 14,72:PRINT XMAXPOT;"mV"
3060 LOCATE 9,29:PRINT XMINPOT;" mV"
3070 LOCATE 23,50:PRINT "POTENTIAL/mV"
3080 LOCATE 3,25:PRINT YL
3090 YLIMI=-YLIMIT
3100 YLI=YLIMI/1000*FACT
3110 LOCATE 21,25:PRINT YLI
3120 PRINT NTH
3130 FOR I=1 TO NPOINTS STEP NTH
3140 LN(I)=180-LN(I)*YDIV
3150 Z(I)=Z(I)*XDIV+300
3160 CIRCLE(Z(I),LN(I)),0
3170 NEXT I
3180 GOTO 3700
```

```
3190 LINE(300,25)-(755,330),1,B
3200 DRAW "bm 300,330"
3210 FOR I= 0 TO 9
3220 DRAW "r 45; bu 5;d 5"
3230 NEXT I
3240 DRAW "l 450"
3250 FOR J= 0 TO 9
3260 DRAW "u 30;bl 5;r 5"
3270 NEXT J
3280 IF NOT LOGP$="Y" GOTO 3370
3290 LOCATE 1,1:PRINT "LOG(CURRENT) vs. LOG(TIME) PLOT"
3300 LOCATE 5,1:PRINT "LOG(CURRENT/";CUR$;")"
3310 LOCATE 23,50:PRINT "LOG(TIME/s)"
3320 LOCATE 22,70:PRINT XLIMIT
3330 LOCATE 2,25:PRINT YLIMIT
3340 LOCATE 20,29:PRINT "0"
3350 LOCATE 22,73:PRINT "0"
3360 GOTO 3020
3370 LOCATE 21,27:PRINT YMIN
3380 LOCATE 22,31:PRINT "0"
3390 LOCATE 22,75:PRINT XLIMIT
3400 LOCATE 23,50:PRINT "TIME/s"
3410 LOCATE 2,25:PRINT YL
3420 IF EXPER$="CC" GOTO 3480
3430 LOCATE 1,1:PRINT "A CONSTANT POTENTIAL"
3440 LOCATE 2,6:PRINT "EXPERIMENT"
3450 LOCATE 3,1:PRINT CST;" mV applied"
3460 LOCATE 5,15:PRINT "CURRENT/";CUR$
3470 GOTO 3520
3480 LOCATE 5,15:PRINT "POTENTIAL/";POT$
3490 LOCATE 1,1:PRINT "A CONSTANT CURRENT"
3500 LOCATE 2,4:PRINT "EXPERIMENT"
3510 LOCATE 3,1:PRINT CST;" mA applied"
3520 IF NOT LOGP$="Y" GOTO 3600
3530 FOR I=XMPT TO XMAPT STEP NTH
3540 LN(I)=330-LN(I)*YDIV
3550 Z(I)=Z(I)*XDIV+300
3560 CIRCLE(Z(I),LN(I)),0
3570 NEXT I
3580 GOTO 3650
3590 PRINT NTH
3600 FOR I= 1 TO NPOINTS STEP NTH
3610 LN(I)=330+YMIN*YDIV-LN(I)*YDIV
3620 Z(I)=Z(I)*XDIV+300
3630 CIRCLE(Z(I),LN(I)),0
3640 NEXT I
3650 IF NOT EXPER$="CP" GOTO 3700
3660 BEEP
3670 IF LOGP$="Y" GOTO 3730
3680 LOCATE 6,1:INPUT "LOG-LOG PLOT -Y- ";LOGP$
3690 IF LOGP$="Y" GOTO 2260
3700 LOCATE 7,1:PRINT "CHANGE THE SCALE OR # PTS.";BEEP
3710 LOCATE 8,1:INPUT "ENTER - Y - ";YUP$
3720 IF YUP$="Y" GOTO 2200
3730 LOCATE 9,1:PRINT "MAKE HARDCOPY ON HP"
```

```
3740 LOCATE 10,1:INPUT "TYPE - Y - ";YEA$
3750 IF YEA$="Y" GOTO 2200
3760 END
3770 REM - HP VIA RS232C PORT B
3780 LOCATE 11,1:BEEP:PRINT "LOAD PAPER TO PLOTTER ' ' '"
3790 LOCATE 12,1:INPUT "pen down enter - PD - ";PD$
3800 LOCATE 13,1:INPUT "TYPE -L- IF 11*17 PAPER -";LPAPER$
3810 INCREM=(YLIMIT-YMIN)/10
3820 INCRE=XLIMIT/10
3830 XLAB=INCRE*5
3840 YLAB=YMIN-INCREM/2
3850 YLABEL=INCREM/2 + YLIMIT
3860 OPEN "O",1,"SERIALB"
3870 IF LPAPER$="L" GOTO 3900
3880 PRINT#1, "IN;IP 800,750,10000,7300;"
3890 GOTO 3910
3900 PRINT#1, 'IN;IP750,700,15000,9500;"
3910 IF EXPER$="CV" GOTO 5000
3920 IF NOT LOGP$="Y" GOTO 4470
3930 XMIN=0:YMIN=INT(YMIN)
3940 PRINT YMIN,"YMIN":BEEP
3950 XLIMIT=INT(XLIMIT)+1:YLIMIT=INT(YLIMIT)+1
3960 INCREM=(YLIMIT-YMIN)/10
3970 INCRE=XLIMIT/10
3980 XLAB=INCRE*5
3990 YLAB=INCREM/2
4000 YLABEL=INCREM/2*21
4010 PRINT#1, "SC";XMIN;XLIMIT;YMIN;YLIMIT
4020 FOR J=1 TO 500:NEXT J
4030 PRINT XMIN,XLIMIT,YMIN,YLIMIT
4040 PRINT#1, "SP1;"
4050 X=Z(XMPT):Y=LN(XMPT)
4060 PRINT#1, "PU";X;Y
4070 W=NTH+XMPT
4080 FOR I=W TO XMAPT STEP NTH
4090 J=I-NTH
4100 XA=Z(J):YA=LN(J)
4110 X=Z(I):Y=LN(I)
4120   IF NOT PD$="PD" GOTO 4150
4130 PRINT#1, "PA";XA;YA;";PD";X;Y
4140 GOTO 4160
4150 PRINT#1, "PU";X;Y;";PD;"
4160 NEXT I
4170 PRINT#1, "PU;"
4180 FOR J=1 TO 500:NEXT J
4190 YOYO=YMIN-YLAB:YLAA=YLABEL+YMIN
4200 PRINT#1, "PA";XLAB;YOYO;";LO5;LBLOG(TIME/S)";CHR$(3)
4210 PRINT#1, "PA0,";YLAA;";LO14;LBLOG(CURRENT/";UNIT$;")";CHR$(3)
4220 PRINT#1, "SP2;"
4230 FOR J=1 TO 500:NEXT J
4240 PRINT#1, "PU";XMIN;YMIN;";EA";XLIMIT;YLIMIT
4250 PRINT #1, "SI .2,.3;IL 1.5,0;"
```

```
4260 FOR Y=YMIN TO YLIMIT STEP INCREM
4270   PRINT#1,"PA0,";Y;";YT;"
4280   PRINT #1, "LO8;LB";Y;+CHR$(3)
4290 NEXT Y
4300 FOR J=1 TO 500:NEXT J
4310 FOR X=0 TO XLIMIT STEP INCRE
4320   PRINT#1, "PA";X;YMIN;";XT;"
4330   PRINT#1, "LO16;LB";X;+CHR$(3)
4340 NEXT X
4350 FOR I=1 TO 500:NEXT J
4360 PRINT#1, "SP3;PA";XLAB;YLAA;";SI.3,.45;LO4;"
4370 PRINT#1, "LBA LOG - LOG PLOT"+CHR$(13)+CHR$(3)
4380 PRINT#1, "SI.2,.3;LO16;"
4390 PRINT#1, "LB(";CST;" mV potenti  was applied)"+CHR$(3)
4400 PRINT#1, "PA";XLIMIT;YLAA;";SI..,.3;LO17;"
4410 BEEP
4420 LOCATE 14,1:INPUT "ENTER DATE:";D$
4430 PRINT#1, "LBDATE"+CHR$(13)+CHR$(3)
4440 PRINT#1, "SI.15,.2;LO19;"
4450 PRINT#1, "LB";D$;+CHR$(3)
4460 GOTO 5620
4470 PRINT#1, "SC";XMIN;XLIMIT;YMIN;YLIMIT
4480 PRINT#1, "SP1;"
4490 X=Z(1):Y=LN(1)
4500 PRINT#1, "PA";X;Y;";PU";X;Y
4510 FOR J=1 TO 500:NEXT J
4520 W=NTH+1
4530 FOR I=W TO NPOINTS STEP NTH
4540 J=I-NTH
4550 XA=Z(J):YA=LN(J)
4560 X=Z(I):Y=LN(I)
4570   IF NOT PD$="PD" GOTO 4600
4580 PRINT#1, "PA";XA;YA;";PD";X;Y
4590 GOTO 4610
4600 PRINT#1, "PU";X;Y;";PD;"
4610 NEXT I
4620 PRINT#1, "PU;"
4630 FOR J=1 TO 200:NEXT J
4640 PRINT#1, "PA";XLAB;YLAB;";LO5;LBTIME/s"+CHR$(3)
4650 IF EXPER$="CC" GOTO 4680
4660 PRINT#1, "PA0,";YLABEL;";LO14;LBCURRENT/";CUR$;+CHR$(3)
4670 GOTO 4690
4680 PRINT#1, "PA0,";YLABEL;";LO14;LBPOTENTIAL/";POT$;+CHR$(3)
4690 PRINT#1, "SP2;"
4700 FOR J = 1 TO 500:NEXT J
4710 PRINT#1, "PU";XMIN;YMIN;";EA";XLIMIT;YLIMIT
4720 PRINT #1, "SI .2,.3;TL 1.5,0;"
4730 FOR Y=YMIN TO YLIMIT STEP INCREM
4740   LY=Y/1000*FAC1
4750   PRINT#1,"PA0,";Y;";YT;"
4760   PRINT #1, "LO8;LB";LY;+CHR$(3)
4770 NEXT Y
```

```
4780 FOR X=0 TO XLIMIT STEP INCRE
4790   PRINT#1, "PA";X;YMIN;";XT;"
4800   PRINT#1, "LO16;LB";X;+CHR$(3)
4810 NEXT X
4820 FOR J=1 TO 500:NEXT J
4830 PRINT#1, "SP3;PA";XLAB;YLABEL;";SI.3,.45;LO4;"
4840 IF  EXPER$="CC" GOTO 4890
4850 PRINT#1, "LBA CONSTANT POTENTIAL EXPERIMENT"+CHR$(13)+CHR$(3)
4860 PRINT#1, "SI.2,.3;LO16;"
4870 PRINT#1, "LB(";CST;" mV potential was applied)"+CHR$(3)
4880 GOTO 4930
4890 PRINT#1, "SP3;PA";XLAB;YLABEL;";SI.3,.45;LO4;"
4900 PRINT#1, "LBA CONSTANT CURRENT EXPERIMENT"+CHR$(13)+CHR$(3)
4910 PRINT#1, "SI.2,.3;LO16;"
4920 PRINT#1, "LB(";CST;" mA current was applied)"+CHR$(3)
4930 PRINT#1, "PA";XLIMIT;YLABEL;";SI.2,.3;LO17;"
4940 BEEP
4950 LOCATE 14,1:INPUT "ENTER DATE:";D$
4960 PRINT#1, "LBDATE"+CHR$(13)+CHR$(3)
4970 PRINT#1, "SI.15,.2;LO19;"
4980 PRINT#1, "LB";D$;+CHR$(3)
4990 IF NOT EXPER$="CV" GOTO 5620
5000 PRINT#1, "SC";XMIN;XLIMIT;YLIMI;YLIMIT
5010 PRINT#1, "SP1;"
5020 X=Z(1):Y=LN(1)
5030 PRINT#1, "PA";X;Y;";PU";X;Y
5040 FOR J= 1 TO 500:NEXT J
5050 W=NTH+1
5060 FOR I=W TO NPOINTS STEP NTH
5070 J=I-NTH
5080 XA=Z(J):YA=LN(J)
5090 X=Z(I):Y=LN(I)
5100 IF NOT PD$="PD" GOTO 5130
5110 PRINT#1, "PA";XA;YA;";PD";X;Y
5120 GOTO 5140
5130 PRINT#1, "PU";X;Y;";PD;"
5140 NEXT I
5150 PRINT#1, "PU;"
5160 FOR J= 1 TO 500:NEXT J
5170 PRINT#1, "SI.2,.3;TL1.5,0;"
5180 PRINT#1, "PA";XLAB;YLIMI;"LO16;LBPOTENTIAL/mV vs. S.C.E."+CHR$(3)
5190 PRINT#1, "PA0,";YLABEL;";LO14;LBCURRENT/";CUR$;+CHR$(3)
5200 INCR=YLIMIT/5
5210 PRINT#1, "SP2;"
5220 FOR J= 1 TO 500:NEXT J
5230 PRINT#1, "SI.2,.3;TL1.5,0;"
5240 PRINT#1, "PU";XMIN;YLIMI;";EA";XLIMIT;YLIMIT
5250 PRINT#1, "EU";XLIMIT;",0;PD0,0;"
5260 PRINT#1, "PU;"
5270 FOR Y=YLIMI TO YLIMIT STEP INCR
5280   FY=Y/1000*FACT
5290   PRINT#1, "PA0,";Y;";YT;"
5300   PRINT#1, "LO8;LB";FY;+CHR$(3)
```

```
5310 NEXT Y
5320 YLABEL =INCREM/2*21+INCREM/4
5330 FOR J= 1 TO 500:NEXT J
5340 PRINT#1, "SP3;PA";XLAB;YLABEL;";SI.3,.45;LO14;"
5350 PRINT#1, "LBA CYCLIC VOLTAMMETRY EXPERIMENT"+CHR$(13)+CHR$(3)
5360 PRINT#1, "SI.2,.3;LO16;"
5370 PRINT#1, "LB(from ";XMINPOT;"to ";XMAXPOT;"mV at ";RATE;"mV/s"+CHR$(3)
5380 PRINT#1, "PA";XLIMIT;YLABEL;";SI.2,.3;LO17;"
5390 BEEP
5400 LOCATE 14,1:INPUT "ENTER DATE:";D$
5410 PRINT#1, "LBDATE"+CHR$(13)+CHR$(3)
5420 PRINT#1, "SI.15,.2;LO19;"
5430 PRINT#1, "LB";D$;+CHR$(3)
5440 PRINT#1, "SP1;SI.1,.2;TL1.0,0;"
5450 DIF=XMAXPOT-XMINPOT
5460 NUM = DIF/100
5470 ONE=1
5480  DIFF = ABS(DIF)
5490  IF DIFF> 1500 THEN ONE = 2
5500  IF DIFF> 3500 THEN ONE = 5
5510 IF NUM<0 THEN ONE=-1
5520  IF DIFF> 1500 AND NUM < 0 THEN  ONE = -2
5530  IF DIFF> 3500 AND NUM < 0 THEN  ONE = -5
5540 AB=XMINPOT
5550 NUMB=100*ONE
5560 FOR I=0 TO NUM STEP ONE
5570  ABC=I/NUM*XMAX
5580  PRINT#1, "PA";ABC;",0;XT;"
5590  PRINT#1, "LO16;LB";AB;+CHR$(3)
5600  AB=AB+NUMB
5610 NEXT I
5620 BEEP
5630 REM - ENTER CONDITIONS OF EXP.
5640 PRINT#1, "SP2;SI .1,.175;"
5650 PRINT#1, "PA";XLIMIT;YLIMIT;";LO19;LB";HEAD$;+CHR$(13)+CHR$(3)
5660 NYL=YLIMIT-INCREM/24*7
5670 PRINT#1, "PA";XLIMIT;NYL
5680 PRINT#1, "LO19;LB";HEA$;+CHR$(3)
5690 IF NOT LOGP$="Y" GOTO 5950
5700 BEEP
5710 LOCATE 17,1:INPUT "FOR SLOPE ENTER STARTING PT.";STPT
5720 LOCATE 18,1:INPUT "                    ENDING PT.";ENPT
5730 N=ENPT-STPT+1
5740 XY=0:XX=0:X=0:Y=0
5750  FOR I = STPT TO ENPT
5760   XY=Z(I)*LN(I)+XY
5770   X=Z(I)+X
5780   Y=LN(I)+Y
5790   XX=Z(I)*Z(I)+XX
5800  NEXT I
5810 SLOPE=((N*XY)-(X*Y))/((N*XX)-(X*X))
5820 PRINT "SLOPE",SLOPE
5830 NN=STPT + (ENPT-STPT)/4
5840 NN=INT(NN)
```

```
500 BEEP:BEEP:BEEP: FOR J=1 TO   500
510         JJJ=  500:FFF=J/15 :KKF=CINT(KFF)
520         LLL JJJ/ 15 - FFF
530         LOCATE 22,1:PRINT "PAUSING FOR ";LLL;" sec."
540     NEXT J:LOCATE 22,1:PRINT "                              "
550 IF EXPER$="Y" GOTO 960
560 PRINT:INPUT "IS EXPERIMENT READY TO RUN ? ENTER  Y   ";EXPER$:BEEP:[illegible]
570 INPUT "COM FILE used in exp. is RUNOCD  -- another file [illegible]  Y  ";YOYO$
580 CO$ "RUNOCD":IF NOT YOYO$="Y" GOTO 600
590 INPUT "          ENTER EXP. COM  FILENAME";CO$
600 PRINT:INPUT "ENTER  #  POINTS YOU WISH EXP. TO STOP AT [illegible]
610 COUNT= CNT
620 PRINT:INPUT "ENTER THE FILENAME YOU WISH TO STORE THE DATA UNDER    ";[illegible]
630 PRINT "ENTER EXPERIMENTAL CONDITIONS (stored 1st line of file)"
640 INPUT "                         - - ";FL$
650 HEAD$=FL$
660 FLA$="NO"
670 INPUT "MORE CONDITIONS or type NO - ";FLA$
680  IF FLA$="NO" THEN HEA$=" "
690 IF NOT FLA$ "NO" THEN HEA$=FLA$
700 FIL="B:"+DA$
710 OPEN "O",#2,FI$
720 PRINT #2,FL$
730  PRINT#2,HEA$
740 PRINT:INPUT "ENTER POTENTIAL LIMITS IN   VOLTS' - AS MIN.,MAX.   [illegible]
750  XDIV=450/CNT
760 DELTAY=YMAX YMIN
770  YDIV=400/DELTAY
780 SCREEN 2,0:WIDTH 80:CLS 2
790  LINE(300,25) (755,330),1,B
800  DRAW "bm 300,330"
810  FOR I= 0 TO 9
820  DRAW "r 45: bu 5:d 5"
830  NEXT I
840  DRAW "l 450"
850  FOR J= 0 TO 9
860  DRAW "u 30:bl 5:r 5"
870  NEXT J
880  LOCATE 21,29:PRINT YMIN
890  LOCATE 22,31:PRINT "0"
900  LOCATE 22,75:PRINT CNT
910  LOCATE 23,50:PRINT "DATA PTS"
920  LOCATE 2,25:PRINT YMAX
930  LOCATE 5,15:PRINT "POTENTIAL/V"
940  LOCATE 1,1:PRINT "A CONSTANT CURRENT"
950  LOCATE 2,4:PRINT "LI INSERTION EXP."
960 GOSUB 1430
970 OPEN488
980 IERGIN,2:TERMOUT,2
990 TAG,10:OUTLOG,CHARGE:UNLISTEN
1000 TAG,10
1010       D$=STRING$(5," "):X$=STRING$(5," ")
1020       INBUS,D$
1030       INBUS,X$
1040       [illegible] VAL(D$)
```

Appendix I(b)

```
6
CONSTANT CURRENT EXPERIMENT
15
MODE 1
I/E -2
CELL -100 5
SIE 2
FP 0
TMB 50000
MM 0
S/P 1
LP 3600
NC
CELL 1
TC
WCD
CELL 0
DC 0 3600
0
3600
```

```
A
C.V. +900 TO 1100 mV at 50 mV/s
14
MODE 2
KEY 15
KEY 3
KEY 6
KEY 38
CELL 1
P 5
I/E -3
CV 900 -1100 900 3
NC
TC
WCD
CELL 0
DC 0 6143
0
6143
```

```
A.
A CONSTANT POTENTIAL PROG. FOR +-3V
41
KEY 26
KEY 7
KEY 14
KEY 3
KEY 38
P 10
MODE 2
KEY 15
KEY 14
KEY 6
I/E -2
KEY 38
P 3
FP 0
LP 220
MR 2
MM 1
TMB 50000
S/P 1
BIAS -1000
INITIAL 0 4000
VERTEX 19 4000
VERTEX 20 -8000
VERTEX 220 -8000
NC
CELL 1
TC
WCD
CELL 0
BIAS 1000
FP 221
LP 800
INITIAL 221 -4000
VERTEX 240 -4000
VERTEX 241 8000
VERTEX 800 8000
CELL 1
TC
WCD
CELL 0
DC 0 220
0
220
DC 221 800
221
800
```

Appendix II(a)

```
10 EXPER$="N"
20 N=0 : NNN=0
30 SCREEN 2,0:WIDTH 80:CLS 2
40 LOCATE 2,22:PRINT "OPEN CIRCUIT Li INSERTION PROGRAM"
50 LOCATE 4,15:PRINT "saves charge and circuit potential in one data file"
60 BEEP:FOR I=1 TO 10
70 LOCATE 6,15:PRINT "CHECK DEFAULT COMMAND VALUES  BEFORE STARTING ' ' ' "
80       FOR J=1 TO 40:NEXT J
90 LOCATE 6,15:PRINT "                                                    "
100       FOR J=1 TO 20:NEXT J
110     NEXT I
120 SCREEN 2,0:WIDTH 80:CLS 2
130 LOCATE 4,22:PRINT "OPEN CIRCUIT Li INSERTION PROGRAM"
140 CO$="SETOC"
150 PRINT "COM FILE ";CO$:PRINT
160 FIL$="A:"+CO$
170 OPEN FIL$ FOR INPUT AS #1
180 LINE INPUT #1,LIN$
190 LINE INPUT #1,LIN$:NUM=VAL(LIN$)
200   FOR I=1 TO NUM-2
210     LINE INPUT #1,LIN$:LOCATE 8,1:PRINT "                "
220                        LOCATE 8,1:PRINT LIN$
230       GOSUB 1430
240       OPEN488
250       TERMIN,2:TERMOUT,2
260 FOR J=1 TO 60:NEXT J
270       LAG,10:OUTBUS,LIN$:UNLISTEN
280 IF NOT LIN$= "Q" GOTO 360
285 IF NNN<1  GOTO 360
290 FOR J=1 TO 60:NEXT J
300   TAG,10
310    QQ$=STRING$(5," "):I$=STRING$(5," ")
320     INBUS,QQ$
330     INBUS,I$
340    QQ=VAL(QQ$):LOCATE 19,1:PRINT "OKEE DOKEE ";QQ
350 UNTALK
360 IF NOT LIN$= "READE" GOTO 440
365 IF NNN<1  GOTO 440
370 FOR J=1 TO 60:NEXT J
380  TAG,10
390     PP$=STRING$(5," "):J$=STRING$(5," ")
400       INBUS,PP$
410       INBUS,J$
420     PP=VAL(PP$):LOCATE 20,1:PRINT "HUNKY DOREE ";PP
430  UNTALK
440 FOR J=1 TO 60:NEXT J
450       CLOSE488
455   NNN = NNN + 1
460 NEXT I
470 LINE INPUT #1,CHARG$:LOCATE 8,1:PRINT "       ":LOCATE 8,1:PRINT CHARG$
480 LINE INPUT #1,POT$:LOCATE 8,1:PRINT "       ":LOCATE 8,1:PRINT POT$
490 CLOSE #1
```

```
500 BEEP:BEEP:BEEP: FOR J=1 TO   500
510        JJJ=  500:FFF=J/15 :KKF=CINT(FFF)
520        LLL JJJ/ 15 - FFF
530        LOCATE 22,1:PRINT "PAUSING FOR ";LLL;" sec."
540    NEXT J:LOCATE 22,1:PRINT "                              "
550 IF EXPER$="Y" GOTO 960
560 PRINT:INPUT "IS EXPERIMENT READY TO RUN ? ENTER  Y  ";EXPER$:BEEP:PRINT
570 INPUT "COM FILE used in exp. is RUNOCD  - another file (Y)   ";YOYO$
580 CO$="RUNOCD":IF NOT YOYO$="Y" GOTO 600
590 INPUT "        ENTER EXP. COM  FILENAME";CO$
600 PRINT:INPUT "ENTER #  POINTS YOU WISH EXP. TO STOP AT (NO. KNOWN ...
610 COUNT=  CNT
620 PRINT:INPUT "ENTER THE FILENAME YOU WISH TO STORE THE DATA UNDER   ";FI$
630 PRINT "ENTER EXPERIMENTAL CONDITIONS (stored 1st line of file)"
640 INPUT "                    - - - ";FL$
650 HEAD$=FL$
660 FLA$="NO"
670 INPUT "MORE CONDITIONS or type NO - ";FLA$
680 IF FLA$="NO" THEN HEA$=" "
690 IF NOT FLA$="NO" THEN HEA$=FLA$
700 FI$="B:"+DA$
710 OPEN "O",#2,FI$
720 PRINT #2,FL$
730  PRINT#2,HEA$
740 PRINT:INPUT "ENTER POTENTIAL LIMITS IN  VOLTS - AS MIN.,MAX.   ...
750  XDIV=450/CNT
760 DELTAY=YMAX-YMIN
770  YDIV=400/DELTAY
780 SCREEN 2,0:WIDTH 80:CLS 2
790  LINE(300,25)-(755,330),1,B
800  DRAW "bm 300,330"
810  FOR I=0 TO 9
820  DRAW "r 45; bu 5;d 5"
830  NEXT I
840  DRAW "r 450"
850  FOR J=0 TO 9
860  DRAW "u 30;bl 5;r 5"
870  NEXT J
880  LOCATE 21,29:PRINT YMIN
890  LOCATE 22,31:PRINT "0"
900  LOCATE 22,75:PRINT CNT
910  LOCATE 23,50:PRINT "DATA PTS"
920  LOCATE 2,25:PRINT YMAX
930  LOCATE 5,15:PRINT "POTENTIAL/V"
940  LOCATE 1,1:PRINT "A CONSTANT CURRENT"
950  LOCATE 2,4:PRINT "LI INSERTION EXP."
960 GOSUB 1430
970 OPEN488
980 TERGIN,2:TERMOUT,2
990 TAG,10:OUTBUS,CHARG$:UNLISTEN
1000 TAG,10
1010      U$=STRING$(5," "):X$=STRING$(5," ")
1020      INBUS,U$
1030      INBUS,X$
1040      U=VAL(U$)
```

```
1050 UNTALK
1060 LAG,10:OUTBUS,POT$:UNLISTEN
1070 TAG,10
1080      P$=STRING$(5," "):Y$=STRING$(5," ")
1090      INBUS,P$
1100      INBUS,Y$
1110      P=VAL(P$)
1120 UNTALK
1130 CLOSE488
1136  IF NNN =1.5 THEN  GOTO 1140
1137  QQ=Q : PP=P
1140 PRINT #2,Q,P,QQ,PP
1150 P=P/1000
1152 PP=PP/1000
1160 A = P
1170 LOCATE 10,1:PRINT "    CHARGE     POTENTIAL"
1180 LOCATE 11,1:PRINT "(as stored)      /V"
1190 LOCATE 12,1:PRINT "                      "
1200 LOCATE 13,1:PRINT "    ";Q;"         ";P
1210 LOCATE 15,1:PRINT "                      "
1220 LOCATE 15,1:PRINT "CC ";QQ;"POT     ";PP
1230      P=330+YMIN*YDIV-P*YDIV
1240      PP=330+YMIN*YDIV-PP*YDIV
1250      X=  N*XDIV+300
1260  CIRCLE(X,P),2
1270  CIRCLE(X,PP),4
1280 N=N+1
1290 IF N COUNT GOTO 1320
1300 LOCATE 17,1:PRINT "PT. # ";N
1310 GOTO 160
1320 LOCATE 17,1:PRINT "          "
1330 PRINT:BEEP:PRINT "EXP. IS DONE TO ";CNT
1340 PRINT" POT. OF LAST PT. IS ";A;" V"
1350 PRINT:INPUT "TO CONTINUE ENTER - Y - ";CON$
1360 IF NOT CON$= "Y" GOTO 1410
1370 PRINT:INPUT " # PTS. YOU WISH EXTRA ";CNT
1380 COUNT=  CNT
1390 N=.5
1400 GOTO 160
1410 CLOSE #2
1420 END
1430    REM "IEEE 488 Interface Tool"  Set-up  Routine  Version 1.01 (C)1985,84
1440    REM Dedicated variables description
1450   IEEESEG%=&H2DD  :REM To be set according to Loading Segment
1460    ERR488%=0        :REM Returned Error Code
1470    IEEE488%=&H7:GOSUB 1560:IEEE488%=&HA
1480    ON ERROR GOTO 1550:RETURN
1490    REM
1500    REM BASIC Program Trapping by Service Request
1510    REM
1520    :GOSUB &55310
1530    TERMINATE
1540    REM
1550    GOSUB 1560:IF ERR488% 0 THEN GOTO 1570 ELSE RESUME NEXT
1560    DEF SEG=IEEESEG%:CALL IEEE488%:DEF SEG:RETURN
1570    PRINT "BASIC Error # ";ERR:END
```

Table 6.1. Chemical analysis of deposits made by cyclic voltammetry from 0.0 to -0.5 V (SCE) at 50 mV/s from aqueous NH_4VO_3, 0.2 mol/L followed by thermal decomposition.

temp. of heating /°C (time of heating/h)	V(IV) /10^{-5} mol	total V /10^{-4} mol	mass /mg	Mole ratio V(VI)/V(V)	formula of deposit from chemical analysis
180 (2.0)	7.83	2.463	26.00	0.466	$(NH_4)_4V_6O_{16.04}$
200 (0.5)	11.94	3.602	37.34	0 496	$(NH_4)_{3.6}V_6O_{15.8}$
200 (2.0)	4.22	1.747	17.50	0.318	$(NH_4)_{2.4}V_6O_{15.5}$
250 (16)	7.39	10.019	99.46	0.080	$(NH_4)_{1.75}V_6O_{15.7}$
300 (10)	1.85	10.877	100.51	0.017	$V_2O_{4.98}$
350 (12)	0.28	4.606	42.20	0.006	$V_2O_{5.00}$
DTA*	0.52	9.653	88.37	0.005	$V_2O_{5.00}$

* After DTA experiment, see section 6.2.2.2.

Appendix II(b)

```
A:TYPE SETOL
SETUP COMMAND FILE - initializes and sets c.c. to 3mA READS first U & pot.
15
KEY 26
KEY 3
KEY 14
KEY 3
KEY 38
P 10
I/E -7
MODE 1
KEY 15
KEY 6
KEY 4
KEY 38
P 3
0
READE
```

```
A.
RUNNING COM FILE FOR OPEN CIRCUIT POT. - CHARGE  L) INSERTIONS
11
CELL 1
I/E -3
P 180
I/E -7
CELL 0
STIR 1
P 100
STIR 0
I/E -7
0
READE
```

[18] P.J. Kulesza and L.R. Faulkner, J. Electroanal. Chem. Interfacial Electrochem., 248 (1988) 305.

[19] A.S. Goncharenko and O.A. Suvorova, Zh. Prikl. Khim. (Leningrad) 33 (1960) 846; J. Appl. Chem. USSR (Engl. Transl.) 33 (1960) 847.

[20] A.S. Goncharenko, Zh. Prikl. Khim. (Leningrad) 34 (1961) 2575; J. Appl. Chem. USSR (Engl. Transl.) 34 (1961) 2439.

[21] A.S. Goncharenko and O.A. Suvorova, Zh. Prikl. Khim., (Leningrad) 34 (1961) 1515; J. Appl. Chem. USSR (Engl. Transl.) 34 (1961) 1444.

[22] M.V. Ptitsyn, Ya.R. Rakhmilevich, K.I. Tikhonov and A L. Rotinyan, Electrokhimiya 16 (1980) 740; Sov. Electrochem. (Engl. Transl.) 16 (1980) 640.

[23] M.V. Ptitsyn, T.V. Amelina and K.I. Tikhonov, Electrokhimiya 15 (1979) 1782; Sov. Electrochem. (Engl. Transl.) 15 (1979) 1527.

[24] J. Bernard, F. Theobald and A. Vidonne, Bull. Soc. Chim. Fr. (1970) 2108.

[25] U.M. Levanto, Acta Polytechnica Scandinavica Ch 82 (1969) Thesis, Helsinki.

[26] F.R. Theobald, J.C. Theobald, J.C Vedrine, R. Clad and J Renard, J. Phys. Chem. Solids 45 (1984) 581.

[27] M. Pouchard, J. Galy, L. Rabardel and P. Hagenmuller, C.R. Hebd. Acad. Sci. 264C (1967) 1943.

[28] M. Pouchard, Ph.D., Bourdeaux University, 1967.

[29] P. Hagenmuller, *in* J.C. Bailar, H.J. Emeleus, R. Nyholm and A.F. Trotman-Dickenson, eds., Comprehensive Inorganic Chemistry Vol. 4, Pergamon Press (1973). pp. 569-601.

[30] J. Galy and A. Carpy, Acta Cryst. B31 (1975) 1794.

[31] Duncan McKie and Christine McKie, Crystalline Solids, Nelson Publishing (1974) p. 187.

[32] J.E.B. Randles, Trans. Faraday Soc., 44 (1948) 327.

[33] A. Sevčik, Coll. Chech. Chem. Comm., 13 (1958) 349

[34] R.S. Nicholson, Anal. Chem., 37 (1965), 1351.

[35] J. Ross MacDonald, J. Electroanal. Chem., 223 (1987) 25.

LIST OF REFERENCES

[1] W.R. McKinnon and R.R. Haering, Modern Aspects of Electrochemistry, Vol 15 ed. by R.E. White, J. O'M. Bockris, and B.E. Conway (plenum, N.Y., 1983), p.235.

[2] J.R. Dahn and W.R. McKinnon, Physics in Canada, July (1988) 93.

[3] M.B. Armand, *in* Fast Ion Transport in Solids, ed. by P. Vashista, J.N. Mundy and G.K. Shenoy, Elsevier-North Holland, Amsterdam, 1979, p. 131.

[4] D.A. Winn, J.M. Shemilt and B.C.H. Steele, Mat. Res. Bull., 11 (1976) 559.

[5] M.S. Whittingham, Prog. Solid State Chem. 12 (1978) 41.

[6] R. Hall, Canadian Research, March (1986) 20.

[7] W.F. Linke, Solubilities: Inorganic and Metal-Organic Compounds. Vol. II, 4th ed. A.C.S., Washington, D.C., 1965.

[8] D.W. Murphy and P.A. Christian, Science 205 (1979) 651.

[9] D.W. Murphy, P.A. Christian, F.J. DiSalvo and J.V. Waszczak, Inorg. Chem. 18 (1979) 2800.

[10] D.W. Murphy, P.A. Christian, J.N. Carides and F.J. Di Salvo, *in* Fast Ion Transport in Solids, ed. by P. Vashista, J.N. Mundy and G.K. Shenoy, Elsevier-North Holland, Amsterdam, 1979, p. 137.

[11] K. West, B. Zachau-Christiansen, M.J.L. Ostergard, and T. Jacobsen, J. Power Sources, 20 (1987) 165.

[12] G. Betz and H. Tributsch, Prog. Solid State Chem. 16 (1985) 195; see sect. 2.4.

[13] M. Salomon, Pure Appl. Chem., 59 (1987) 1165.

[14] E. Plichta, M. Salomon, S. Slane and M. Uchiyama, J. Solution Chem., 16 (1987) 225.

[15] D.W. Murphy, P.A. Christian, F.J. DiSalvo and J.N. Carides, J. Electrochem. Soc., 126 (1979) 497.

[16] D.M. Abraham, J.L. Goldman and M.D. Dempsey, J. Electrochem. Soc., 128 (1981) 2493.

[17] T. Yoshino, N. Baba and Y. Kouda, Jap. J. Appl. Phys., 26 (1987) 782.

[36] V.G. Levich, Physicochemical Hydrodynamics, Prentice Hall, 1962.

[37] Instrumental Methods in Electrochemistry, ed. T.J. Kemp, Ellis Horwood Ltd. 1985.

[38] P.G. Bruce, *in* Polymer Electrolyte Reviews-1, ed. by J.R. MacCallum and C.A. Vincent, Elsevier Applied Science 1987, p. 237.

[39] W.R. McKinnon and J.R. Dahn, J. Phys C: Solid State Phys., 19 (1986) 5121.

[40] S.T. Coleman, W.R. McKinnon and J.R. Dahn, Phys. Rev. B, 29 (1984) 4147.

[41] E. Bishenden, M.Sc. thesis, The University of Western Ontario, 1989.

[42] R. Crandall, P. Wojtowicz and B. Faughnan, Solid State Comm., 18 (1976) 1409.

[43] H.R. Grady, Treatise on analytical chemistry II, Vol. 8 (Wiley, New York, 1963) p. 228.

[44] H.R. Grady, Treatise on analytical chemistry II, Vol. 1 (Wiley, New York, 1963) p. 373.

[45] Berman Density Balance Instruction Sheet, 1971.

[46] ASTM, Philadelphia, PA, 1962, Cards 7-332, 11-673.

[47] M.J. Lasalle and James W. Cobble, J. Phys. Chem, 59 (1955) 519.

[48] A.D. Kelmers, J. Inorg. Nucl. Chem.,21 (1961) 45.

[49] A.S. Goncharenko, Zh. Prikl. Khim. (Leningrad) 35 (1962) 2449; J. Appl. Chem. USSR (Engl. Transl.) 35 (1962) 2350.

[50] C.F. Baes and R.E. Mesmer, The Hydrolysis of Cations. Wiley, New York, 1976, section 10.2.8.

[51] J. Lemerle, L. Nejem and J. Lefebvre, J. Inorg. Nucl. Chem. 42 (1980) 17.

[52] H. Freundlich, New Conceptions in Colloidal Chemistry, Methuen, London, 1926, p. 103.

[53] R.A. Robinson and R.H. Stokes, Electrolyte Solutions, 2nd Ed., Butterworth and Co. Ltd. (1959) pp. 515.

[54] J.M. Hale, in N.S. Hush (ed), Reaction of Molecules at Electrodes, Wiley, Interscience (1971) pp. 229.

[55] J. Bernard and F. Theobald, C.R. Hèbd. Acad. Sci., 256C (1963) 4916.

[56] I. Lukàcs, C. Strusievici and C. Liteanu, Rev. Roumaine Chim., 15 (1970) 935; ASTM, Philidelphia, PA, 1970, Card 28-845.

[57] ASTM, Philadelphia, PA, 1962, Cards 11-210.

[58] O. Glemser and E. Schwarzmann, Z. Anorg. Chemie., 278 (1955) 249.

[59] Joint Committee on Powder Diffraction Standards, US Dept. of Commerce, NBS. Crystal Data, 3rd. ed., Vol.II, 1973.

[60] L. Abello, E. Husson, Y. Repelin and G. Lucazeau, Spectrochim. Acta, 39A (1983) 641.

[61] T. Yoshino, N. Baba and Y. Kouda, J. Surf. Sci. Soc. Jpn., 6 (1985) 198.

[62] K. Post and R.G. Robins, Electrochim. Acta 21, 401 (1976)

[63] Walter A. VanSchalkwijk, Ph.D., University of Ottawa, 1986.

[64] U. von Sacken and J.R. Dahn. Journal of Power Sources, 26 (1989) 461.

[65] D.W. Murphy, P.A. Christian, F.J. DiSalvo, J.N. Carides and J.V. Waszczak, J. Electrochem. Soc., 128 (1981) 2053.

[66] ASTM, Philidelphia, PA, 1962, Card 9-387, 27-1318.

[67] National Bureau of Standards Circular, 539,(8) (1958) 66.

[68] H.G. Bachman, F.R. Ahmed and W.H. Barnes, Z. Kristallog. Kristallgeom. Kristallphys. Kristallchem. 115 (1961) 110.

[69] R.W.G. Wyckoff, Crystal Structures, Vol. 2, Chap. 5, (1964) pp.184-7.

[70] P. Aldebert, N. Baffier, N. Gharbi and J. Livage, Mater. Res. Bull. 16 (1981) 669.

[71] P. Aldebert, N. Baffier, N. Gharbi and J. Livage, Mater. Res. Bull. 16 (1981) 949.

[72] D. Lemordant, A. Bouhaouss, P. Aldebert and N. Baffier, J. Chim. Phys. Chim. Biol. 83 (1986) 105.

[73] K. Wilhelmi, K. Waltersson and L. Kihlborg, Acta Chem. Scand., 25 (1971) 2675.

[74] A. Deschanvres, G. Nouet and B. Raveau, C.R. Hèbd. Acad. Sci., 261 (1965) 3144.

[75] E. Andrukaitis, P.W.M. Jacobs, E.A. Bishenden and J.W. Lorimer, J. Power Sources, 26 (1989) 475.

[76] F. Theobald, R. Cabala and J. Bernard, C.R. Hèbd. Acad. Sci., 266C (1968) 1534.

[77] M.S. Whittingham, J. Electrochem. Soc. 122 (1975) 713.

[78] E. Andrukaitis, P.W.M. Jacobs and J.W. Lorimer, Solid State Ionics, 27 (1988) 19.

[79] P.G. Dickens, A.M. Chippindale and S.J. Hibble, Solid State Ionics, 34 (1989) 79.

[80] R. Larsson, B. Folkesson and G. Schon, Chem. Scr., 3 (1973) 88.

[81] I.M. Curelaru, E. Suoninen and E. Minni, J. Chem. Phys. 78 (1983) 2262.

[82] B. Liaw, I.D. Raistrick and R.A. Huggins, Solid State Ionics, 18/19 (1986) 828.

[83] S.H. Liu, Phys. Rev. Let., 55 (1985) 529.

[84] S.H. Liu, T. Kaplan, and L. J. Gray, Proceedings of the IEEE International Symposium on Circuits and Systems, Philadelphia, Penn., May 1987, 942.

[85] P.G. Dickens, S.J. French, A.T. Hight and M.F. Pye, Mater. Res. Bull. 14 (1979) 1295.

[86] M.S. Whittingham, J. Electrochem. Soc. 123 (1976) 315.

[87] M.V. Ptitsyn, K.I. Tikhonov and A.L. Rotinyan, Electrokhimiya 16 (1980) 737; Sov. Electrochem. (Engl. Transl.) 16 (1980) 637.

[88] R.J. Cava, A. Santoro, D.W. Murphy, S.M. Zahurak, R.M. Fleming, P. Marsh, R.S. Roth, J. Solid State Chem. 65 (1986) 63.

[89] M.V. Ptitsyn, K.I. Tikhonov and A.L. Rotinyan, Electrokhimiya 17 (1981) 1558; Sov. Electrochem. (Engl. Transl.) 17 (1981) 1297.

[90] A. Honders and G.H.J. Broers, Solid State Ionics, 15 (1985) 173.

[91] A. Honders, J.M. der Kinderen, A.H. van Heeren, J.H.W. deWitt and G.H.J. Broers, Solid State Ionics, 15 (1985) 265.

[92] S. Atlung, K. West and T. Jacobsen, J. Electrochem. Soc., 126 (1979) 1311.

[93] B.W. Faughnan, R.S. Crandall and M.A. Lampert, Appl. Phys. Lett. 27 (1975) 275.

[94] B.W. Faughnan and R.S. Crandall, Topics in Applied Physics, Vol. 40, Display Devices (1980) pp. 180-211.

[95] Anthony J. Vaccaro, T. Palanisamy, R.L. Kerr and J.T. Maloy, J. Electrochem. Soc., 129 (1982) 682.

[96] R. Crandall, P. Wojtowicz and B. Faughnan, Solid State Comm., 18 (1976) 1409.

[97] P.W.M. Jacobs, J.W. Lorimer, A. Russer and M. Wasiucionek, Journal of Power Sources, 26 (1989) 503.

[98] P.W.M. Jacobs, J.W. Lorimer, A. Russer and M. Wasiucionek, Journal of Power Sources, 26 (1989) 483.

[99] E. Andrukaitis, P.W.M. Jacobs, J.W. Lorimer, A. Russer and M. Wasiucionek, 72nd Canadian Chemical Conference, Victoria B.C., 1989.

[100] M.B. Armand, *in* Polymer Electrolyte Reviews-1, ed. by J.R. MacCallum and C.A. Vincent, Elsevier Applied Science 1987, p. 1.

[101] M.R. Worboys Ph.D. Thesis, University of Kent 1985.

[102] P.G. Bruce and F. Krok, Solid State Ionics, 36 (1989) 171.

[103] E. Andrukaitis, P.W.M. Jacobs, P. Kurek and J.W. Lorimer, to be presented, J. Electrochem. Soc. Meeting, Montreal, Canada, June, 1990.

[104] Jiqiang Wang, I.D. Raistrick and R.A. Huggins, J. Electrochem. Soc., 133 (1986) 457.

[105] J.C. Thevenin and R.H. Muller, J. Electrochem. Soc., 134, (1987) 273.